Growth controls of rhodoliths (*Lithothamnion glaciale*) and relationships between structural complexity and macrofaunal diversity in subarctic rhodolith beds

by

© David Bélanger

A thesis submitted to the School of Graduate Studies

in partial fulfillment of the requirements for the degree of

Doctor of Philosophy, Biology

Department of Biology

Memorial University of Newfoundland

St. John's, Newfoundland, Canada

November 2020

Abstract

Coastal benthic ecosystems are major contributors to oceans global productivity and biodiversity. Research has historically focused on charismatic ecosystems such as coral reefs, kelp beds and seagrass meadows. This paradigm may overshadow the biogeochemical functions and ecological importance to coastal oceans of other less studied communities. Rhodoliths are benthic, unattached, slow-growing coralline red algae. Rhodoliths may aggregate into extensive and diverse communities called rhodolith beds, which occur within the photic zone in all oceans, from the tropics to the poles. This thesis used long-term laboratory and field experiments as well as seasonal surveys to characterize controls of growth in *Lithothamnion glaciale* rhodoliths and to investigate the relationship between structural complexity and the diversity of rhodolith-associated macrofauna in a subarctic rhodolith bed from southeastern Newfoundland. Results showed that rhodolith growth is negatively affected by elevated nutrient (N and P) concentrations and biofouling. Rhodolith growth was mainly controlled by irradiance and was unaffected by temperatures between ~1 and 17°C, but appeared to be inhibited by temperatures ≤ 0.5°C. Rhodolith bed structure showed little annual spatial and temporal variations. Macrofaunal density scaled positively with total rhodolith volume per surface area, whereas biomass did not. Results also suggest that rhodolith morphology exerts a control on the diversity of macrofauna associated to rhodoliths. Macrofaunal assemblages varied spatially and temporally in most taxonomic groups with few, uncommon taxa being generally responsible for dissimilarity between sites and among seasons. These findings provide novel insights into the ecology and vulnerability of rhodoliths to anthropogenic threats and climate change while elevating the importance of subarctic *L. glaciale* beds as a key ecosystem in the Northwest Atlantic.

Acknowledgements

I would like to thank my supervisor Dr. Patrick Gagnon for his encouragement, guidance, and dedication throughout this project and also my committee members, Dr. Paul Snelgrove, and Dr. Robert Gregory for their support and constructive comments throughout the stages of this thesis. I am especially thankful for all the hard work and dedication of Anne Provencher St-Pierre, Samantha Trueman, Kyle Millar, and Desta Frey for their invaluable help with field work, and to laboratory assistants Philip Schryburt, Ítalo Lima, and Jadson Lima for their help with laboratory work. A special thanks to Dr. David Schneider for his help with statistical analyses and for having greatly contributed in developing my skills and understanding of modern statistics. I thank Sandra Fraser, Gina Doyle, and Gary Maillet for their time and the logistical support they provided to complete nutrient analyses, and Jennifer Wacasey for having graciously supplied fertilizer. I am also grateful to my parents who have always supported me in my endeavours and, most importantly, to my wife, Bárbara de Moura Neves, who was always there to listen and encourage me through the ups and downs all along these years. This research was supported by Natural Sciences and Engineering Research Council (NSERC- Discovery Grant), Canada Foundation for Innovation (CFI- Leaders Opportunity Funds), Research & Development Corporation of Newfoundland and Labrador (Ignite R&D), and Department of Fisheries and Aquaculture of Newfoundland and Labrador (DFA) grants to Patrick Gagnon. David Bélanger was supported by the Memorial University President's Doctoral Student Investment Fund program.

Table of Contents

List of Tables

List of Figures

List of Appendices

Co-Authorship Statement

The work described in this thesis was conducted by David Bélanger with guidance from Patrick Gagnon, Paul Snelgrove, and Robert Gregory. David Bélanger was responsible for the development of experimental designs, field and laboratory data collection and analysis (with assistance by Patrick Gagnon). All chapters were written by David Bélanger with intellectual and editorial input by Patrick Gagnon. An abridged version of Chapter II is published in *Marine Ecology Progress Series* (full reference below). Chapter III has been submitted to *Marine Ecology Progress Series* and is currently under revision. A shortened version of Chapter IV is currently being prepared for publication in the primary literature. Any additional publication in the primary literature resulting from this work will be co-authored by David Bélanger and Patrick Gagnon.

Bélanger D, Gagnon P (2020) Low growth resilience of subarctic rhodoliths (*Lithothamnion glaciale*) to coastal eutrophication. Mar Ecol Prog Ser 642:127-132

Bélanger D, Gangon P (in review) High growth resilience of subarctic rhodoliths (*Lithothamnion glaciale*) to ocean warming and chronic low irradiance. Mar Ecol Prog Ser

CHAPTER I

General introduction

1.1. MARINE CALCIFIERS

Marine calcifiers are organisms that use carbonate and calcium ions dissolved in seawater to construct their shells and skeletons. They range in size from <1 mm (coccolithophorids and foraminifera) to several meters (corals) and occupy both pelagic and benthic zones from the ocean surface to the deep sea (Tendal 1992, Watling et al. 2013, Lischka et al. 2018). Marine calcifiers play a key role in the global carbon cycle through carbon sequestration into the carbonate structure they form (Perry et al. 2008, Tsuji et al. 2015). Benthic calcifiers such as molluscs, bryozoans, hermatypic and cold-water corals, and calcareous algae build biological structures that modify and often enhance the structural complexity of the marine benthic seascape (Meadows et al. 2012). These biogenic constructions provide new substrate for attachment, shelter, and feeding to other species (Nelson 2009, Buhl-Mortensen 2012). Marine calcifiers are facing mounting threats including global warming, ocean acidification, and costal eutrophication (Tomascik & Sander 1985, Kawahata et al. 2019). Responses to these threats are often species-specific (Fabry 2006, Ries et al 2009). Understanding how the changing environment will impact marine calcifiers and their associated communities is important to predict large-scale ecosystem response.

1.2. RHODOLITHS AND RHODOLITH BEDS

Rhodoliths are unattached, benthic nodules primarily composed of coralline red algae (Rhodophyta, Corallinales) (Bosellini & Ginsburg 1971). They occur in all oceans from the intertidal zone down to the lower limit of the photic zone (Foster 2001). Under favorable conditions, rhodoliths aggregate and form structurally complex benthic habitats

named rhodolith beds, also know as maërl beds. These beds vary in size from 100s of m^2 to 1000s of km^2 and generally host biodiverse communities including endemic and commercially important species (Steller & Cáceres-Martínez 2009, Amado-Filho & Pereira-Filho 2012). Because of their free-living nature, rhodoliths normally accumulate in environment where water motion is not so high or directional as to cause destruction or transport to unfavourable environments (Foster 2001). To survive, rhodoliths also need to stay free from burial by sediments, which is normally accomplished through occasional movement caused by water motion and bioturbation (Hinojosa-Arango et al. 2009, Pascelli et al. 2013). The role of bioturbation is particularly important in environment where hydrodynamic forces are insufficient to move rhodoliths (Millar & Gagnon 2018).

The importance of sexual and asexual reproduction in enabling rhodolith bed expansion varies among coralline species, with a generally high reliance on tissue fragmentation (Bosence 1976, Irvine and Chamberlain 1994, Peña et al. 2014a, Pardo et al. 2017). Rhodoliths may also occasionally shed asexual spores (Adey & McKibbin 1970, Woelkerling & Irvine 1986, Peña & Barbara, 2004). However, rhodoliths bearing sexual reproductive structures have seldomly been reported in rhodolith beds (Mendoza & Cabioch 1998). In general, rhodolith accumulate on the sea floor at a remarkably slow rate of 0.1 to 1.5 m kyr^{-1}, and persist over thousands of years (Aguirre et al. 2017).

1.3. GLOBAL DISTRIBUTION

Rhodoliths are distributed worldwide from the poles to the tropics and predominate in the Gulf of California (Steller et al. 1995, Steller et al. 2003), Northeast Atlantic (Blake Maggs 2003, Grall & Hall-Spencer 2003), Mediterranean Sea (Basso et al. 2016), and

southwest Atlantic where the largest known rhodolith bed (~21 000 km^2) occurs off the coast of Brazil (Amado-Filho et al. 2012). Beds have also been reported in the Caribbean (Peña et al. 2014b), Gulf of Mexico (Fredericq et al. 2019), North-Pacific (Konar et al. 2006, Matsuda & Iryu 2011, Sletten et al. 2017) and South-Pacific (Nelson 2012, Darrenougue et al. 2013, Macaya et al. 2015), Northwest Atlantic (Gagnon et al. 2012, Adey et al. 2015), and the Arctic (Freiwald & Henrich 1994, Teichert et al. 2014). A review of herbariums collections and scientific grey literature revealed that rhodoliths are common along 70% of Australian coastline where they were considered to be uncommon until recently (Harvey et al. 2016). Similarly, recently published works on habitat mapping indicate that rhodolith beds are widely distributed along the coast of southern Greenland where they had not been officially reported before (Jørgensbye & Halfar 2017, Schoenrock et al. 2018). Growing interest in rhodolith research over the past two decades has highlighted the global importance of rhodolith beds as one of the world's largest macrophyte-dominated communities ranking with kelp beds, seagrass meadows, and coralline reefs, which have historically received more attention from the scientific community (Foster 2001).

1.4. GROWTH AND CALCIFICATION

Growth in rhodolith-forming coralline species is slow and does not typically exceed a few mm y^{-1} (Nelson 2009). Rhodolith in cold-water environments grow at even slower rates, generally < 1 mm y^{-1} (see Chapters II & III and Halfar et al. 2000). Temperature and light are important factors controlling rhodolith distribution and growth (see Chapter III and Adey & Hayek 2011). Coralline red algae are low-light adapted and rhodoliths are a

characteristic element of the mesophotic environment in many oceanic offshore banks and continental or insular margins, where limited irradiance prevent growth in other benthic primary producers (Adey & MacIntyre 1973). With live, actively growing specimens collected at depth of 268 m in the Bahamas, coralline red algae are the deepest known plant life in the ocean (Littler et al. 1985). To our knowledge, only one published study reported growth estimates in Northwest Atlantic rhodoliths (Halfar et al. 2000). Little is known about the environmental controls of growth in subarctic and Arctic environments (see section 1.8).

Growth in rhodoliths consists in the successive deposition of layers of heavily calcified cells originating from an intercalary meristem (Nash et al. 2019). Several techniques have been used to measure rhodolith growth and calcification including differential weight (Steller et al. 2007, Teed et al. 2020), annual banding count (Halfar et al. 2000), and mechanical (William et al. 2019) and chemical marking (Blakes and Magg 2003, Lewis & Diaz-Pulido, 2017). For example, rhodolith immersed in a solution of the biological stain Alizarin red, incorporate the stain into calcified walls of newly produced cells with no effect on growth (Andrake & Johansen 1980). Quantifying growth by measuring the thickness of coralline tissue deposited above the stain mark is therefore an effective and reliable technique that has been used extensively in laboratory and *in situ* field experiments (see Chapters II & III and Blake and Maggs 2003, Darrenougue et al. 2013).

1.5. HABITAT COMPLEXITY AND BIODIVERSITY

Rhodoliths vary in size and shape from few centimeter-long twig-like thalli to large (> 10 cm diameter) spheroidal nodules (Foster 2001). They can be monospecific (composed

of one species) or plurispecific (composed of two or more species) (Villas-Boas et al 2014) and present a variety of growth forms including warty, lumpy, fruticose, and foliose (Woelkerling 1993). In rhodolith beds, live rhodoliths generally overlay a sedimentary layer composed mainly of coralline hashes originating from dead or live rhodoliths (Adey et al. 2015). The complex three-dimensional matrix arising from the accumulation of rhodoliths of different shapes, sizes, and growth forms provides a variety of ecological niches to highly diverse communities composed of epiphytic, epibenthic, cryptofaunal, and infaunal species (Steller et al. 2003, Figueiredo et al. 2007, Amado-Filho et al. 2010).

Rhodolith beds function is intimately linked to the composition of resident communities. Rhodoliths have been designated holobionts of critical importance to the establishment and maintenance of marine biodiversity (Fredericq et al. 2019). Coralline algae, including rhodolith-forming species, can induce larval settlement and metamorphosis, while creating nursery habitats for several ecologically and economically important species (Pearce & Sheibling 1990, Kamenos et al. 2004ab, Steller & Cáceres-Martínez 2009). It has been suggested that enhanced larval settlement on rhodolith surfaces results in part from rhodolith-associated microalgae representing food for settlers (Krayesky-Self et al. 2017). Rhodolith beds can host large numbers of suspension feeders, including bivalves and brittle stars (see Chapter IV and Castriota et al. 2005, Gagnon et al. 2012), whose water filtering capacity may help mitigate the negative effect of coastal eutrophication by removing excess phytoplankton from the water column (Officer et al. 1982, Hily 1991).

1.6. CARBON SINK AND CLIMATE ARCHIVE

Deposition of calcium carbonate by marine algae is an important aspect of the global carbon cycle. Approximately one-third of total shelf carbonate production takes place in non-tropical coastal waters with a significant amount coming from rhodoliths deposits (Nelson 2009). Capacity to store carbon is significant in rhodoliths because of the substantial preservation potential and longevity (> 5500 y) of their deposits (Grall & Hall-Spencer 2003, van der Heijden & Kamenos 2015). Corallines' net calcification decreases with increasing ocean acidity and temperature (Sordo et al. 2019), with no strong consensus on how climate change will affect the stability of this significant carbon store.

In addition to sequestering carbon, the calcified tissues of rhodoliths archive information on ocean climate conditions at the time of their formation. Analyses of the geochemical composition of their calcium carbonate skeleton can be used to backtrack paleoceanographic conditions (Halfar et al. 2000, Darrenougue et al. 2018). Adey et al. (2015) found that specimens of *Clathromorphum compactum* (a long-lived encrusting coralline) collected within rhodolith beds were on average 6 times older (i.e. 6 times thicker) than those collected outside the beds, thus extending their climate archiving potential to ~1200 y. The authors attributed the extended longevity of these specimens of *C. compactum* to the limited boring activity occurring within the anoxic sediment layer underlying the rhodolith bed in which they were partly buried, thus promoting their longevity and climate archiving potential.

1.7. THREATS AND CONSERVATION

Threats to rhodolith beds are numerous and include both anthropogenic activities and climate change impacts. Rhodoliths are commercially harvested in the Northeast Atlantic and transformed into a variety of agricultural and horticultural products (Blunden et al. 1975). Besides marine habitats destruction associated with the physical extraction of rhodoliths, dredging activities resuspend large amounts of fine particles that settle back on, and smother live rhodoliths and resident biota (Grall & Hall-Spencer 2003). Similarly, breakage of rhodoliths by towed demersal fishing gear reduce habitat complexity and strongly impact associated fauna and flora (Hall-Spencer & Moore 2000, Bernard et al. 2019). Nutrient and organic-enriched sediment inputs near aquaculture facilities or urban or industrial waste discharges decrease the functional and species diversity of rhodolith-associated communities and facilitate the proliferation of fast growing opportunistic macrophytes that may ultimately outcompete slow growing rhodoliths (Grall & Glémarec 1997, Aguado-Guímenez & Ruiz-Fernández 2012). Moreover, high phosphate concentrations often present in wastewaters interfere with calcification processes and negatively impact rhodolith growth and survival (see Chapter II and Simkiss 1964, Björk et al. 1995). Combined effects of ocean acidification and ocean warming are expected to significantly affect the structure and function of rhodolith beds (Brodie et al. 2014). Rhodoliths are primarily composed of high-Mg calcite, the most soluble form of calcium carbonate (Williamson et al. 2014). In the long-term, the combined and potentially synergistic effects of ocean acidification and global warming on calcification processes is expected to significantly impact the distribution, diversity and functioning of rhodolith habitats worldwide (Büdenbender et al. 2011, Sordo et al. 2019).

Because of their low growth and accumulation rates, rhodoliths and the beds they form are considered non-renewable resources with high conservation interest. In Europe, rhodolith beds are included in several conservation initiatives, including the EU's Habitats Directive, and the Bern Convention (Riosmena-Rodríguez 2017). Destructive fishing over Mediterranean rhodolith bottoms is prohibited by European law (Barbera et al. 2003). In New Zealand, rhodolith beds have been identified as ecologically significant marine sites (Davidson et al. 2011) and rhodolith-forming species have been included in the list of "sensitive marine habitats" (MacDiarmid et al. 2013). In Atlantic Canada, rhodoliths beds have been reported within at least two marine protected areas (Copeland et al. 2013, Novaczek et al. 2017). However, despite growing evidence of their wide range distribution along the Canadian Atlantic coast, rhodoliths are not listed in the latest Department of Fisheries and Oceans Canada's report on Atlantic Ecosystems (Bernier et al. 2018).

1.8. NORTHWEST ATLANTIC BEDS

There are only two rhodolith-forming species in the Northwest Atlantic: 1) the wide-ranging *Lithotanmion glaciale* encountered from the Gulf of Maine to the Arctic, and 2) the more arctic *L. tophiforme* (Adey & Hayek 2011). In subarctic environments, *L. glaciale* strongly dominates rhodolith bed composition at depths < 20 m, with an increasing prevalence of *L. tophiforme* at greater depth and dominance at depths > 25 m (Adey et al. 2015). Rhodoliths are generally composed of either one of the two species, but nodules made of both species are not uncommon where both species occur in the same bed (personal observation). Contrary to commonly encountered monospecific *L. glaciale* beds (Gagnon et al. 2012), beds composed exclusively of *L. tophiforme* rhodoliths have not been reported

yet. Although the first published account of rhodolith beds occurrence in the northwest Atlantic dates back the mid-1960s (Adey 1966), information about their distribution and ecological function in the region remained mostly anecdotal, with no formal rhodolith habitat mapping initiative taking place until recently. Gagnon et al. (2012) were the first to describe and quantify variation in rhodolith morphology and associated macrofaunal assemblages in subarctic *L. glaciale* beds in southeastern Newfoundland. Adey et al. (2015) provided the first sedimentological description of a rhodolith bed in central Labrador. These papers set the basis for a series of research initiatives addressing fundamental biological and ecological aspects of subarctic rhodoliths and rhodolith beds, including sedimentological processes (Millar & Gagnon 2018), calcification rate (Teed et al. 2020), and trophodynamics of rhodolith-associated macrofaunal communities (Hacker Teper et al. in prep).

1.9. THESIS OUTLINE

The present thesis aims at characterizing important aspects of the biology and ecology of subarctic rhodoliths and the beds they form. More specifically we aimed at quantifying, for the first time, the impact of coastal eutrophication on *L. glaciale* rhodoliths. The growing fishfarming industry and associated nutrient loading is likely to increase nutrient inputs in eastern Canadian coastal waters. Understanding the effects of eutrophication on rhodolith growth and survival is key to science-based decision making in terms of implementation of mitigation strategies. Another important aspect of the thesis was to extend the range of environmental conditions over which growth has been tested for *L. galciale* rhodoliths to include temperature and irradiance levels representative of

subarctic and arctic environments. This information will assist our capacity to forecast future effects of ongoing ocean warming and expected higher turbidity of costal waters due to increased freshwater runoffs (Węsławski et al. 2010) on the productivity of subarctic rocky dominated by *L. glaciale*. The last overall objective of the thesis was to describe the structural complexity and the full spectrum of rhodolith-associated macrofaunal diversity in a Northwest Atlantic *L. glaciale* bed, and to characterize the relationships between the two. Quantifying the abundance and diversity of macrofaunal assemblages associated with rhodoliths and their relationship with rhodolith beds structural complexity is essential to understand the ecological function of rhodolith communities and the potential effects of climate and anthropogenic threats on these benthic communities in the subarctic Northwest Atlantic.

Besides this introductory chapter (I) this thesis contains three data chapters (II-IV) and a conclusion and summary chapter (V). In Chapter II, we used a combination of long-term (6 mo) laboratory mesocosm and field experiments to test the hypothesis that nutrient (ammonia, nitrate and phosphate) enrichment and biofouling reduce rhodolith growth. Rhodoliths in the laboratory were exposed to one of three nutrient concentrations (ambient, intermediate, and high) and either of two levels of manual cleaning (cleanned and uncleanned), while rhodolith in the field were exposed to one of two nutrient concentrations (ambient and enriched). In Chapter III, we used a similar methodological approach based on 1-y complementary laboratory mesocosm and field experiments to test the hypothesis that growth in *L. glacial* rhodoliths in mainly controlled by irradiance. Rhodoliths in the laboratory were exposed to one of five seawater temperatures (ambient, 2, 4, 7, and 10°C), and to one of three irradiances (low, intermediate and high), while rhodoliths in the field

were held in cages at three depths (8, 15 and 25 m). In Chapter IV, we used univariate and multivariate statistics applied to quadrat collections and video imagery to test the hypotheses that: 1) rhodolith bed structure varies spatially within the bed but is temporally stable because of prevalent low hydrodymamics at the study site, and 2) that rhodolith-associated macrofaunal assemblages vary spatially with rhodolith abundance and rhodolith bed structure, as well as seasonally driven by macrofaunal life cycles. Data collection was carried out in spring, summer, fall, and winter at two sampling sites (15 m and 18 m) within the same bed characterized by different rhodolith morphologies. Chapter V summarises the results and main conclusions from the three data chapters, and points to future research directions.

CHAPTER II

Low growth resilience of subarctic rhodoliths (*Lithothamnion glaciale*) to coastal eutrophication[1]

[1] Bélanger D, Gagnon P (2020) Low growth resilience of subarctic rhodoliths (*Lithothamnion glaciale*) to coastal eutrophication. Mar Ecol Prog Ser 642: 117-132.

2.1. ABSTRACT

Eutrophication is one of the most important drivers of changes in coastal marine ecosystems worldwide. Given their slow growth, rhodoliths and the biodiverse communities they support are regarded as non-renewable resources threatened by human activity. Consequences of nutrient enrichment on growth and calcification in crustose coralline algae are equivocal, and even more so in cold-water rhodoliths. We paired a 183-d laboratory mesocosm experiment and a 193-d field experiment with Newfoundland rhodoliths (*Lithothamnion glaciale*) to test the hypothesis that nutrient (nitrate, ammonia, and phosphate) enrichment and biofouling reduce rhodolith growth. Rhodoliths in the laboratory were exposed to one of three nutrient concentrations (ambient, intermediate, or high) and either of two levels of manual cleaning (cleaned or uncleaned) to control biofouling. We exposed rhodoliths in the field to one of two nutrient concentrations (ambient or elevated). Eutrophication in the laboratory did not affect biofouling, however manual cleaning reduced biofouling by ~4 times relative to uncleaned rhodoliths. Rhodoliths grew two times slower at elevated than ambient concentrations, and ~27% more in cleaned than uncleaned rhodoliths at all concentrations. Rhodoliths in the field also grew significantly slower under elevated than ambient phosphate concentrations, but only during the first 6 wk, indicating some capacity for long-term recovery. We conclude that despite some growth resilience to low levels of infrequent increases in nutrient concentrations, subarctic *L. glaciale* rhodoliths cannot cope with prolonged exposure to modest eutrophication.

2.2. INTRODUCTION

Eutrophication is one of the most important drivers of change in coastal marine ecosystems worldwide (Andersen & Conley 2009). Fossil fuel emissions, urban wastewaters, industrial effluents, agriculture runoffs, and fish farming produce major anthropogenic inputs of nitrogen (N) and phosphorus (P) to coastal environments (Selman et al. 2008, Conley et al. 2009). N and P often limit ocean primary production, more specifically in their dissolved inorganic forms; nitrate (NO_3^-), ammonia (NH_3), and phosphate (PO_4^{3-}) (Ryther & Dunstan 1971). Higher N and P concentrations can increase primary production, ultimately altering bottom-up forces that trigger important changes in the structure and function of coastal assemblages (Valiela et al. 1997). Typically, in marine systems undergoing eutrophication, rapid growth of benthic algae and epiphytes exceeds the ability of grazers to control them, resulting in gradual replacement of perennial, canopy-forming vegetation (Duarte 1995).

Many studies consider nitrogen as the main limiting nutrient for marine primary producers (Smith 1984, Larned 1998, Blomqvist et al. 2004), yet phosphorus limitation also occurs, particularly in environments with high N concentration (Krom et al. 1991). Although high concentrations of N, P, or both, generally enhance the growth of marine primary producers (Delgado & Lapointe 1994), excessive phosphate can inhibit growth and calcification (Simkiss 1964), as seen in corals (Dunn et al. 2012) and coralline algae (Björk et al. 1995, Belliveau & Paul, 2002, Littler et al. 2010). Growth in coralline algae correlates positively with the rate of addition of new layers of calcified tissue (McCoy & Pfister 2014). Few studies in warm-water coral reef environments have examined the effects of nutrient enrichment on growth and calcification of crustose coralline algae (Björk et al. 1995, Belliveau & Paul 2002, Tanaka et al. 2017). These studies generally conclude that nutrient enrichment does not improve coralline algal growth. For

example, Björk et al. (1995) reported a ~45% decrease in growth rate of *Lithophyllum kotschyanum* and a ~24% decrease in coralline algal abundance near sewer outfalls. Whether this conclusion extends to cold-water coralline algae or to species with more complex morphologies remains unknown.

Rhodoliths are non-geniculate, unattached, benthic coralline algae with highly calcified tissues that grow only a few millimetres per year (Foster 2001). Depending on species and environmental conditions, rhodoliths vary in size, shape, and growth form, ranging from small twig-like thalli to large (> 10 cm across) and highly branched ellipsoids (Woelkerling et al. 1993). They occur in all oceans from the low intertidal zone down to the lower photic zone (Riosmena-Rodriguez et al. 2017), accumulating in structurally complex and biologically diverse communities known as rhodolith beds (Foster, 2001). Given their slow growth and accumulation rates, most researchers consider rhodoliths as non-resilient and non-renewable resources threatened by human activity (Nelson 2009, Riosmena-Rodriguez et al. 2017).

Multiple studies report alteration of rhodolith beds by anthropogenic stressors, including eutrophication, and anticipate further global increases (Grall & Hall-Spencer 2003, Gabara et al. 2018). In the Northwest Atlantic, the coralline red alga *Lithothamnion glaciale* dominates coralline assemblages at depths of 15 to 25 m (Adey & Hayek 2011). Rhodoliths (*L. glaciale*) and extensive rhodolith beds develop within this depth range, near natural, urbanized, and industrialized areas along the coast of Newfoundland and Labrador (Gagnon et al. 2012, Millar and Gagnon 2018, Teed et al. 2020). This region provides an excellent opportunity to study the vulnerability of subarctic rhodoliths to eutrophication because of: (1) predominantly cold water environments in which these beds develop (Caines & Gagnon 2012, Blain & Gagnon 2013); and (2) general absence

of epiphytes on rhodoliths in the Newfoundland beds studied thus far (Gagnon et al. 2012, Adey et al. 2015, Millar & Gagnon 2018).

We paired a 183-d laboratory mesocosm experiment and a 193-d field experiment with Newfoundland rhodoliths (*L. glaciale*) to test the hypothesis that nutrient enrichment (nitrogen and phosphorous) and biofouling reduce rhodolith growth. This hypothesis stems from (1) inhibitory effect of phosphate on calcification processes as seen in the crustose coralline alga *L. kotschyanum* (Björk et al. 1995); and (2) expected proliferation of epiphytes, reducing rhodolith access to light and nutrients, and hence photosynthetic activity and growth, as seen in the seagrasses *Thalassia testudinum* and *Zostera marina* (Drake et al. 2003). Rhodoliths in the laboratory experiment experienced different combinations of nutrient concentrations (ambient, intermediate, or high) and manual cleaning of their surface to control biofouling (cleaned or uncleaned). We held rhodoliths in the field experiment in cages and exposed them to ambient or elevated nutrient concentration. In both experiments, (1) rhodoliths experienced natural variation in sea temperature and photoperiod; (2) slow release of an agricultural fertilizer determined nutrient concentrations; and (3) we compared rhodolith growth to identify individual and interactive effects of nutrient enrichment and biofouling on growth.

2.3. MATERIALS AND METHODS

2.3.1. Rhodolith collection and staining

On 30 May and 4 June, 2015, divers hand collected spheroidal *Lithothamnion glaciale* rhodoliths measuring 40 to 45 mm in diameter (Figure 2.1A) haphazardly at ~15 m depth from the middle of a rhodolith bed in St. Philip's (southeastern Newfoundland, Canada [47.5926° N, 52.8926° W]) (see Gagnon et al. 2012 and Millar et al. 2018 for a detailed description of the bed).

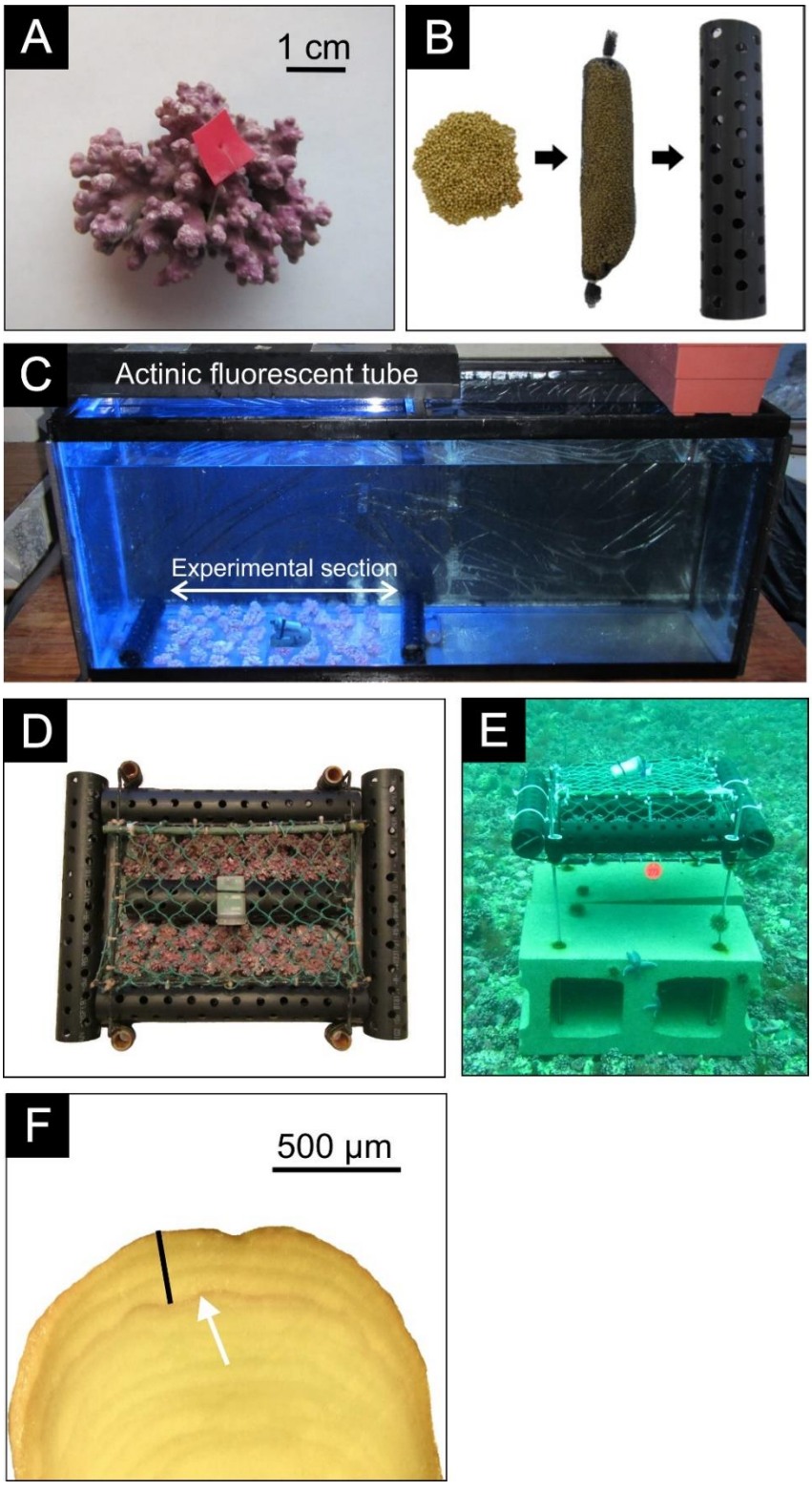
A
1 cm
B
C
Actinic fluorescent tube
Experimental section
D
E
F
500 µm

Figure 2.1. (A) One of the rhodoliths in the laboratory mesocosm experiment with a colour-coded identifier. (B) Nutrient dispenser: Osmocote® fertilizer prills [left]; fiberglass screen bag [1.5-mm mesh size] with prills [centre]; and perforated [9-mm diameter holes] ABS pipe with bag [right]. (C) One of the six, 180-L mesocosms with location of the experimental section containing rhodoliths, two 25-cm-long nutrient dispensers [bottom], one temperature and light logger [in the centre of the rhodoliths], and one actinic fluorescent tube [top]. (D) One of the rhodolith cages [26 x 18 x 7 cm] used in the field experiment with four peripheral and one internal nutrient dispensers, 30 stained rhodoliths on each side of the internal dispenser, and one temperature and light logger attached to the top. (E) One of the cages in the rhodolith bed in St. Philip's. (F) Longitudinal section across the tip of a rhodolith branch showing the Alizarin stain mark [white arrow] used to measure growth [black bar].

Rhodoliths were transported in plastic containers filled with seawater to the Ocean Sciences Center (OSC) of Memorial University and transferred into two 180-L glass tanks (360 rhodolith in each tank) supplied with flow-through seawater pumped in from a depth of ~5 m in adjacent Logy Bay. We exposed rhodoliths in these tanks for 35 d to natural irradiance and photoperiod of indirect sunlight.

From 26 to 28 June, 2015, we inspected each rhodolith and removed all cryptofauna and epiphytes with forceps and a smooth nylon brush in preparation for rhodolith staining. On 29 June, 2015, we stopped seawater delivery to each tank and lowered the water volume to 90 L prior to adding 10 L of seawater containing 8.5 g of dissolved Alizarin Red S (a biological stain commonly used to stain rhodoliths; Riosmena-Rodriguez et al. 2017), yielding a concentration of ~85 mg Alizarin L^{-1}. We held rhodoliths for 48 h in the staining solution at ~6°C with immersion probe coolers (IP-35RCL; PolyScience) controlled by timers. During staining, we aerated each tank with a pump (Elite802; Rolf C. Hagen) that delivered 1500 cm^3 of air min^{-1} to prevent deoxygenation and acidification althought this was done preemptively and we did not monitor these two parameters. Two 61-cm long, actinic fluorescent tubes [Marine-GLO, T8, 20W; Rolf C. Hagen] located ~50 cm above the water surface [one tube per half section of the tank] emitted light daily from 06:00 to 20:00 to reflect a natural photoperiod. These actinic tubes, designed to emulate shallow marine coastal light conditions, emitted predominantly in the lower PAR range (400-580 nm). After staining, we reinstated water flow in the tanks, gradually flushing the staining solution.

2.3.2. Nutrient release

Marine ecologists use slow-release agricultural fertilizers to simulate and study the impacts of nutrient enrichment on plant growth and community structure (Worm et al. 2000). These fertilizers simulate nutrient composition of terrestrial water runoffs and outfalls, while enabling long-term in-situ enrichment experiments through gradual release of nutrients over time. In both the laboratory mesocosm experiment ("Mesocosm enrichment experiment") and field experiment ("Field enrichment experiment"), we used slow-release fertilizer prills (Osmocote® Classic, 19-6-12; Everris) containing 10% ammoniacal nitrogen (NH_3-N), 9% nitrate nitrogen (NO_3-N), 6% phosphorus pentoxide (P_2O_5), and 12% potassium oxide (K_2O). In each experiment, we used custom-built nutrient dispensers to establish the desired nutrient concentrations. Each dispenser consisted of a cylindrical fiberglass screen bag (mesh size = 1.5 mm) filled with fertilizer prills and placed in a perforated (9-mm diameter holes, 13 holes per dm^2) ABS pipe (diameter = 3.8 cm) (Figure 2.1B). Dispenser size was constrained by mesocosm width and inner-cage length (25 cm, 76 holes), and outer-cage perimeter (30 cm, 92 holes) (Figure 2.1B). We carried out pre-experimental trials to study patterns of nutrient release (see Figure A.1, Appendix A) and create repeatable patterns with detectable levels of nitrate, ammonia, and phosphorus in our experiments.

2.3.3. Mesocosm enrichment experiment

To test individual and interactive effects of nutrient enrichment and biofouling on rhodolith growth, we exposed stained rhodoliths in a 183-d laboratory mesocosm experiment, in a fully crossed design, to one of six combinations of nutrient concentrations (ambient, intermediate, and high) and biofoulers of rhodolith surfaces (cleaned and uncleaned). We measured the thickness of

new layers of tissue added at the tip of branches since marking (see "Rhodolith growth" for details of growth measurement).

The experiment used six, 180-L glass mesocosms (120 cm long x 30 cm wide x 50 cm deep) with flow-through ambient seawater (1 L min^{-1}). We assigned each mesocosm one of two replicates for each of the three nutrient concentrations. Experimental manipulations were carried out in the half section of each mesocosm opposite the sea water inflow to limit rhodolith exposure to non-enriched ambient water input. One 61 cm-long, actinic fluorescent tube (Marine-GLO, T8, 20W; Rolf C. Hagen) located ~10 cm above the water surface and emitting ~15 µmol photons m^{-2} s^{-1} of photosynthetically active radiation (PAR), lit this section of the mesocosms, hereafter the "experimental section" (Figure 2.1C). Electrical timers controlled light emission, adjusted to natural photoperiod throughout the experiment. Opaque canvas on the sides of each mesocosm blocked sunlight coming through the lab windows making actinic light the only significant source of irradiance. We achieved desired nutrient concentrations by placing one nutrient dispenser (Figure 2.1B) at each end of the experimental section. Mesocosm dispensers for ambient, intermediate, and high nutrient concentrations were filled with respectively 0, 125, or 250 g of fertilizer equally divided between the two dispensers in each mesocosm.

On 3 July, 2015 (onset of experiment), we placed two groups of 30 stained rhodoliths on the bottom of the experimental section of each mesocosm. A small (1 x 1 cm) coloured plastic tag affixed to each rhodolith with fishing line (Figure 2.1A) provided a unique identifier between "Cleaned" and "Uncleaned" rhodolith groups in each mesocosm. Every ~14 d, we transferred all 60 individuals from each mesocosm into a bucket filled with water from their mesocosm, and gently scrubbed rhodoliths in the "Cleaned" treatment with a smooth nylon brush to remove

surface biofoulers; individuals in the "Uncleaned" treatment were left untouched. Rhodoliths were then haphazardly redistributed homogeneously within their mesocosms.

We removed five cleaned and five uncleaned rhodoliths from each mesocosm on each collection event (see Table 2.1 for collection dates) to measure the biomass of biofoulers growing on rhodoliths and rhodolith growth. The latter collection marked the end of the experiment. We introduced ten live, unstained "Replacement rhodoliths" to the bottom of each mesocosm after each of the six collection events to maintain constant rhodolith density throughout the experiment.

Replacing nutrient dispensers every three to five weeks during the experiment maintained consistently higher nutrient concentrations in the intermediate and high concentration treatments (see "Nutrient release"). Nutrient concentrations were monitored by collecting water samples every ~7 d from each mesocosm (see "Water sampling and nutrient analysis"). A temperature and light logger (HOBO Pendant; Onset Computer Corporation) placed in the center of the experimental section, with the light sensor facing the water surface (Figure 2.1C) recorded water temperature and downwelling illuminance every 5 min. We converted illuminance to photosynthetically active radiation (PAR) using:

$$\mathrm{PAR} = \frac{\mathrm{I}}{\mathrm{CF}} \qquad (1)$$

where PAR is photosynthetically active radiation in µmol photons m^{-2} s^{-1}, I is illuminance in lux (lx), and CF is a lux to PAR conversion factor for high irradiance of $\frac{22.1\ \mathrm{lx}}{\mu\mathrm{mol\ photons\ m^{-2}s^{-1}}}$ obtained from simultaneous measurement of illuminance and irradiance for artificial actinic light in the mesocosms (see details of actinic light PAR conversion factor in Table B.1 (Appendix B).

Table 2.1. Rhodolith collection dates for the laboratory ("mesocosm enrichment experiment") and field ("Field nutrient enrichment") experiments.

Experiment	Collection	Date	Days since onset of experiment
Mesocosm experiment	1	31 Jul, 2015	29
	2	1 Sep, 2015	61
	3	1 Oct, 2015	91
	4	1 Nov, 2015	122
	5	1 Dec, 2015	152
	6	1 Jan, 2016 (end of experiment)	183
Field experiment	1	10 Aug, 2015	39
	2	4 Sep, 2015	64
	3	5 Oct, 2015	95
	4	4 Nov, 2015	125
	5	3 Dec, 2015	154
	6	11 Jan, 2016 (end of experiment)	193

We calculated daily light integral (DLI), the total amount of photosynthetically active photons received by a given surface over 24 h, for each day and mesocosm using:

$$\mathrm{DLI} = \sum_{i=1}^{288} \frac{300 x_i}{10^6} \qquad (2)$$

where DLI is daily light integral in mol photons m^{-2} d^{-1}, 288 is the number of PAR readings over 24 h, x_i is the i^{th} PAR value in µmol photons m^{-2} s^{-1}, 300 is the number of seconds separating two consecutive readings (one reading every 5 min), and 10^6 is the µmol to mol scaling factor.

2.3.4. Field nutrient enrichment

To test rhodolith response to nutrient enrichment in a natural habitat, we ran a 193-d experiment at 16 m depth in the rhodolith bed in St. Philip's, monitoring biofouling and growth of stained rhodoliths exposed to ambient or elevated nutrient concentration. We ran this experiment simultaneously with the laboratory mesocosm enrichment experiment described above. Three hundred and sixty (360) rhodoliths were held in 12 rectangular cages (26 cm long x 18 cm wide x 7 cm deep) made of a metal frame covered in tightly stretched nylon netting with 2-cm mesh (Figure 2.1D). We exposed rhodoliths in those cages to either ambient or elevated nutrient concentrations. Four 30-cm-long nutrient dispensers surrounded each cage, with an additional 25-cm-long central dispenser inside each cage (Figure 2.1D). Ambient treatments contained dispensers with no fertilizer prills. The 30- and 25-cm-long dispensers in the enriched treatment contained 250 and 200 g of prills, respectively, for a total of 1,200 g of fertilizer per cage. We based this quantity (~5 times the amount of fertilizer in the high concentration treatment of the laboratory experiment) on pre-experimental determination of nutrient concentration in water

samples taken from cages containing various amounts of fertilizer. Metal rods attached to each corner of the cage and secured to cinder blocks raised cages ~35 cm above the seabed to limit cages' access by benthic grazers such as sea urchins, chitons, and gastropods (Figure 2.1E). Separating cages by at least ~5 m limited nutrient contamination among cages. Ambient and enriched treatments were randomly assigned to cages.

The experiment began on 3 July, 2015, when we removed stained rhodoliths from the flow-through mesocosms at the OSC and transported them to the rhodolith bed in 70-L plastic containers filled with seawater. Divers introduced 15 rhodoliths to each preassembled cage on each side of the internal nutrient dispenser (for a total of 30 rhodoliths per cage). This arrangement resulted in similar exposure to light and nutrients for each rhodolith. Approximately every month thereafter, divers removed five rhodoliths from each cage to measure biofouling and rhodolith growth (see Table 2.1 for collection dates).

We collected two water samples from each cage twice monthly to monitor nutrient concentrations (immediately before, and ~15 d after replacing the nutrient dispensers). Two temperature and light loggers (HOBO Pendant; Onset Computer Corporation) attached to different cages, with the light sensor facing the sea surface, recorded sea temperature and downwelling illuminance every 5 min throughout the experiment. Illuminance was converted to PAR with equation (1) using a conversion factor of $\frac{23.5\ \mathrm{lx}}{\mu\mathrm{mol\ photons\ m^{-2}s^{-1}}}$ obtained from simultaneous measurement of illuminance and irradiance of sunlight at a depth of 15 m in the rhodolith bed (see sunlight PAR conversion factor details in Table B.2, Appendix B). We calculated DLI for each of the 193 d of the field experiment with equation (2).

2.3.5. Biofouling

We measured the amount of biofoulers on rhodoliths after each of the six collections in the laboratory and field experiments. For each collection, we oven dried rhodoliths at 40°C for 48 h and weighed individuals to obtain rhodolith gross dry weight, W_g. We subsequently scrubbed each rhodolith with a smooth nylon brush to remove all biofoulers growing on rhodoliths' surfaces and weighed again, yielding rhodolith net dry weight, W_n. We calculated the relative weight of biofoulers for each rhodolith using:

$$\mathrm{R}W_b = \frac{W_g - W_n}{W_n} \quad (3)$$

where $\mathrm{R}W_b$ is the relative dry weight of biofoulers for each rhodolith in mg of biofoulers per g of rhodolith, W_g is the gross dry weight of a given rhodolith in mg, and W_n is the net dry weight of the same rhodolith, also in mg.

2.3.6. Rhodolith growth

Growth in branched rhodoliths can be estimated by measuring the thickness of new layers of calcified tissue added at the apices of branches since marking. We chose this widely used method of growth estimation (Blake & Maggs 2003, Kamenos & Law, 2010, Kamenos et al. 2008, Amado-Filho et al. 2012, Darrenougue et al. 2013, Sletten et al. 2017) because it allowed comparison with other growth estimates reported in the literature. Following oven drying of laboratory and field rhodoliths, we haphazardly chose five branches per rhodolith, and filed them longitudinally to their center with a rotary tool (3000; Dremel) fitted with a 240-grit sanding disc. Filed branch tips were then hand-polished with a 600-grit sandpaper to expose stain marks and

photographed at a 40X magnification with a microscope equipped with a digital camera (BA300; Motic). Digital photographs and image analysis software (Motic Images Plus 2.0; Motic) provided measurements of branch elongation, defined as the maximum length of the axis perpendicularly joining the stain mark and apex of the tip (Figure 2.1F). We then calculated mean rhodolith growth, hereafter referred to as growth, by averaging the five branch elongation measurements.

2.3.7. Water sampling and nutrient analysis

On days of collection, divers transported 12 syringes in a sealed, plastic bag to the rhodolith cages, and slowly approached each cage to avoid stirring up sediment. They removed a syringe from the bag, inserted it in the cage through the netting, completely filled it with water from ~1cm above the rhodoliths, capped it, and placed it back inside the sealed bag to minimize the risk of contamination with surrounding water. Upon surfacing, we transferred 40 mL of water from each syringe into a 50 mL polypropylene centrifuge tube, placed it on ice in a cooler, and transported to the OSC for storage at -20°C.

We measured concentrations of nitrate (NO_3^-), ammonia (NH_3), and phosphate (PO_4^{3-}) in water samples with a continuous flow autoanalyzer (AA3 HR; Seal Analytical). Frozen samples were thawed in a refrigerator and filtered with 0.7 µm borosilicate glass microfiber filters (Whatman GF/F; GE Healthcare's Life Sciences). We presoaked all materials used for water sample collection and nutrient analysis in a 10% hydrochloride solution for 24 h before rinsing them three times with deionized water, and air drying.

2.3.8. Statistical analysis

We used ANCOVA (Sokal & Rohlf, 2012) to examine differences in rates of change of rhodolith growht among our various experimental treatments. Although we measured growth in rhodoliths collected at various time intervals, interpreting statistical differences among regression slopes of experimental treatments effectively compared differences in rhodolith growth rates among treatments (Quinn & Keough, 2002). As detailed below, we applied linear mixed-effects models (LMEM) to various ANCOVA designs with both fixed and random factors to properly handle the dependency structure of the data and account for pseudoreplication (Zuur et al. 2009).

2.3.8.1. Laboratory mesocosm experiment

Two LMEMs applied to split-plot ANCOVA experimental designs (Quinn & Keough, 2002) with Concentration (ambient, intermediate, or high concentrations) as a fixed, between-plots factor, Mesocosm (each of the six experimental mesocosms) as a random factor nested within Concentration, Biofouling (cleaned or uncleaned rhodoliths) as a fixed, within-plots factor, and covariate Time (days elapsed since the onset of the experiment) compared: (1) rhodolith biofouling; and (2) rhodolith growth rate among the six experimental treatments [n=360 for each analysis]. For each model, we implemented a specific variance structure to satisfy the assumption of homogeneity of variance; an identity variance (varIdent) structure for the 1st analysis accounted for the lower variance in the abundance of biofoulers on cleaned than uncleaned rhodoliths, and a power of the variance covariate (varPower) structure for the 2nd analysis accounted for increasing variance in rhodolith growth over time (Zuur et al., 2009).

2.3.8.2. Field experiment

We applied two LMEMs to nested ANCOVA experimental designs with Concentration (ambient or elevated concentrations) as a fixed factor, Cage (each of the 12 cages) as a random factor nested within Concentration (six cages per nutrient concentration), and Time (days elapsed since the onset of the experiment) as covariate to test the effect of nutrient concentration on: 1) biofouling of rhodoliths; and (2) rhodolith growth rate [n = 360 for each analysis]. We implemented a power of the variance covariate (varPower) structure for each model for the same reason explained above.

For all analyses, we verified homogeneity of variance and normality of residuals by examining the distribution of the residuals and the normal probability plot of the residuals, respectively (Snedecor & Cochran, 1989). Paired t-test comparisons detected differences among levels within a factor (ANCOVAs). All analyses were carried out with R 3.6.1 (R Core Team, 2017), using a significance level of 0.05. Rhodolith annual growth reported for the laboratory and field experiments describe model predicted values at Time = 365 d (number of days in one year) assuming no growth at the onset of experiment (i.e. intercept corrected to 0).

2.4. RESULTS

2.4.1. Laboratory mesocosm experiment

2.4.1.1. Temperature and light environment

As expected, daily mean water temperature (DMWT) in the mesocosms during the 183-d laboratory experiment varied seasonally, increasing from 10.6 ± 0.2 (SD) °C at the onset (3 July, 2015) to a maximum of 15.3 ± 0.2°C fifty-three (53) days later (24 August, 2015), and then declined steadily afterwards to a minimum of 2.6 ± 0.2°C at the end (1 January, 2016) (Figure

2.2A). Contrary to DMWT, daily light integral (DLI) in the mesocosms averaged 0.46 ± 0.14 (SD) mol photons m^{-2} d^{-1} and was relatively stable throughout the experiment (no seasonal variation), ranging between 0.21 ± 0.07 and 0.81 ± 0.03 mol photons m^{-2} d^{-1} (Figure 2.2C). Our modifications to daily lighting in the mesocosms to track the declining photoperiod resulted in a ~75% decrease in mean DLI over the course of the experiment (Figure 2.2C).

2.4.1.2. Nutrients

Compared to the ambient treatment (no fertilizer added), nutrient concentration in the intermediate (125 g of fertilizer) and high (250 g) enrichment treatments was ~3 and 9 times higher for nitrate respectively, 4 and 10 times higher for ammonia, and 2 and 5 times higher for phosphate (Table 2.2). Differences in mean nitrate, ammonia, and phosphate concentrations between the intermediate and high enrichment treatments (Table 2.2) largely resulted from sudden increases to peak concentrations in the high enrichment treatment following replacement of the nutrient dispensers (Figure 2.3A-C). Nitrate concentration in between peaks was similar in the intermediate and high enrichment treatments, but less so for ammonia and phosphate, which were lower in the high than in the intermediate treatment (Figure 2.3A-C). Concentration peaks in the intermediate and high enrichment treatments of the laboratory experiment were ~1 to 2, and 3 to 4 times higher respectively than those in pre-experiment trials for corresponding treatments (Figure. 2.3A-C and A.1, Appendix A).

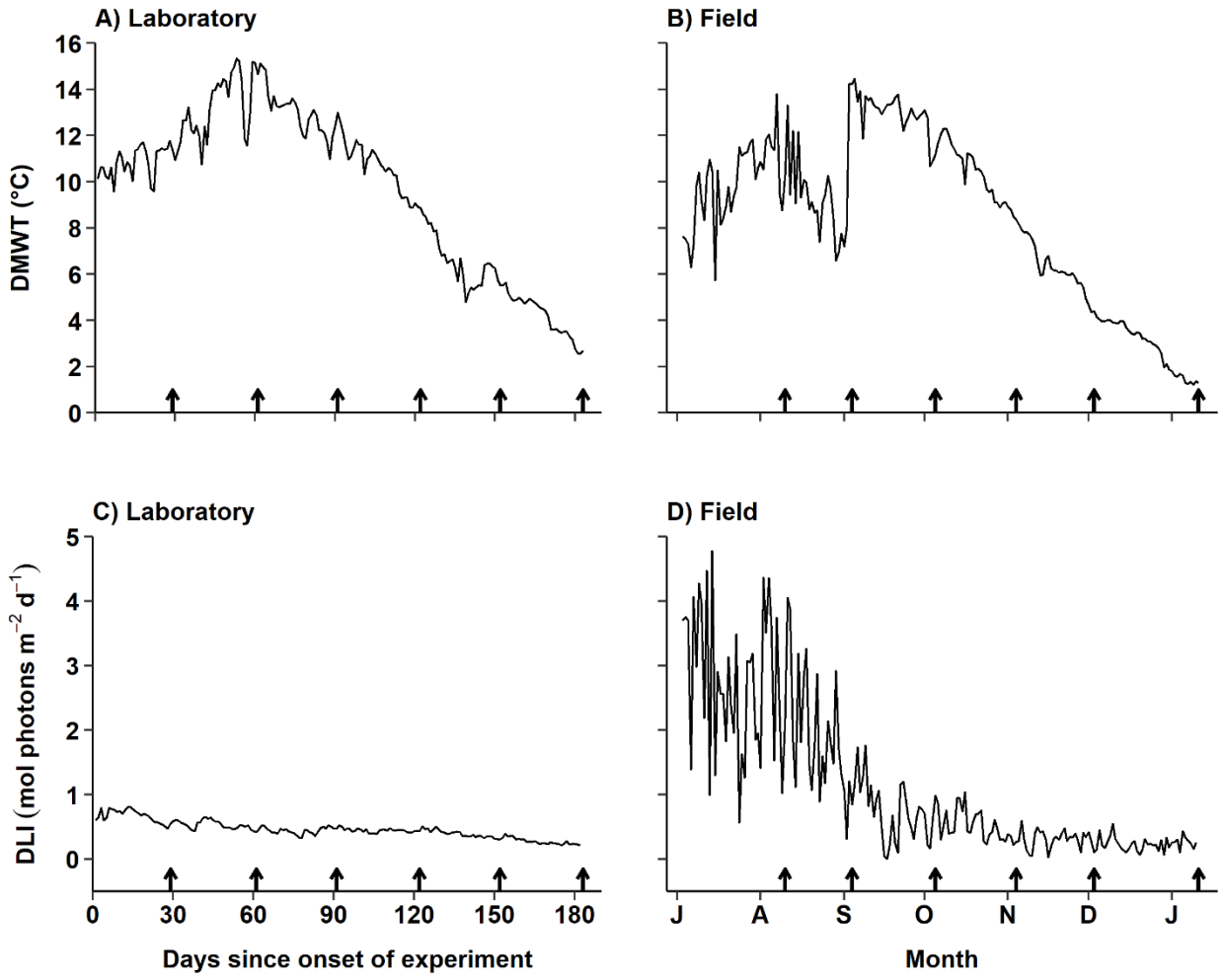

Figure 2.2. Daily mean water temperature (DMWT) and daily light integral (DLI) in (A, C) the mesocosms [temperature and irradiance averaged over the six mesocosms: two for each of the ambient, intermediate and high nutrient concentration treatments] throughout the 183-d laboratory experiment (3 July to 1 January, 2016); and (B, D) at a depth of 16 m in the rhodolith bed throughout the 193-d field experiment (3 July to 11 January, 2016). Arrows along abscissas mark days since the onset of the laboratory or field experiments on which 10 laboratory (five per fouling treatment) or 5 field rhodoliths were removed from each mesocosm or cage to measure biofouling and growth (see Table 2.1 for collection dates).

Table 2.2. Mean (± SD) concentration of nitrate (NO_3^-), ammonia (NH_3), and phosphate (PO_4^{3-}) for each nutrient concentration treatment (ambient [0 g of fertilizer], intermediate [125 g] and high [250 g]) in the 183-d laboratory mesocosm experiment, and for each nutrient concentration treatment (ambient [0 g of fertilizer] and elevated [250 g of fertilizer]) in the 193-d field experiment. Concentrations in the laboratory experiment were averaged over the 26 water collections and two mesocosms per concentration treatment (n = 52). Concentrations in the field experiment were averaged over the 12 water collections and six rhodolith cages per concentration treatment (n = 72).

		Nutrient concentration (µmol L^{-1})		
Experiment	Treatment	NO_3^-	NH_3	PO_4^{3-}
Laboratory	Ambient	3.2 (1.8)	3.5 (3.2)	0.6 (0.4)
	Intermediate	10.2 (6.7)	14.4 (11.5)	1.3 (0.7)
	High	29.5 (52.2)	33.9 (42.7)	2.9 (5.0)
Field	Ambient	1.0 (1.3)	3.3 (2.0)	0.4 (0.1)
	Elevated	3.3 (1.0)	5.1 (1.7)	1.2 (0.3)

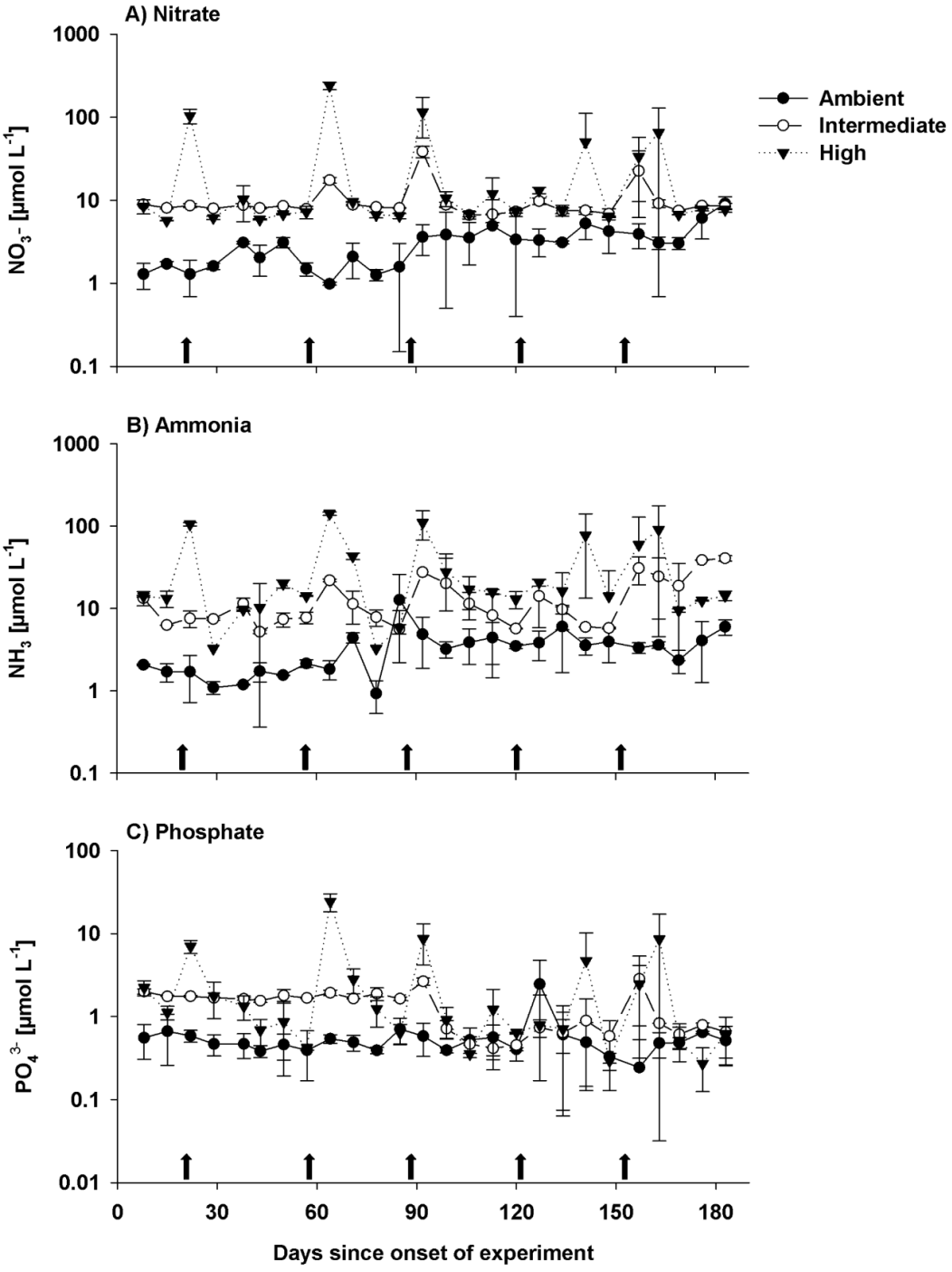
A) Nitrate
1000
100
10
1
0.1
NO_3^- [µmol L^{-1}]
Ambient
Intermediate
High
B) Ammonia
1000
100
10
1
0.1
NH_3 [µmol L^{-1}]
C) Phosphate
100
10
1
0.1
0.01
PO_4^{3-} [µmol L^{-1}]
0
30
60
90
120
150
180
Days since onset of experiment

Figure 2.3. Mean (±SD) concentration of (A) nitrate [NO_3^-], (B) ammonia [NH_3], and (C) phosphate [PO_4^{3-}] for each nutrient concentration treatment (ambient, intermediate, and high) for each of the 26 water collections during the 183-d laboratory mesocosm experiment. Each water collection's concentration is the average from the two replicate mesocosms per concentration treatment (n = 2). Note the change in scale along the (Log-scaled) ordinates. Arrows along the abscissas of panels (A), (B), and (C) mark days since the onset of the experiment on which nutrient dispensers were replaced with new ones: 20 [22 Jul, 2015]; 57 [28 Aug, 2015]; 88 [28 Sep, 2015]; 121 [31 Oct, 2015]; and 153 [2 Dec, 2015] d.

2.4.1.3. Biofouling

Rhodolith biofoulers in the laboratory (and field) experiment consisted primarily of a thin brownish microalgal film, filamentous green and red algae, and bryozoans. Technical considerations prevented finer taxonomic identification. Relative dry weight of biofoulers did not differ significantly among the three nutrient concentration treatments, which did not change over time (Table 2.3). Nonetheless, biofouler biomass differed significantly and was nearly four times greater in uncleaned (0.78 ± 0.12 [CI] mg biofoulers g^{-1} rhodolith) than cleaned (0.20 ± 0.04 mg biofoulers g^{-1} rhodolith) rhodoliths (Tables 2.3 and 2.4, Figure 2.4A).

2.4.1.4. Rhodolith growth

Rate of change in rhodolith growth differed significantly among the three nutrient concentration treatments, with growth rates approximately two times higher at ambient concentrations than at intermediate and high concentrations (Tables 2.4 and 2.5). Mean branch tip elongation at the end of the experiment (after 183 d) was ~2 (high concentration) to 3 (ambient) times higher than measured initially (after 29 d) (Figure 2.5A). Resulting annual rhodolith growth rates were nearly twice as high under ambient (398 ± 25 [CI] µm y^{-1}) than intermediate (230 ± 25 µm y^{-1}) or high (208 ± 25 µm y^{-1}) nutrient concentrations (Figure 2.6A). Rates of change in growth and associated annual growth rates were ~27% higher in cleaned (314 ± 23 µm y^{-1}) than uncleaned (248 ± 23 µm y^{-1}) rhodoliths in all three nutrient concentrations (Tables 2.4 and 2.5; Figure. 2.5B, 2.6B).

Table 2.3. Summary of split-plot ANCOVA (applied to raw data) examining the effects of between-plot factor nutrient Concentration (C; three levels: ambient, intermediate, and high), within-plot factor Biofouling (B; two levels: cleaned and uncleaned rhodoliths), and covariate Time (T; number of days elapsed since the onset of the experiment on each rhodolith sampling event [29, 61, 91, 122, 152, and 183 d]), while correcting for the random factor Mesocosm (each of the six experimental mesocosms) nested within Concentration (two mesocosms per level of Concentration), on relative dry weight of biofoulers on rhodoliths in the laboratory mesocosm experiment (see "Mesocosm enrichment experiment" for a description of the experiment). Random-factor effects are not relevant to the present study, and hence not shown for simplicity.

Source of variation	**numDF**	**denDF**	**F-ratio**	***p***
Intercept	1	345	200.05	< 0.001
C	2	3	0.01	0.986
B	1	345	83.54	< 0.001
T	1	345	0.03	0.871
C x B	2	345	0.30	0.738
C x T	2	345	0.03	0.972
B x T	1	345	3.04	0.082
C x B x T	2	342	0.73	0.481

numDF = F-ratio numerator; denDF = F-ratio denominator; *p* = p-value.

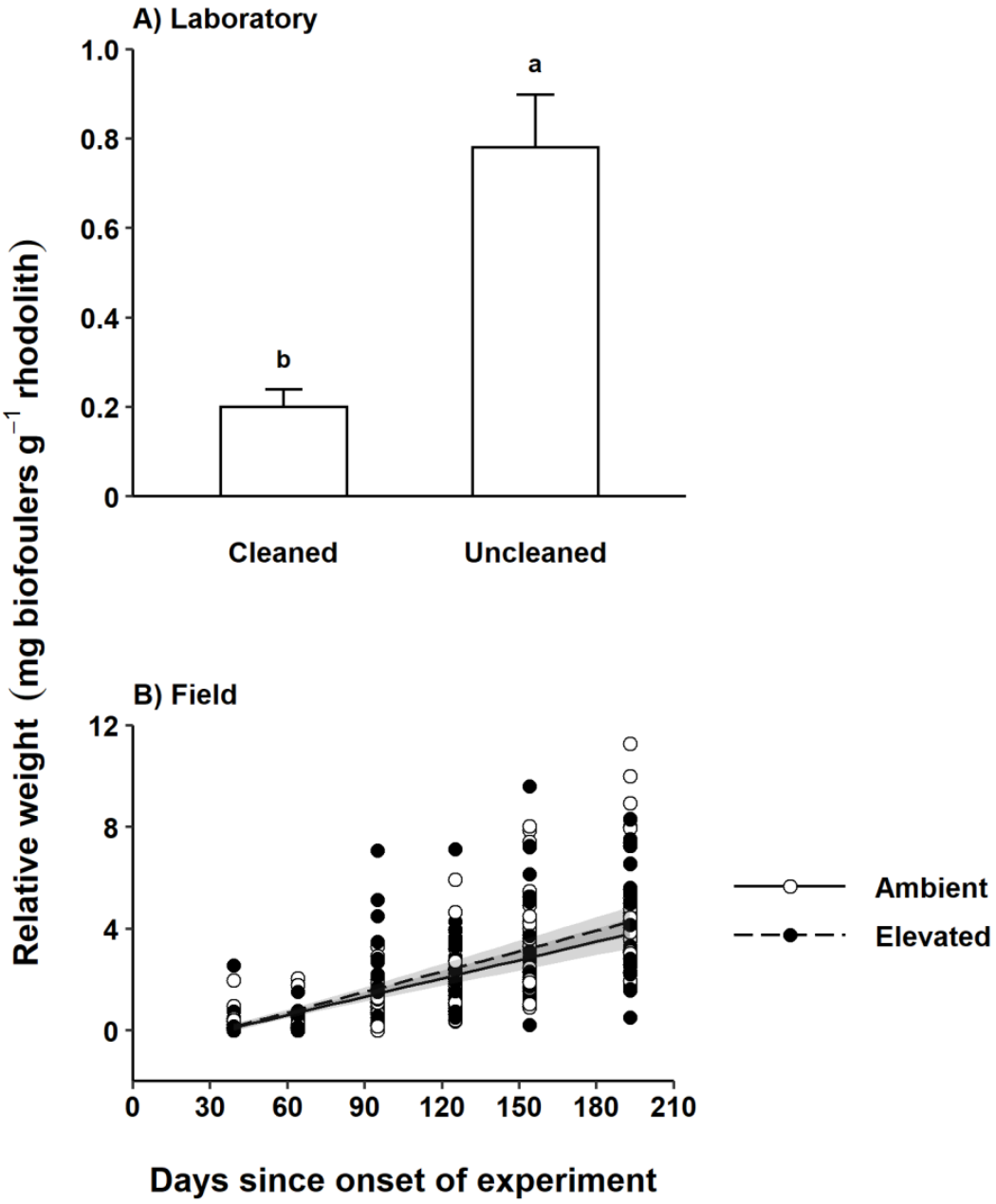
A) Laboratory
1.0
0.8
0.6
0.4
0.2
0
a
b
Cleaned
Uncleaned
B) Field
12
8
4
0
0
30
60
90
120
150
180
210
Days since onset of experiment
Relative weight (mg biofoulers g^{-1} rhodolith)
Ambient
Elevated

Figure 2.4. (A) Relative dry weight [+95% CI] of biofoulers on rhodoliths for each level of rhodolith cleaning [cleaned and uncleaned; pooled over nutrient concentration treatments] in the laboratory mesocosm experiment. Bars not sharing the same letter differ statistically (LS means test, $p < 0.05$; $n = 36$ for each level of cleaning). (B) Increase in relative dry weight [± 95% CI] of biofoulers throughout the field experiment for each nutrient concentration treatment [ambient and elevated]. (See Table 2.1 for collection dates and Table 2.2 for details of coefficients of regression slopes presented in (B)).

Table 2.4. Summary of regression coefficients of the two split-plot ANCOVAs in the laboratory experiment, and two nested ANCOVAs in the field experiment (applied to raw data) examining the relationships between relative dry weight of biofoulers on rhodoliths or rhodolith growth, and time elapsed since the onset of the 183-d laboratory mesocosm and 193-d field experiments at the various nutrient concentrations and levels of manual cleaning of rhodoliths (biofouling) tested.

Experiment/ Response variable	**Factor/Level**	**N**	**Intercept (SE)**	**Slope (SE)**
Laboratory/	Concentration			
Relative dry	Ambient	120	0.49 (0.13)	-0.000 (0.001)
weight of biofoulers	Intermediate	120	0.34 (0.13)	0.001 (0.001)
	High	120	0.40 (0.13)	0.001 (0.001)
	Biofouling			
	Cleaned	180	0.20 (0.02)	-0.000 (0.000)
	Uncleaned	180	0.78 (0.06)	0.002 (0.001)
Laboratory/	Concentration			
Rhodolith growth	Ambient	120	69.6 (3.6)	1.086 (0.043)
	Intermediate	120	87.9 (3.6)	0.644 (0.043)
	High	120	90.4 (3.6)	0.567 (0.043)
	Biofouling			
	Cleaned	180	78.3 (4.2)	0.855 (0.038)
	Uncleaned	180	86.6 (3.9)	0.679 (0.038)
Field/	Concentration			
Relative dry	Ambient	180	-0.84 (0.13)	0.024 (0.002)
weight of biofoulers	Elevated	180	-0.91 (0.13)	0.027 (0.002)
Field/	Concentration			
Rhodolith growth	Ambient	180	118.6 (7.2)	1.272 (0.085)
	Elevated	180	99.7 (6.9)	1.313 (0.085)

Table 2.5. Summary of split-plot ANCOVA (applied to raw data) examining the effects of between-plot factor nutrient Concentration (C; three levels: ambient, intermediate, and high), within-plot factor Biofouling (B; two levels: cleaned and uncleaned rhodoliths), and covariate Time (T; number of days elapsed since the onset of the experiment on each rhodolith sampling event [29, 61, 91, 122, 152, and 183 d]), while correcting for the random factor Mesocosm (each of the six experimental mesocosms) nested within Concentration (two mesocosms per level of Concentration), on rhodolith growth in the laboratory mesocosm experiment (see "Mesocosm enrichment experiment" for a description of the experiment). Random-factor effects are not relevant to the present study, and hence not shown for simplicity.

Source of variation	**numDF**	**denDF**	**F-ratio**	***p***
Intercept	1	345	13793.56	< 0.001
C	2	3	16.55	0.024
B	1	345	1.72	0.191
T	1	345	979.12	< 0.001
C x B	2	345	0.70	0.498
C x T	2	345	43.57	< 0.001
B x T	1	345	12.63	< 0.001
C x B x T	2	342	0.66	0.515

numDF = F-ratio numerator; denDF = F-ratio denominator; *p* = p-value.

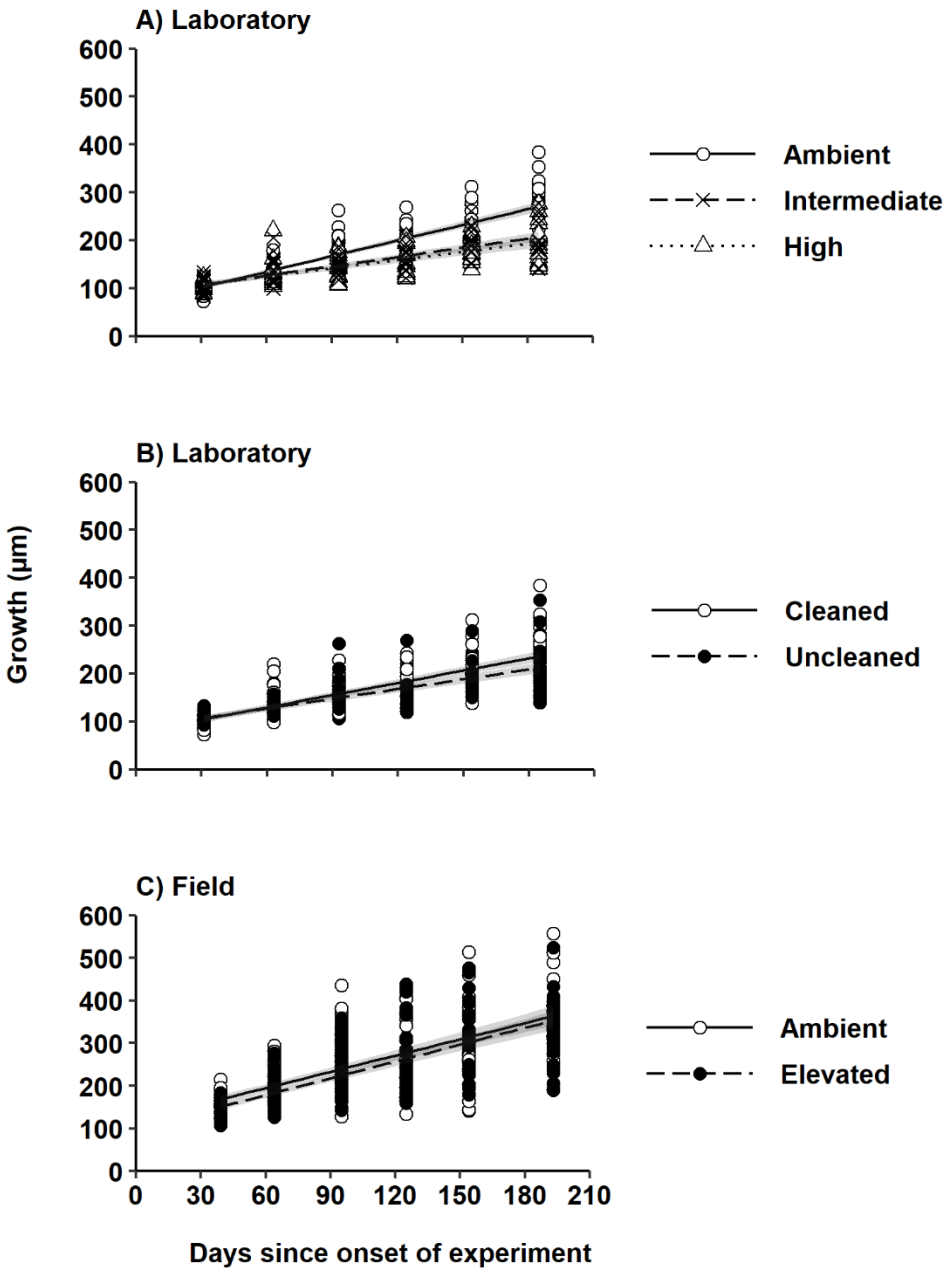
A) Laboratory
600
500
400
300
200
100
0
Ambient
Intermediate
High
B) Laboratory
Growth (µm)
Cleaned
Uncleaned
C) Field
Ambient
Elevated
0
30
60
90
120
150
180
210
Days since onset of experiment

Figure 2.5. growth (± 95% CI) of rhodoliths over time for the (A) three nutrient concentration treatments [ambient, intermediate, and high; pooled over rhodolith cleaning treatments] in the laboratory mesocosm experiment; (B) two levels of rhodolith cleaning [cleaned and uncleaned; pooled over nutrient concentration treatments] in the laboratory mesocosm experiment; and (C) two nutrient concentration treatments [ambient and elevated] in the field experiment (see Table 2.1 for collection dates and Table 2.2 for details of coefficients of regression slopes presented in all panels).

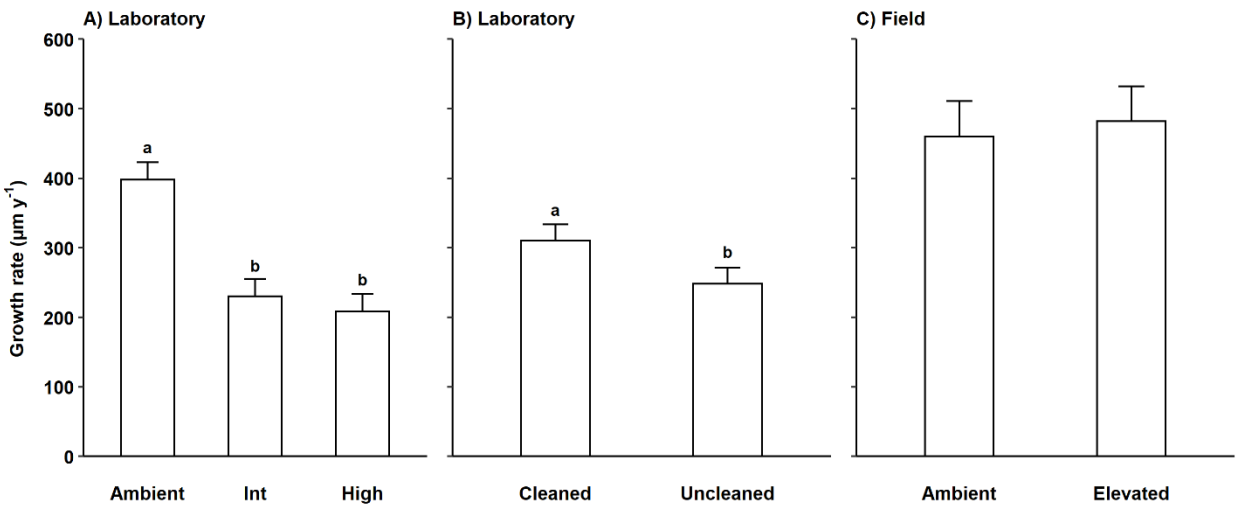

Figure 2.6. Mean (+95% CI) annual growth rate of rhodoliths for the (A) three nutrient concentration treatments [ambient, intermediate, and high; pooled over rhodolith cleaning treatments] in the laboratory mesocosm experiment; (B) two levels of rhdolith cleaning [cleaned and uncleaned; pooled over nutrient concentration treatments] in the laboratory mesocosm experiment; and (C) two nutrient concentration treatments [ambient and elevated] in the field experiment. Annual growth rates were calculated from the slopes of the linear regressions (presented in Table 2.2). Bars not sharing the same letter differ statistically (pairwise t-test comparisons).

2.4.2. Field experiment

2.4.2.1. Temperature and light environment

Seasonal variation in DMWT in the rhodolith bed during the 193-d field experiment paralleled the laboratory experiment, increasing from 7.6 ± 0.9°C at the onset (3 July, 2015) to a maximum of 14.5 ± 0.7°C during the first week of September, and then declining to a minimum of 1.2 ± 0.1°C near the end (11 January, 2016) (Figure 2.2B). The thermocline position during summer overlapped the experimental depth (16 m), causing larger variation in DMWT during the first two months than in the laboratory experiment, including relatively sudden changes of up to ~6°C over 24 h (Figure 2.2B). Mean DMWT during the field experiment was 8.4±3.7 (SD) °C. Contrary to the laboratory experiment, DLI in the rhodolith bed varied strongly seasonally, peaking at 4.78 mol photons m^{-2} d^{-1} and averaging 2.52 ± 1.11 (SD) mol photons m^{-2} s^{-1} from July to August, before declining by 80% from September to January to values as low as 0.46 ± 0.34 mol photons m^{-2} s^{-1}, i.e. similar to mean DLI in the laboratory mesocom experiment (Figure 2D). Mean DLI during the field experiment, 1.10 ± 1.17 mol photons m^{-2} s^{-1}, was two times higher than mean DLI during the laboratory experiment.

2.4.2.2. Nutrients

Mean concentrations of nitrate, ammonia, and phosphate during the experiment were ~1.5, 1.5, and 2 times higher respectively in the elevated [250 g of fertilizer added] than ambient [no fertilizer added] treatments (Table A.1, Appendix A). Nutrient concentration was lower for the ambient cages than in elevated concentration treatments on the 12 collection dates (Figure 2.7A-C).

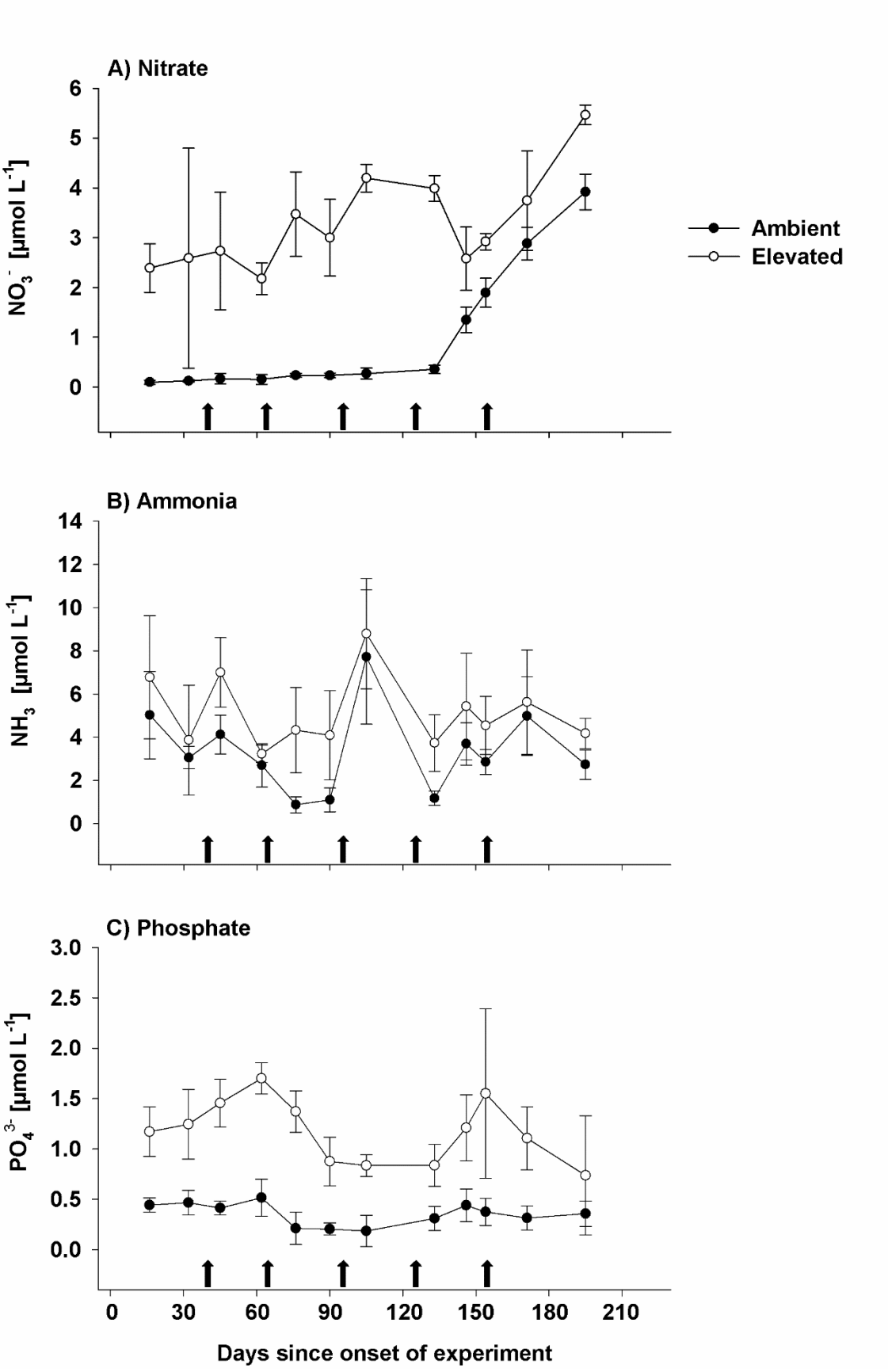
A) Nitrate
NO_3^- [µmol L^{-1}]
Ambient
Elevated
B) Ammonia
NH_3 [µmol L^{-1}]
C) Phosphate
PO_4^{3-} [µmol L^{-1}]
Days since onset of experiment

Figure 2.7. Mean (± SD) concentration of (A) nitrate [NO_3^-], (B) ammonia [NH_3], and (C) phosphate [PO_4^{3-}] for each nutrient concentration treatment (ambient and enriched) for each of the 12 water collections during the 193-d field experiment. Each water collection's concentration is the average from the six rhodolith cages per concentration treatment. Arrows along the abscissas of panels (A), (B), and (C) mark days since the onset of the experiment on which nutrient dispensers were replaced with new ones: 39 (10 Aug, 2015), 64 (4 Sep, 2015), 95 (5 Oct, 2015), 125 (4 Nov, 2015), and 154 (3 Dec, 2015) d.

Nitrate in the ambient treatment remained low, ~0.21 ± 0.11 (SD) µmol L^{-1}, from July to early November, when it increased by one order of magnitude and further increased to a maximum of 3.92 ± 0.36 µmol L^{-1} at the end of the experiment, on 11 January (Figure 2.7A). Nitrate in the elevated treatment exhibited a similar pattern, only with higher concentrations. Ammonia varied considerably in both treatments throughout the experiment, ranging from 0.88 ± 0.47 µmol L^{-1} on 14 September (ambient) to 8.79 ± 2.55 µmol L^{-1} on 13 October (elevated) (Figure 2.7B). Phosphate remained fairly low and stable throughout the experiment, peaking to 0.52 ± 0.18 (ambient) and 1.70 ± 0.15 (elevated) µmol L^{-1} on 31 August (Figure 2.7C). Mean nutrient concentrations in the field elevated treatment were up to 9 times lower than those in the intermediate and high nutrient concentration treatments in the laboratory experiment (Table 2.2).

2.4.2.3. Biofouling

Relative dry weight of rhodolith biofoulers did not differ significantly between the ambient and elevated nutrient concentration treatments (Table 2.6). It consistently increased, at an average rate of 0.03 ± 0.00 (CI) mg biofoulers g^{-1} rhodoliths d^{-1}, from 0.23 ± 0.02 mg biofoulers g^{-1} rhodolith on the first collection (10 August), to 4.71 ± 0.34 mg biofoulers g^{-1} rhodolith at the end of experiment (11 January) (Table 2.6, Figure 2.4B). At the end of the experiment, relative dry weight of rhodolith biofoulers was ~24 and 6 times higher than at the start for the cleaned and uncleaned rhodoliths in the laboratory experiment, respectively (Figure 4A, B).

Table 2.6. Summary of nested ANCOVA (applied to raw data) examining the effects of nutrient Concentration (C; two levels: ambient and elevated) and covariate Time (T; number of days elapsed since the onset of the experiment on each rhodolith sampling event [39, 64, 95, 125, 154, and 193 d], while correcting for the random factor Cage (each of the 12 rhodolith cages) nested within Concentration (six cages per level of Concentration), on relative dry weight of biofoulers on rhodoliths in the field experiment (see "Field nutrient enrichment" for a description of the experiment). Random-factor effects are not relevant to the present study, and hence not shown for simplicity.

Source of variation	**numDF**	**denDF**	**F-ratio**	***p***
Intercept	1	346	139.30	< 0.001
C	1	10	0.84	0.380
T	1	346	296.35	< 0.001
C x T	1	346	0.92	0.339

numDF = F-ratio numerator; denDF = F-ratio denominator; p = p-value.

2.4.2.4. Rhodolith growth

Growth was significantly lower in rhodoliths exposed to elevated than ambient nutrient concentrations during the 39 d separating the onset of the field experiment and the first rhodolith collection (Table 2.7, Figure 2.5C). Growth then stabilized for the remainder of the experiment, increasing at similar rates of 460 ± 51 (CI) and 482 ± 50 μm y^{-1} in the ambient and elevated treatments, respectively (Table 2.7, Figures 2.5C, 2.6C). Mean growth rate in the field was ~18% higher than the ambient nutrient concentration treatment of the laboratory experiment, and about two times higher than the intermediate and high concentration treatments (Figure 2.6A, C).

2.5. DISCUSSION

The laboratory mesocosm and field experiments showed that biofouling and elevated nutrient concentration can reduce growth in *Lithothamnion glaciale* rhodoliths. In the laboratory, growth in rhodoliths exposed for six months to nutrient concentrations between ~2 (phosphate; PO_4^{3-}) and 9 (ammonia; NH_3) times higher than the ambient concentrations, decreased by ~46%. Yet, in the field, nutrient concentrations between ~1 (ammonia) and 3 (nitrate; NO_3^-) times higher than the ambient ones had no effect on growth over six months. Contrary to our expectation, increasing nutrient concentration did not increase biofouling in either experiment. This was possibly due to the timing of the experiments and reduced algal spores or larval recruitment from July to January. In the laboratory experiment, however, biofouling was ~4 times lower, and growth ~27% higher, in cleaned compared to uncleaned rhodoliths treatments regardless of nutrient concentration.

Table 2.7. Summary of nested ANCOVA (applied to raw data) examining the effects of nutrient Concentration (C; two levels: ambient and elevated) and covariate Time (T; number of days elapsed since the onset of the experiment on each rhodolith sampling event [39, 64, 95, 125, 154, and 193 d], while correcting for the random factor Cage (each of the 12 rhodolith cages) nested within Concentration (six cages per level of Concentration), on rhodolith growth in the field experiment (see "Field nutrient enrichment" for a description of the experiment). Random-factor effects are not relevant to the present study, and hence not shown for simplicity.

Source of variation	**numDF**	**denDF**	**F-ratio**	***p***
Intercept	1	346	5022.20	< 0.001
C	1	10	8.12	0.017
T	1	346	460.17	< 0.001
C x T	1	346	0.13	0.722

numDF = F-ratio numerator; denDF = F-ratio denominator; *p* = p-value.

2.5.1. Biofouling

In laboratory mesocosms, most rhodolith biofoulers consisted of a thin, brownish microalgal film with a few occasional filamentous algae and bryozoans. Devlin et al. (2007) propose eutrophication threshold concentrations of DIN, including nitrate and ammonia, between 13 and 20 µmol L^{-1} for UK coastal waters. Combined nitrate and ammonia concentrations in the intermediate and high concentration treatments of 88% of water samples from our laboratory experiment were within or above, the latter threshold range. The generally lower irradiance in the laboratory mesocosms, particularly during the first ~60 d of the experiment, may have been insufficient to promote continuous growth of epiphytes as seen in the field cages. Admiraal (1976) reported peak growth rates of four estuarine benthic diatom species at daily quantum irradiances of 2.5 to 5 mol photons m^{-2} d^{-1}, which are 3 to 6 times higher than the mean irradiance in our mesocosms. The relatively high turnover rate of seawater in our mesocosms presumably limited supply and settlement of spores or larvae of potential biofoulers. Nonetheless, consistently higher biofouling in uncleaned than in cleaned rhodoliths did not prevent rhodolith growth (see below), indicating suitable physical and chemical conditions in the mesocosms to sustain rhodoliths and biofouler recruits.

In the field, a thin film of mainly filamentous algae developed on the surface of rhodoliths. Yet, contrary to the laboratory experiment, biofouling increased consistently over time, with at least six times more fouling in field than laboratory rhodoliths by the end of the experiment. Biofouling occurred at a similar rate for rhodoliths exposed to ambient and elevated nutrient concentrations, despite nitrate, ammonia, and phosphate concentrations ~2 to 3 times higher in the elevated treatment. Combined nitrate and ammonia concentrations in the latter treatment, however, still fell below the lower DIN limit of 13 µmol L^{-1} noted above for eutrophication in cold-water

systems, except perhaps on those few occasions when we replaced nutrient dispensers with fresh ones and nutrient concentrations increased for a few hours as suggested by the observed nutrient release profiles. Presumably, prolonged exposure to sub-threshold nutrient concentrations prevented increased epiphyte growth. Rasher et al. (2012) observed nutrient-driven macroalgal blooms in coral reefs only where herbivore grazing was suppressed. These findings suggest that top down control could be more important than bottom-up processes in controlling macroalgal blooms in eutrophic environments. By cagingrhodoliths we limited grazing by some large grazers (e.g. fish and adult sea urchins). However, smaller grazers (e.g. gastropods and juvenile sea urchins) likely entered the cages and offset biofouling in cages with elevated nutrient concentration. Interestingly, Lapointe et al. (1993) reported N and P thresholds for bottom-up control of macroalgal growth in tropical coral reefs ~4 times lower than ambient concentrations at our study site, which suggests a greater vulnerability of rhodoliths to eutrophication-induced biofouling in tropical (largely oligotrophic) than polar or temperate (largely eutrophic) systems.

2.5.2. Rhodolith growth

In the laboratory mesocosm experiment, 27% lower growth of uncleaned rhodoliths than that of cleaned rhodoliths represented a considerable difference considering that biofoulers, which were four times more abundant on uncleaned rhodoliths formed only a thin and scattered film on their surface. Irradiance strongly influences growth of *L. glaciale* rhodoliths (Teichert & Freiwald 2014), so that a greater abundance of biofoulers than in our study could block light or reduce nutrient availability, thus further limiting rhodolith growth. Our rhodolith growth rate of ~221 µm y^{-1} (pooled rate) was also statistically similar between the two elevated nutrient concentrations in the laboratory experiment despite phosphate and nitrate concentrations two and three times higher

respectively in the high compared to intermediate concentration treatments. Differences in nutrient concentrations between both treatments mostly resulted from higher peaks in the high concentration treatment shortly after replacing the nutrient dispensers. In between peaks, rhodolith treatments experienced similar concentrations of nitrate, ammonia, and phosphate, which may explain similar rhodolith growth in both treatments.

Previous studies draw mixed conclusions about the effect of elevated nitrogen concentration on growth and calcification in coralline algae. For example, Björk et al. (1995) reported no effect on growth of nitrogen concentrations up to 5 µmol L^{-1} above ambient levels. Johnson and Carpenter (2018) showed a 90 to 130% increase in calcification with elevated nitrate, nitrite, and ammonium concentrations through a significant increase in photosynthetic pigment content. No study reported an inverse relationship between nitrogen concentration and growth or calcification in coralline algae. Nonetheless, Björk et al. (1995) showed a linear decrease in growth with increasing phosphate concentration between ~0.5 to 18 µmol L^{-1}. Their study also reported a ~9 to 33% increase in coralline algal cover with increasing distance from sewer outfalls, with greatest increases at phosphate concentrations < 0.3 µmol L^{-1}. Other studies reported significant decreases in coralline algal cover at phosphate concentrations of 0.31 µmol L^{-1} (Belliveau & Paul 2002), and 0.69 to 0.94 µmol L^{-1} (Littler et al. 2010). These phosphate concentrations, measured in naturally oligotrophic coral reef systems, presumably mismatch our more nutrient-rich, temperate coastal systems. In our study, ambient phosphate concentrations in the laboratory and field experiments were 0.6 and 0.4 µmol L^{-1} respectively, which approaches or exceeds the most detrimental levels reported for oligotrophic systems. In all cases, the negative impact of phosphate on coralline algal growth was likely caused by the inhibitory effect of phosphorous on calcification processes (Simkiss 1964).

The significant decrease in rhodolith growth rates in our laboratory experiment occurred at phosphate concentrations of 1.31 µmol L^{-1} (intermediate enrichment) and 2.88 µmol L^{-1} (high enrichment), comparable to concentrations at the outlet of a heavily drained, subtropical coastal catchment discharging nutrient-laden water into an estuarine system (Santos et al. 2013). Our results compare with those of Shubert et al. (2019) who reported that net photosynthetic performance of Brazilian *Melyvonnea erubescens* rhodoliths decreased significantly at phosphate concentrations of 5.6 µmol L^{-1}.

Rhodoliths in our field experiment also grew significantly slower under elevated (1.2 µmol L^{-1}) than ambient (0.4 µmol L^{-1}) phosphate concentrations, but only during the first ~6 wk, after which growth resumed and remained similar between treatments. Apparently, abnormally high phosphate concentrations may impact *L. glaciale* rhodoliths initially, but they have some capacity to recover in the long run. Nutrient release profiles from our pre-experimental trials carried out in laboratory mesocosms suggest that nutrient pulses occurred in the field shortly after we replaced nutrient dispensers, but we could not detect this effect because of the timing of our field sampling. Nutrients dispersed more efficiently in the field cages than in the laboratory mesocosms as indicated by similar mean levels of enrichment in the field obtained with a quantity of fertilizer ~10 times higher than in the laboratory. As in the laboratory experiment, we replaced nutrient dispensers in the field experiment six times (once every 25 to 39 d), limiting the number of potential nutrient pulses. Most likely, the magnitude and duration of the phosphate pulses in the field cages were less than in the laboratory mesocosms and below the inhibitory threshold for growth in *L. glaciale* rhodoliths. These results confirm those of Tanaka et al. (2017) who reported no effect of phosphate concentrations between 1 to 2 µmol L^{-1} on calcification rates of the coralline red alga *Porolithon onkodes*. Although we did not measure water flow in the field, wave and tidal

currents certainly contributed to the greater dispersal of nutrients away from the rhodoliths than in the more stagnant water of the laboratory mesocosms. More research is needed to elucidate the sole effect of water flow on the response of rhodoliths to nutrients. In Chapter III, we demonstrate the predominant role of irradiance on *L. glaciale* rhodolith growth. In the present study, irradiance in the field was about twice higher than in the laboratory, which may largely explain our observed 15% faster rhodolith growth at ambient nutrient concentration in the field.

2.5.3. Conclusions and future research directions

Our laboratory experiment supported our overall hypothesis that nutrient enrichment (nitrogen and phosphorus) and biofouling reduce rhodolith (*L. glaciale*) growth, though this was less clear from the field experiment. Contrary to our expectation, elevated concentrations of nitrate and ammonia in the laboratory experiment triggered very little growth of biofoulers on rhodoliths, suggesting that the inhibitory effect of phosphate on (presumably) rhodolith calcification processes primarily explained decreased rhodolith growth in the enriched treatments. Our laboratory experiment clearly demonstrated, and the field experiment suggested, less effects of nutrient pulses on rhodolith growth than the relatively stable and lower, yet still elevated, concentrations that prevailed most of the time. These findings indicate some degree of growth resilience (*sensu* DeSoto et al. 2020) in subarctic *L. glaciale* rhodoliths to modest and infrequent (approximately once a month) increases in nutrient concentrations, yet an inability to cope with prolonged (several months) exposure to slightly eutrophic conditions.

Rhodolith beds are globally distributed, representing a pervasive and important marine biological system (Foster 2001, Riosmena-Rodriguez et al. 2017). As coralline red algae, rhodoliths form an important carbon sink, particularly on temperate and cold-water shelves where

they play a significant role in marine carbon cycling (Basso 2012, van der Heijden & Kamenos 2015, Teed et al. 2020). Despite the implementation of antipollution laws to reduce the direct discharge of nutrients and toxic substances into coastal waters, anthropogenic inputs of nitrogen and phosphorus in coastal waters have globally increased because of ever-increasing urbanization and industrialization of coastal areas (Small & Nicholls 2003). In subarctic and Arctic regions, ongoing changes in nutrient cycling and freshwater runoff resulting from permafrost thawing and snow melting will likely increase coastal nutrient inputs (Walvoord & Striegl 2007, Kendrick et al. 2018). Our study documents, for the first time, the effects of nutrient enrichment and associated biofouling on growth in *L. glaciale*, a dominant reef-building and rhodolith-forming species in Atlantic subarctic and Arctic marine systems (Adey & Hayek, 2011). Like other marine calcifiers, rhodoliths face increasing threats from ocean acidification and warming (Kamenos et al. 2013). Predicting changes in their abundance and the rich biological communities they support requires better understanding of the impacts of nutrient enrichment on rhodolith growth and calcification and their interaction with ocean acidification and warming.

CHAPTER III

High growth resilience of subarctic rhodoliths (*Lithothamnion glaciale*) to ocean warming and chronic low irradiance

3.1. ABSTRACT

Impacts of ongoing changes in sea temperature and irradiance on algal growth are difficult to separate because these two factors often co-vary and interact in the marine environment, while thermal optima for growth can vary with irradiance, and vice versa. We paired a 361-d laboratory mesocosm experiment and a 383-d field experiment with Newfoundland (eastern Canada) rhodoliths (*Lithothamnion glaciale*) to test the overall hypothesis that growth in subarctic rhodoliths is chiefly controlled by irradiance. Rhodoliths in the laboratory were exposed to one of five water temperatures (ambient, 2, 4, 7 and 10°C) and either of three irradiances (low, intermediate, and high). Rhodoliths in the field were held in cages at three depths (8, 15, and 25 m). Laboratory results unequivocally demonstrated that growth is unaffected by temperature between ~1 and 16°C. Field results indicated that growth ceases at temperatures near or below 0.5°C and that *L. glaciale*'s annual growth profile comprises three distinct phases - two of positive growth separated by one of arrested growth - and that the switch from one phase to the next coincides with seasonal shifts in sea temperature and light regimes. We conclude that growth is chiefly controlled by irradiance and that temperature effects may override, but not interact with, those of irradiance over only a few months yearly. Subarctic *L. glaciale* rhodoliths are quite resilient to changes in sea temperature over a relatively broad thermal range, with sustained growth even at temperatures that exceed those prevailing most of the year in Newfoundland coastal waters and northwards.

3.2. INTRODUCTION

Sea temperature largely determines physiological basis and responses in marine algae, with most species growing and reproducing within specific temperature ranges that often correlate with latitude (Lüning 1984). Temperature also varies with depth, more so in cold-temperate seas where strong thermoclines can form during the warm season (Hickman et al. 2012) that place a higher demand on species as they approach their tolerance limits (Gillooly et al. 2001, Eggert 2012). By powering photosynthesis, irradiance also influences algal physiology and bathymetric distribution. Seawater and its constituents scatter and absorb sunlight, affecting the spectral composition of light, with a generally deeper penetration by short than long wavelengths (Wozniak 2007). Algae in the three major taxonomic groups (Chlorophyta, Ocrophyta, and Rhodophyta) have evolved photosynthetic characteristics to harvest light within specific depth ranges or parts of the light spectrum (Dring 1990, Figueroa et al. 1997), with some capacity to adapt to daily and seasonally changing light quality and quantity (Figueroa et al. 2009, Hanelt 1998).

Impacts of changes in sea temperature and irradiance on algal growth are difficult to separate because these two factors often co-vary and interact in the marine environment (White et al. 1997), while thermal optima for growth can vary with irradiance (Spilling et al. 2015). Rhodoliths are non-geniculate, unattached, benthic coralline algae (Rhodophyta: Corallinales, Hapalidiales, and Sporolithales) with highly calcified tissues that grow only a few millimetres per year (Foster 2001). Depending on species and environmental conditions, rhodoliths vary in size, shape, and growth form, ranging from small twig-like thalli to large (> 10 cm across) and highly branched ellipsoids (Woelkerling et al. 1993). They thrive in all oceans from the low intertidal zone down to the lower photic zone, accumulating in structurally complex and biologically diverse communities known as rhodolith beds (Foster, 2001). Despite rhodolith beds' global distribution,

ecological importance as nursery habitats, and significant role in marine carbon cycling (van der Heijden & Kamenos 2015, Teed et al. 2020), only a handful of studies examined the impacts of changes in sea temperature and irradiance on rhodolith growth (Freiwald & Henrich 1994, Kamenos & Law 2010, Teichert & Freiwald 2014). For example, Blake and Maggs (2003) tested the effect of water temperature and depth (a proxy for light) on growth of several European corallines, concluding to species-specific responses. Although informative, these studies are short term, or lack the necessary temporal resolution for proper testing and partitioning of the effects of both factors on rhodolith growth. With ongoing global ocean warming (Levitus et al. 2012) and alteration to precipitation, runoffs, and turbidity of coastal waters (Ahn et al. 2005, Ogston & Field 2010, Fabricius et al. 2013), the need to characterize and predict rhodoliths' growth response to individual and combined effects of changes in temperature and irradiance has become even more important.

In the Northwest Atlantic, the coralline red alga *Lithothamnion glaciale* dominates coralline assemblages at depths of 15 to 25 m (Adey & Hayek 2011). Rhodoliths (*L. glaciale*) and extensive rhodolith beds develop within this depth range along the coast of Newfoundland and Labrador (Gagnon et al. 2012, Millar and Gagnon 2018, Teed et al. 2020). A recent study shows that Newfoundland rhodoliths are somewhat resilient to low levels of infrequent increases in nutrient concentrations, yet cannot cope with prolonged exposure to modest eutrophication (see Chapter II). The latter study's entirely experimental approach, along with relatively long duration and complementarity of the laboratory (183-d) and field (193-d) experiments used, helped disentangle effects of eutrophication and biofouling on rhodolith growth. A similar approach to the study of rhodholith growth response to changes in water temperature and irradiance would also help characterize these factors' individual and additive effects, if any, while increasing the strength

of the conclusions. Shallow (0 to 25 m deep) Newfoundland rhodoliths can undergo considerable seasonal variation in sea temperature (~ -1 to 16°C) and irradiance (~ 0 to 14 mol photons m^{-2} d^{-1}; present study, see Chapter III and Caines & Gagnon 2012, Blain & Gagnon 2013, Frey & Gagnon 2015), and hence represent excellent subjects to gain a better understanding of their resilience to thermal and light variability.

In the present study, we paired a 361-d laboratory mesocosm experiment and a 383-d field experiment with Newfoundland rhodoliths (*L. glaciale*) to examine individual and interactive effects of water temperature and irradiance on rhodolith growth. Rhodoliths in the laboratory experiment experienced different combinations of water temperature (ambient, 2, 4, 7, and 10°C) and irradiance (low, intermediate, and high). We predicted that growth is unrelated to temperature, while increasing non-linearly with irradiance. We held rhodoliths in the field experiment in cages at three depths (8, 15, and 25 m). We predicted that growth decreases non-linearly with increasing depth, while varying seasonally with irradiance. These predictions stem from studies suggesting that growth in *L. galciale* (and other *Lithothamnion* species) (1) does not correlate with seasonal changes in sea temperature (Kamenos and Law, 2010;Darrenougue et al., 2013); and (2) correlates positively with intensity and duration of solar radiation (Teichert & Freiwald 2014). The expected non-linear relationship between growth and irradiance is based on Burdett et al. (2012) who proposed adaptation to low-light environments in *L. glaciale* rhodoliths based on measurement of relatively low light saturation point.

3.3. MATERIALS AND METHODS

3.3.1. Rhodolith collection and staining

We carried out the two experiments described below with medium-sized (40-45 mm in diameter) *Lithothamnion glacial*e rhodoliths (Figure 3.1A). Divers hand collected rhodoliths on

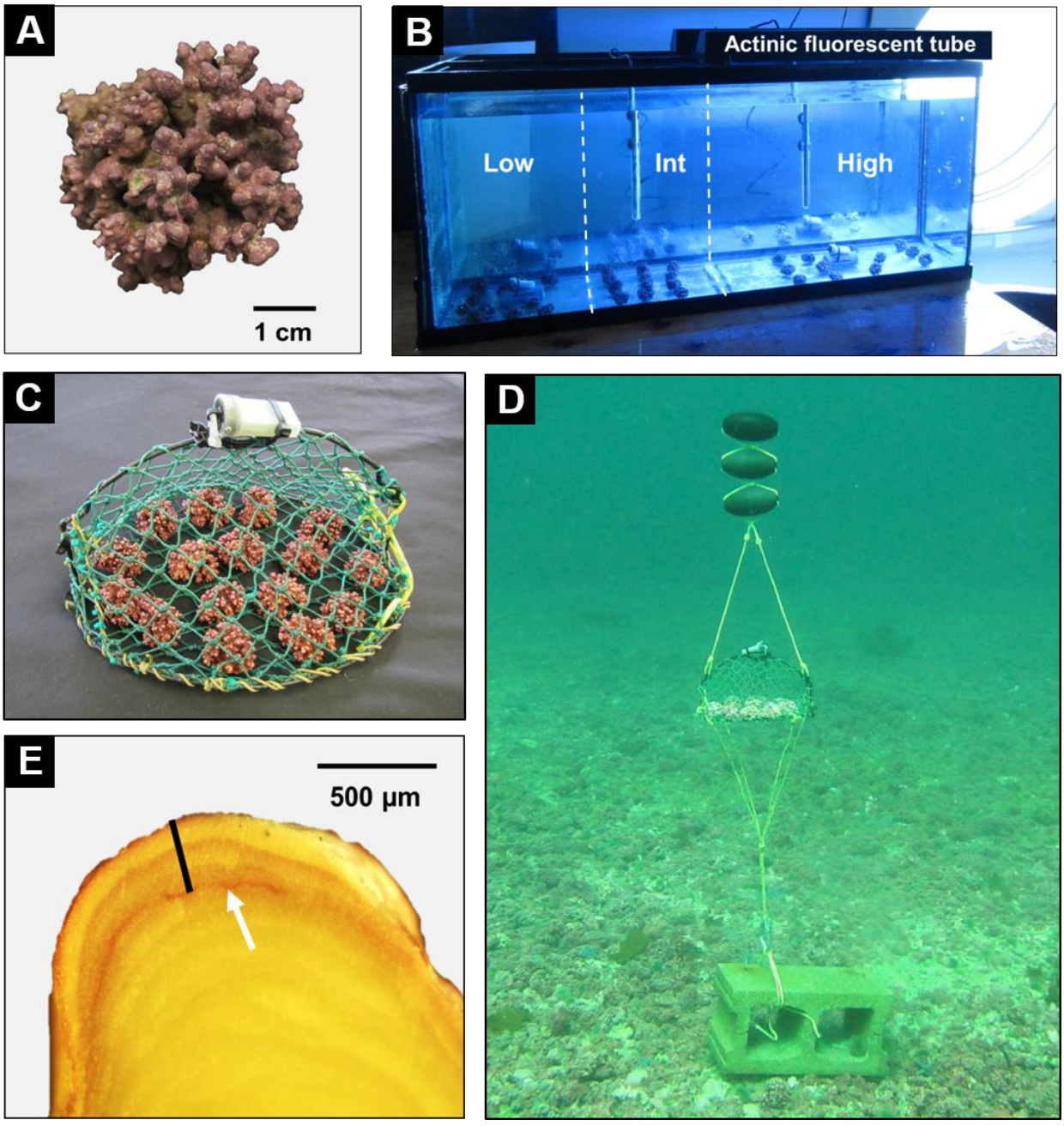
A
1 cm
B
Actinic fluorescent tube
Low
Int
High
C
D
E
500 µm

Figure 3.1. (A) Shape [primarily spheroidal] and size of sample rhodolith used in laboratory mesocosm and field experiments. (B) One of the five, 180-L mesocosms with location of the three irradiance treatment sections [low, intermediate (Int), and high], two temperature loggers [bottom], actinic fluorescent tube, and circular window [right] overlooking Logy Bay. (C) One of the rhodolith cages used in the field experiment [~25-cm diameter x 15-cm high] with a temperature and light logger attached to the top. (D) One of the cages attached to a cinder block and suspended in the water column by small floats at a depth of 15 m in the rhodolith bed in St. Philip's. (E) Longitudinal section of the tip of a rhodolith branch showing the stain mark [white arrow] used to measure growth, defined as the maximum length of the axis perpendicularly joining the stain mark and apex of the branch [black bar].

25 Aug, 2012, at a depth of ~15 m in the middle of a relatively large (0.025 km^2) rhodolith bed off St. Philip's (47°35'33.3" N, 52°53'33.4" W) in Conception Bay, Newfoundland, Canada. See Gagnon et al. (2012) for a detailed description of the bed. Rhodoliths were transported in plastic containers filled with seawater to the Ocean Sciences Center (OSC) of Memorial University. Upon arrival at the OSC, we transferred rhodoliths into two, 180-L glass tanks (~150 ind. per tank), each supplied with ambient flow-through seawater (~1 L min^{-1}) pumped from ~5 m depth in the adjacent Logy Bay. In these tanks, we exposed rhodoliths for seven days to indirect, natural light passing through 1-m-diameter circular windows overlooking Logy Bay. We removed any visible epibiont and cryptofauna from the surface of each rhodolith with a smooth nylon brush or forceps.

Andrake and Johansen (1980) marked coralline algae with Alizarin Red with no impact on growth. Many authors have since used Alizarin Red S to study growth in coralline algae, including rhodoliths (Blake & Maggs 2003, Kamenos et al. 2008, Amado-Filho et al. 2012, Darrenougue et al. 2013, Sletten et al. 2017). On 1 Sep, 2012, we interrupted water delivery in both tanks and lowered the volume of water to 90 L prior to adding 10 L of seawater containing 8.5 g of dissolved Alizarin Red S, yielding a final concentration of ~85 mg L^{-1} in each tank. Rhodoliths were maintained in this stain-laden seawater for 48 h at ~10°C with immersion probe coolers (one per tank) (IP-35RCL; PolyScience) controlled by timers. During staining, we used a pump (Elite802; Rolf C. Hagen) to aerate the water in each tank by delivering 1500 cm^3 of air per minute to prevent deoxygenation and acidification. We controlled light conditions in each tank to emulate natural photoperiod and diel fluctuations in irradiance with: (1) two, 61-cm long, actinic fluorescent tubes [Marine-GLO, T8, 20W; Rolf C. Hagen] located ~50 cm above the water surface [one tube per half section of the tank] and emitting ~20 µmol m^2 s^{-1} of light daily from 10:00 to 15:00; and (2) indirect, natural light entering the lab as described above. These actinic tubes emit mainly in the

lower range (400-580 nm) of the PAR spectrum. We resumed seawater flow in both tanks at the end of the staining period to eliminate residual stain in the water.

3.3.2. Effects of temperature and irradiance on rhodolith growth (laboratory mesocosm experiment)

Growth in branched rhodoliths can be measured as the thickness of new layers of calcified tissue added at the apices of branches since marking (Blake & Maggs 2003, Darrenougue et al. 2013). To test individual and combined effects of water temperature and irradiance on rhodolith growth, we carried out a laboratory mesocosm experiment in which we exposed stained rhodoliths for one year (361 d) to seawater at one ambient and four controlled temperatures (2, 4, 7, and 10°C) under three irradiances (low, intermediate, and high). These temperatures fall within the typical thermal range of -1 to 16°C for shallow (< 25 m deep) coastal waters in southeastern Newfoundland. Limited chilling capacity constrained our ability to test temperatures below 2°C. As with staining, we used both indirect natural lighting and direct artificial lighting from above the experimental tanks (see below) to ensure exposure of rhodoliths to daily and seasonal variation in natural light regimes, as well as to shorter wavelengths of photosynthetically active radiation (PAR) range (400-700 nm) that predominate in shallow coastal water environments.

The experiment utilized five, 180-L glass tanks (L x W x H: 120 x 30 x 50 cm) supplied with flow-through seawater (1 L min^{-1}). We arranged four of the tanks in a 2 x 2 grid arrangement alongside a wall of the laboratory with two circular windows, staggering them relative to windows to locate their right ends near one of the windows. We covered the left end of the four tanks with opaque canvas to block natural light penetration through that end, leaving the other sides of the four tanks unobstructed (no canvas). This particular arrangement, together with orientation of the

windows relative to the daily trajectory of sun, created similar gradients of indirect, natural light in the four tanks, with progressively more light from right to left ends. We subdivided each tank in three sections based on visual delineation of differences in irradiance: (1) low, in the first quarter of the tank flanking the covered end; (2) intermediate, in the second quarter of the tank adjacent to the low irradiance quarter; and (3) high, in the remaining half of the tank flanking the uncovered end (Figure 3.1B).

No structures in the tanks physically separated rhodoliths and water among sections, and we lit each tank with one 61-cm-long, actinic fluorescent tube (Marine-GLO, T8, 20W; Rolf C. Hagen, also used for staining) located ~10 cm above the water surface in the high irradiance section and emitting light daily from 10:00 to 15:00 (Figure 3.1B). The actinic fluorescent tube contributed ~1, 5, and 14 µmol photons m^{-2} s^{-1} in the low, intermediate, and high irradiance sections, respectively to total irradiance, as measured with a PAR meter (LI-250A; LI-COR) fitted to an underwater quantum sensor (LI-192; LI-COR). We randomly assigned each tank one of the four temperature treatments, and set up the fifth tank, located at the margin of the 2 x 2 grid, to recreate the same light environment as in the four other tanks, but supplied with ambient seawater that reflected Logy Bay water temperature.

On 4 Sep, 2012 (onset of experiment), we uniformly distributed 12 stained rhodoliths to the bottom of each section in each of the five mesocosms, resulting in a total of 36 rhodoliths per mesocosm with similar light exposure (Figure 3.1B). Logistics prevented replication of mesocosms, and we therefore repeated the experiment below in 2013 (see below). Ambient seawater temperature could not be replicated from one year to another, so the second experimental run only included the four controlled temperature treatments. The 2, 4, and 7°C treatments were gradually cooled from the 10°C onset temperature at slightly different rates: (1) 2°C: 2°C wk^{-1} for

four weeks; (2) 4°C: 2°C wk^{-1} for three weeks; (3) 7°C: 1°C wk^{-1} for three weeks to reduce the likelihood of thermal shock. We maintained water temperature in the 2, 4, 7, and 10°C mesocosms by continuously injecting seawater at 4°C from a main chilled reservoir or, when required, with 300-W water heaters (Fluval M300; Rolf C. Hagen) for the 7 and 10°C mesocosms and immersion probe coolers (IP 35RCL; PolyScience) for the 2°C mesocosm.

We sought to characterize temporal variation in rhodolith growth. Accordingly, we removed three rhodoliths from each section of each mesocosm every three months (Table 3.1) for growth measurement (see "Growth measurement"). Once a month, we carefully inspected the surface of each rhodolith and removed any visible epibiont with a smooth nylon brush. Remaining rhodoliths were randomly overturned and assigned different locations within their respective mesocosm section. We terminated the experiment on 30 Aug, 2013, after a total duration of 361 d. Available resources limited us to one mesocosm for each temperature treatment. To account for possible confounding of temperature and mesocosm effects, we carried out a second, shorter run of the same experiment from 3 Sep to 30 Nov, 2013, with the 2, 4, 7, and 10°C temperature treatments assigned to different mesocosms within the 2 x 2 grid. This run omitted a mesocosm treatment with ambient seawater because we could not replicate thermal conditions from the previous year. Collection, staining, and acclimation of rhodoliths to temperature treatments followed the protocol described above, and we measured rhodolith growth only once at the end of this 89-d run.

Table 3.1. Rhodolith collection dates for the laboratory ("Laboratory mesocosm experiment") and field ("Field experiment") experiments.

Experiment	Collection	Date	Days since onset of experiment
Laboratory (First run)	1	1 Dec, 2012	89
	2	1 Mar, 2013	179
	3	2 Jun, 2013	272
	4	30 Aug, 2013	361
Laboratory (Second run)	1	30 Nov, 2013	89
Field	1	3 Dec, 2012	65
	2	10 Jan, 2013	103
	3	2 Mar, 2013	154
	4	2 Apr, 2013	185
	5	27 May, 2013	240
	6	17 Jul, 2013	291
	7	29 Aug, 2013	334
	8	17 Oct, 2013	383

Two temperature and light loggers (HOBO Pendant; Onset Computer Corporation) placed horizontally in the center of the low and high irradiance sections (one logger per section) recorded water temperature and downwelling illuminance at the bottom of each mesocosm every 5 min throughout the experiment. A 5-d preliminary trial during which we recorded temperature and illuminance in the three irradiance sections of one mesocosm showed: (1) similar temperature in the three sections; and (2) 31% illuminance in the intermediate irradiance section relative to that in the high irradiance section. Accordingly, we estimated illuminance throughout the experiment in the intermediate irradiance section of each mesocosm by multiplying illuminance values in the high irradiance section by 0.31.

3.3.3. Growth along a depth gradient (field experiment)

We monitored growth of stained rhodoliths held at depths of 8, 15, and 25 m in the rhodolith bed at St. Philip's. These depths correspond roughly to the shallow, middle, and deep sections of the bed, respectively (see Chapter III and Gagnon et al. 2012, Millar & Gagnon 2018). Expected sea temperature and irradiance decreases from shallow to deep sections presumably yielded increasingly less favorable conditions for rhodolith growth. We set the duration of the field experiment to ~12.5 mo (383 d) to capture potential seasonal differences in growth over at least one year.

Three dome-shaped cages held rhodoliths at each depth (nine cages in total). Each cage consisted of a roughly circular metal ring (25 cm in diameter) topped by a semi-circular metal arch (15 cm at highest point), both fully covered in tightly stretched nylon netting with 2-cm mesh (Figure 3.1C). A 15-kg cinder block placed horizontally on the rhodolith bed anchored the bottom (circular metal ring) of each cage, whereas three small buoys held the top (semi-circular arch) cage

upright (Figure 3.1D). The three cages at each depth were located ~5 m from one another. This particular set-up: (1) minimized alteration of natural light and water flow passing through cages; and (2) continuously maintained the bottom of the cages ~50 cm above the bed, greatly limiting benthic grazer access.

To facilitate installation on the rhodolith bed we preassembled cages and their rhodolith content in the laboratory a few days prior to the start of the experiment. We added 16 stained rhodoliths one by one to each cage through a collapsible section of the netting, and permanently attached each rhodolith to the bottom with fishing line to prevent movement and abrasion in the field. The attachment process distributed rhodoliths evenly on cage bottoms, thus ensuring similar access to light and exposure to other environmental influences among individuals. Attachment of rhodoliths took less than 10 min per cage and was completed in a cool, moist, dim environment to limit emersion stress in rhodoliths. Upon completion of attachment, we submerged and maintained cages with rhodoliths in large flow-through tanks until transport to the study site.

The experiment began on 30 Sep, 2012, when we removed caged rhodoliths from the flow-through tanks and transported them in seawater-filled containers to install them at three experimental depths in the rhodolith bed in St. Philip's. Approximately every 1.5 mo thereafter, divers removed two rhodoliths from each cage at each depth and placed them in pre-labeled plastic bags, which were transported to the OSC for growth measurement (see "Growth measurement"). We terminated the experiment on 17 Oct, 2013 (383 d after it commenced), with collection of the last rhodoliths in all cages. In total, we completed eight rhodolith collections at 15 and 25 m depths, between December 2012 and October 2013 (Table 3.1). Storm damaged cages and destroyed all rhodoliths at 8 m in January 2013 yielding only two rhodolith collections at that depth. One temperature and light logger (HOBO Pendant; Onset Computer Corporation) attached horizontally

to the top of one of the three cages with the light sensor oriented towards the sea surface recorded sea temperature and downwelling illuminance at each depth every 5 min throughout the experiment.

3.3.4. Growth measurement

Growth in branched rhodoliths can be estimated by measuring the thickness of new layers of calcified tissue added at the apices of branches since marking (Blake & Maggs 2003, Darrenougue et al. 2013). Measurements of growth in rhodoliths in the laboratory mesocosm and field experiments used an identical protocol. Following oven drying at 40°C for 48 h, we filed down rhodolith branches (distal ends) of 10 haphazardly chosen individuals to their center with a precision rotary tool (3000; Dremel) fitted with a 240-grit sanding bit. We then gently broke off the filed branches, hand-polished them with a 600-grit sandpaper to expose stain marks and photographed them at a 40X magnification with a microscope equipped with a digital camera (BA300; Motic). Digital photographs and image analysis software (Motic Images Plus 2.0; Motic) were used to measure branch elongation, defined as the maximum axis length between the stain mark and apex of the branch (Figure 3.1E). We then calculated mean rhodolith branch elongation, hereafter referred to as growth, by averaging the ten growth measurements.

3.3.5. Light conversion

Our light loggers for the laboratory and field experiments measured illuminance, in lux (lx), between 150 and 1200 nm. To compare results among the lab and field experiments and published studies, we converted all illuminance values to PAR equivalents (photosynthetically

active radiation, referring to the segment of the electromagnetic spectrum between 400 and 700 nm used for most photosynthesis) using the following procedures derived from Long et al. (2012):

$$\mathrm{PAR} = \frac{\mathrm{I}}{\mathrm{CF}} \quad (1)$$

where PAR is photosynthetically active radiation in μmol photons m^{-2} s^{-1}, I is illuminance in lux (lx), and CF is a lux to PAR conversion factor in $\frac{\mathrm{lx}}{\mu\mathrm{mol\ photons\ m^{-2}s^{-1}}}$ obtained from simultaneous measurement of illuminance and irradiance for artificial actinic light in the mesocosms (low irradiance section = 14.7, intermediate = 18.1, and high = 22.1 lx) and sunlight in the field (23.4) (see Tables B.1, B.2, Appendix B). For the laboratory mesocosm experiment, we used actinic light conversion factors to convert illuminance data acquired each day between 10:00 and 15:00, when artificial light provided most of the irradiance, and a sunlight conversion factor for illuminance data acquired between 15:05 and 09:55, when lights were off. The mixture of natural and artificial lighting prevented establishing a conversion factor for sunlight in the mesocosms during the experiment. Accordingly, we applied a conversion factor for sunlight in the field (23.4) to all mesocosms' illuminance data measured in the absence of actinic light.

We calculated daily light integral (DLI), a time-integrated irradiance (PAR) integral indicating the amount of photosynthetically active photons received by a given surface over 24 h (Korczynski et al. 2002), for each of the three irradiance treatments in the laboratory mesocosm experiment on each of the 361 and 89 d that the first and second experimental runs lasted, respectively. We also calculated DLI in the field experiment for each of the three depths on each of the 383 d that the experiment lasted using the following equation (adapted from Korczynski et al., 2002):

$$\mathrm{DLI} = \sum_{i=1}^{288} \frac{300 x_i}{10^6} \qquad (2)$$

where DLI is daily light integral in mol photons m^{-2} d^{-1}, 288 denotes the number of PAR readings over 24 h, x_i refers to the i^{th} PAR value in µmol photons m^{-2} s^{-1}, 300 is the number of seconds separating two consecutive readings (one reading every 5 min), and 10^6 is the µmol to mol scaling factor.

3.3.6. Statistical analysis

We used ANCOVA (Sokal & Rohlf 2012) to examine differences in rates of change of rhodolith growth among our various experimental treatments. Although we measured growth in rhodoliths collected at various time intervals, interpreting statistical differences among regression slopes of experimental treatments effectively compared differences in rhodolith growth rates among treatments (Quinn & Keough 2002). As detailed below, we applied linear mixed-effects models (LMEM) to various ANCOVA designs with both fixed and random factors to properly handle the dependency structure of the data and account for pseudoreplication (Zuur et al. 2009).

3.3.6.1. Laboratory mesocosm experiment

We used one LMEM applied to split-plot ANCOVA experimental designs (Quinn & Keough 2002) to compare rhodolith growth rates among temperature and irradiance treatments (n =216), with the fixed, between-plots factor Temperature (the five water temperature treatments: ambient, 2, 4, 7, and 10°C), random factor Mesocosm (each of the nine experimental mesocosms) nested within Temperature (two mesocosms per fixed temperature treatment [one in each of the two experimental runs], and one mesocosm for the ambient treatment [first experimental run

only]), fixed, within-plots factor Irradiance (the three irradiance treatments: low, intermediate, and high), and covariate Time (number of days elapsed since the onset of the experiment). Growth data from the mesocosm with ambient water temperature were available for the first run of the experiment only because we could not replicate this temperature in the second run. We implemented a power of the variance covariate (varPower) structure to account for the increasing variance in rhodolith growth over time (Zuur et al. 2009).

3.3.6.2. Field experiment

We applied one LMEM to nested ANCOVA experimental design with the fixed factor Depth (8, 15, and 25 m), random factor cage (each of the nine cages) nested within Depth (three cages per depth) to compare rhodolith growth rates among depths (n = 36) during the first 103 d of the experiment, i.e. before the storm destroyed rhodolith cages at 8 m (see "Growth along a depth gradient"). Non-linear growth patterns at 15 and 25 m over the full duration (383 d) of the experiment (see Results) prevented using the ANCOVA approach to compare growth rates among the two depth treatments. Instead, we used one LMEM applied to two-way ANOVA (Quinn & Keough 2002) experimental design with the fixed factors Time (the eight rhodolith collection events) and Depth (15 and 25 m), and random factor Cage (each of the six cages) nested within Depth (three cages per depth) to compare rhodolith growth between the two uninterrupted growth time series at 15 and 25 m and among the eight rhodolith collections (n = 96). We implemented an identity variance (varIdent) structure to both models to account for different variances in rhodolith growth among depth levels (Zuur et al. 2009). All analyses were applied to raw (non-transformed) data.

In all LMEMs, we verified homogeneity of the variance and normality of the residuals by examining the distribution of the residuals and the normal probability plot of the residuals, respectively (Snedecor & Cochran 1989). We used paired t-test comparisons to detect differences among levels within a factor (ANCOVAs and ANOVA). All analyses were carried out with R 3.6.1 (R Core Team 2019), using a significance level of 0.05. Rhodolith annual growth reported for the laboratory experiment describe model predicted values at Time = 365 d (number of days in one year) assuming no growth at the onset of experiment (i.e. intercept corrected to 0).

3.4. RESULTS

3.4.1. Laboratory mesocosm experiment

3.4.1.1. Temperature

Mean daily mean water temperature (DMWT) in the controlled temperature mesocosms differed by no more than 0.5°C (in the 10°C treatment) from the targeted temperatures during the post-acclimation period (days 29-361) (Table 3.2, Figure 3.2A). DMWT in the ambient temperature mesocosm averaged 6.7°C and varied more than in the controlled temperature mesocosms (Table 3.2, Figure 3.2B); as expected, it declined seasonally from ~15.6°C at the onset of the experiment in early September 2012, to ~0.5°C in mid-February 2013, followed by an overall increase to ~16.5°C near the end of the experiment in late July 2013 (Figure 3.2B). Ambient DMWT was < 1°C only 3% of the time, over less than five consecutive days. DMWT patterns in the controlled temperature mesocosms during the first 89 d of the first experimental run were similar to those throughout the 89-d duration of the second run (Table 3.2, Figures 3.2C-D; C.1A-D, Appendix C).

Table 3.2. Mean (± SD) water temperature and daily light integral (DLI) in the laboratory mesocosms for various segments of the first and second experimental runs. Temperatures for the controlled (2, 4, 7, and 10°C) and ambient mesocosms are averaged daily means. DLI for the low, intermediate, and high irradiance treatments are averaged over all temperature treatments (see Figures 2 and 3 for daily mean water temperatures and DLI, respectively).

		First run			Second run
Factor	**Treatment**	**Full run (361 d)**	**Post-acclimation (day 29-361)**	**First 89 d**	**Full run (89 d)**
Temperature (°C)	2	2.6 (1.6)	2.3 (0.8)	3.4 (2.7)	3.6 (3.3)
	4	4.6 (1.1)	4.4 (0.8)	5.0 (1.7)	5.3 (2.1)
	7	7.4 (1.0)	7.4 (1.0)	7.3 (1.0)	7.4 (1.0)
	10	10.4 (1.1)	10.5 (1.0)	10.0 (1.1)	9.9 (1.1)
	Ambient	6.7 (4.7)	---	---	---
Irradiance (DLI) (mol photons m^{-2} d^{-1})	Low	0.02 (0.01)	---	0.01 (0.01)	0.01 (0.01)
	Intermediate	0.11 (0.02)	---	0.10 (0.02)	0.09 (0.02)
	High	0.29 (0.05)	---	0.28 (0.05)	0.24 (0.04)

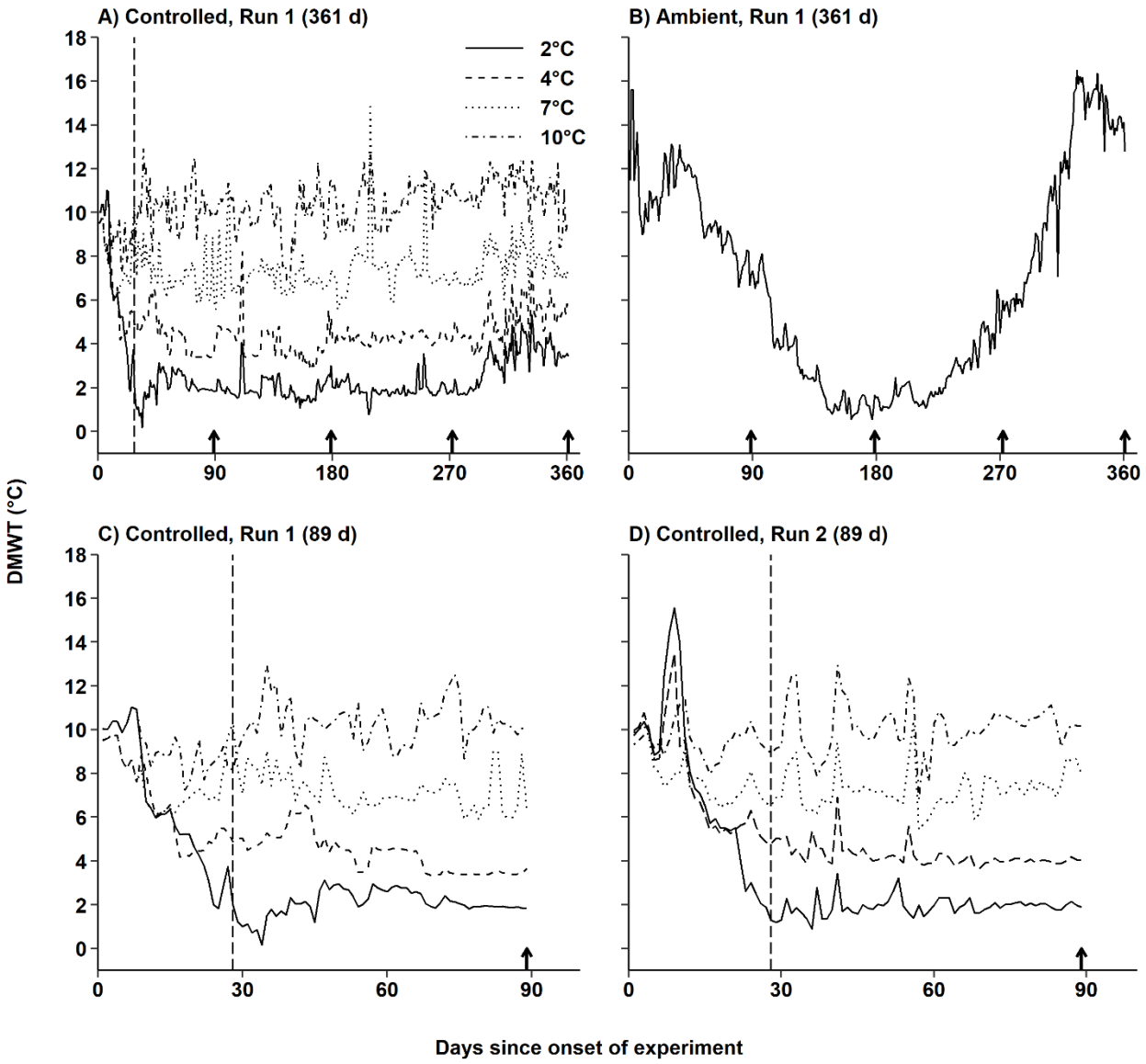
A) Controlled, Run 1 (361 d)
B) Ambient, Run 1 (361 d)
C) Controlled, Run 1 (89 d)
D) Controlled, Run 2 (89 d)
2°C
4°C
7°C
10°C
DMWT (°C)
Days since onset of experiment

Figure 3.2. Daily mean water temperature (DMWT) in (A) each of the four mesocosms with controlled temperature [2, 4, 7, and 10°C] throughout the first experimental run; (B) the mesocosm with ambient temperature throughout the first experimental run; (C) each of the four mesocosms with controlled temperature during the first 89 d of the first experimental run; and (D) each of the four mesocosms with controlled temperature throughout the second experimental run. The vertical dashed line in panels (B), (C), and (D) marks the end of the acclimation during which rhodoliths in mesocosms at 2, 4, and 7°C were exposed to decreasing temperatures from an initial temperature of 10°C. Arrows along abscissas mark days since the onset of both experimental runs on which nine rhodoliths (three per irradiance treatment) were removed from each mesocosm to determine growth (see Table 3.1 for collection dates).

3.4.1.2. Irradiance

At 0.29 (± 0.05, SD) mol photons m^{-2} d^{-1}, mean daily light integral (DLI) throughout the first experimental run (361 d) in the high irradiance treatment was ~3 and 15 times higher than in the intermediate and low irradiance treatments, respectively (Table 3.2). This pattern closely resembled that during the first 89 d of the first experimental run and 89 d of the second run, with differences of no more than 0.05 mol photons m^{-2} d^{-1} in any of the irradiance treatments (Table 3.2). Mean DLI remained fairly constant throughout both experimental runs, with smallest to largest daily fluctuations in the lowest to highest irradiance treatments, respectively (Table 3.2, Figure 3.3A, B). Mean instantaneous irradiance (the average of all measures of irradiance at a given time of day) over the first experimental run exhibited a clear, daily cycle in all three irradiance treatments with: (1) low [< 1 µmol photons m^{-2} s^{-1}] values from 0600 to 0900, followed by; (2) a 2.5-h increase to peak values [up to 15.2 µmol photons m^{-2} s^{-1} under high irradiance] that persisted from 1130 to 1400, followed by; (3) a 2-h decrease to low values from 1600 to 2030, ending with; (4) nearly complete darkness until 0600 the next day (Figure 3.3C). Mean instantaneous irradiance during the peak period in the high irradiance treatment was 3 and 13 times higher than in the intermediate and low irradiance treatments, respectively (Figure 3.3C).

3.4.1.3. Rhodolith growth

There was no interactive effect of temperature and irradiance on growth. Growth was ~20% lower at 10 than at 4 and 7°C during the 89 days separating the onset of the laboratory experiment and the first rhodolith collection (Table 3.3, Figure 3. 4A). Growth then stabilized for the rest of the experiment, increasing at similar rates in all temperature treatments (Tables 3.3, 3.4; Figure 3.4A). Mean branch tip elongation after 361 d (end of the experiment) was between 2.4 (at 7°C)

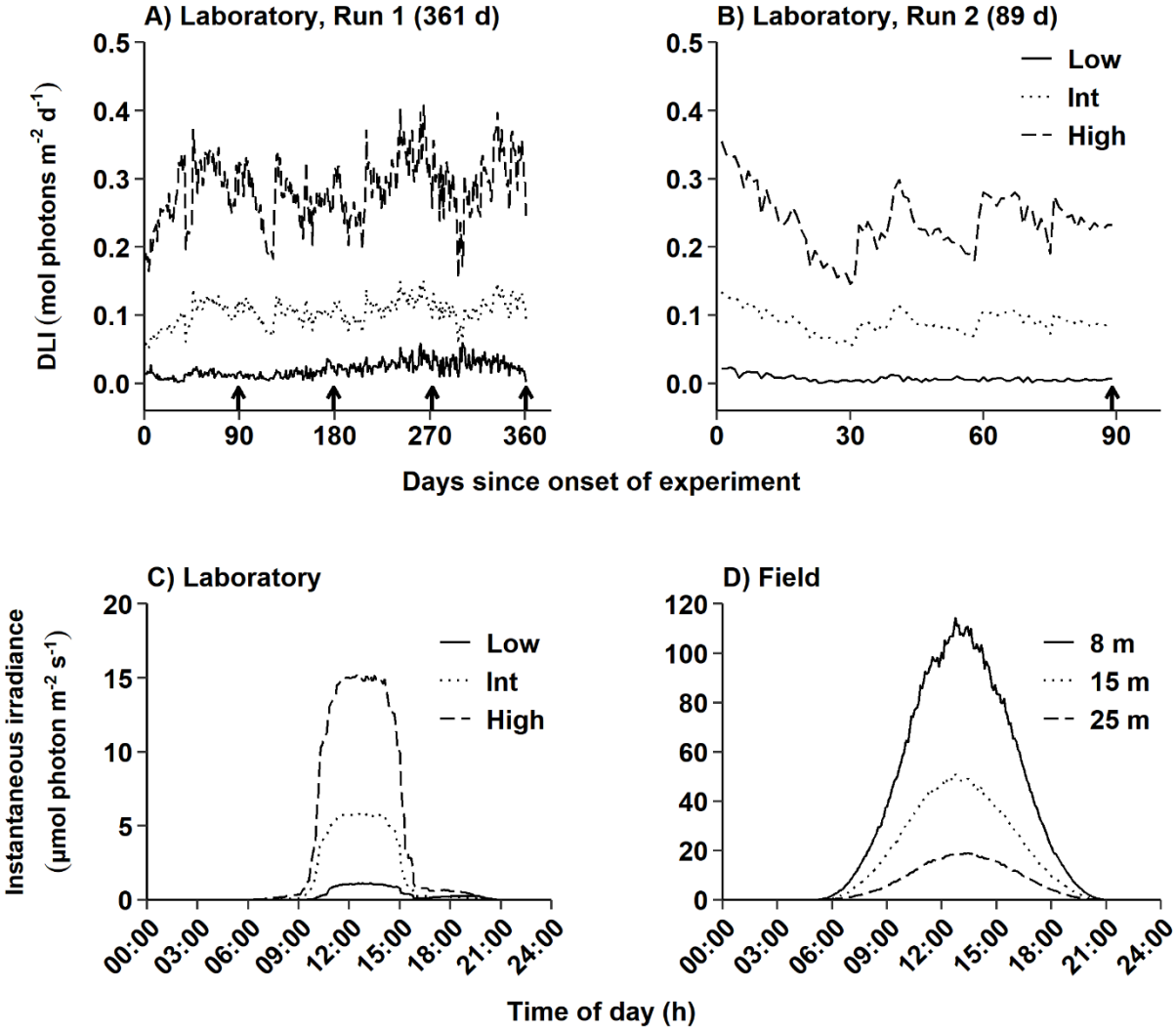
A) Laboratory, Run 1 (361 d)
B) Laboratory, Run 2 (89 d)
DLI (mol photons m-2 d-1)
0.5
0.4
0.3
0.2
0.1
0.0
0
90
180
270
360
30
60
Low
Int
High
Days since onset of experiment
C) Laboratory
D) Field
Instantaneous irradiance (µmol photon m-2 s-1)
20
15
10
5
120
100
80
60
40
8 m
15 m
25 m
00:00
03:00
06:00
09:00
12:00
15:00
18:00
21:00
24:00
Time of day (h)

Figure 3.3. Mean daily light integral (DLI, data pooled across all mesocosms) for the low, intermediate, and high irradiance treatments in the laboratory mesocosm experiment throughout the (A) first experimental run [361 d]; and (B) second experimental run [89 d]. Arrows along the abscissas mark days since the onset of both experimental runs on which nine rhodoliths (three per irradiance treatment) were removed from each mesocosm to determine growth. Mean instantaneous irradiance regimes for (C) the low, intermediate, and high irradiance treatments in the first run of the laboratory mesocosm experiment [data pooled across all mesocosms]; and (D) at 8, 15, and 25 m depths in the field experiment. Each regime averages irradiance measured every five minutes throughout (C) the first run of the laboratory experiment; and (D) the 383-d field experiment (note the change of scale between panels C and D; see Table 3.1 for collection dates).

Table 3.3. Summary of split-plot ANCOVA (applied to raw data) examining the effect of between-plot factor water Temperature (T; five levels: ambient, 2, 4, 7 and 10°C), within-plot factor Irradiance (I; three levels: low, intermediate, and high), and covariate Time (t; number of days elapsed since the onset of the experiment on each rhodolith sampling event in the first [89, 179, 272 and 361 d] and second [89 d] experimental runs), while correcting for the random factor Mesocosm (each of the 9 experimental mesocosms [respectively 5 and 4 mesocosms in the first and second experimental runs]) nested within Temperature (two mesocosms per controlled temperature [2, 4, 7, and 10°C]) on rhodolith (*Lithothamnion glaciale*) growth in the laboratory mesocosm experiment (see "Effects of temperature and irradiance on rhodolith growth" for a description of the experiment). Random-factor effects are not relevant to the present study, and hence not shown for simplicity.

Source of variation	numDF	denDF	F-ratio	*p*
Intercept	1	182	4341.292	< 0.001
T	4	4	7.162	0.041
I	2	182	17.779	< 0.001
t	1	182	316.473	< 0.001
T x I	8	182	0.694	0.697
T x t	4	182	0.878	0.478
I x t	2	182	20.013	< 0.001
T x I x t	8	182	0.681	0.708

numDF = F-ratio numerator; denDF = F-ratio denominator; *p* = p-value.

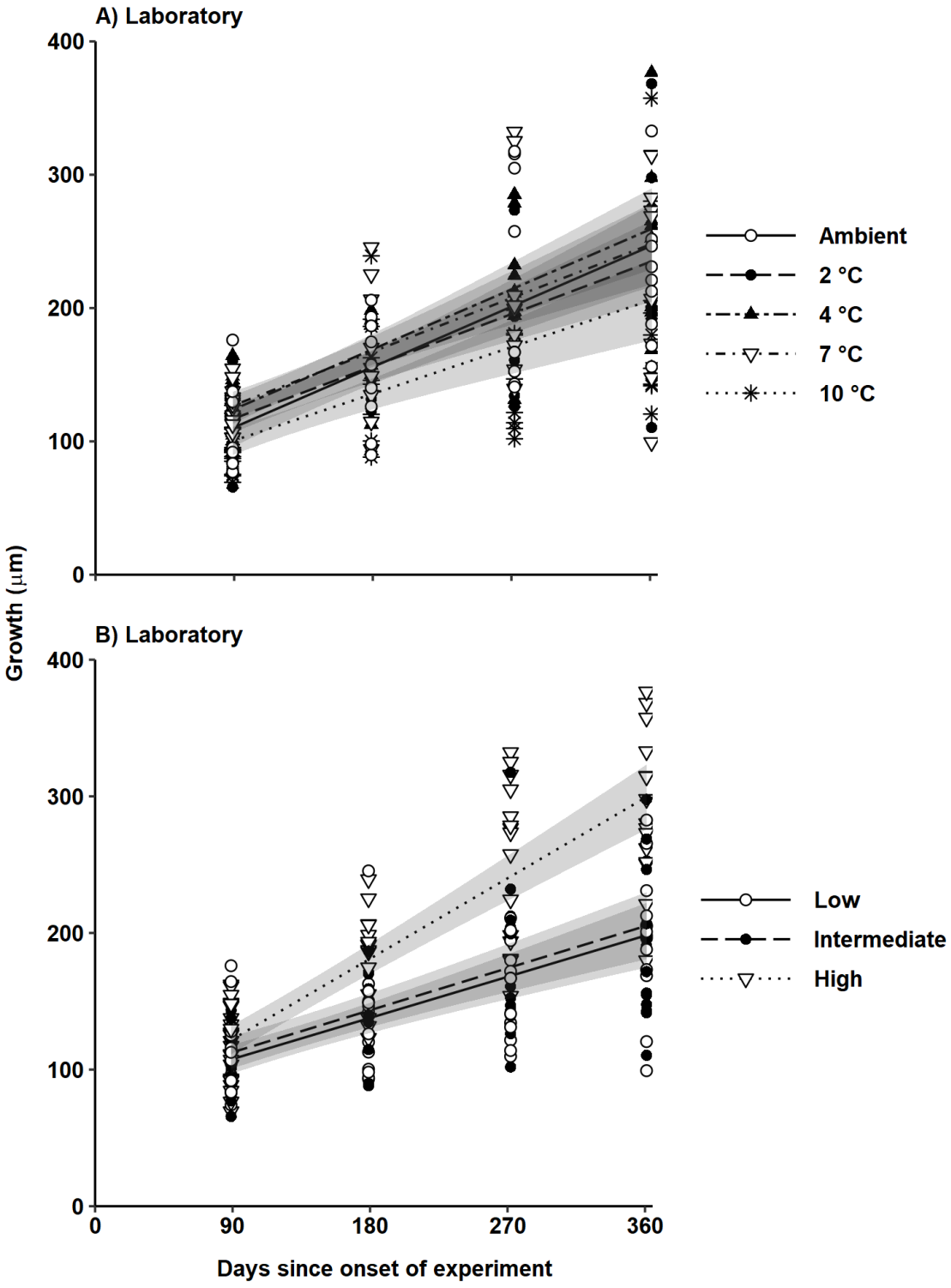
A) Laboratory
B) Laboratory
Growth (μm)
Days since onset of experiment
0
100
200
300
400
90
180
270
360
Ambient
2 °C
4 °C
7 °C
10 °C
Low
Intermediate
High

Figure 3.4. Relationship between rhodolith (*Lithothamnion glaciale*) growth (± 95% CI) and number of days elapsed since the onset of (A) the laboratory experiment for each of the five water temperatures tested [data pooled across the first and second experimental runs and irradiance treatments; n = 45 for 2, 4, 7 and 10°C, and n = 36 for ambient temperature]; (B) the laboratory experiment for each of the three irradiances tested [data pooled across the two experimental runs and controlled temperature treatments; n = 72 for each irradiance].

Table 3.4. Summary of regression coefficients of the spit-plot ANCOVA in the laboratory experiment, and nested ANCOVA in the field experiment (both applied to raw data) examining the relationships between rhodolith (*Lithothamnion glaciale*) growth and time elapsed since the onset of the 361-d laboratory mesocosm experiment at the various water temperatures and irradiances tested, and between the onset of the field experiment and the second rhodolith collection (103 d) at the three experimental depths.

Experiment	Factor/Level	N	Intercept (SE)	Slope (SE)
Laboratory	Temperature (°C)			
	2	45	78.1 (9.2)	0.43 (0.06)
	4	45	79.3 (9.2)	0.50 (0.06)
	7	45	87.0 (9.2)	0.45 (0.06)
	10	45	65.6 (9.2)	0.39 (0.06)
	Ambient	36	65.2 (11.7)	0.50 (0.07)
	Irradiance			
	Low	72	77.7 (9.7)	0.33 (0.05)
	Intermediate	72	81.9 (8.3)	0.34 (0.05)
	High	72	63.4 (7.8)	0.65 (0.05)
Field	Depth			
	8 m	12	30.7 (19.0)	0.68 (0.22)
	15 m	12	19.7 (35.8)	1.39 (0.42)
	25 m	12	77.0 (27.0)	0.94 (0.31)

and 4.6 (2°C) times higher than after 89 d (first growth measurement) (Figure 3.4A). Contrary to temperature, the rate of change in rhodolith growth differed significantly among the three irradiances tested (Table 3.3); it was twice as high at high than at low or intermediate irradiances (Table 3.4, Figure 3.4B). Branch tips after 361 d were between 2.8 (low irradiance) and 4.5 (high irradiance) longer than after 89 d (Figure 3.4B). Annual growth rate did not differ significantly among the five temperature treatments, ranging from 142 ± 31 (CI) μm y^{-1} (at 10 °C) and 183 ± 31 μm y^{-1} (at ambient), yet it was nearly twice as high at high (239 ± 24 μm y^{-1}) than at low (122 ± 24 μm y^{-1}) or intermediate (125 ± 26 μm y^{-1}) irradiances (Figure 3.5A, B). Overall, these results suggest a larger effect of irradiance on rhodolith growth than water temperature.

3.4.2. Field experiment

3.4.2.1. Temperature

Daily mean water temperature (DMWT) throughout the 383-d field experiment averaged 0.6°C warmer at 8 than 15 m deep, and 1.6°C warmer at 15 than 25 m. DMWT varied similarly at 8, 15, and 25 m depths during the first ~5 mo of the field experiment, steadily decreasing from ~12°C in early October 2012, to a minimum of ~ -0.4°C by late February 2013 (Figure 3.6A-C). DMWT generally increased at all depths during the remainder of the experiment, although at an increasingly lower and more variable rate with increasing depth (Figure 3.6A-C). It peaked at all depths between early August and October 2013, to 17.1, 15.9, and 13.2°C at 8, 15, and 25 m, respectively (Figure 3.6A-C). These patterns suggest that a thermocline developed over spring and summer that kept the shallowest (8 m) rhodoliths in a warmer and more stable thermal environment than deeper (15 and 25 m) rhodoliths (Figure 3.6A-C).

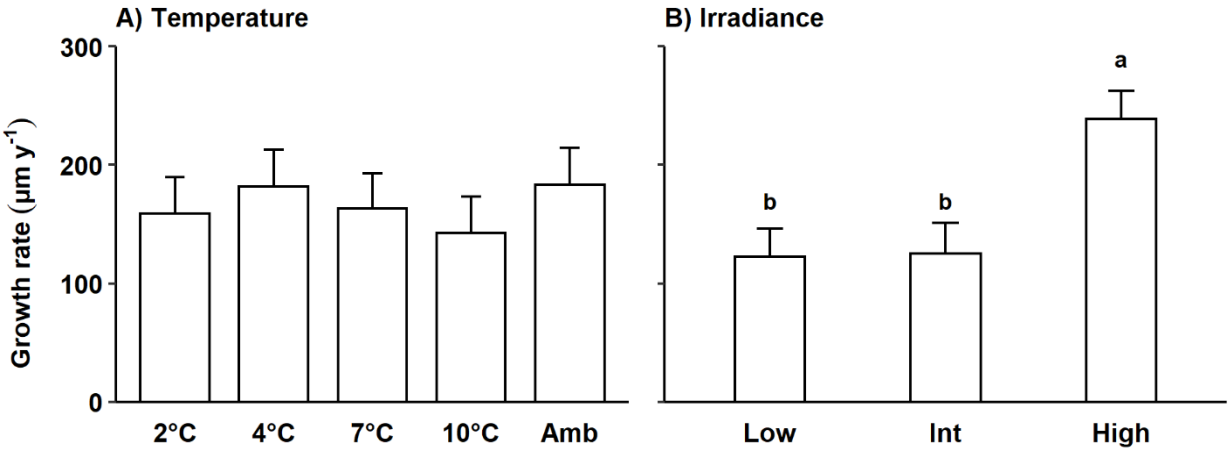

Figure 3.5. Growth rate (+95% CI) of rhodoliths (*Lithothamnion glaciale*) at (A) the five water temperatures [data pooled across irradiances] and (B) the three irradiances [data pooled across controlled temperatures] tested in the laboratory experiment. Annual growth rates are model (split-plot ANCOVA) predictions at Time = 365 d derived from regression slopes (± 95% CI) of growth as a function of time assuming null growth at Time = 0 (see Figure 3.4). Bars not sharing the same letters differ statistically (paired t-test comparison; $p < 0.05$).

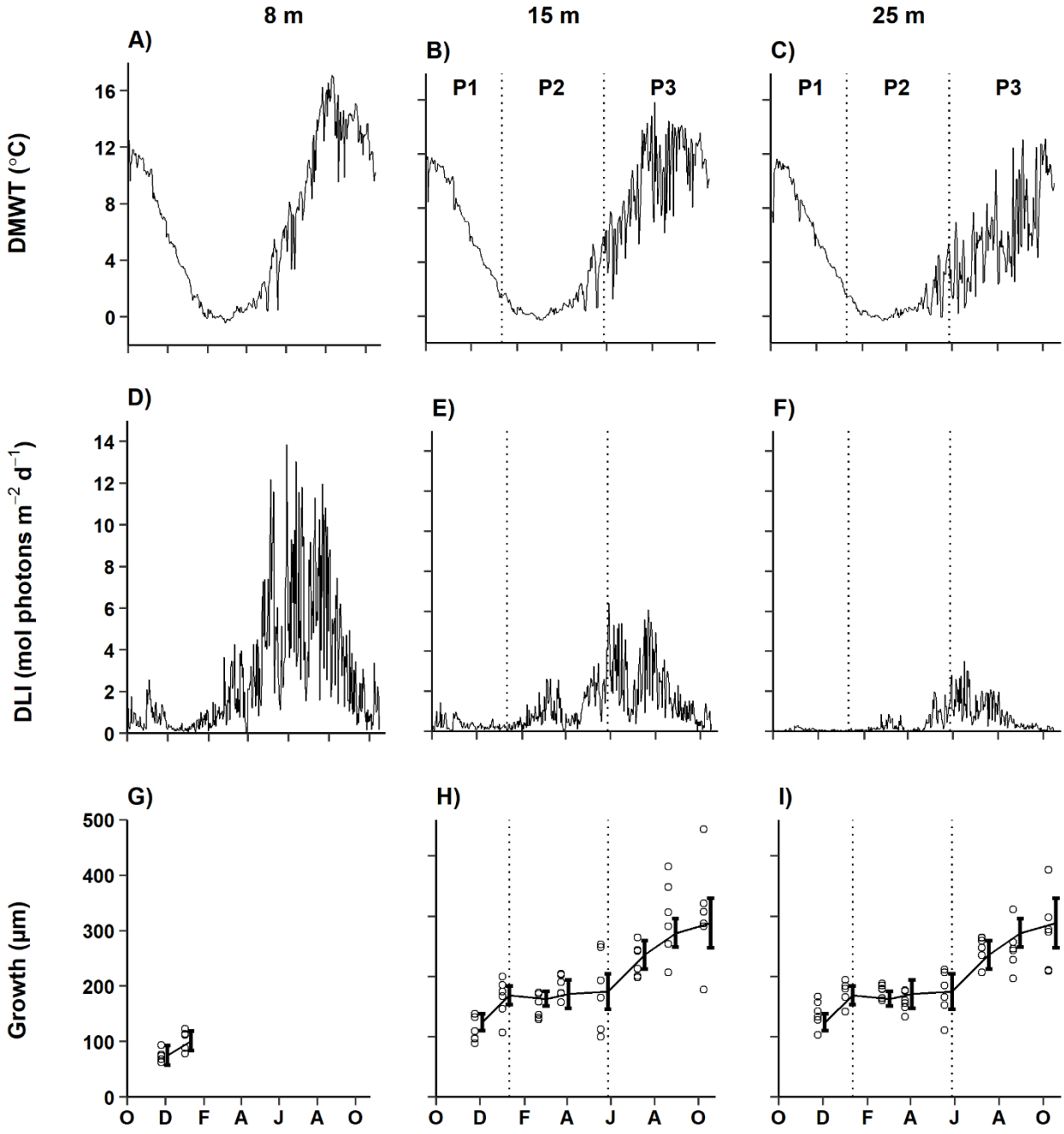
8 m
15 m
25 m
A)
B)
C)
P1
P2
P3
DMWT (°C)
D)
E)
F)
DLI (mol photons m^{-2} d^{-1})
G)
H)
I)
Growth (µm)
O D F A J A O

Figure 3.6. Daily mean water temperature (DMWT; A to C), daily light integral (DLI; D to F), and growth of rhodoliths (*Lithothamnion glaciale*; G to I) at 8, 15, and 25 m depths during the 383-d field experiment. Vertical dotted lines separate three main growth phases: Phase 1 (P1) and Phase 3 (P3), which denote positive growth, and Phase 2 (P2), which denotes arrested growth (see "Growth along a depth gradient" and "Light conversion" for experimental details and calculation of DLI).

3.4.2.2. Irradiance

Like temperature, mean irradiance throughout the field experiment decreased with increasing depth, with 55% higher irradiance at 8 than at 15 m and 58% higher at 15 than at 25 m (Figure 3.6D-F). During the first ~5 months (October 2012, to February 2013) irradiance remained consistently low, < 2.6 mol photons m^{-2} d^{-1}, at all depths, followed by a brief increase (up to two times higher at 8 m) in March 2013 (Figure 3.6D-F). Irradiance at all depths decreased to low levels for a few weeks in April (most likely as a result of the annual phytoplankton bloom), then increased markedly (more so at 8, than at 15, than at 25 m) over the remainder of spring and early summer (Figure 3.6D-F). It peaked at all depths in June or July 2013, to 13.0, 6.1, and 3.5 mol photons m^{-2} d^{-1} at 8, 15, and 25 m, respectively (Figure 3.6D-F). Mean daily peak irradiance at 8 m was ~2 and 6 times higher than at 15 and 25 m, respectively (Figure 3.3D). Daily irradiance patterns were similar in the field and laboratory experiments, though peaks at 8, 15, and 25 m depths were ~8, 9, and 17 times higher than in the high, intermediate, and low irradiance treatments, respectively (Figure 3.3C, D).

3.4.2.3. Rhodolith growth (overall)

Rhodolith growth was ~40% lower at 8 than at 15 and 25 m depths between the onset of experiment and the first rhodolith collection, 65 d later (Table 3.5, Figure 3.7A). Growth then stabilized over the following 38 d that separated the 1st and 2nd rhodolith collections, increasing at similar rates among depths (Table 3.5, Figure 3.7A). Mean branch tip elongation after 103 d was between 26% (at 25 m) and 49% (at 15 m) higher than after 65 d (Figure 3.6G-I).

Table 3.5. Summary of (A) nested ANCOVA (applied to raw data) examining the effects of factor Depth (D; three levels: 8, 15 and 25 m) and covariate Time (t; numbers of days elapsed since the onset of the field experiment on each of the first two rhodolith collection events [65 and 103 d] wile correcting for the random factor Cage (each of the nine cages [three cages per depth treatment]) nested within Depth, on rhodolith (*Lithothamnion glaciale*) growth; and (B) two-way ANOVA examining the effects of fixed factors Depth (D; two levels: 15 and 25 m) and Collection (C; eight levels: each of the eight rhodolith collection events) while correcting for the random factor Cage (each of the six cages [three cages per depth treatment]) nested within Depth, on rhodolith (*L. glaciale*) growth (see "Growth along a depth gradient" for a description of the experiment). Random-factor effects are not relevant to the present study, and hence not shown for simplicity.

	Source of variation	**numDF**	**denDF**	**F-ratio**	***p***
A. First two collections (8, 15, and 25 m depths)	Intercept	1	24	1336.762	< 0.001
	D	2	6	49.171	< 0.001
	t	1	24	27.580	< 0.001
	D x t	2	24	1.205	0.317
B. All (eight) collections (15 and 25 m depths)	Intercept	1	83	3968.350	< 0.001
	D	1	83	4.854	0.092
	C	7	4	29.533	< 0.001

numDF = F-ratio numerator; denDF = F-ratio denominator; p = p-value

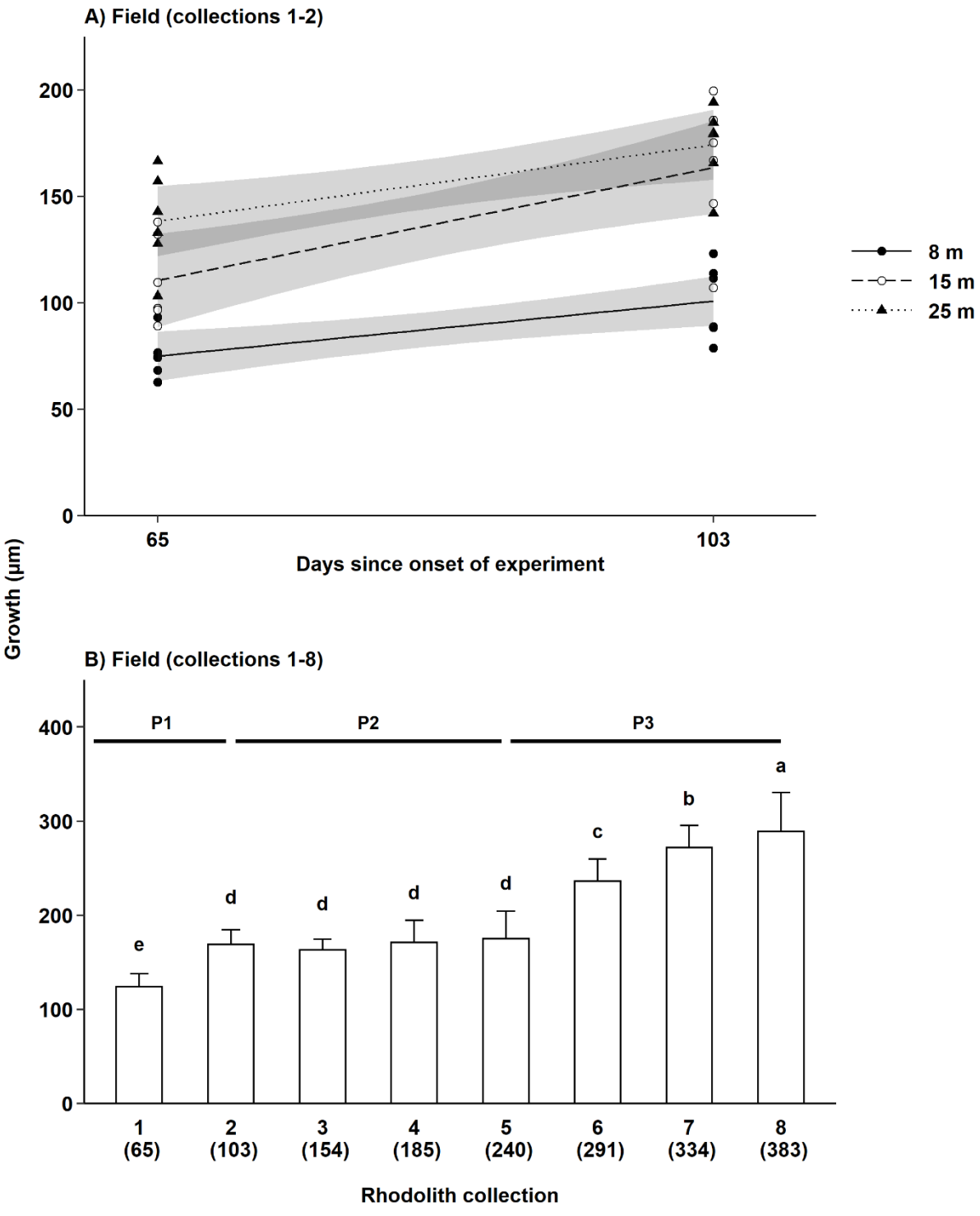
A) Field (collections 1-2)
200
150
100
50
0
65
103
Days since onset of experiment
Growth (µm)
8 m
15 m
25 m
B) Field (collections 1-8)
P1
P2
P3
400
300
200
100
0
e
d
d
d
d
c
b
a
1 (65)
2 (103)
3 (154)
4 (185)
5 (240)
6 (291)
7 (334)
8 (383)
Rhodolith collection

Figure 3.7. (A) Relationship between rhodolith (*Lithothamnion glaciale*) growth (± 95% CI) and number of days elapsed since the onset of the field experiment during the first two rhodolith collections when rhodoliths were present at the three experimental depths (n = 12 per depth). (B) Mean growth (± 95% CI) [data pooled across the 15 and 25 m depths] on each of the eight rhodolith collection events (n = 12 per collection). Numbers in parentheses under each rhodolith collection event number on the abscissa indicate the number of days elapsed since the onset of experiment. Phase 1 (P1) and Phase 3 (P3) denote periods of positive growth, whereas Phase 2 (P2) denotes a period of arrested growth (see Figure 6 for timing of phases and "Growth along a depth gradient" for a description of the experiment).

For the 383-d uninterrupted time series at 15 and 25 m, growth was similar between depths but differed among collection events (Table 3.5, Supplement 3, Figure 3.7B), and more than two times higher at 383 d (end of experiment; 289 ± 21 µm) than at 65 d (first rhodolith collection; 124 ± 7 µm) (Figure 3.7B).

3.4.2.4. Rhodolith growth (seasonal phases)

Rhodolith growth pooled across the 15 and 25 m depths increased by 36% during the 38 d that separated the 1st and 2nd rhodolith collections (Phase 1) and remained remarkably stable (Phase 2) during the following 137 d (i.e. until the 5th collection, Figure 3.7B). Growth then resumed and increased (Phase 3) by 35%, 15%, and 6% within each time block separating respectively the 5th and 6th (51 d), 6th and 7th (43 d), and 7th and 8th (49 d) collections (Figure 3.7B). During Phase 1 (1st phase of positive growth), DMWT decreased from ~12 to 1°C and DLI was consistently lowest, averaging 0.20 µmol photons m^{-2} s^{-1} (Figure 3.6B, C, E, F). During Phase 2 (nearly arrested growth), DMWT ranged between ~ -0.3 and 6°C, averaging ~1°C. It remained below 0.5°C (which is the lowest water temperature attained in the ambient mesocosm of the laboratory experiment) 77% of the time. DLI was ~4 times higher than during Phase 1, averaging 0.70 µmol photons m^{-2} s^{-1} (Figure 3.6B, C, E, F). During Phase 3 (2nd phase of positive growth), DMWT increased from ~5 to 16°C and always was above 0.5°C (Figure 3.6B, C). DLI peaked, averaging 1.48 µmol photons m^{-2} s^{-1}, which was ~7 and 2 times higher than during Phase 1 and Phase 2, respectively (Figure 3.6E, F).

3.5. DISCUSSION

The laboratory mesocosm and field experiments showed that growth in *Lithothamnion glaciale* rhodoliths is primarily controlled by irradiance at sea temperatures between ~1 and 16°C, yet virtually ceases when temperature reaches and drops below 0.5°C. Growth rate of rhodoliths exposed in the laboratory to various combinations of temperature (ambient, 2, 4, 7, and 10°C) and irradiance (low, intermediate, and high) over ~1 y, increased at high irradiance regardless of temperature, shedding new light on temperature-light interactive effects reported in previous studies of *L. glaciale* (Adey, 1970) and *Lithophyllum margaritae* rhodoliths (Steller et al. 2007).

3.5.1. Temperature

Growth in rhodoliths exposed to 10°C in the laboratory experiment was significantly lower than at 2 and 4°C during the 90 d that preceded the first rhodolith collection. Possibly, growth was temporarily stimulated by a steeper thermal acclimation at the two lowest temperature treatments during the ~1-mo acclimation period. Adey (1970) reported transitory effects of temperature change on growth in subarctic coralline crusts, including *L. glaciale*, although, contrary to our results, growth decreased with decreasing temperature. Rhodolith growth was however unaffected by temperature in the remaining 9 mo of the experiment, averaging 158 µm y^{-1} across the ambient temperature regime (0.5 to 16.5°C) and four controlled temperature treatments [2 to 10°C]. These results are consistent with those of Kamenos & Law (2010) who found no difference in growth in *L. glaciale* rhodoliths grown for one year at controlled temperatures between 8 and 15°C. Our results thus extend the thermal range for relatively unimpaired growth in this species.

Several other studies support the notion that rhodoliths are generally insensitive to relatively large variation in water temperature. For example, Blake and Maggs (2003) reported no temperature effect between 10 and 18°C on growth of European *Phymatolithon calcareum*

rhodoliths. Wilson et al. (2004) found no significant difference in photosynthetic activity of *P. calcareum* rhodoliths exposed to temperatures between 9 and 25°C over 4 to 5 wk. Steller et al. (2007) documented no significant change in net photosynthesis of Californian *Lithophyllum margaritae* rhodoliths exposed to temperatures between 10 and 30°C and irradiance < 100 µmol photons m^{-2} s^{-1}. However, at ~150 µmol photons m^{-2} s^{-1}, photosynthesis was ~5 times lower at 10 than 25°C, suggesting interactive effects of temperature and light above a threshold irradiance. In the present study, irradiance in the low, intermediate, and high irradiance treatments of the laboratory experiment was up to two orders of magnitude lower than the average maximum daily ambient irradiance in the field. Temperature effects on physiological processes which influence growth in *L. glaciale* rhodoliths may only occur at higher irradiance.

Studies of effects of water temperature on metabolism show that some freshwater copepods (Epp & Lewis 1979) and rotifers (Epp & Lewis 1980) maintain constant metabolic rates within the thermal range of their natural environment, likely as a result of evolutionary adaptation to rapidly changing environments. These findings align with similar growth rates in the ambient and fixed temperature treatments of our laboratory experiment, suggesting that some coralline algae, including *L. glaciale*, are able to maintain a relatively stable metabolic rate over their natural habitat's temperature range. Other studies, however, yielded contrasting results. For example, Martin et al. (2013) reported strong temperature-driven seasonal variation in the metabolic activity of *Lithophyllum cabiochae*. Adey (1970) measured a positive temperature effect on the marginal growth rate of several boreal and Arctic coralline species, including *L. glaciale*, until temperature exceeded thresholds beyond which growth decreased. Ichiki et al. (2000) found a > 50% reduction in marginal growth in *Lithophyllum yessoense* crusts at 10°C and 25°C, compared to 15°C and 20°C, with no significant difference between the latter two temperatures, suggesting no

temperature effect on growth within a certain range. Overall, temperature effects on coralline algal growth appear species specific and, in some cases, may depend on irradiance. However, the present study and Kamenos & Law (2010) indicate a quite limited influence of temperature on growth in *L. glaciale* rhodoliths in the 1 to 18°C range.

3.5.2. Irradiance

Our laboratory experiment, together with the findings of other studies, provide several indications that growth in *L. glaciale* rhodoliths is chiefly driven by irradiance, with increased growth above a relatively low threshold irradiance that may correspond to the species' light compensation point. Growth in our low (~1 µmol photons m^{-2} s^{-1}) and intermediate (~5 µmol photons m^{-2} s^{-1}) irradiance treatments remained similarly low (~124µm y^{-1}), while twice lower than in the high (~15 µmol photons m^{-2} s^{-1}) irradiance treatment (~239 µm y^{-1}). Kamenos and Law (2010) measured similar growth rates (~90 to 160 µm y^{-1}) in *L. glaciale* rhodoliths exposed in the laboratory to ~5 µmol m^{-2} s^{-1} and water temperatures comparable to those in the present study. Kamenos et al. (2008) also measured similar growth rates (~146 to 173 µm y^{-1}) in *L. glaciale* rhodoliths exposed in the field to temperature between ~7 to 16°C and in the lab to some (unspecified) ambient water temperature and light regimes.

Our laboratory experiment was not designed to specifically characterize light compensation or saturation points in *L. glaciale* rhodoliths. Nevertheless, results were consistent with (1) Schwarz et al.'s [2005] compensation point of ~0.1 µmol photons m^{-2} s^{-1} in coralline algal crusts under thick ice cover in the Antarctic Ross Sea; and (2) Burdett et al.'s [2012] light saturation irradiance between ~5 and 55 µmol photons m^{-2} s^{-1} in *L. glaciale* rhodoliths measured in the lab and at a depth of ~6 m in the field. Rhodoliths in our high irradiance treatment likely

experienced irradiance closer to, or above, light saturation for growth, yet still below photoinhibitory level, resulting in a higher growth rate compared to the low and intermediate irradiance treatments. Consistency among our findings and those of the studies described above, together with Teichert et al.'s (2012) observation that *L. glaciale*'s lower distribution limit in the Svalbard Arctic Archipelago is near ~80 m deep, where mean irradiance is only ~0.1 µmol photons m^{-2} s^{-1}, further reinforces the notion that *L. glaciale* is well adapted to low-light conditions.

Our field experiment yielded mixed conclusions about the effect of irradiance on *L. glaciale* rhodolith growth. Growth during the first ~2 mo was ~40% lower at 8 (~75 µm) than at 15 and 25 m (~124 µm), but similar across the three depths afterwards. This finding aligns with an ~50% lower growth at 5 than at 10 m depths in Irish *Phymatolithon calcareum* rhodoliths attributed to photoinhibition at the former depth (Blake & Maggs 2003). Accordingly, we propose that our observed initially lower growth at 8 m depth was because of photoinhibition, followed by photosynthetic acclimation of low-light-adapted *L. glaciale* (Burdett et al. 2012). This explanation is also supported by the ~70% decrease in irradiance between the first and second growth measurements, when growth at 8 m became similar to that of deeper rhodoltihs. Growth at 15 and 25 m was similar throughout the experiment despite a 58% decrease in irradiance at the latter depth. Schwarz et al. (2005) reported little variation in photosynthetic activity in Antarctic coralline red algal crusts at depths of 16 to 20 m, indicating low downregulation of photosynthesis at irradiance below the light saturation point. Our findings that *L. glaciale* rhodolith growth was similar at 15 and 25 m depths in the field, and at low and intermediate irradiances in the laboratory experiment, yet still below growth at high irradiance in the laboratory, further support the notion that irradiance plays a key role in regulating growth in *L. glaciale* rhodoliths.

3.5.3. Seasonal growth phases

Our field experiment showed, for the first time, that growth in subarctic *L. glaciale* rhodoliths exhibits three distinct seasonal phases. The two phases of positive growth were when (1) sea temperature decreased from ~12 to 1°C and irradiance was consistently lowest, ~0.20 µmol photons m^{-2} s^{-1} [Phase 1 - December to mid-January]; or (2) sea temperature increased from ~5 to 16°C and irradiance was at least twice higher than in the two other phases [Phase 3 - June to mid-October]. Interestingly, these two phases were separated by the only phase of arrested growth (Phase 2 - mid-January to end of May), when sea temperature plummeted near or below 0.5°C 77% of the time, but irradiance was nevertheless four times higher than during one of the two phases of positive growth (Phase 1) and ~35 times higher than in the low irradiance treatment of the laboratory experiment under which positive growth occurred.

These findings reinforce the notion discussed above that growth in *Lithothamnion glaciale* rhodoliths is primarily controlled by irradiance at sea temperatures between ~1 and 16°C. The species appears unable to cope with prolonged exposure to chronic low temperatures of ~0.5°C or less and responds to it by ceasing growth momentarily. Temperature effects may, therefore, override (but not interact with) those of irradiance over only a few months yearly. Growth inhibition at low temperature has also been reported in several cold-water macroalgae (Wiencke & Dieck 1990) and coralline algae (Ichiki et al. 2000). Blain and Gagnon (2013) showed that frond length (a proxy for growth) in the highly acidic (H_2SO_4) annual brown seaweed *Demarestia viridis* in Newfoundland waters also exhibits three distinct phases (increase, no change, decrease). However, contrary to *L. glaciale* rhodoliths, sea temperature is as a key driver of switches from one growth phase to the next (Blain & Gagnon 2013), driven by the attainment in late summer of an upper lethal temperature limit of ~12°C for *D. viridis* (Gagnon et al. 2013). That these two

taxonomically quite distant benthic primary producers both exhibit three distinct growth phases under similar thermal environments, yet respond to temperature in quite opposite ways (i.e. *L. glaciale* rhodoliths thrive at 12°C, whereas *D. virids* dies), is a neat example of the various life-history strategies and adaptations of marine flora to subarctic environmental conditions.

3.5.4. Conclusion and future directions

Our ~1-year long laboratory and field experiments supported our overall hypothesis that growth in subarctic *L. glaciale* rhodoliths is chiefly controlled by irradiance, while showing some inhibitory effect of exposure to chronic low sea temperature. Laboratory results demonstrated that growth is unaffected by temperature between ~1 and 16°C. Our field results indicated that growth ceases at temperatures near or below 0.5°C. They also revealed that *L. glaciale*'s annual growth profile in predominantly cold subarctic waters comprises three dominant phases and that the switch from one phase to the next coincides with seasonal shifts in both sea temperature and light regimes. Overall, these findings (1) extend the known temperature range [~1 to at least 16°C] over which growth in *L. glacilale* rhodoliths remains unaffected; (2) identify the lower temperature limit [~0.5°C] below which growth ceases momentarily; and (3) demonstrate that temperature effects may override, but not interact with, those of irradiance over only a few months yearly.

Lithothamnion glaciale rhodolith beds are a pervasive and dominant marine biological system in the predominantly cold waters of subarctic North Atlantic (Blake & Maggs, 2003, Gagnon et al. 2012, Adey et al. 2015, Schoenrock et al. 2018). In Chapter III, we show that Newfoundland *L. glaciale* rhodoliths are somewhat resilient to low levels of infrequent increases in nutrient concentrations, yet cannot cope with prolonged exposure to modest eutrophication. Results from this chapter show that *L. glaciale* rhodoliths are nevertheless quite resilient to changes in sea temperature over a relatively broad thermal range, with sustained growth even at

temperatures that exceed those prevailing most of the year in Newfoundland coastal waters and northwards. The Arctic is warming at a rate almost twice the global average, with a clear decrease in sea-ice and ice cover that ultimately increases light availability to marine organisms (Lang et al. 2017, Bindoff et al. 2019). The present study therefore also suggests that ongoing ocean warming will benefit subarctic *L. glaciale* rhodoliths (and the highly biodiverse beds they form) by shortening the yearly period over which near-zero sea temperatures prevent their growth. Further studies should address the vulnerability of *L. glaciale* rhodoliths to ocean acidification and its consequences on the structure and function of Arctic and subarctic benthic communities.

CHAPTER IV

Spatiotemporal variation in structural complexity and macrofaunal diversity of a subarctic rhodolith (*Lithothamnion glaciale*) bed

4.1. ABSTRACT

Benthic marine macrofaunal abundance and diversity generally increase with habitat complexity. Rhodolith beds are benthic communities organized around the primary production of free-living, non-geniculate coralline red algae known as rhodoliths. Rhodoliths provide three-dimensional habitat structure to macrofauna including ecologically and economically important species. Knowledge about rhodolith-associated macrofaunal communities and their relationships with habitat complexity is limited in subarctic compared to temperate and tropical environments. We carried out four seasonal surveys at two locations in a Northwest Atlantic subarctic rhodolith (*Lithothamnion glaciale*) bed in St. Philips, Newfoundland, to test the hypotheses that: 1) seafloor composition and rhodolith abundance and morphology are temporally stable but vary spatially within the same bed, 2) the abundance and diversity of rhodolith-associated macrofauna vary with rhodolith abundance, and 3) macrofaunal assemblages vary spatially and seasonally. We applied univariate and multivariate statistics to quadrat collections and video imagery to characterize habitat complexity and faunal assemblages in a subarctic rhodolith bed. Seafloor composition within the bed varied spatially and seasonally but rhodolith density and biomass remained stable at both sites across all seasons. Macrofaunal density related positively to total rhodolith volume per surface area, whereas diversity showed contrasting relationships with rhodolith volume between sites. Macrofaunal biomass did not vary with rhodolith volume but was higher in spring than in summer. Spatial and seasonal variation in the diversity of rhodolith-associated macrofauna varied among taxonomic groups, with crustaceans contributing most to macrofaunal assemblage dissimilarities. We conclude that rhodolith beds of *L. glaciale* in the subarctic Northwest Atlantic provides a structurally complex and temporarily stable habitat to a diverse macrofaunal communities dominated by suspension-feeders and characterized by moderate seasonal variation.

4.2. INTRODUCTION

Ecologists define habitat as the place where an organism, or a community of organisms, live (Hine 2019). Habitat structure refers to the physical arrangement of objects in space and is characterized by the complexity and the heterogeneity of structural elements (McCoy & Bell 1991). Positive relationship between habitat structural complexity and faunal diversity has been described in terrestrial (Camargo et al. 2018), and aquatic (Beck 1998, Buhl-Mortensen et al. 2012, Carvalho et al. 2017) ecosystems. Early studies on the topic focused on the positive relationship between habitat complexity and colonizable surface to explain high faunal density and diversity (Preston 1960, MacArthur & Wilson 1967, Connor & McCoy 1979). More recent work suggested that habitat structure also regulates microhabitat and niche availability through food foraging, intra- and interspecific competition, and predator-prey interaction (Dean & Connell 1987, Hixon & Menge 1991, Bell et al. 2012, Myhre et al. 2013).

In addition to physical elements (sediment, pebbles, cobbles, bedrocks, etc.), some organisms modify, maintain, or add structural components. These organisms, sometimes called ecosystem engineers (Jones et al. 1994), may enhance species abundance and diversity within communities by increasing habitat complexity at both local and regional scales (Buhl-Mortensen et al. 2010). Several studies have highlighted the positive impact of biological structure formed by macroalgae (Steneck et al. 2002, Eriksson et al. 2006, Hauser et al. 2006) and marine calcifiers such as bivalves (Koivisto & Westerbom 2010) and corals (Buhl-Mortensen et al. 2012) on biodiversity.

Rhodoliths are non-geniculate, free-living, benthic coralline red algae (Adey & MacIntyre 1973). Under favorable conditions, rhodoliths aggregate over extensive areas of the seafloor to form structurally complex benthic communities called rhodolith beds (Foster 2001). The calcium

carbonate skeletons of rhodoliths function as autogenic ecosystem engineers (*sensu* Jones et al. 1994) providing a three-dimensional habitat matrix for diverse macrobenthic communities (Nelson 2009). Rhodoliths display various size, shape, and growth forms, thus significantly contributing to benthic habitat structural complexity (Woelkerling et al. 1993, Gagnon et al. 2012). Moreover, they are long-lived (up to 100 years) (Frantz & Kashgarian 2000, Teed et al. 2020) and slow-growing (generally < 1 mm y^{-1}) (see Chapters II & III and Nelson 2009), and may thus provide a temporally stable habitat in locations where water motion is insufficient to frequently move the rhodolith matrix.

Rhodoliths reproduce mainly by fragmentation but may also originate from spore settlement on hard particles that the coralline tissue eventually overgrows (Freiwald & Henrich 1994). Whereas the former scenario results in non-nucleated rhodoliths composed entirely of algal tissue, the latter scenario produces nucleated rhodoliths bearing an exogenous core. Nuclei size and shape may strongly influence rhodolith morphology and reduce the space available for colonization by macrofauna (Ballantine et al. 2000, Teichert 2014).

Past studies link the high biodiversity generally associated with rhodolith beds to the structural complexity of the habitat they provide (Hinojosa-Arango 2004, Gabara et al. 2018). This functional aspect of rhodolith beds is especially important given that they normally form over comparatively featureless sedimentary bottom. Rhodolith beds also act as nursery ground for several ecologically and economically importance species (Foster 2001, Riosmena-Rodriguez et al. 2017) by enhancing larval settlement of specific molluscs (Hinojosa-Arango 2004, Gabara et al. 2018), echinoderms (Pearce & Scheibling 1990), corals (Heyward & Negri 1999), and sponges (Whalan et al. 2012).

Reports of rhodolith beds along the eastern Canada coast date back more then 60 y (Adey 1966, Bosence 1983). Newfoundland beds are essentially composed of *Lithothamnion glaciale* rhodoliths, a dominant species within the photic zone in subarctic environments (Adey & Hayek 2011). Past studies widely acknowledge the ecological importance of rhodolith beds as a biodiversity hotspot (Foster 2001). However, few studies have described spatiotemporal variations in rhodolith bed structure and associated macrofaunal assemblages, and even fewer studies have focused on cold water environments.

Our study builds on previous work by Gagnon et al. (2012), who provided a general description of rhododith abundance and mophology as well as the diversity of rhodolith-associated macrofauna in two subarctic beds from southeastern Newfoundland (Canada) including one located off St. Philip's. Here we use seasonal surveys that combined rhodolith collections and underwater imagery to quantify spatiotemporal variation in structural complexity and associated biodiversity in the St. Philip's bed. By sampling the bed in spring, summer, fall, and winter at two different sites during one year, we tested the hypotheses that: 1) seafloor composition and rhodolith abundance and morphology are temporally stable due to prevailing low hydrodynamic forces and sedimentation rate at the study site, but vary spatially within the bed, 2) the abundance and diversity of rhodolith-associated macrofauna vary with total rhodolith volume per surface area, and 3) macrofaunal assemblages vary spatially within rhodolith bed structure, and seasonally with macrofauna life cycles.

4.3. MATERIALS AND METHODS

4.3.1. Study sites

We studied a rhodolith bed located off St. Philip's on the eastern shore of Conception Bay, Newfoundland, Canada (see Figure 1 in Millar and Gagnon, 2018 for a map and image of the bed).

The steep rocky shoreline at this location extends into the ocean to ~10 m depth before grading into a gently sloping sedimentary bottom interspersed with rocky outcrops protruding up to two meters above the seabed. From 12 to 20 m, rhodoliths occur in high density over the sedimentary sections of the seafloor. We selected two sites on the basis of noticeable differences in rhodolith morphology. The first site (SP15, 47.5933° N, 52.8926° W) was located at a depth of 15-17 m in the middle section of the bed. It was partially enclosed by low (≤ 50 cm) rocky outcrops, and densely covered with spheroidal rhodoliths with no visible signs of nucleation (Figure 4.1A, B). The second site (SP18, 47.5936° N, 52.8919° W), ~ 50 m away, was located at a depth of 18-20 m near the deeper limit of the bed. This location was almost entirely enclosed by high (~2 m) rocky outcrops, with dense coverage by two types of rhodoliths: 1) spheroidal rhodoliths with no observable signs of nucleation (e.g. no visible pebbles or shells in the rhodoliths structure), and 2) bladed rhodoliths built around horse mussel (*Modiolus modiolus*) shell nuclei (Figure 4.1B).

4.3.2. Habitat structure and faunal diversity

In 2013, we carried out four seasonal surveys at both sites at ~3-month intervals to quantify spatial and temporal variations in rhodolith bed habitat structure and rhodolith-associated macrofaunal assemblages. Sampling took place when sea temperatures were at their annual minimum (early spring), maximum (early fall), and intermediate (early summer and early winter) (see Table 4.1 for sampling dates). Sampling consisted of a combination of video transects and rhodolith collections carried out by scuba divers.

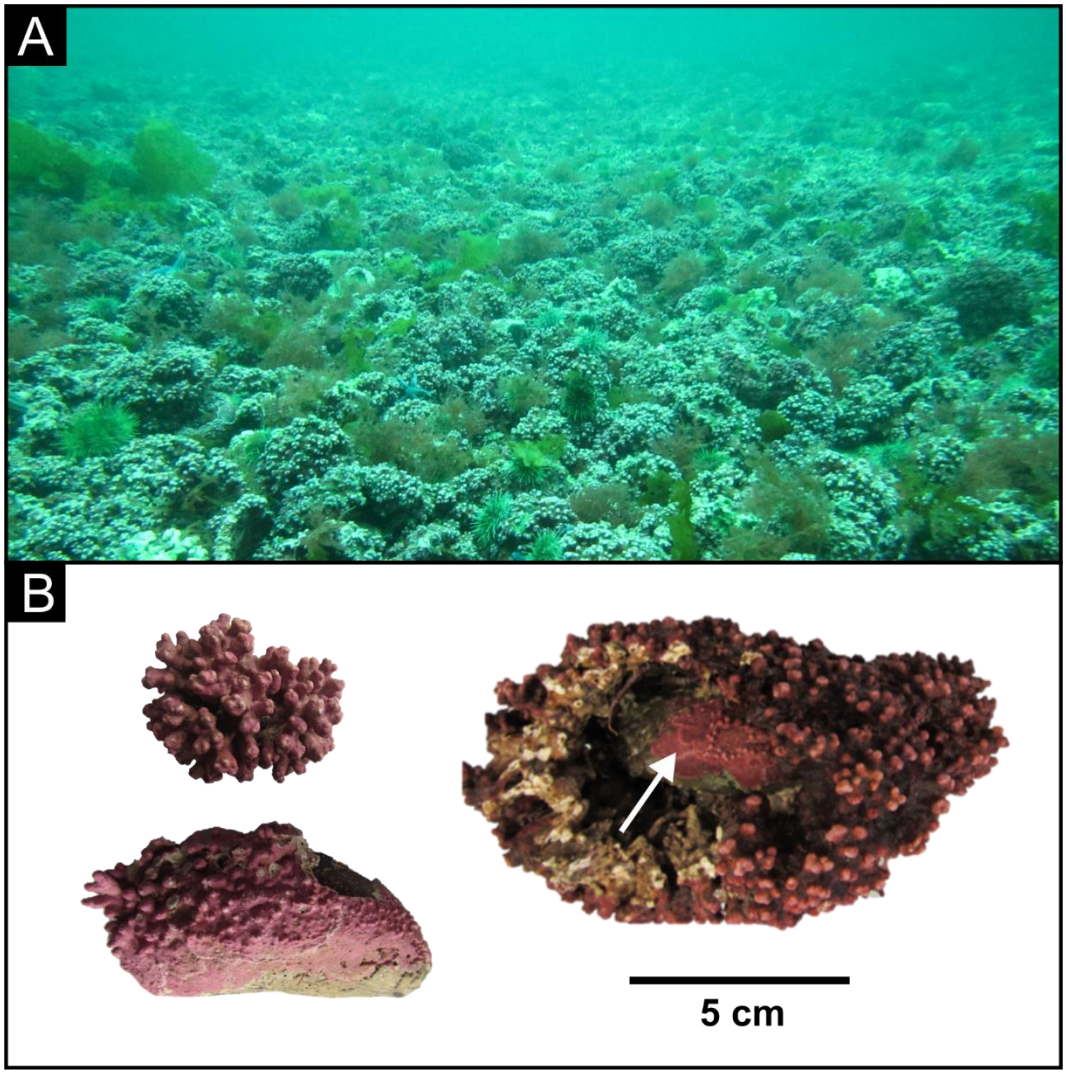

Figure 4.1. (A) St. Philip's rhodolith bed (Newfoundland, Canada). (B) Non-nucleated compact rhodoliths (top left), bladed mussel-shell nucleated rhodolith (bottom left), and large (~12 cm across), partially fragmented mussel-shell nucleated rhodolith (right) with the shell nucleus (white arrow) in the center.

4.3.2.1. Seafloor composition

During each seasonal survey, we deployed three 20-m transects haphazardly ~4 m apart in the middle of each site and filmed both sides of each transect with a submersible video camera system (Sony HDV 1080i/MiniDV with an Amphibico Endeavor housing) equipped with a scaling bar and propelled by a diver at a fixed height (1.5 m) above the seabed. We then converted videos to sequential, non-overlapping frames with the VLC media player 2.2.3 (VideoLan Organization) and randomly selected 20 frames from each transect. Using ImageJ (U.S. National Institutes of Health), we randomly placed a 0.5 x 1 m rectangle on each frame and superimposed grid points with 10-cm spacing. The type of sea bottom encountered under each of the 50 points within the 0.5 m^2 rectangle was assigned to one of six seafloor type categories: live rhodoliths, dead rhodoliths, dead shells, sediment, pebble, and cobble. Live/dead rhodoliths consisted of pigmented/unpigmented (i.e. purple/white) rhodoliths. Dead shell consisted of entire of large fragments of dead bivalve shells, almost exclusively horse mussel shells. The sediment category consisted of coarse carbonate sands dominated by dead rhodolith fragments < 0.4 cm. We categorized rocks with maximum diameter of 4-64 mm and 65-256 mm mm as pebble and cobble, respectively, following the Wentworth scale for grain size classification (Wentworth 1922). Together, these six categories covered the entirety of the seafloor types encountered in the two studied sites. By summing seafloor type occurrences across the 20 randomly selected frames, we estimated seafloor composition for each filmed transect.

Table 4.1. Dates at which video transects and rhodolith collections were carried out at the two sites (SP15 and SP18) and four seasons (spring, summer, fall and winter) in the St. Philip's rhodolith bed.

Season	Station	Sampling date
Spring	SP15	14 Mar, 2013
	SP18	4 Mar, 2013
Summer	SP15	17 Jun, 2013
	SP18	10 Jun, 2013
Fall	SP15	17 Sep, 2013
	SP18	1 Oct, 2013
Winter	SP15 & SP18	15 Dec, 2013

4.3.2.2. Rhodolith abundance and morphology

After videotaping the transects (see section 4.3.2.1) for each seasonal survey, divers collected all rhodoliths within three 30 x 30 cm quadrats placed on the right side of each transect at 2, 10 and 18 m marks for a total of 72 quadrats (3 quadrats x 3 transects x 2 sites x 4 collections). Placing quadrats at predetermined distances along haphazardly deployed transects prevented bias in choosing sampling location. All rhodoliths laying on top of sediment within each quadrat were placed in separate sealed plastic bags filled with seawater, brought to surface, and transported to the Ocean Science Center (OSC). Upon arrival at the OSC, we transferred bags containing rhodolith samples into large flow-through tanks supplied with ambient seawater pumped from the adjacent embayment (Logy Bay) at a depth of ~ 5 m. We replaced the water content of each bag three times per day to keep organisms alive throughout the ~48 h necessary to process all samples.

For each quadrat sample, we counted all rhodoliths and measured their longest [L], intermediate [I] and shortest [S)] axes to determine their size and shape. We estimated the volume of each rhodolith based on the following equation:

$$V = \frac{4}{3}\pi abc \qquad (4)$$

where V describes the volume of an ellipsoid, *a* denotes the radius of the longest axis (L/2), *b* denotes the radius of the intermediate axis (I/2), and *c* is the radius of the shortest axis (S/2). We used ternary diagrams created with the open source software TRIPLOT (https://www.lboro.ac.uk/microsites/research/phys-geog/tri-plot/index.html) developed by Graham and Midgley (2000) and based on the work by Sneed and Folk (1958) on particle shapes to visualize variation in rhodolith shape distribution: 1) within and between the two sites, and 2)

among non-nucleated, pebble-nucleated, and shell-nucleated rhodoliths. The software uses mathematical relationships between the three rhodolith axes [S/L, I/L, and (L-I)/L-S)] to calculate the proportion of rhodoliths within each of ten shape classes ranging from compact, to platy, bladed, and elongate shapes. We then carefully fragmented all rhodoliths into ~2-cm^3 pieces to determine the presence and the type of nucleus (pebble or shell). By oven drying the fragments at 40 °C to constant weight after removing all macrofauna, we determined total rhodolith biomass per quadrat (see "Diversity of rhodolith-associated macrofaunal" below).

4.3.2.3. Diversity of rhodolith-associated macrofauna

For each quadrat sample, we inspected rhodolith fragments and extracted all visible macrofauna. We then transferred the fragments into a 5-L bucket filled with filtered sea water, manually stirred for ~1 min to dislodge remaining macrofauna, and poured the content onto a sieve stack composed of one 5-mm mesh sieve to retain rhodolith fragments, placed atop a 500-µm sieve to retain macrofauna. The material collected in the 500-µm sieve was preserved in a 4% formaldehyde.

We sorted macrofauna from each sample into twelve taxonomic groups (Ophiuroidea, Asteroidea, Echinoidea, Holothuroidea, Polyplacophora, Gastropoda, Bivalva, Polychaeta, Crustacea, Porifera, Nemertea and Sipuncula) and measured the total wet weight for each group after gently blotting the samples. We chose to express macrofaunal biomass in wet weight rather than dry weight in order to preserve samples integrity for future studies. We then identified and tallied all organisms to the lowest possible taxonomic rank. Because of time constraints associated with identification of high numbers of small and often immature specimens we identified polychaetes to family level. However, using one randomly chosen sample per site and per season

(n = 8 samples), we produced a list of all identifiable polychaete species. Sponge specimens collected in the samples were highly fragmented and could only be tallied as present or absent.

Morphological similarities among collected rhodoliths and DNA-based identification performed on two specimens suggested that rhodoliths in the St. Philip's bed were monospecific and composed of *Lithothamnion gaciale*. We used American Seashells (Abbott 1974) as the main guide for mollusc identification. We used detailed identification keys by Pettitbone (1963), Fauchald (1977), Appy et al. (1980), and Pocklington (1989) to identify polychaetes families and species. Amphipods were identified by professionals. We used field guides by Gosner (1978), Pollock (1998), Abbott & Morris (2001), and Squires (1990) to complete macrofaunal identification.

4.3.3. Statistical analysis

4.3.3.1. Habitat structure

We used a two-way permutational multivariate analysis of variance (PERMANOVA) (Anderson 2001) with fixed factors Site (SP15 and SP18) and Season (spring, summer, fall, and winter) to compare spatial and seasonal variability in: 1) seafloor composition based on six seafloor types: live rhodoliths, dead rhodoliths, dead shells, sediment, pebbles, and cobbles (n = 24: 3 transects x 2 sites x 4 seasons); and 2) rhodolith shapes based on four shapes: compact [i.e. compact, compact-platy, compact-bladed, and compact-elongate classes], platy [plate and very-platy], bladed [bladed and very-bladed], and elongate [elongate and very elongate] (n = 72: 9 quadrats x 2 sites x 4 seasons). We used a negative binomial regression (Quinn & Keough 2002) with the fixed factor Site (SP15 and SP18), to compare rhodolith density (counts per quadrat) between the two sites. A negative binomial (rather than Poisson distribution) distribution

accounted for the overdispersed rhodolith counts data. We used two one-way ANOVAs, each with the fixed factor Site (SP15 and SP18), to compare 1) rhodolith biomass, and 2) total rhodolith volume per quadrat between sites (n = 72 for each ANOVA: 2 sites x 9 quadrats per sites x 4 collections). Two binomial regressions (Quinn & Keough 2002) with the fixed factor Site, enabled comparison of: 1) the proportion of nucleated rhodoliths (nucleated or non-nucleated), and 2) the proportion of each nucleus type (pebble or shell) between sites (n = 72 each: 2 sites x 9 quadrats per sites x 4 collections). We used one two-sample Kolmogorov-Smirnov (KS) test (Sokal & Rohlf 2012) to compare the cumulative distributions of rhodolith sizes between SP15 (n = 2489) and SP18 (n = 2802).

4.3.3.2. Density, biomass, and diversity of rhodolith-associated macrofauna

As rhodolith volume increase, so does the available space available for colonization by macrofauna both on the outer and inner surfaces between branches. Therefore, we included rhodolith volume as an explanatory term in our analyses on macrofaunal biomass, diversity, and density. We used two analyses of covariance (ANCOVA), each with fixed factors Site (SP15 and SP18) and Seasons (spring, summer, fall, and winter) and covariate Volume (total rhodolith volume per quadrat) to compare macrofaunal biomass and diversity (Shannon diversity index) between sites and among seasons. We used negative binomial regressions to model overdispersed macrofaunal count data with fixed factors Site (SP15 and SP18) and Season (spring, summer, fall, and winter) to compare macrofaunal density between sites and among seasons. PERMANOVAs detected differences in macrofaunal assemblages between sites and among seasons. We applied all of these statistical analyses to all taxa pooled, and to each of four taxonomic subsets: Echinodermata, Polychaeta, Mollusca, and Crustacea (n = 72 each).

For all ANOVAs and ANCOVAs, we verified homogeneity of variance and normality of the residuals by examining the distribution and normal probability plot of the residuals, respectively (Snedecor & Cochran 1989). Tukey HSD multiple comparison tests based on least-square means detected differences among levels within a factor. All statistical analyses were carried out with R 3.6.1 R (Core Team 2019). We used R packages MASS and VEGAN to fit GLMs (binomial and negative binomial regressions) and PERMANOVA models, respectively. PERMANOVAs were based on Bray-Curtis dissimilarity for square-root transformed data. We used pairwise comparisons to detect differences among levels within factors and similarity percentage (SIMPER) analyses with 9999 permutations to identify taxa that significantly contributed to overall between-group dissimilarity. For PERMANOVA and SIMPER analyses, we used a significance level of 1% ($\alpha = 0.01$) as recommended by Manly (1997) for > 4500 permutations. All other analyses used a 5% significance level ($\alpha = 0.05$). We present all means with standard errors (mean ± SE) unless stated otherwise.

4.4. RESULTS

4.4.1. Rhodolith bed habitat structure

4.4.1.1. Seafloor composition

Of the seafloor types, live rhodolith and sediment were encountered most frequently, with mean percent cover of 63% and 23% respectively. Dead rhodoliths followed with 9% surface cover, pebbles (3.6%), dead shells (2.4%), and cobbles (< 1%). PERMANOVA showed significant spatial variation in seafloor composition (Table 4.2, Figure 4.2) and SIMPER analysis identified the lower percent cover of dead shell at SP15 compared to SP18 as the only significant contributor to the 11% dissimilarity between the two sites (Table D.1, Appendix D). Seafloor composition also varied between spring and winter (Table 4.2, Figure 4.2) with higher percent cover of

Table 4.2. Summary of permutational multivariate analysis of variance (PERMANOVA), based on Bray-Curtis dissimilarity for square-root transformed count data, examining the effect of (A) the fixed factors Site (SP15 and SP18) and Season (spring, summer, fall, and winter) on seafloor type percent cover based on six categories: live rhodoliths, dead rhodoliths, sediment, pebble, and mussel shell), and (B), the effect of the fixed factor Site (SP15 and SP18) on rhodolith shape distribution based on ten shape classes: compact, compact-platy, platy, very-platy, compact-bladed, bladed, very-bladed, compact-elongate, elongate, very-elongate. All analyses were performed on balanced design using Type I sums of squares and a 1% significance level ($\alpha = 0.01$).

Source of variation	df	MS	Pseudo-*F*	*p*(perm)
A. Seafloor type				
Site	1	0.025	7.717	< 0.001
Season	3	0.010	3.080	0.003
Site x Season	3	0.005	1.381	0.211
Residuals	16	0.003		
Total	23			
B. Rhodolith shape				
Site	1	0.132	2.984	0.033
Season	3	0.106	3.988	0.015
Site x Season	3	0.014	0.325	0.097
Residuals	64	0.044		
Total	71			

p-values obtained using 9999 permutations.

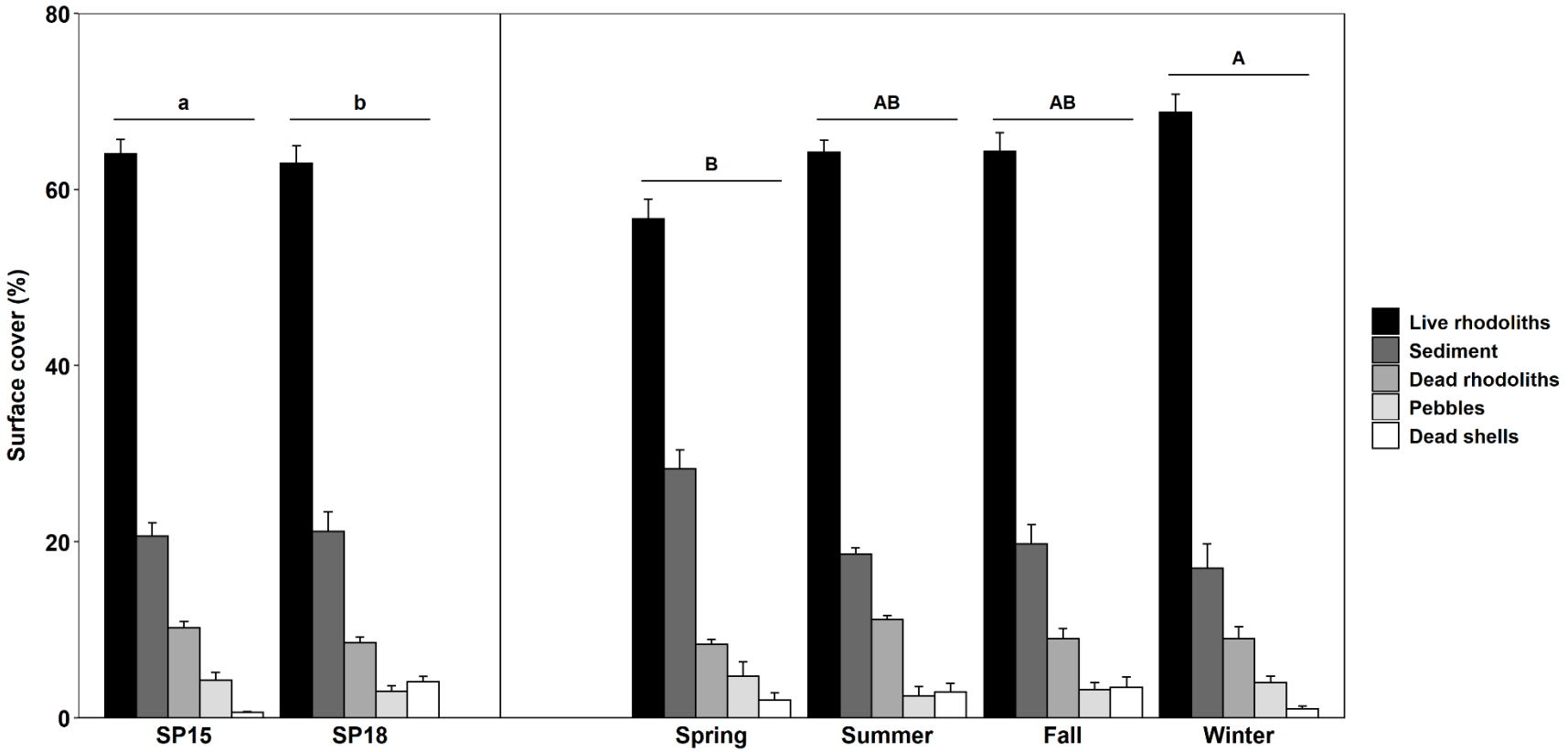

Figure 4.2. Variation in mean surface cover (± SE) of different seafloor types between the two sampling sites (data pooled across seasons, n = 12 per station), and among the four sampling seasons (data pooled across stations; n = 6 per season). Group of bars with different letters indicate significant differences in seafloor composition between sites (SP15 and SP18) or among seasons ($p < 0.05$).

sediment, along with lower percent cover of live rhodolith in spring compared to winter as the only two significant contributors to the 11% dissimilarity between the two seasons (Table D.1, Appendix D).

4.4.1.2. Rhodolith abundance and morphology

Rhodolith density and biomass did not differ significantly between sites or among seasons, averaging 74 ± 4 rhodoliths quadrat^{-1} and 1.039 ± 0.042 kg quadrat^{-1}, respectively (Tables 4.3 and 4.4, Figure 4.3A, B). Rhodolith size distribution also varied spatially (K-S test, $D = 0.079$, $p < 0.001$). Rhodoliths ranged in size from 0.6 to 527.2 cm^3 at SP15, and from 0.2 to 392.0 cm^3 at SP18, corresponding to a mean rhodolith size 1.4 times higher at SP15 (25.6 ± 0.87 cm^3) than at SP18 (18.8 ± 0.54 cm^3). Despite similar rhodolith size distributions at both sites for the 5-50 cm^3 size classes, the proportion of smaller (< 5 cm^3) and larger (> 50 cm^3) rhododoliths was 7% lower and 5% higher at SP15 than at SP18, respectively (Figure 4.4). Total rhodolith volume per 30 x 30 cm quadrat (0.09 m^{-2}) averaged 1.4 times higher at SP15 (25 600 cm^3) than at SP18 (18 800 cm^3) but did not vary seasonally (Table 4.4, Figure 4.3C).

The proportion of nucleated rhodoliths was similar at both sites (Table 4.3), averaging 18 ± 1% at SP15, and 20 ± 2% at SP18 (Figure 4.5). Nuclei consisted of either small pebbles (< 2 cm across), or entire or fragmented horse mussel (*Modiolus modiolus*) shells except for one gastropod shell and one small (~2 cm) piece of wood. The proportion of the two main nucleus types (pebble and dead shell), however, significantly differed between sites with 12% more pebble-nucleated, and 14% fewer shell-nucleated rhodoliths at SP15 compared to SP18 (Table 4.4, Figure 4.5).

Table 4.3. Analysis of deviance (ANODEV) tables for (A) negative binomial regression examining the effect of fixed factors Site (SP15 and SP18) and Season (spring, summer, fall, and winter) on rhodolith density, and for (B) and (C) binomial regressions examining the effect of the fixed factor Site (SP15 and SP18) on rhodolith nucleation (nucleated and non-nucleated) and nucleus type (pebble-nucleated and shell-nucleated), respectively. All analyses were performed on balanced design using Type I sums of squares and a 5% significance level ($\alpha = 0.05$).

Tested parameter	GLM family	Source	df	Dev	Resid.*df*	Resid. Dev	*p* (>Chi)
A. Rhodolith density	Negative binomial	Null			71	82.642	
		Site	1	1.768	70	80.874	0.184
		Season	3		67	75.048	0.120
		Site x Season	3		64	73.126	0.589
B. Rhodolith nucleation	Binomial	Null			71	218.220	
		Site	1	0.134	70	218.090	0.715
C. Nucleus type	Binomial	Null			71	624.350	
		Site	1	463.930	70	160.410	< 0.001

Null = null model (intercept only); Resid. *df* = residual degrees of freedom; Resid. Dev = residual deviance

Table 4.4. Summary of two-way ANOVAs examining the effect of fixed factors Site (SP15 m and SP18 m) and Seasons (spring, summer, fall, and winter) on (A) the biomass of *Lithothamnion glaciale* rhodoliths, and (B) total rhodolith volume per quadrat 30 x 30 cm quadrat (0.09 m^2). All analyses were performed on balanced design using Type I sums of squares and a 5% significance level ($\alpha = 0.05$).

Source	df	A. Rhodolith biomass			B. Total rhodolith volume		
		MS	F-value	*p*	MS	F-value	*p*
Site	1	6299	0.053	0.821	1663151	4.547	0.037
Season	3	893920	2.448	0.072	400282	1.094	0.358
Site x Season	3	383279	1.050	0.377	202501	0.554	0.648
Residuals	64	7790578			365747		
Total	71						

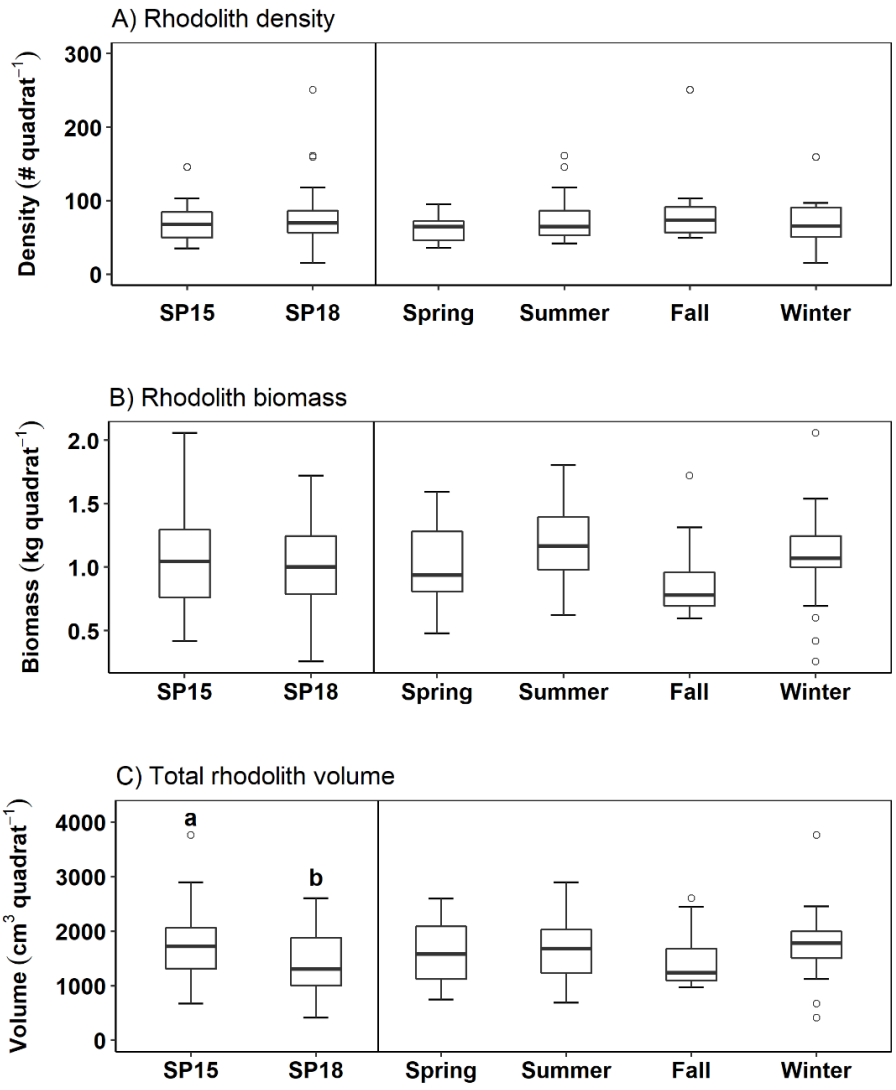

Figure 4.3. Boxplots of (A) rhodolith density, (B) rhodolith biomass, and (C) total rhodolith volume per 30 cm x 30 cm quadrats (0.09 m^2) at sampling sites SP15 and SP18 (data pooled across seasons, n = 36 per site) and on each seasonal collection (data pooled across sites, n = 18 per season). Lower and upper box boundaries represent the interquartile range (IQR: 25th to 75th percentiles, respectively), line inside the box represents the median, and lower and upper error bars extend to the lowest and highest values within 1.5 x IQR, respectively. Open circles represent outliers. Boxplots with different letters indicate statistically different means ($p < 0.05$).

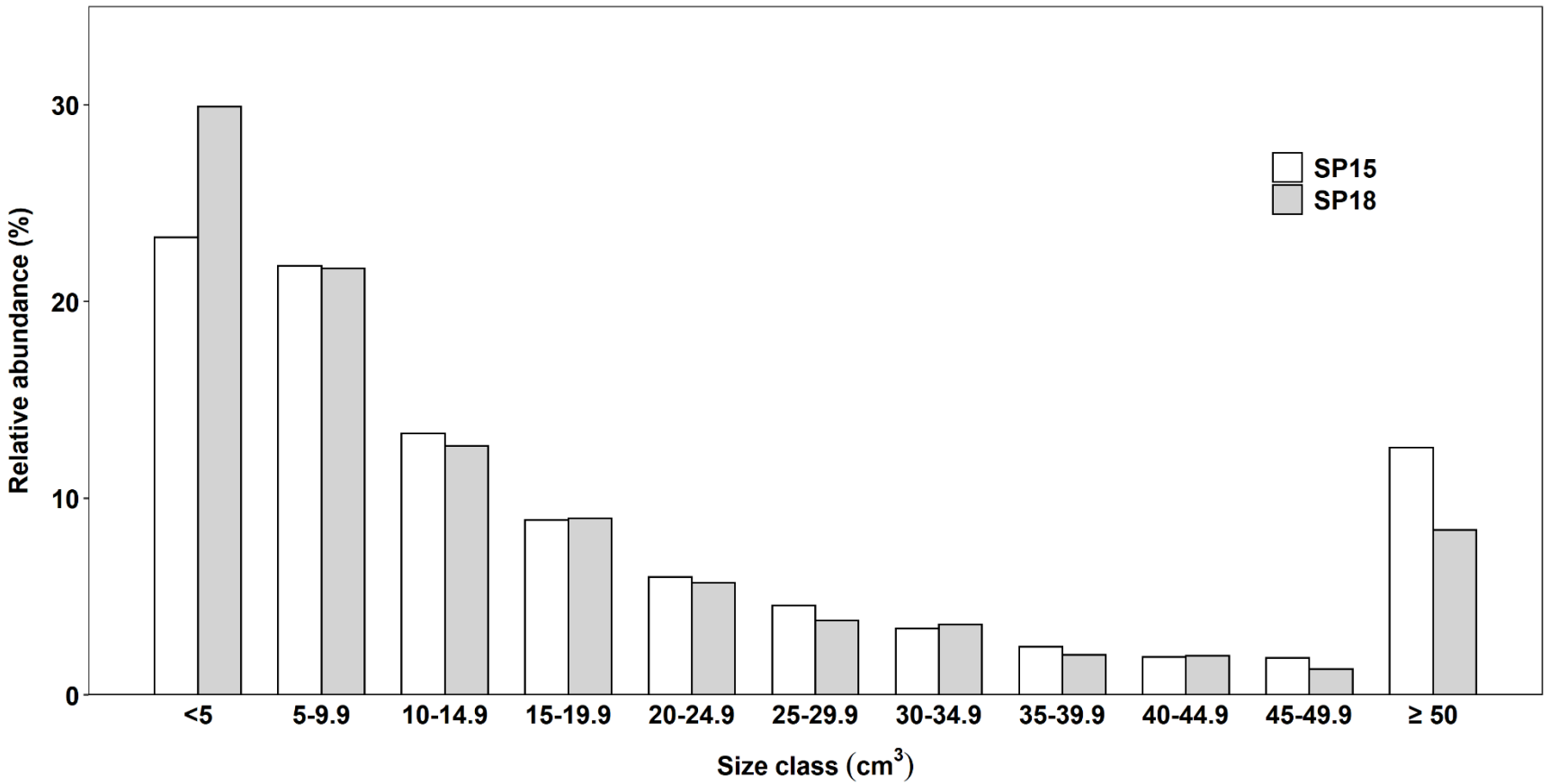

Figure 4.4. Relative abundance of rhodoliths per 5-cm^3 size class intervals at the two sampling sites. Relative abundances were calculated using all rhodoliths collected during the four seasonal surveys at SP15 (n = 2849) and SP18 (n = 2805).

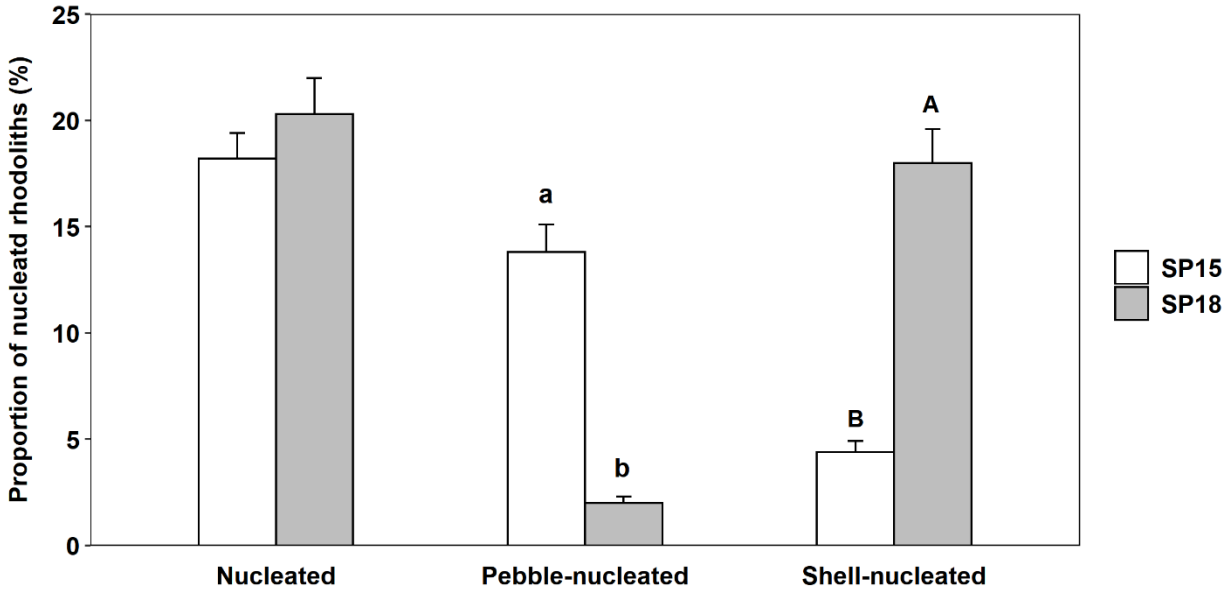

Figure 4.5. Mean proportion (+SE) of nucleated rhodoliths and main nucleus type at the two sampling sites (n = 36 for each station). Bar with different letters differ statistically ($p < 0.05$).

Large (≥ 50 cm^3) rhodoliths were 47% nucleated at SP15, including 34% pebble-nucleated rhodoliths. At SP18, the proportion of large nucleated rhodoliths increased to 68%, including 61% shell-nucleated rhodoliths.

Compact shapes (i.e. rhodoliths in any one of the four compact shape classes) dominated SP15 (73%) and SP18 (62%) rhodoliths, followed by bladed (bladed and very-bladed; 16% and 22%), elongate (elongate or very-elongate; 6% and 9%), and platy (platy or very-platy; 5% and 6%) shapes (Figure 4.6A, B). PERMANOVA analysis, showed no significant differences in the distribution of rhodolith shape (compact, elongate, bladed and platy) between sites or among seasons (Table 4.2).

Rhodoliths distribution among shape classes was similar in non-nucleated and pebble-nucleated rhodoliths with compact shapes dominating, followed by bladed, elongate, and platy shapes (Figure 4.7). Elongate shapes were nonetheless 5% more abundant in pebble-nucleated than non-nucleated rhodoliths (Figures 4.6, 4.7). Shell-nucleated rhodoliths were predominantly bladed or elongate (79%), whereas compact shapes were the least represented (9%) (Figures 4.6, 4.7). The proportion of very-bladed and very-elongate shapes were 32% and 16% higher in shell-nucleated than in non-nucleated or pebble-nucleated rhodoliths, respectively (Figures 4.6, 4.7).

4.4.2. Rhodolith-associated macrofauna

4.4.2.2. All taxa

We identified a total of 53, 172 macrofaunal species, from 109 taxa (Table E.1, Appendix E). Echinoderms and molluscs numerically dominated macrofaunal abundance accounting for 39 and 34% of total specimens, respectively.

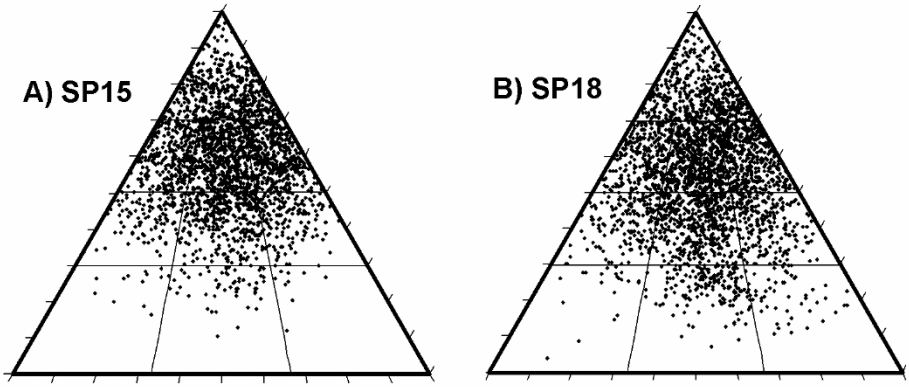
A) SP15
B) SP18

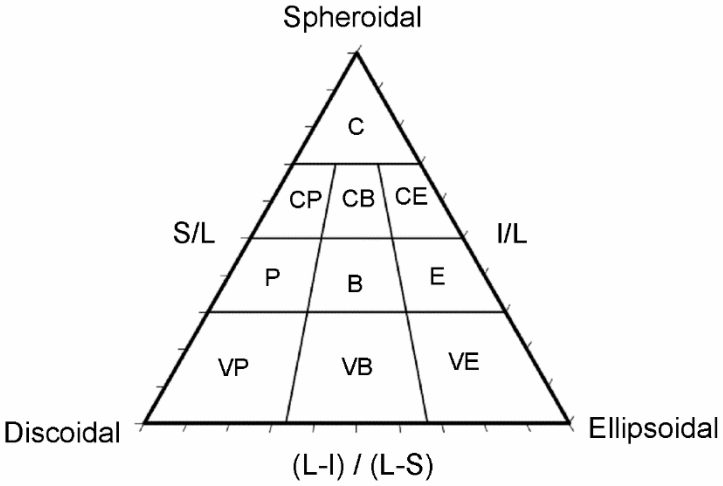
Spheroidal
C
CP
CB
CE
S/L
I/L
P
B
E
VP
VB
VE
Discoidal
Ellipsoidal
(L-I) / (L-S)

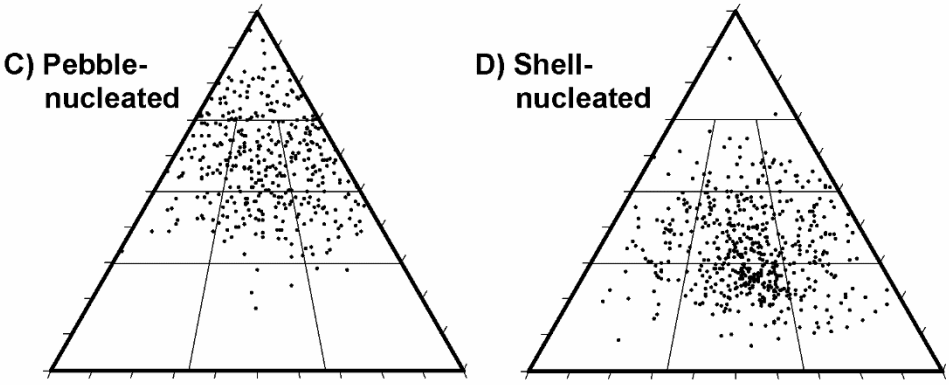
C) Pebble-nucleated
D) Shell-nucleated

Figure 4.6. Ternary diagrams showing the distribution of rhodoliths among the ten shape classes (compact [C], compact-platy [CP], compact-bladed [CB], compact-elongate [CE], platy [P], bladed [B], elongate [E], very-platy [VP], very-bladed [VB], very-elongate [VE]) defined by Sneed & Folk (1958) at (A) sampling site SP15 (n = 2489) and (B) sampling site SP18 (n = 2802), and for (C) pebble-nucleated rhodoliths (n = 383), and (D) shell-nucleated rhodoliths (n = 538). Rhodoliths at SP15 and SP18 were pooled across seasons (spring, summer, fall, and winter). Pebble- and shell-nucleated rhodoliths were pooled across sites and seasons.

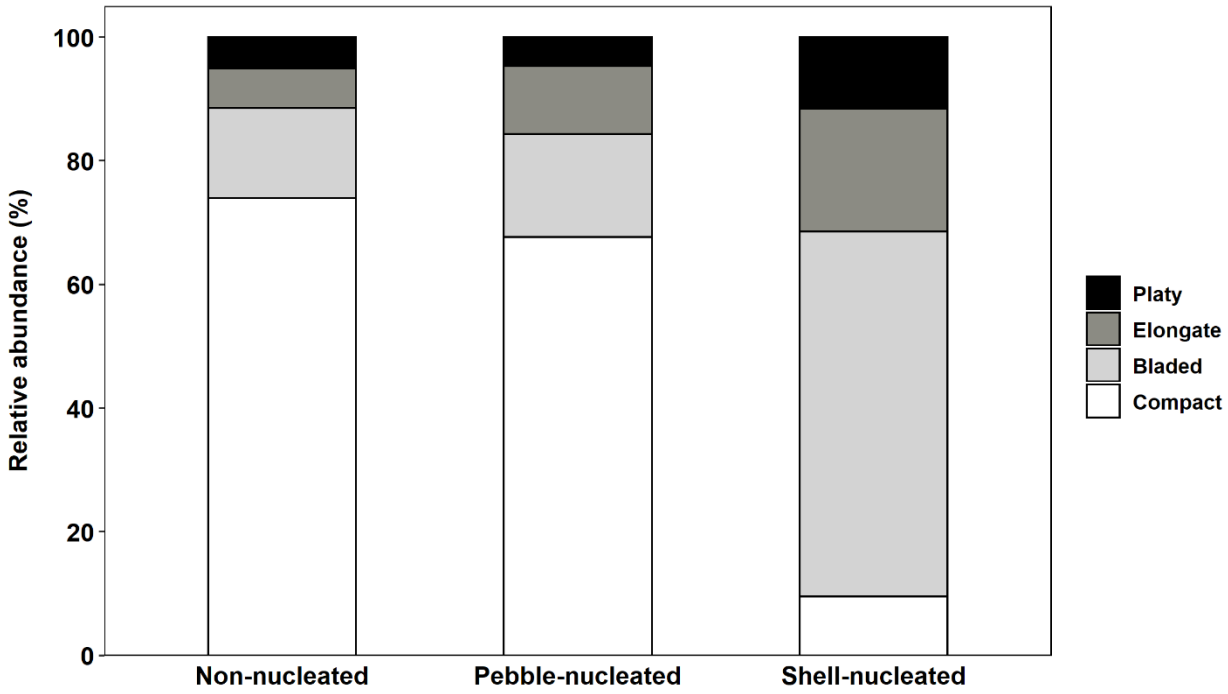

Figure 4.7. Relative abundance of each of four rhodolith shape categories (Platy: platy and very-platy; Elongate: elongate and very-elongate; Bladed: bladed and very-bladed; Compact: compact, compact-platy, compact-bladed, and compact-elongate) for non-nucleated (n = 4371), pebble-nucleated rhodoliths (n = 383) and shell-nucleated (n = 538) rhodoliths (data pooled across sites [SP15 and SP18] and seasons [spring, summer, fall, and winter]).

Polychaetes and crustaceans accounted for 13% and 7% of total abundance, respectively, followed by nematodes (3%), nemerteans, and sipunculids (1.3% each). Tunicates, Platyhelminthes, and cnidarians also occurred in low abundance. Total macrofaunal density ranged from 91 to 2216 and averaged 739 ± 42 ind. quadrat^{-1}.

Macrofaunal density increased with total rhodolith volume per surface area at a similar rate at both sites, but a lower rate in summer compared to spring and winter (Table 4.5; Figure 4.8A, 4.9A). Total macrofaunal biomass ranged from 3.53 g to 103.84 g per quadrat and did not vary with rhodolith volume (Table 4.6, Figure 4.10A). Biomass per quadrat was 1.6 times higher at SP15 (31.2 ± 2.7 g) than at SP18 (19.6 ± 2.7 g), and 2.5 times higher in spring (32.3 ± 3.7 g) than in summer (12.9 ± 3.1 g). Diversity of rhodolith-associated macrofauna (Shannon index) increased with total rhodolith volume per surface area at SP15 but decreased with increasing rhodolith volume at SP18 (Table 4.7, Figure 4.11A).

PERMANOVA indicated differences in macrofaunal assemblages between SP15 and SP18 (Table 4.8, Figure 4.12A), and SIMPER analysis identified 24 taxa (nine crustaceans, five molluscs, six polychaetes, one nematode, one sipunculid, and one cnidarian) that contributed significantly to the 32% dissimilarity between the two sites (Table D.2, Appendix D)**.** Assemblages also varied seasonally (Table 4.8, Figure 4.13A) with eight taxa (three molluscs, two polychaetes, one crustacean, one nematode, and one tunicate) contributing to the 30% dissimilarity between summer and fall, and six taxa (four crustaceans, one polychaete, and one mollusc) contributing to 32% dissimilarity between summer and winter (Table D.2, Appendix D).

Table 4.5. Analysis of deviance (ANODEV) tables for negative binomial linear models (applied to non-transformed count data) examining the effect of fixed factors Site (Si: SP15 and SP18) and Season (Se: spring, summer, fall, and winter), and and the covariate Volume (V: total rhodolith volume per 30 x 30 cm quadrat) on macrofaunal density for (A) all macrofaunal taxa, and for each of four taxonomic subsets: (B) Mollusca, (C) Echinodermata, (D) Polychaeta, and (E) Crustacea. All analyses were performed on balanced design using Type I sums of squares and a 5% significance level ($\alpha = 0.05$).

			A. All taxa			B. Mollusca			C. Echinodermata		
Source	df	Res *df*	Dev	Res Dev	*p* (>Chi)	Dev	Res Dev	*p* (>Chi)	Dev	Res Dev	*p* (>Chi)
Null		71		259.711			243.878			220.572	
V	1	70	153.255	106.457	< 0.001	133.625	110.253	< 0.001	113.090	107.482	< 0.001
St	1	66	0.186	88.755	0.666	0.739	85.807	0.390	3.975	95.062	0.046
Se	3	67	17.516	88.941	< 0.001	23.707	86.546	< 0.001	8.445	99.038	0.038
V x St	1	62	0.284	73.100	0.594	0.237	74.071	0.627	4.199	74.112	0.040
V x Se	3	63	15.371	73.384	0.002	11.499	74.308	0.009	16.752	78.311	0.001

			D. Polychaeta			E. Crustacea		
Source	df	Res *df*	Dev	Res Dev	*p* (>Chi)	Dev	Res Dev	*p* (>Chi)
Null		71		177.725			155.608	
V	1	70	77.553	100.172	< 0.001	38.246	117.363	< 0.001
St	1	66	0.735	77.105	0.391	31.156	78.887	< 0.001
Se	3	67	22.232	77.840	< 0.001	7.319	110.043	0.062
V x St	1	62	0.240	74.374	0.624	0.771	74.167	0.380
V x Se	3	63	2.491	74.615	0.477	3.949	74.939	0.267

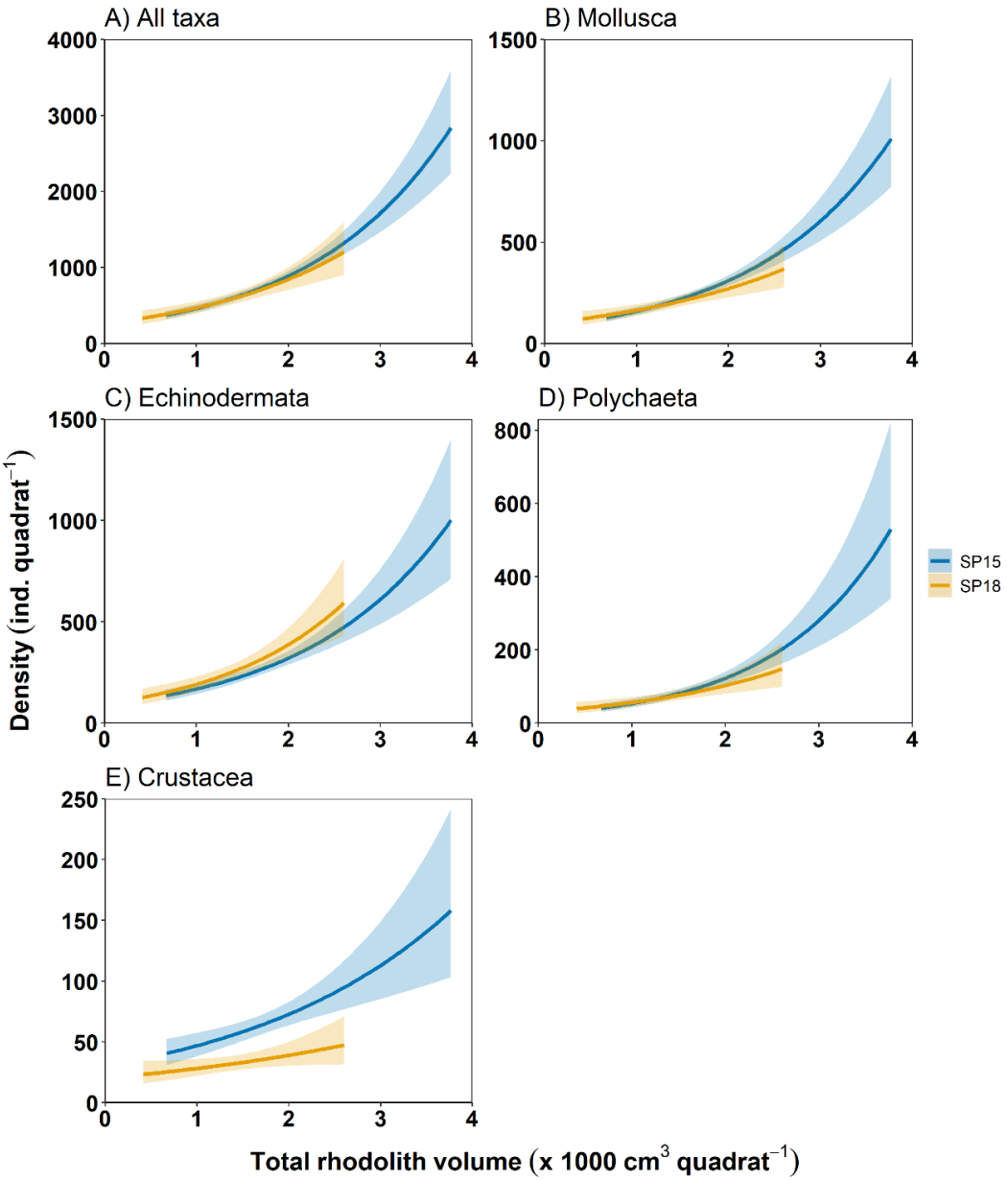

Figure 4.8. Relationship between macrofaunal density and total rhodolith volume per 30 x 30 cm quadrat (0.09 m^{-2}) at the two sampling sites (SP15 and SP18) for (A) all macrofaunal taxa, and for each of four taxonomic subsets: (B) Mollusca, (C) Echinodermata, (D) Polychaeta, and (E) Crustacea (n = 36 for each). Lines indicate negative bionomial regression (± SE) applied to macrofaunal counts.

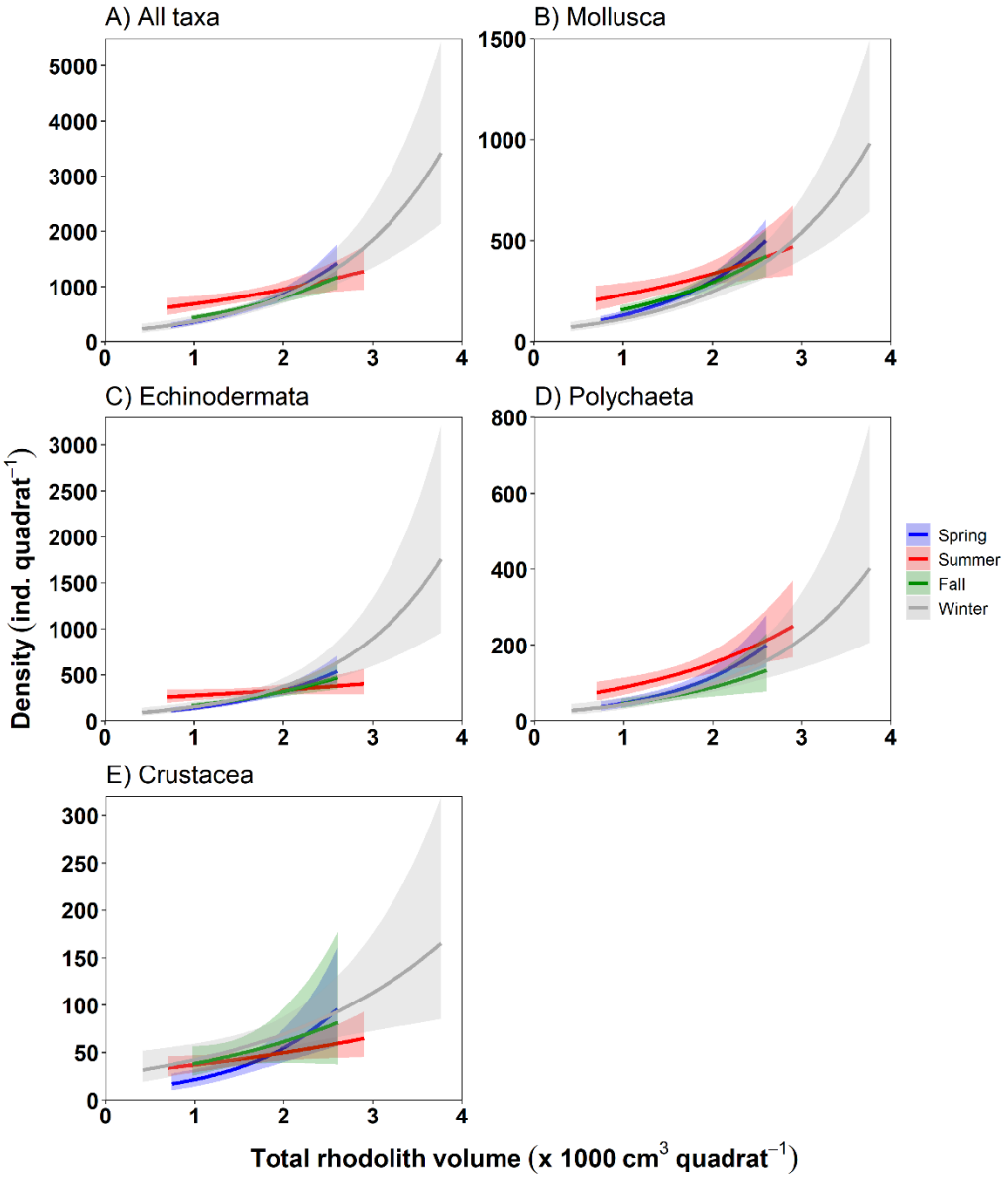

Figure 4.9. Relationship between macrofaunal density and total rhodolith volume per 30 x 30 cm quadrat (0.09 m^{-2}) during each sampling season (spring, summer, fall, and winter) for (A) all macrofaunal taxa, and for each of four taxonomic subsets: (B) Mollusca, (C) Echinodermata, (D) Polychaeta, and (E) Crustacea (n = 18 each). Lines indicate negative bionomial regression (± SE) applied to macrofaunal counts.

Table 4.6. Summary of ANCOVA examining the effect of fixed factors Site (Si: SP15 and SP18) and Season (Se: spring, summer, fall, and winter), and the covariate Volume (V: total rhodolith volume per 30 x 30 cm quadrat) on rhodolith-associated macrofaunal biomass (wet weight) of (A) all macrofaunal taxa, and for each of four taxonomic subsets: (B) Mollusca, (C) Echinodermata, (D) Polychaeta, and (E) Crustacea. All analyses were performed on balanced design using Type I sums of squares and a 5% significance level ($\alpha = 0.05$).

		A. All taxa			B. Mollusca			C. Echinodermata		
Source	df	MS	F	p	MS	F	p	MS	F	p
V	1	0.24	0.001	0.975	0.007	0.001	0.971	0.85	0.005	0.944
Si	1	1879.92	7.844	0.007	75.059	14.880	< 0.001	1101.46	6.494	0.013
Se	3	771.79	3.220	0.029	22.189	4.399	0.007	488.35	2.879	0.043
V x Si	1	22.11	0.092	0.762	1.563	0.310	0.580	12.04	0.071	0.791
V x Se	3	393.77	1.643	0.189	3.361	0.666	0.576	287.86	1.697	0.177
Resid	62	239.68			5.044			169.62		
Total	71									

		D. Polychaete			E. Crustacea		
Source	df	MS	F	p	MS	F	p
V	1	0.472	0.847	0.361	0.000	0.097	0.756
Si	1	0.860	1.545	0.219	0.007	1.635	0.206
Se	3	1.661	2.983	0.038	0.005	1.034	0.384
V x Si	1	0.012	0.022	0.883	0.001	0.208	0.650
V x Se	3	0.897	1.611	0.196	0.001	0.322	0.810
Resid	62	0.557			0.004		
Total	71						

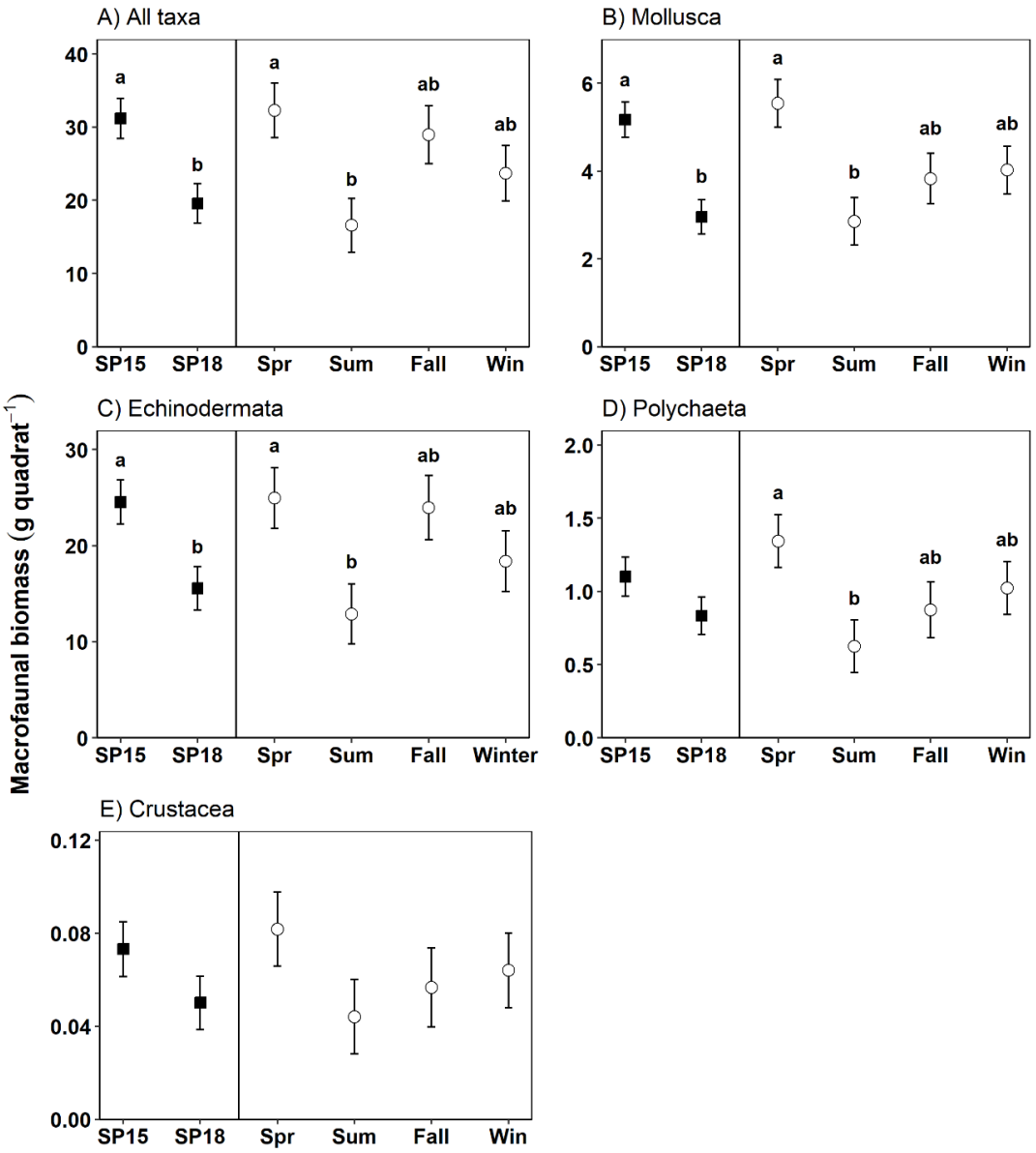

Figure 4.10. Rhodolith-associated macrofaunal biomass (± SE) per sampling site (SP15 and SP18; n = 36 each) and season (spring [Spr], summer [Sum], fall [Fall], and winter [Win]; n = 18 each). Mean biomasses represent least square means derived from linear models (see section 4.3.2.3 for details on linear models) applied to biomass data for (A) all macrofaunal taxa, and for each of four taxonomic subsets of the data: (B) Mollusca, (C) Echinodermata, (D) Polychaeta, and (E) Crustacea. Station (solid squares) or seasons (open circles) with different letters differ statistically ($p < 0.05$).

Table 4. 7. Summary of ANCOVA examining the effect of fixed factors Site (SP15 and SP18) and Season (spring, summer, fall, and winter), and covariate Volume (total rhodolith volume per 30 x 30 cm quadrat) on Shannon diversity index (H) for (A) all macrofaunal taxa, and for each of four taxonomic subsets: (B) Mollusca, (C) Echinodermata, (D) Polychaeta and (E) Crustacea. All analyses were performed on balanced design using Type I sums of squares and a 5% significance level ($\alpha = 0.05$).

		A. All taxa			B. Mollusc			C. Echinodermata		
Source	df	MS	F	*p*	MS	F	*p*	MS	F	*p*
V	1	0.000	0.000	0.997	0.112	7.201	0.009	0.007	0.547	0.462
Si	1	0.419	18.222	< 0.001	0.047	3.035	0.086	0.097	7.461	0.008
Se	3	0.033	1.441	0.239	0.475	10.176	< 0.001	0.043	3.350	0.025
V x Si	1	0.172	7.493	0.008	0.006	0.398	0.531	0.003	0.267	0.607
V x Se	3	0.023	0.982	0.407	0.093	2.002	0.123	0.020	1.560	0.208
Resid	62	0.023			0.964			0.013		
Total	71									

		D. Polychaete			E. Crustacea		
Source	df	MS	F	*p*	MS	F	*p*
V	1	0.066	1.768	0.189	0.000	0.000	0.989
Si	1	0.131	3.499	0.066	0.002	0.030	0.864
Se	3	0.142	3.796	0.015	0.342	4.470	0.007
V x Si	1	0.023	0.628	0.431	0.016	0.210	0.648
V x Se	3	0.034	0.914	0.440	0.139	1.823	0.152
Resid	62	0.037			0.077		
Total	71						

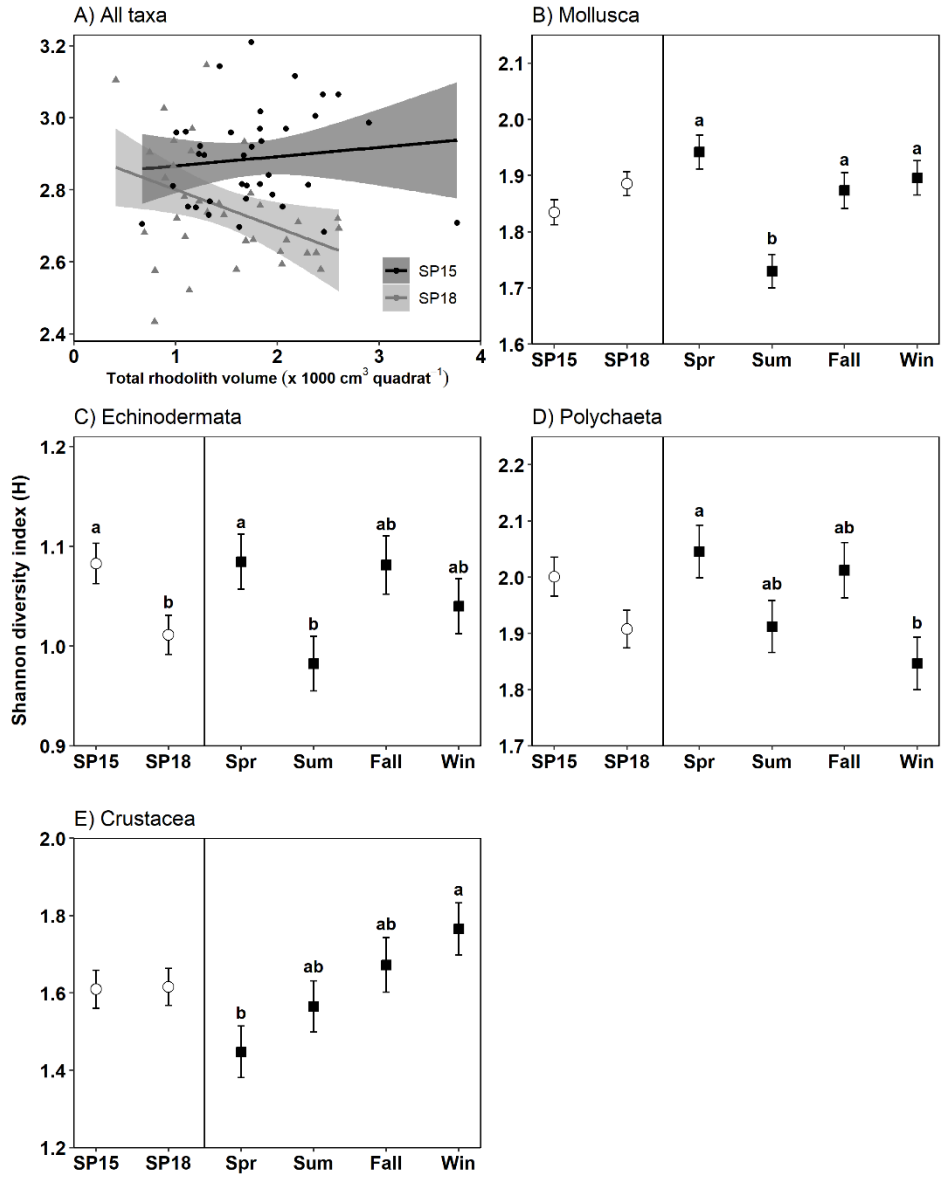

Figure 4.11. (A) Relationship (± SE) between diversity of rhodolith-associated macrofauna and total rhodolith volume per 30 x 30 cm quadrat (0.09 m^{-2}) for all identified taxa (88 taxa) and (B) to (E) mean (± SE) diversity per sampling site (SP15 and SP18; n = 36 each) and season (spring [Spr], summer [Sum], fall [Fall], and winter [Win]; n = 18 each). Mean diversity indices represent least square means derived from linear models applied to (A) all macrofaunal taxa, and for each of four taxonomic subsets: (B) Mollusca, (C) Echinodermata, (D) Polychaeta, and (E) Crustacea. Station or seasons with different letters differ statistically ($p < 0.05$).

Table 4.8. Summary of permutational multivariate analysis of variance (PERMANOVA) based on Bray-Curtis dissimilarity measure for square-root transformed data examining the effect of fixed factors Site (SP15 and SP18) and Season (spring, summer, fall, and winter), and covariate Volume (total rhodolith volume per quadrat) on assemblage dissimilarity for (A) all macrofaunal taxa, and for each of four taxonomic subsets: (B) Mollusca; (C) Echinodermata; (D) Polychaeta and (E) Crustacea. All analyses were performed on balanced design using Type I sums of squares and a 1% significance level ($\alpha = 0.01$).

		A. All (88 taxa)			B. Molluscs (32 taxa)			C. Echinoderm (7 taxa)		
Source	df	MS	Pseudo-*F*	*P*(perm)	MS	Pseudo-*F*	*P*(perm)	MS	Pseudo-*F*	*P*(perm)
V	1	1.717	31.711	< 0.001	0.789	0.789	< 0.001	0.626	38.671	< 0.001
Si	1	0.264	4.880	< 0.001	0.148	0.148	< 0.001	0.028	1.736	0.163
Se	3	0.230	4.242	< 0.001	0.417	0.139	< 0.001	0.174	1.074	0.371
Resid	66	0.054			1.918	0.291		0.162		
Total	71									

		D. Polychaete (21 taxa)			E. Crustaceans (22 taxa)		
Source	df	MS	Pseudo-*F*	*P*(perm)	MS	Pseudo-*F*	*P*(perm)
V	1	0.846	14.678	< 0.001	0.294	3.674	0.004
Si	1	0.177	3.069	0.001	0.772	9.650	< 0.001
Se	3	0.158	2.740	0.001	1.102	13.767	< 0.001
Resid	66	0.058			0.080		
Total	71						

p-values obtained using 9999 permutations.

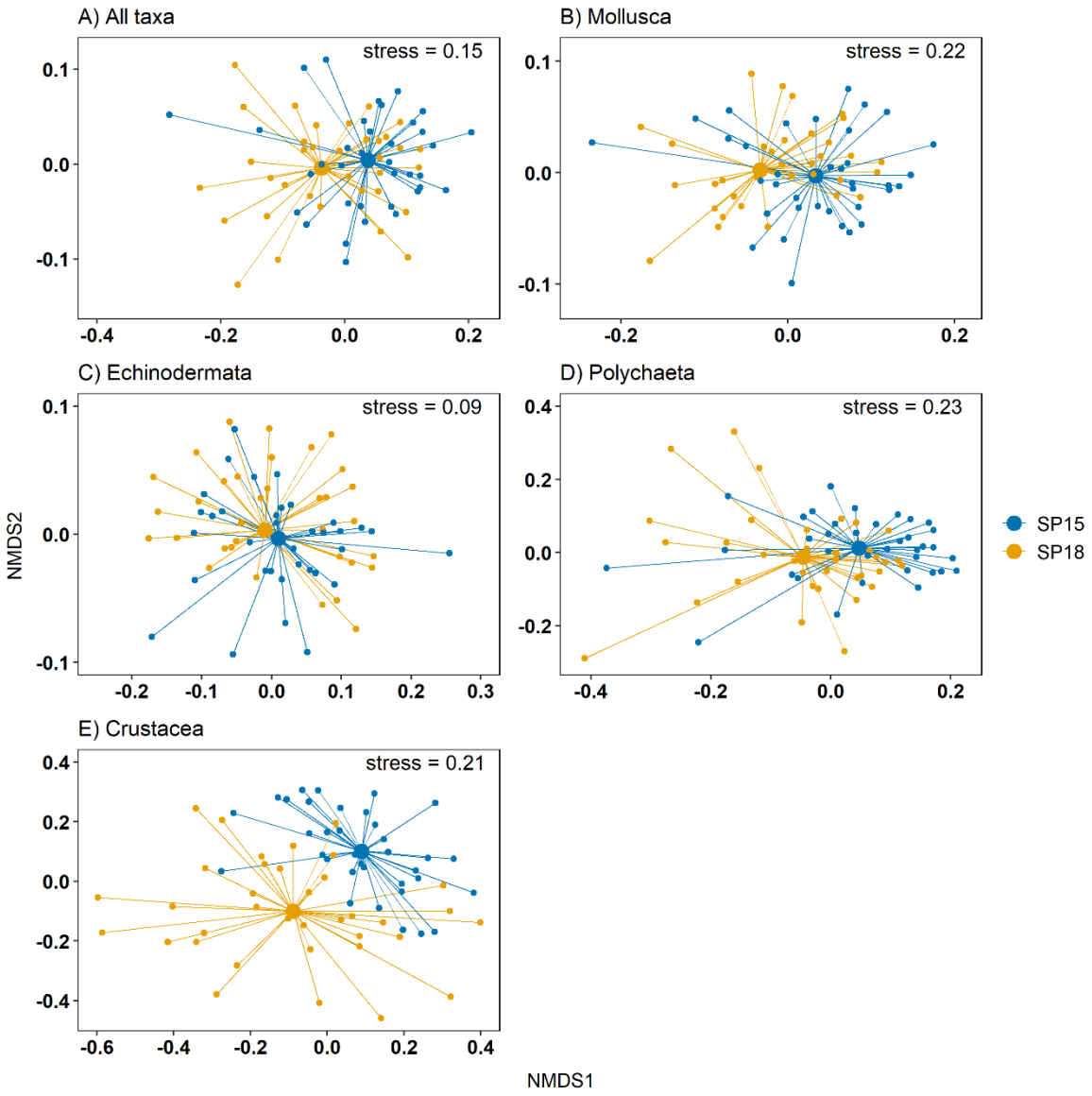

Figure 4.12. NMDS plots showing spatial dissimilarities in macrofaunal assemblage between sampling sites (SP15 and SP18) for (A) all macrofaunal taxa [88 taxa], and for each of four taxonomic subsets: (B) molluscs [31 taxa], (C) echinoderms [7 taxa], (D) polychaetes [21 taxa], and (E) crustaceans [27 taxa]. Smaller dots represent samples, and larger solid circles in the center of each cluster represent site centroids. All NMDS are based on Bray–Curtis dissimilarities of square-root transformed data. Stations or Seasons that share different letters differ significantly ($p < 0.05$).

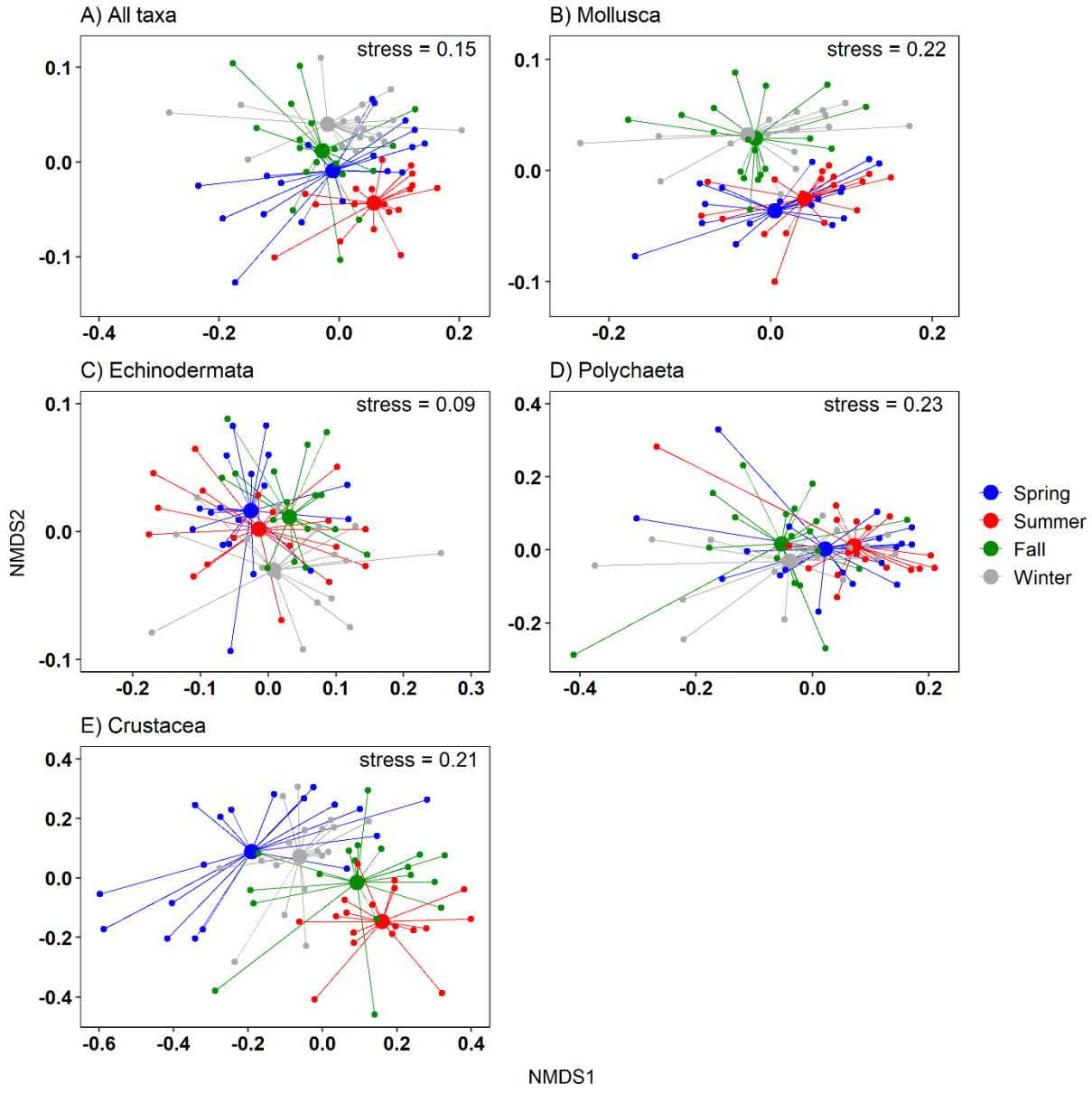

Figure 4.13. NMDS plots showing seasonal dissimilarities in macrofaunal assemblage for (A) all macrofaunal taxa [88 taxa], and for each of four taxonomic subsets: (B) molluscs [31 taxa], (C) echinoderms [7 taxa], (D) polychaetes [21 taxa], and (E) crustaceans [27 taxa]. Smaller dots represent samples and larger solid circles in the center of each cluster represent group season centroids. All NMDS are based on Bray–Curtis dissimilarities of square-root transformed data. Stations or Seasons that share different letters differ significantly ($p < 0.05$).

4.4.2.3. Molluscs

We identified 32 mollusc taxa (Table D.3, Appendix D). Chitons numerically dominated abundance, accounting for 50% of total collected mollusc, followed by gastropods (31%), and bivalves (19%). The mottled red chiton *Tonicella marmorea* was the most abundant mollusc species. Linné's puncturella (*Puncturella noachina)*, the ribbed moelleria (*Moelleria costulata*), the northern rosy margarite (*Margarites costalis*), and *Boreocingula castanea* were the most abundant gastropods, whereas bivalve abundance was dominated by the wrinkled rock borer *Hiatella arctica.* Mollusc density averaged 251 ± 14 ind. quadrat^{-1} and increased with total rhodolith volume per surface area at a similar rate at SP15 and SP18, but at a lower rate in summer compared to winter and spring (Table 4.5, Figures 4.8B, 4.9B).

Molluscs made up 16% of total macrofaunal biomass and did not vary with total rhodolith volume per surface area. Biomass per quadrat was 1.7 times higher at SP15 (5.2 ± 0.4 g) than at SP18 (3.0 ± 0.4 g), and 1.9 times higher in spring (5.5 ± 0.5 g) than in summer (2.9 ± 0.5 g) (Table 4.6, Figure 4.10B). Chitons, bivalves, and gastropods accounted for 48%, 44%, and 8% of total mollusc biomass, respectively. Mollusc diversity did not vary with total rhodolith volume per surface area or between sites but was significantly lower in summer than in other seasons (Table 4.7, Figure 4.11B). PERMANOVA indicated significant spatial differences in mollusc assemblages (Table 4.8, Figure 4.12B) and SIMPER analysis identified six taxa that contributed significantly to the 30% dissimilarity between SP15 and SP18 (Table D.3, Appendix D). Mollusc assemblages also varied seasonally (Table 4.8, Figure 4.13B) with 3 taxa contributing to 28% dissimilarity between summer and fall (Table D.3, Appendix D).

4.4.2.4. Echinoderms

We identified 7 echinoderm taxa: two brittle stars, one sea urchin, two sea stars, and two sea cucumbers (Table E.1, Appendix E). Brittle stars accounted for 86% of total echinoderms, followed by sea urchins (9%) and sea stars (5%). *A. rubens* dominated sea stars, whereas *C. papposus* accounted for < 1% of sea star abundance. Our sampling collected only 29 sea cucumbers. Echinoderm density averaged 295 ± 20 ind. quadrat^{-1}, increasing with total rhodolith volume per surface at a lower rate at SP15 than SP18, and in summer compared to spring (Table 4.5, Figures 4.8C, 4.9C).

Echinoderms accounted for 79% of the total macrofaunal biomass, with brittle stars accounting for 81% of total echinoderm biomass, followed by sea urchins (16%) and sea stars (3%). All sea cucumbers collected during the study were small (<1 cm) individuals at early developmental stages, accounting for < 0.1% of the biomass. Mean biomass per quadrat was 1.6 times higher at SP15 (24.5 ± 2.3) than at SP18 (15.6 ± 2.3), and 1.4 times higher in spring (18.4 ± 3.1) than summer (25.0 ± 3.1); biomass did not vary with total rhodolith volume per surface area (Table 4.6, Figure 4.10C). Echinoderm diversity also did not vary with total rhodolith volume per surface area but was significantly higher at SP15 than at SP18, and in spring compared summer (Table 4.7, Figure 4.11C). PERMANOVA analysis showed no spatial or seasonal variation in echinoderm assemblages (Table 4.8, Figures 4.12C, 4.13C).

4.4.2.5. Polychaetes

We identified 39 polychaete taxa from 21 families (Table E.1, Appendix E). The family Sabellidae accounted for 33% of total polychaetes, followed by Terebellidae (15%), Cirratulidae (13%), Orbiniidae (9%), and Phyllodocidae (9%). Maldanidae, Capitellidae, Spionidae, Syllidae,

Flabelligeridae and Nereididae were also common, each accounting for 2-5% of total collected specimens. All families occurred at both sites and in all seasons except for Glyceridae which was only present at SP15 in spring and summer, and Paraonidae which occurred only at SP15 in summer and fall (Table E.1, Appendix E). Polychaete density increased with total rhodolith volume per surface area at a similar rate at both sites and in all seasons but averaged 1.6 times higher in summer (133 ± 16 ind. quadrat^{-1}) than in other seasons (84 ± 8 ind. quadrat^{-1}) (Table 4.5, Figures 4.8D, 4.9D).

Polychaetes accounted for 4% of total macrofaunal biomass. Mean biomass per quadrat averaged 0.9 ± 0.1 g and did not vary with total rhodolith volume per surface area nor between sites. Nonetheless, biomass was 2.2 times higher in spring (1.3 ± 0.2 g) than in summer (0.6 ± 0.2 g) (Table 4.6, Figure 4.10D). Polychaete diversity did not vary with total rhodolith volume per surface area and was similar at both sites, but higher in spring than in winter (Table 4.7, Figure 4.11D). PERMANOVA indicated significant spatial differences in polychaete assemblages (Table 4.8, Figure 4.12D) and SIMPER analysis identified six families (Cirratulidae, Orbiniidae, Phyllodocidae, Scalibregmidae, Glyceridae, and Paraonidae) that contributed significantly to 37% dissimilarity between SP15 and SP18 (Table D.4, Appendix D). Assemblages also varied seasonally (Table 4.8, Figure 4.13D) with only one family (Arenicolidae) contributing significantly to 38% dissimilarity between summer and spring (Table D.4, Appendix D).

4.4.2.6. Crustaceans

We identified 23 crustacean taxa from five classes: Amphipoda, Isopoda, Decapoda, Copepoda, and Ostracoda (Table E.1, Appendix E). Amphipods accounted for 39% of total crustaceans, followed by harpacticoid copepods (35%), isopods (14%), ostracods (7%), and

decapods (5%). At 80% of the total, *Dexamine thea* dominated amphipod abundance. *C. bonelli*. *Hardametopa carinata. Deflexilodes tesselatus, Pontogeneia inermis* and *Pleusymtes glaber* were also common, and each contributed 2-7% of amphipod abundance. *Munna* sp. comprised 98% of isopods, whereas Hippolytidae shrimp represented 90% of decapods. Crustacean density increased with total rhodolith volume per surface area at a similar rate at both sites and all seasons but averaged 1.2 times higher at SP15 (54 ± 6 ind. quadrat^{-1}) than SP18 (46 ± 5 ind. quadrat^{-1}) (Table 4.5, Figure 4.8E, 4.9E).

Crustaceans accounted for only 0.2% of total macrofaunal biomass, averaging 0.06 ± 0.02 g quadrat^{-1}), and did not vary with total rhodolith volume per surface area, nor between sites or among seasons. (Table 4.6, Figure 4.10E). Crustacean diversity was similar at both sites but higher in spring than in summer (Table 4.7, Figure 4.11E). PERMANOVA indicated significant spatial variation in crustacean assemblages (Table 4.8, Figure 4.12E) and SIMPER analysis identified seven taxa that significantly contributed to 50% dissimilarity between SP15 and SP18. Crustacean assemblages also varied among all seasons (Table 4.8, Figure 4.13E). Five taxa contributed significantly to 57% dissimilarity between spring and summer, three taxa to 47% dissimilarity between spring and fall, three taxa to 47% dissimilarity between summer and winter, and two taxa to 43% dissimilarity between fall and winter. No taxa contributed significantly to 47% dissimilarity between spring and winter, nor to 44% dissimilarity between summer and fall (Table D.5, Appendix D).

Nematodes, sipunculids, and nemerteans occurred at both sites and in all seasons (Table E.1, Appendix E). Nematode density averaged 20 ind. quadrat $^{-1}$, which was ~2 times more than for sipunculids and nemerteans. Although sipunculids and nematodes contributed negligibly to macrofaunal biomass (< 0.02 g quadrat^{-1}), nemertean biomass 0.14 ± 0.01 g quadrat^{-1} which was

~2 times higher than for crustaceans. One sponge genus (*Sycon* sp.) also occurred at both sites and in all seasons, along with fragments of other indeterminate sponge species (Table E.1, Appendix E). We could not accurately determine sponge density from fragmented specimens, but biomass ranged from 0 to 0.64 and averaged 0.09 ± 0.01 g quadrat^{-1}.

4.5. DISCUSSION

Seasonal surveys indicated that the St. Philip's rhodolith bed offer a structurally stable habitat to a diverse macrofaunal community at depth of 15-20 m. Rhodolith density and biomass did not vary seasonally nor spatially but differences in seafloor composition between the two study sites was reflected in rhodolith morphology with more shell-nucleated rhodolith at deeper (SP18) compared the shallower (SP15) site. Macrofaunal density was positively related with total rhodolith volume per surface area. Contrasting relationship between the diversity of rhodolith-associated macrofauna and total rhodolith volume per surface area at SP15 (positive relationship) and SP18 (negative relationship) was presumably due to differences in rhodolith morphology, more specifically to nucleus types, between the two sites. Crustaceans were responsible for most of the seasonal dissimilarity in rhodolith-associated macrofaunal assemblages.

4.5.1. Rhodolith bed structure

4.5.1.1. Seafloor composition

Seasonal variation in seaflor composition suggested a reorganization of the rhodolith matrix over time as reported in beds elsewhere (Steller & Foster 1995, Pascelli et al. 2013). Millar and Gagnon (2018), however, concluded that hydrodynamic forces at depth ≥ 12 in the St. Philip's bed were insufficient to move rhodoliths, and they demonstrated that benthic bioturbators such as sea urchins and sea stars play an important role in rhodolith movement. James (2000), reported

that sea urchins could transport rhodoliths over ~20 m d^{-1}. During the first week of March 2013, (approximately 1 week before the first rhodolith survey) a major storm affected Conception Bay. The storm moved 15-kg concrete blocks located at 10-m depth near SP15 several meters (see Chapter II for effects of storm on experimental setup). Hydrodynamic forces at 15-17 m were likely sufficient to move and concentrate rhodoliths into areas of reduced bottom flow, thus exposing the underlying sedimentary bottom. Gradual dispersion of rhodoliths by bioturbators in the months following the storm may explains the overall 12% increase in live rhodolith cover concurrent with an 11% decrease in sediment cover over the 9 months separating the spring and winter surveys.

4.5.1.2. Rhodolith abundance and morphology

Rhodolith density at SP15 (15-17 m) and SP18 (18-20) m was comparable to that reported by Gagnon et. (2012) for a shallower (8-10 m) section of the same bed, and to those reported for tropical Brazilian beds at depth between 5 and 15 m (Bahia et al. 2010, Pascelli et al. 2013). Densities 4 to 26 times lower have been reported by several authors (Riul 2008, Avila & Riosmena-Rodríguez 2011, Amado-Filho et al. 2012), but few studies report higher densities (up to ~14 times) (Steller et al. 2003, Bahia et al. 2010). Rhodolith density along an 8-20 m depth gradient in St. Philip's were similar to those reported by Riul et al. in 2008, who also found density differences between 10 and 20 m. However, other studies report increasing (Bahia et al. 2010), or decreasing (Amado-Filho et al. 2007, Pascelli et al. 2013) rhodolith densities with increasing depth. In protected waters, *L. glaciale* often dominates among coralline algae from the low intertidal to the photic limit, with peak abundance peak between 15 and 25 m (Adey & Hayek 2011). We therefore anticipated its high abundance within the depth range covered by our study.

Rhodolith biomass did not significantly vary between the two sites despite a higher proportion of larger rhodoliths at SP15 compared to SP18. Biomass at 15-20 m was, however, ~2 times lower than the biomass reported by Gagnon et al. (2012) at 8-10 m in the same bed for a similar density, suggesting that rhodolith size generally decreases with increasing depth. Several studies also reported a similar trend in coastal waters (Steller & Foster 1995, Riul 2008, Bahia et al. 2010, Pascelli et al. 2013). Our study found that more than half of the larger ($\geq$ 50 cm^3) rhodoliths were nucleated. Similarly, a New Zealand study reported that all rhodoliths > 60 mm across were pebble-nucleated (Basso et al. 2009), suggesting the importance of rhodolith genesis in explaining size and shape distribution.

More than 60% of rhodoliths at SP15 and SP18 were compact, i.e. mostly spheroidal. Several previous authors report the predominance of compact shapes (Amado-Filho 2007, Basso et al. 2009, Bahia et al. 2010, Avila & Riosmena-Rodríguez 2011, Teichert et al. 2012, Gagnon et al. 2012, Pascelli et al. 2013), which appears to be a general feature of rhodolith beds worldwide. Although we detected no significant variation in the abundance of compact, platy, bladed, and elongate rhodolith shapes between the two sites, the proportion of compact shapes averaged 10% lower, and the proportion of bladed and elongate shapes 9% higher, at the shallow site (SP15) compared to the deep (SP18) site. A similar trend of fewer compact shapes and more flattened and elongate with increasing depth was reported in Brazilian beds by Bahia et al. (2010) from 15 and 25 m, and by Amado-Filho et al. (2007) from 4 to 55 m. Previous studies suggest that spheroidal shapes result from frequent overturning, whereas flattened shapes typify calmer environments (Bosellini & Ginsburg 1971, Bosence 1983). Other authors concluded that rhodolith morphology cannot be used as indicators of energy conditions (Adey & MacIntyre 1973, Teichert et al. 2014). Prevalence of spheroidal shapes in environments with insufficient hydrodynamic forces to move

rhodoliths (Millar & Gagnon 2018) suggests that other factors influence rhodolith morphology. Shell-nucleated rhodoliths were predominantly bladed (59%) and elongate (20%), but seldom compact (10%). The higher proportion of dead shells on the sea bottom at SP18 likely produced comparatively more bladed and elongate shell-nucleated rhodoliths than at SP15. Small pebble nuclei had less impact on rhodolith shape than large shells. Pebble-nucleated rhodoliths nonetheless produced ~5% more elongate shapes than non-nucleated ones. Our results suggest that nucleation exerts greater control on rhodolith shape than hydrodynamic forces in the St. Philip's bed.

4.5.2. Rhodolith-associated macrofauna

4.5.2.1 Abundance and diversity

Echinoderms, molluscs, and polychaetes dominated the macrofaunal community numerically. Mean total density of > 8,000 ind. m^{-2} in the St. Philip's bed was 5 to 10 times higher than densities reported for Mediterranean (Bordehore et al. 2003, Sciberras et al. 2009) and Arctic (Teichert et al. 2012) beds, but comparable densities to those reported by Grall et al. (2006) from grab samples in Northeast Atlantic beds. Doyle et al. (2014) highlighted the importance of rhodolith beds as nursury habitats for brittle stars in the subarctic Northwest Atlantic. Suspension feeders comprised four of the six most abundant taxa in St. Philip's (brittle stars *Ophiura robusta* and *Ophiopholis aculeata*, sabellid polychaetes, and the bivalve *Hiatella arctica*), accounting for 44% of total abundance. Hily (1991) estimated that brittlestars density of ~2200 ind. m^{-2} significantly mitigated eutrophication effects by filtering ~30% of the total volume of the Bay of Brest daily. In our study, density of suspension feeders often surpassed 5000 ind. m^{-2}. Suspension feeders exert a natural control on eutrophication in shallow coastal by actively removing excess

phytoplankton from the water column (Officer et al. 1982). Consequently, our results highlight the potentially important ecological function of rhodolith beds as a natural eutrophication control in coastal waters.

Macrofaunal density related positively to total rhodolith volume per surface area in all taxonomic subsets. The small size of many macrofaunal organisms (< 1 cm) meant they could colonize interstices down to the core. Moreover, boring species such as the rock-boring clam *Hiatella arctica* and spionid polychaetes can colonize calcified tissues of rhodoliths (Brookes & Stevens 1985, Radashevsky & Pankova 2013). Therefore, internal space available to colonization increased with rhodolith volume in non-nucleated rhodoliths. Previous studies reported similar positive relationship between macrofaunal abundance and rhodolith volume in another Newfoundland bed (Gagnon et al. 2012), and in the Gulf of California (Steller et al. 2003, Foster et al. 2007).

At 80% of total macrofaunal biomass, molluscs and echinoderms dominated, at densities 1.6 times higher at Sp15 than at SP18. Biomass, in contrast to density, did not increase with rhodolith volume in any of the taxonomic subsets, indicating that mean organism size decreased with increasing density. Only cryptofauna can colonize rhodoliths' interstices down to their core whereas larger macrofauna such as brittle stars that dominated macrofaunal biomass often occurred on or near rhodolith surfaces. Given the exponential nature of the surface area to volume ratio of spheroidal objects such as rhodoliths, the internal space that macrofauna could colonize increased at a higher rate than the space near rhodolith surfaces normally occupied by large organisms, thus explaining why macrofaunal biomass did not increase significantly increase with total rhodolith volume per surface area, as we observed with density.

Higher biomass occurred in spring (March) than in summer (June) in all taxonomic subsets except crustaceans. Zhang et al. (2015) reported an increase in benthic suspension feeders and opportunistic/predatory taxa biomass during the phytoplankton spring bloom in the Northeast Atlantic followed by a rapid decline at the end of the bloom. Phytoplankton concentration generally begins to increase in early March in coastal waters around the study site and the spring bloom generally ends by June (Parrish et al. 2005, Maillet et al. 2019). Parrish et al. (2005) also reported a rapid transfer of high-energy material to the benthos during the spring bloom in Conception Bay, likely increasing benthic production. These results align with the ~50% decrease in rhodolith-associated macrofaunal biomass observed between spring (March) and summer (June).

We identified a total of 109 macrofaunal taxa, a number > 2 times more than richness reported for Arctic (Teichert et al. 2012) and sub-tropical (McConnico et al. 2017) beds. The positive relationship between diversity and rhodolith volume at SP15 aligns with observations from Foster et al. (2007) for Californian beds. In contrast, diversity at SP18 decreased with increasing rhodolith volume. Previous work links increased diversity to an increase in available habitat in structurally complex environments (Connor & McCoy 1979). Because volume increases exponentially with radius, the presence of a few large rhodoliths greatly impacts the total rhodolith volume per surface area. Because of their size, mussel-shell nuclei produce large rhodoliths. However, large and relatively smooth shell nuclei may decrease rhodolith internal structural complexity and reduce the amount and variety or microniches available for colonization by cryptofaunal organisms. Shell-nucleated rhodoliths were ~4 times more abundant at SP18 than at SP15, which may explain the negative relationship between diversity and total rhodolith volume at SP18.

4.5.2.3 Spatial and seasonal variation in macrofaunal assemblage

Total macrofaunal assemblage varied spatially, as did mollusc, polychaete, and crustacean assemblages. In all cases, higher faunal densities at SP15 than at SP18 largely drove assemblage dissimilarity. Fifteen of the 22 taxa that contributed significantly to spatial dissimilarity in total macrofaunal assemblages were 1.6 to 9 times more abundant at SP15 than at SP18 whereas six taxa were present at SP15 in low density. Echinoderm assemblages did not vary between SP15 (~15 m) and SP18 (~18 m), contrasting results from Gondim et al. (2014), who reported decreasing echinoderm abundance and richness along a 10 to 20 m gradient in Brazilian bed. However, only seven echinoderm taxa were present in St. Philip's compared to 32 for Gondim et al., and all occurred in relatively high densities at both sites, except for the common sun star *Crossaster papposus,* which we observed only occasionally.

Total macrofaunal assemblages also varied between summer and fall, as did mollusc, polychaete, and crustacean assemblages. One and three (uncommon) taxa drove dissimilarities in mollusc and polychaete assemblages between summer and fall. For molluscs, *Lacuna vincta*, and *Mytilus edulis,* generally occurred in densities < 1 ind. quadrat^{-1} and *M. edulis* was absent in spring and winter. Arenicolid polychaetes occurred in densities < 1 ind. quadrat^{-1} in all seasons. Crustacean assemblages displayed the strongest seasonality with significant variation between all seasons. As with molluscs and polychaetes, most taxa that contributed significantly to seasonal dissimilarity were uncommon and often absent from samples. However, common taxa such as Hippolytidae shrimps, the amphipods *Corophium bonelli* and *Dexamine thea*, harpacticoid copepods, and ostracods also contributed to dissimilarity. Given the short (~1 y) life cycle of most small crustaceans (Wolff & Gerberding 2015) their assemblages generally vary strongly seasonally

(Ansari & Parulekar 1993, Taylor 1997, Hull 1997). Not surprisingly, crustaceans were the most represented group (6 taxa) among organisms that significantly contributed to seasonal variation in total macrofaunal assemblages. Mean seasonal overall dissimilarity for crustaceans was also 11% and 21% higher than for polychaetes and molluscs, respectively.

4.5.3. Conclusions and future research directions

Our results from seasonal surveys of the St. Philip's bed partly supported our first hypothesis that seafloor composition and rhodolith abundance and morphology exhibit temporal stability but vary spatially. Unusual extreme weather conditions that affected the study site ~1 week prior to the surveys apparently contributed to seasonal variation in seafloor composition. Although rhodolith density, biomass, and shape did not vary spatially, we observed higher total rhodolith volume per surface area at SP15 than at SP18. The proportion of pebble vs shell nucleated rhodoliths also varied between the two sites. Our results partly supported our second hypothesis of increases macrofaunal abundance and diversity with increased rhodolith volume per surface area, in that macrofaunal biomass did not vary with rhodolith volume. Our results also suggest that the higher proportion of shell-nucleated rhodoliths at SP18 explained the negative relationship between diversity and rhodolith volume at that site. Spatial and seasonal variation in macraofaunal assemblages supported our third hypothesis. However, few and typically uncommon taxa, drove seasonal dissimilarities between macrofaunal assemblages in all taxonomic groups, suggesting a degree of temporal stability in rhodolith-associated macrofaunal communities.

As ecosystem engineers, rhodolith beds support highly diverse communities and play a central role in recruitment processes (Nelson 2009). Conservation measures adapted by various European and international frameworks recognize the ecological importance and vulnerability of

rhodoliths to climate change and anthropogenic activities (Riosmena-Rodriguez et al. 2017). Mounting evidences suggest that rhodolith beds are ubiquitous in the subarctic Northwest Atlantic, (personnel observations and Gagnon et al. 2012, Adey et al. 2015). Yet, little information exists on their ecological function in cold water systems. Our study showed that rhodolith beds may provide stable habitats for diverse macrofaunal communities. The St. Philip's bed was dominated by suspension-feeders, with remarkably high densities of brittle stars with a potentially high filtration capacity that may play a key role in controlling water quality in subarctic coastal regions. Fully grasping the functional importance of these widely distributed, and yet poorly studied, subarctic coastal communities requires studies aimed at describing large-scale spatial distribution of rhodolith beds and their associated biodiversity.

CHAPTER V

Summary and general conclusions

5.1. OVERALL OBJECTIVE OF THE STUDY

Lithothamnion glaciale rhodoliths are important components of subtidal benthic habitats in the North Atlantic (Adey and Hayek 2011). Their complex morphology and accumulation into large aggregates (beds) create habitat for a variety of associated macroalgae and macrofaunal communities (Foster 2001). Until recently, most ecological knowledge on *L. glaciale* rhodoliths and rhodolith beds came from Europe (Freiwald & Henrich 1994, Blake & Maggs 2003, Kamenos & Law 2010) and the Gulf of California (Steller & Foster 1995, Foster et al. 2007, Steller & Cáceres-Martínez 2009). Discovery of *L. glaciale* rhodolith beds in southeastern Newfoundland (Gagnon et al. 2012) triggered a series of studies aimed at diversifying the geographical locations and types of studied beds as well as increasing knowledge about the ecology of northwest Atlantic *L. glaciale* rhodoliths and rhodolith beds (Millar & Gagnon 2018, Teed et al. 2020). The present study adds to a more comprehensive understanding of the ecology of subarctic *L. glaciale* rhodoliths and rhodolith beds, and adds particular novelty in evaluating the factors that influence rhodolith growth and associated fauna.

The overall objective of the present thesis was twofold: 1) to test the effects of key abiotic (nutrients, temperature and irradiance) and biotic (presence or absence of biofoulers) factors on rhodolith growth, and 2) to describe spatial and temporal variation in rhodolith bed habitat structure and associated macrofaunal assemblages. Our research involved paired laboratory mesocosm and field experiments (see Chapters II and III) as well as seasonal surveys of a rhodolith bed located off St. Philip's in Conception Bay, Newfoundland (see Chapter IV). Laboratory experiments were carried out at the Ocean Sciences Centre of Memorial University with rhodoliths collected from the St. Philip's bed.

5.2. EFFECT OF NUTRIENT ENRICHMENT ON RHODOLITH GROWTH (CHAPTER II)

This chapter tested the effect of nutrient enrichment on biofouling and rhodolith growth. Using Newfoundland rhodoliths (*Lithothamnion glaciale*), We paired a 183-d laboratory mesocosm experiment and a 193-d field experiment to test the hypothesis that increased concentrations of nitrate, ammonia, and phosphate as well as biofouling reduce rhodolith growth. In the laboratory, we exposed rhodoliths to one of three nutrient concentrations (ambient, intermediate, or high) and either of two levels of manual cleaning (cleaned or uncleaned) to control biofouling. In the field, we exposed rhodoliths to one of two nutrient concentrations (ambient or elevated). Nutrient enrichment did not enhance growth in *L. glaciale* rhodoliths as reported for other fleshy macrophytes (Delgado & Lapointe 1994). Rather, prolonged (6 mo) exposure of rhodoliths to ammonia, nitrate, and phosphate concentrations 2 to 10 times higher than ambient levels nearly halved growth in the laboratory mesocosm experiments, presumably mainly because of the inhibitory effect of phosphate on calcification processes. Nutrient enrichment did not promote growth of biofoulers on the surface of rhodoliths as expected. However, rhodolith surfaces cleaned to remove epibionts grew 27% faster than those left untouched, presumably resulting from increased access to light. Ammonia, nitrate, and phosphate concentrations 1.5 to 2 times higher than ambient levels had no effect on rhodolith biofouling and growth in the field experiment, indicating that rhodoliths can withstand moderate eutrophication.

5.3. TEMPERATURE AND LIGHT CONTROLS ON RHODOLITH GROWTH (CHAPTER III)

The interaction between sea temperature and irradiance complicate efforts to evaluate impacts of sea temperature and irradiance on algal growth in the marine environment. We paired a 361-d laboratory mesocosm experiment and a 383-d field to test the overall hypothesis that irradiance primarily controls growth in subarctic *L. glaciale* rhodoliths. In the laboratory, we exposed rhodoliths to one of five water temperatures (ambient, 2, 4, 7 and 10°C) and one of three irradiances (low, intermediate, and high). Rhodoliths in the field were held in cages at three depths (8, 15, and 25 m). Overall, results showed that irradiance primarily controls growth with no significant effect of temperature between ~1 and 17°C. Growth in the laboratory was unaffected by temperature but was ~2 times higher at high compared to low and intermediate irradiance. However, rhodolith growth in the field stopped when water temperature dropped to near or below 0.5°C, despite irradiance ~35 times higher than in the low irradiance treatment of the laboratory mesocosm experiment, where positive growth occurred. These findings indicate that temperature effects may override those of irradiance at extreme low temperature, resulting in a seasonal growth pattern characterized by a period of arrested growth during the coldest months of the year.

5.4. HABITAT STRUCTURE AND ASSOCIATED BIODIVERSITY (CHAPTER IV)

Little knowledge information exists on rhodolith-associated macrofaunal communities and their relationship with habitat complexity. We applied univariate and multivariate statistics to video imagery and quadrat collections to test the hypotheses that: 1) seafloor composition and rhodolith abundance and morphology are temporally stable because of prevailing low hydrodynamic forces and sedimentation rate at the study sites, but vary spatially within the bed,

2) the abundance and diversity of rhodolith-associated macrofauna vary with total rhodolith volume per surface area, and 3) macrofaunal assemblages vary spatially within rhodolith bed structure, and seasonally based on macrofaunal life cycles. We carried out seasonal (spring, summer, fall, and winter) surveys in a *L. glaciale* beds at two sampling sites (15-m and 18-m deep locations) characterized by different rhodolith morphologies. During each survey, we videotaped three transects and collected rhodoliths within nine quadrats per site. The structure of the St. Philip's rhodolith bed remained generally stable throughout the 9-mo survey period as predicted. Rhodolith density, biomass, and shape were similar between sites and among seasons. The highest macrofaunal biomass occurred in spring, corresponding to the spring phytoplankton bloom (late March), with lowest biomass in summer for all taxonomic groups (all taxa combined, Mollusca, Echinodermata, Polychaeta, and Crustacea). Macrofaunal density increased with rhodolith volume per surface area, but the relationship between rhodolith volume and diversity of rhodolith-associated macrofauna varied between sites, presumably because of differences in rhodolith nucleation types, i.e. higher proportion of large shell nucleus at one site than another. Rhodolith-associated macrofaunal assemblages varied seasonally for most taxonomic groups (molluscs, polychaetes, and crustaceans) and were characterized by high density and biomass of suspension feeders.

5.5. IMPORTANCE OF THIS STUDY

This study provides new insights on growth controls of *L. glaciale* rhodoliths and relationships between structural complexity and the diversity of rhodolith-asociated macrofaunain subarctic rhodolith beds. Findings from this study will help understand future response of these non-renewable, biodiverse communities to anthropogenic and climate-related threats. The aquaculture industry is expanding worldwide. In Newfoundland, sea-based finfish farming

dominates the aquaculture industry (Newfoundland Aquaculture Industry Association 2020). On average, salmon aquaculture releases ~60% of nitrogen and 70% of phosphorous of fish feed inputs in aquaculture cages into the environment (Wang et al. 2012). Our study indicated low growth resilience of *L. glaciale* rhodoliths to coastal eutrophication. Fish farming generally takes place in sheltered coastal areas where rhodolith beds frequently occur. Policy makers can potentially use these results to develop mitigating strategies to limit the impact of aquaculture on vulnerable benthic ecosystems, including rhodolith beds. Our findings also provide insights on the large-scale potential impacts on rhodoliths under projected increases in coastal nutrient inputs at high latitudes associated with increased terrestrial runoffs caused by permafrost thawing and snow melting (Walvoord & Striegl 2007, Kendrick et al. 2018).

Our results confirm previous studies that reported a limited effect of temperature on growth of *L. glaciale* rhodoliths, and extends the lower temperature range at which growth remains unaffected to ~1°C. This study is also the first to characterize rhodolith seasonal growth patterns using time series of in-situ growth over a full year in combination with high-resolution monitoring of temperature and irradiance. Our findings that temperature near or below ~0.5°C limits growth in *L. glaciale* rhodoliths has major implications for our ability to estimate and predict rhodolith bed productivity in a warming climate. Indeed, a small increase in water temperature may considerably extend the period of positive growth. Combined increases in water temperature and irradiance from reduced sea ice will likely benefit *L. glaciale* productivity in sub-Arctic and Arctic environments. Higher calcification rates derived from increased productivity of coralline algae may buffer the effect of ongoing ocean acidification through marine carbon sequestration by rhodolith calcified skeletons.

Few previous studies described seasonal variation in rhodolith-associated macrofaunal assemblages, and mine is the first to do so within a *L. glaciale* bed. With 109 identified taxa, this study significantly increases the number of macrofaunal species previously reported for a Northwest Atlantic bed. The abundance and diversity of rhodolith-associated macrofauna found in St. Philip's established the ecological importance of Canadian rhodolith communities. Moreover, the unique community composition characterized by high densities and biomass of suspension-feeding brittle stars and bivalves highlighted the potentially important role of rhodolith beds in bentho-pelagic coupling through the effective transfer of energy in the form of organic matter from the water column to the benthic environment (Griffiths et al. 2017).

5.6. FUTURE DIRECTIONS

Our study provided various answers to the ecology of *L. glaciale* rhodoliths, but it also raised important questions that have yet to be addressed. Chapter II demonstrated that biofoulers impact rhodolith growth, as do high concentrations of ammonia, nitrate, and phosphate. However, our experimental design, meant to simulate the natural eutrophication conditions, did not allow me to discriminate among the individual effects of each of these three nutrients. Outbreaks of fast-growing, opportunistic algae characteristic of eutrophication events generally result from high concentrations of nitrate (Scanlan et al. 2007). Phosphate, in contrast, directly interferes with calcification processes (Simkiss 1964). Parsing the individual, interactive, and possibly synergistic effects of these macronutrients on rhodolith growth and survival will require more research.

Our field experiment in Chapter III demonstrated that growth in *L. glaciale* rhodolith stopped when the temperature dropped below ~0.5°C, resuming again only in spring several weeks after temperature had risen above that threshold. Ambient temperature and light variation in the

field did not permit me to clearly identify the temperature threshold for growth inhibition. Moreover, no study has clearly defined the upper temperature limit for growth and survival for that species. Adey (1970) reported an interactive effect of temperature and irradiance on radial growth in *L. glaciale* crusts from northern Norway, with declining growth rates occurring at temperature thresholds positively related to irradiance and ranging from ~5 to 14°C. In contrast, growth in *L. glaciale* rhodolith from Newfoundland (see Chapter III) and Scotland (Kamenos et al. 2008) was unaffected by temperatures as warm as ~17 and 18°C, respectively. Moreover, we found no interactive effect of temperature and irradiance for water temperatures (see Chapter III). Marine heatwaves have become longer-lasting and more frequent, extensive, and intense in the past few decades and climate models predict an acceleration of this trend under further global warming (Frölicher et al. 2018). Deleterious impacts of heatwaves on foundation species such as corals, seagrasses, and kelps have been observed worldwide (Smale et al. 2019). Coralline red algae are considered foundation species because of their important role in structuring benthic habitats, both as a crust on rocky shores and as rhodoliths on sedimentary bottom (Ólafsson 2017). Our ability to forecast future impacts of global warming on rhodolith bed productivity and geographical distribution crucially depends on delineating the full temperature range over which *L. glaciale* rhodoliths can grow and survive.

Rhodolith beds house biodiverse communities (see Chapter IV and Foster 2001) that a variety of species use as nursery or feeding habitats, including economically important taxa ones such as scallop (Kamenos et al. 2004a, Steller & Cáceres-Martínez 2009) and gadoid fishes (Kamenos et al. 2004b). In Newfoundland and Labrador, *L. glaciale* beds are generally associated with high densities of the commercially fished Icelandic scallop *Chlamys islandica* (personal observations) but no study has evaluated this relationship. The rhodolith-associated macrofaunal

assemblage in St. Philip's included high abundances of early life stages of keystone species such as sea urchins and sea stars, which play critical roles in structuring coastal benthic habitats (Saier 2001, Filbee-Dexter & Scheibling 2014). Sea ravens (*Hemitripterus americanus*) are benthic fish that scientists have used extensively to study a variety of metabolic processes. In Newfoundland, sea ravens use rhodolith beds as spawning grounds, depositing egg masses inside the cavities of hollow rhodoliths (personal observation). Although our study highlighted the importance of rhodolith beds for local and regional biodiversity, a full understanding of their role as ecosystem service providers requires deeper investigation.

Rhodoliths, like other marine calcifiers, face the mounting challenge of ocean acidification, which interferes with key basic life functions including photosynthesis, growth, pigmentation, and calcification processes (Gao & Zheng 2010, Büdenbender et al. 2011). Rhodoliths produce high Mg-calcite skeletons with greater vulnerability to ocean acidification than the aragonite or low-Mg calcite skeleton of scleractinian corals or molluscs (Andersson et al. 2008). Several studies have highlighted the synergistic negative effects of high temperature and ocean acidification on coralline calcification (Martin & Gattuso 2009, Johnson & Carpenter 2012, Sordo et al. 2019). On the other hand, there are indication that ocean acidification may alleviate the effect of low temperature on growth and photosynthesis in some species of red algae (Olischläger & Wiencke, 2013). Little information exists on ocean acidification effects in eutrophic waters where biofoulers, elevated phosphate concentration (see Chapter II), and an extended period of growth inhibition at extreme low temperature (see Chapter III) may already hamper growth and calcification.

Several countries already recognize the ecological importance of rhodolith bed communities through conservation measures (Riosmena-Rodríguez 2017). Despite growing evidences of their wide distribution along the eastern Canadian coastline, Canadian legislation

largely ignores rhodolith beds. Personal observations and communications over near a decade of study suggest that rhodoliths likely rival other foundation species such as kelp and eelgrass in abundance in coastal waters of Newfoundland and Labrador, yet they have received comparatively less attention from scientists and policy makers (Merzouk & Johnson 2011, Joseph et al. 2013, Wong & Dowd 2015, St. Pierre & Gagnon 2020). The scarcity of information on rhodolith distribution and abundance in the Northwest Atlantic certainly contributed to the limited attention received from the scientific community, but also to limited interest from the general public, to which they remain largely unknown. Mapping of rhodolith beds therefore represents a critical step towards full appreciation of these unique, vulnerable, but widely overlooked benthic communities that contribute significantly to Canadian and global natural heritage.

LITERATURE CITED

Abbott RT (1974) American seashells; the marine molluska of the Atlantic and Pacific coasts of North America 2nd ed. Van Nostrand Reinhold, New York

Abbott RT and Morris P (2001) Shells of the Atlantic and Gulf coasts and the West Indies 4th ed. Houghton Mifflin Harcourt, Boston, 512 p.

Adey WH (1966) Distribution of saxicolous crustose corallines in the northwestern North Atlantic. J Phycol 2: 49-54

Adey W (1970) The effects of light and temperature on growth rates in boreal-subarctic crustose corallines. J Phycol 6: 269-276

Adey W, Halfar J, Humphreys A, Suskiewicz T and others (2015) Subarctic rhodolith beds promote longevity of crustose coralline algal buildups and their climate archiving potential. Palaios 30: 281-293

Adey W and Hayek LA (2011) Elucidating marine biogeography with macrophytes: quantitative analysis of the North Atlantic supports the thermogeographic model and demonstrates a distinct subarctic region in the northwestern Atlantic. Northeast Nat 18: 1-128

Adey WH, MacIntyre IG (1973) Crustose coralline algae: a re-evaluation in the geological sciences. Geol Soc Am Bull 84: 883-904

Adey WH, McKibbin DL (1970) Studies on the maerl species *Phymatolithon calcareum* (Pallas) nov. comb. and *Lithothamniun coralloides* Crouan in the Ria de Vigo. Bot Mar 13: 100-106

Admiraal W (1976) Influence of light and temperature on the growth rate of estuarine benthic diatoms in culture. Mar Biol 39: 1-9

Aguado-Guímenez F and Ruiz-Fernández JM (2012) Influence of an experimental fish farm on the spatio-temporal dynamic of a Mediterranean maërl algae community. Mar Environ Res 74: 47-55

Aguirre J, Braga JC, Bassi D (2017) Rhodoliths and rhodolith beds in the rock record. In: Riosmena-Rodríguez R, Nelson W, Aguirre J (eds) Rhodolith/maerl beds: a global perspective. Springer International Publishing, Switzerland, p 105-138

Ahn JH, Grant SB, Surbeck CQ, Digiacomo PM and others (2005) Coastal water quality impact of stormwater runoff from an urban watershed in southern California. Environ Sci Technol 39: 5940-5953

Amado-Filho GM, Maneveldt G, Manso RCC, Marins-Rosa BV and others (2007) Structure of rhodolith beds from 4 to 55 meters deep along the southern coast of Espírito Santo State, Brazil. Cienc Mar 33: 399-410

Amado-Filho GM, Maneveldt GW, Pereira-Filho GH and others (2010) Seaweed diversity associated with a Brazilian tropical rhodolith bed. Cienc Mar 36: 371-391

Amado-Filho GM, Moura RL, Bastos AC and others (2012) Rhodolith beds are major $CaCO_3$ bio-factories in the tropical south west Atlantic. PLoS ONE 7: e35171

Amado-Filho GM, Pereira-Filho GH, Bahia RG, Abrantes DP and others (2012) Occurrence and distribution of rhodolith beds on the Fernando de Noronha Archipelago of Brazil. Aquat Bot 101: 41-45

Andersen J and Conley DJ (2009) Eutrophication in coastal ecosystems: Towards better understanding and management strategies: Selected papers from the second international symposium on research and management of eutrophication in coastal ecosystems, 20-23 June 2006, Nyborg, Denmark. Dordrecht: Springer, Dordrecht

Anderson MJ (2001) A new method for non-parametric multivariate analysis of variance. Austral Ecol 26: 32-46

Anderson MJ, Diebel CE, Blom WM, Landers TJ (2005) Consistency and variation in kelp holdfast assemblages: Spatial patterns of biodiversity for the major phyla at different taxonomic resolutions. J Exp Mar Biol Ecol 320: 35-56

Andersson AJ, Mackenzie FT, Bates NR (2008) Life on the margin: implications of ocean acidification on Mg-calcite, high latitude and cold-water marine calcifiers. Mar Ecol Prog Ser 373: 265-273

Avila E and Riosmena-Rodríguez R (2011) A preliminary evaluation of shallow-water rhodolith beds in Bahia Magdalena, Mexico. Braz J Oceanogr 59: 365-375

Andrake W and Johansen HW (1980) Alizarin red dye as a marker for measuring growth in *Corallina officinalis* L. (Corallinaceae, Rhodophyta). J Phycol 16: 620-622

Ansari Z and Parulekar A (1993) Environmental stability and seasonality of a harpacticoid copepod community. Mar Biol 115: 279-286

Appy TD, Linkleter LE, and Dadswell MJ (1980) A guide to the marine flora and fauna of the Bay of Fundy. Fisheries and marine service technical report no. 920. Fisheries and Oceans, St. Andrews. 124 p.

Bahia RG, Abrantes DP, Brasileiro PS, Pereira GH and others (2010) Rhodolith bed structure along a depth gradient on the northern coast of Bahia State, Brazil. Braz J Oceanogr 58: 323-337

Barbera C, Bordehore C, Borg JA, Glémarec M and others (2003) Conservation and management of northeast Atlantic and Mediterranean maerl beds. Aquatic Conserv Mar Fresw Ecosyst 13: S65-S76

Basso D (2012) Carbonate production by calcareous red algae and global change. Geodiversitas 34: 13-33

Basso D, Babbini L, Kaleb S, Bracchi VA and others (2016) Monitoring deep Mediterranean beds. Aquatic Conserv: Mar Freshw Ecosyst 26: 549-561

Basso D, Nalin R, Nelson CS (2009) Shallow-water *Sporolithon* rhodoliths from North Island (New Zealand). Palaios 24: 92-103

Beck M (1998) Comparison of the measurement and effects of habitat structure on gastropods in rocky intertidal and mangrove habitats. Mar Ecol Prog Ser 169: 165-178

Bell SS, McCoy ED, Mushinsky HR (2012) Habitat structure: The physical arrangement of objects in space. Springer Science & Business Media

Belliveau SA and Paul V (2002) Effects of herbivory and nutrients on the early colonization of crustose coralline and fleshy algae. Mar Ecol Prog Ser 232: 105-114

Bernard G, Romero-Ramirez A, Tauran A, Pentalos M and others (2019) Declining maerl vitality and habitat complexity across a dredging gradient: insights from *in situ* sediment profile imagery (SPI). Sci Rep 9: 16463

Bernier RY, Jamieson RE, Moore AM (eds) (2018). State of the Atlantic Ocean synthesis report. Can Tech Rep Fish Aquat Sci 3167: iii+149 p

Bindoff NL, Cheung WW L, Kairo JG, Arístegui J and others (2019) Changing ocean, marine ecosystems, and dependent communities. In: Pörtner H-O, Roberts DC, Masson-Delmotte V, Zhai P, Tignor M, Poloczanska E, Mintenbeck K, Alegría A, Nicolai M, Okem A, Petzold J, Rama B, Weyer NM (eds) IPCC special report on the ocean and cryosphere in a changing climate. In press

Björk M, Mohammed SM, Björklund M, Semesi A (1995) Coralline algae, important coral reef builders threatened by pollution. Ambio 24: 502-505

Blain C and Gagnon P (2013) Interactions between thermal and wave environments mediate intracellular acidity (H_2SO_4), growth, and mortality in the annual brown seaweed *Desmarestia viridis*. J Exp Mar Biol Ecol 440: 176-184

Blain C and Gagnon P (2014) Canopy-forming seaweeds in sea-urchin-dominated systems in eastern Canada: structural forces or simple prey for keystone grazers? PLoS ONE 9:e98204. doi: 10.1371

Blake C and Maggs CA (2003) Comparative growth rates and internal banding periodicity of maerl species (Corallinales, Rhodophyta) from northern Europe. Phycologia 42: 606-612

Blomqvist S, Gunnars A, Elmgren R (2004) Why the limiting nutrient differs between temperate coastal seas and freshwater lakes: A matter of salt. Limnol Oceanogr 49: 2236-2241

Blunden G, Binns WW, Perks F (1975) Commercial collection and utilization of maërl. Econ Bot 29: 140-145

Bordehore C, Ramos-Esplá AA, Riosmena-Rodríguez R (2003) Comparative study of two maerl beds with different otter trawling history, southeast Iberian Peninsula. Aquat Conserv: Mar Freshwat Ecosyst 13: S43-S54

Bosellini A, Ginsburg RN (1971) Forms and internal structure of recent algal nodules (Rhodolites) from Bermuda. J Geol 79: 669-68

Bosence DW (1983) Coralline algal reef frameworks. J Geol Soc London 140: 365-376

Bosence DWJ (1983) The occurence and ecology of recent rhodoliths - a review. Peryt TM (ed) *Coated grains*. Springer-Verlag, Berlin

Bosence D (1976) Ecological studies on two unattached coralline algae from the western Ireland. Palaeontology 19: 365-395

Brodie J, Williamson CJ, Smale DA, Kamenos NA and others (2014) The future of the northeast Atlantic benthic flora in a high CO_2 world. Ecol Evol 4: 2787-2798

Büdenbender J, Riebesell U, Form A (2011) Calcification of the Arctic coralline red algae *Lithothamnion glaciale* in response to elevated CO_2. Mar Ecol Prog Ser 441: 79-87

Brookes JA and Stevens RK (1985) Radiocarbon age of rock-boring *Hiatella arctica* (linné) and postglacial sea-level change at Cow Head, newfoundland. Can J Earth Sci 22: 136-140

Buhl-Mortensen L, Vanreusel A, Gooday AJ, Levin LA and others (2010) Biological structures as a source of habitat heterogeneity and biodiversity on the deep ocean margins. Mar Ecol 31: 21-50

Buhl-Mortensen L, Buhl-Mortensen P, Dolan M, Dannheim J and others (2012) Habitat complexity and bottom fauna composition at different scales on the continental shelf and slope of northern Norway. Hydrobiologia 685: 191-21

Burdett H, Hennige S, Francis F, Kamenos N (2012) The photosynthetic characteristics of red coralline algae, determined using pulse amplitude modulation (PAM) fluorometry. Bot Mar 55: 499-509

Caines S and Gagnon P (2012) Population dynamics of the invasive bryozoan *Membranipora membranacea* along a 450-km latitudinal range in the subarctic northwestern Atlantic. Mar Biol 159: 1817-1832

Camargo N, Sano NY, Vieira EM (2018) Forest vertical complexity affects alpha and beta diversity of small mammals. J Mammal 99: 1444-1454

Carvalho LRS, Loiola M, Barros F (2017) Manipulating habitat complexity to understand its influence on benthic macrofauna. J Exp Mar Biol Ecol 489: 48-57

Castriota L, Agamennone F, Sunseri G (2005) The mollusc community associated with maerl beds of Ustica Island (Thyrrhenian Sea). Cah Biol Mar 46: 289-297

Cloern JE (1982) Does the benthos control phytoplankton biomass in south San Francisco bay? Mar Ecol Prog Ser 9: 191-202

Conley D, Paerl HW, Howarth RW, Boesch DF and others (2009) Controlling eutrophication: Nitrogen and phosphorus. Science 323: 1014-1015

Connor EF and McCoy ED (1979) The statistics and biology of the species-area relationship. Am Nat 113: 791-833

Copeland A, Edinger E, Devillers R, Bell T and others (2013) Marine habitat mapping in support of a marine protected area management in a subarctic fjord: Gilbert Bay, Labrador, Canada. J Coast Conserv 17: 225-237

Darrenougue N, Deckker P, Eggins S, Fallon S and other (2018) A record of mining and insdustrial activities in New Caledonia based on trace elements in rhodolith-forming coralline red algae. Chem Geol 493: 24-36

Darrenougue N, De Deckker P, Payri C, Eggins S and others (2013) Growth and chronology of the rhodolith-forming, coralline red alga *Sporolithon durum*. Mar Ecol Prog Ser 474: 105-119

Davidson R, Duffy C, Gaze P, Baxter A and others (2011) Ecologically significant marine sites in Marlborough, New Zealand. Marlborough District Council

Dean RL and Connell JH (1987) Marine invertebrates in an algal succession. III. mechanisms linking habitat complexity with diversity. J Exp Mar Biol Ecol 109: 249-273

Delgado O and Lapointe B (1994) Nutrient-limited productivity of calcareous versus fleshy macroalgae in a eutrophic, carbonate-rich tropical marine environment. Coral Reefs 13: 151-159

De Soto L, Cailleret M, Sterck F and others (2020) Low growth resilience to drought is related to future mortality risk in trees. Nat Commun 11: 545

Devlin M, Painting S, Best M (2007) Setting nutrient thresholds to support an ecological assessment based on nutrient enrichment, potential primary production and undesirable disturbance. Mar Pollut Bull 55: 65-73

Dorgan KM (2015) The biomechanics of burrowing and boring. J Exp Biol 218: 176

Doyle GM, Hamel J, Mercier A (2014) Small-scale spatial distribution and oogenetic synchrony in brittlestars (Echinodermata: Ophiuroidea). Estuar Coast Shelf Sci 136: 172-178

Drake LA, Dobbs FC, Zimmerman RC (2003) Effects of epiphyte load on optical properties and photosynthetic potential of the seagrasses *Thalassia testudinum* Banks ex König and *Zostera marina* L. Limnol Oceanogr 48: 456-46

Dring MJ (1990) Light harvesting pigment composition in marine phytoplankton and macroalgae. In: Herring PJ, Campbell AK, Whitfield M, Maddock L (eds) Light and life in the sea. p 59-88

Duarte CM (1995) Submerged aquatic vegetation in relation to different nutrient regimes. Ophelia 41: 87-112

Dunn JG, Sammarco PW, Lafleur G (2012) Effects of phosphate on growth and skeletal density in the scleractinian coral *Acropora muricata*: A controlled experimental approach. J Exp Mar Biol Ecol 411: 34-4

Eggert A (2012) Seaweed responses to temperature. In: Wiencke C and Bischof K (eds) Seaweed biology, novel insights into ecophysiology, ecology and utilization. Ecological Studies 219, Springer-Verlag, Berlin, p 47-6

Epp R and Lewis W (1980) Metabolic uniformity over the environmental temperature range in *Brachionus plicatilis* (Rotifera). Hydrobiologia 73: 145-14

Epp R and Lewis W (1979) Metabolic responses to temperature change in a tropical freshwater copepod (*Mesocyclops brasilianus*) and their adaptive significance. Oecologia 42: 123-138

Eriksson BK, Rubach A, Hillebrand H (2006) Biotic habitat complexity controls species diversity and nutrient effects on net biomass production. Ecology 87: 246-25

Fabricius KE, De'ath G, Humphrey C, Zagorskis I and others (2013) Intra-annual variation in turbidity in response to terrestrial runoff on near-shore coral reefs of the great barrier reef. Estuar Coast Shelf Sci 116: 57-6

Fabry VJ (2008) Marine calcifiers in a high-CO_2 ocean. Science 320: 1020-1022

Fauchald K (1977) The polychaete worms: definitions and keys to the order, families, and genera. Natural History Museum of Los Angeles County, Los Angeles, 188 p.

Figueiredo MAO, Santos de Menezes K, Costa-Paiva EM and others (2007) Experimental evaluation of rhodoliths as living substrata for infauna at the Abrolhos Bank, Brazil. Cienc Mar 33: 427-44

Figueroa FL, Salles S, Aguilera J, Jiménez C and others (1997) Effects of solar radiation on photoinhibition and pigmentation in the red alga *Porphyra leucosticta*. Mar Ecol Prog Ser 151: 81-9

Figueroa F, Martinez B, Israel A, Neori A and others (2009) Acclimation of red sea macroalgae to solar radiation: photosynthesis and thallus absorptance. Aquat Biol 7: 159-172

Filbee-Dexter K, Scheibling RE (2014) Sea urchin barrens as alternative stable states of collapsed kelp ecosystems. Mar Ecol Prog Ser 495: 1-25

Foster M (2001) Rhodoliths: between rocks and soft places. J Phycol 37: 659-667

Foster M, McConnico L, Lundsten L, Wadsworth T and others (2007) Diversity and natural history of a *Lithothamnion muelleri-Sargassum horridum* community in the Gulf of California. Cienc Mar 33: 367-384

Fredericq S, Krayesy-Self S, Sauvage T, Richards J and others (2019) The critical importance of rhodoliths in the life cycle completion of macro- and microalgae, and as holobionts for the establishment and maintenance of marine biodiversity. Front Mar Sci 5: 502

Freiwald A, Henrich R (1994) Reefal coralline algal build-ups within the Arctic circle: morphology and sedimentary dynamics under extreme environmental seasonality. Sedimentology 41: 963-984

Frey DL and Gagnon P (2015) Thermal and hydrodynamic environments mediate individual and aggregative feeding of a functionally important omnivore in reef communities. PLoS ONE 10(3): e0118583

Frölicher TL, Fisher EM, Gruber N (2018) Marine heatwaves under global warming. Nature 560: 360-364

Gabara S, Hamilton S, Edwards M, Steller D (2018) Rhodolith structural loss decreases abundance, diversity, and stability of benthic communities at Santa Catalina Island, CA. Mar Ecol Prog Ser 595: 7

Gagnon P, Blain C, Vad J (2013) Living within constraints: irreversible chemical build-up and seasonal temperature-mediated die-off in a highly acidic (H_2SO_4) annual seaweed (*Desmarestia viridis*). Mar Biol 160: 439-451

Gagnon P, Matheson K, Stapleton M (2012) Variation in rhodolith morphology and biogenic potential of newly discovered rhodolith beds in newfoundland and Labrador (Canada). Bot Mar 55: 85-99

Gao K and Zheng Y (2010) Combined effects of ocean and solar UV radiation on photosynthesis growth, pigmentation and calcification of the coralline alga *Corallina sessilis* (Rhodophyta). Glob Change Biol 16: 2388-239

Gillooly JF, Brown JH, West GB, Savage VM and others (2001) Effects of size and temperature on metabolic rate. Science 293: 2248-2251

Gosner KL (1978) Atlantic seashore: a field guide to sponges, jellyfish, sea urchins, and more. Houghton Mifflin Harcourt, Boston, 329 p.

Gondim AI, Dias TLP, Cristina de SD, Riul P and others (2014) Filling a knowledge gap on the biodiversity of rhodolith-associated Echinodermata from northeastern Brazil. Trop Conserv Sci 7: 87-99

Graham DJ and Midgley NG (2000) Graphical representation of particle shape using triangular diagrams: An excel spreadsheet method. Earth Surf Process Landforms 25: 1473-1477

Grall J, Glémarec M (1997) Using biotic indices to estimate macrobenthic community perturbations in the Bay of Brest. Estuar Coast Shelf Sci 44: 43-53

Grall J, Hall-Spencer JM (2003) Problems facing maerl conservation in Brittany. Aquatic Conserv Mar Freshw Ecosyst 13: S55-S64

Grall J, Le Loc'h F, Guyonnet B, Riera P (2006) Community structure and food web based on stable isotopes (δ 15N and δ 13C) analysis of a North Eastern Atlantic maerl bed. J Exp Mar Biol Ecol 338: 1-15

Griffiths JR, Kadin M, Nascimento FJA, Tamelader T and others (2017) The importance of benthic-pelagic coupling for marine ecosystem functioning in a changing world. Global Change Biol 23: 2179-2196

Halfar J, Zack T, Kronz A, Zachos JC (2000) Growth and high-resolution paleoenvironmental signals of rhodoliths (coralline red algae): a new biogenic archive. J Geophys Res 105: 22107-22116

Hall-Spencer JM and Moore PG (2000) Scallop dredging has profound, long-term impacts on maerl habitats. J Mar Sci 57: 1407-141

Hanelt D (1998) Capability of dynamic photoinhibition in arctic macroalgae is related to their depth distribution. Mar Biol 131: 361-369

Harvey AS, Harvey RM, Merton E (2016) The distribution, significance and vulnerability of the Australian rhodolith beds: a review. Mar Freshw Res 68: 411-428

Hauser A, Attrill M, Cotton P (2006) Effects of habitat complexity on the diversity and abundance of macrofauna colonising artificial kelp holdfasts. Mar Ecol Prog Ser 325: 93-100

Heyward AJ and Negri AP (1999) Natural inducers for coral larval metamorphosis. Coral Reefs 18: 273-27

Hickman A, Moore C, Sharples J, Lucas M and others (2012) Primary production and nitrate uptake within the seasonal thermocline of a stratified shelf sea. Mar Ecol Prog Ser 463: 39-57

Hily C (1991) Is the activity of benthic suspension feeders a factor controling water quality in the Bay of Brest? Mar Ecol Prog Ser 69: 179-188

Hine R (2019) A dictionary of biology. Oxford University Press, Oxford

Hinojosa-Arango G (2004) Influence of rhodolith-forming species and growth-form on associated fauna of rhodolith beds in the Central-West Gulf of California, Mexico. Mar Ecol 25: 109-127

Hinojosa-Arango G, Maggs CA, Johnson MP (2009) Like a rolling stone: the mobility of maerl (Corallinaceae) and the neutrality of the associated assemblages. Ecology 90: 517-528

Hixon MA and Menge BA (1991) Species diversity: Prey refuges modify the interactive effects of predation and competition. Theor Popul Biol 39: 178-200

Hull S (1997) Seasonal changes in diversity and abundance of ostracods on four species of intertidal algae with differing structural complexity. Mar Ecol Prog Ser 161: 71-8

Ichiki S, Mizuta H, Yamamoto H (2000) Effects of irradiance, water temperature and nutrients on the growth of sporelings of the crustose coralline alga *Lithophyllum yessoense* Foslie (Corallinales, Rhodophyceae). Phycol Res 48: 115-120

Irvine LM, Chamberlain YM (1994) Seaweeds of the Brittish Isles. Volume 1 Rhodophyta part 2B Corallinales, Hildenbranchiales, HMSO, London

James D (2000) Diet, movement, and covering behavior of the sea urchin *Toxopneustes roseus* in rhodolith beds in the Gulf of California, México. Mar Biol 137: 913-923

Johnson MD and Carpenter RC (2012) Ocean acidification and warming decrease calcification in the crustose coralline alga *Hydrolithon onkodes* and increase susceptibility to grazing. J Exp Mar Biol Ecol 434-435: 94-101

Johnson MD and Carpenter RC (2018) Nitrogen enrichment offsets direct negative effects of ocean acidification on a reef-building crustose coralline alga. Biol Lett 14: 20180371

Jones CG, Lawton JH, Shachak M (1994) Organisms as ecosystem engineers. Oikos 69: 373-386

Jørgensbye HIØ, Halfar J (2017) Overview of coralline red algal crusts and rhodolith beds (Corallinales, Rhodophyta) and their possible ecological importance in Greenland. Polar Biol 40: 517-531

Joseph V, Schmidt AL, Gregory RS (2013) Use of eelgrass habitats by fish in eastern Canada. Ottawa: Fisheries and Oceans Canada, Science, 12 p.

Kamenos NA, Burdett HL, Aloisio E, Findlay HS, Martin S, Longbone C, Dunn J, Widdicombe S, Calosi P (2013) Coralline algal structure is more sensitive to rate, rather than the magnitude, of ocean acidification. Global Change Biol 19: 3621-362

Kamenos NA, Cusack M, Moore PG (2008) Coralline algae are global palaeothermometers with bi-weekly resolution. Geochim Cosmochim Acta 72: 771-779

Kamenos NA and Law A (2010) Temperature controls on coralline algal skeletal growth. J Phycol 46:331-335

Kamenos NA, Moore PG, Hall-Spencer JM (2004a) Maerl grounds provide both refuge and high growth potential for the juvenile queen scallops (*Aequipecten opercularis* L.) J Exp Mar Biol Ecol 313: 241-254

Kamenos NA, Moore PG, Hall-Spencer JM (2004b) Small-scale distribution of juvenile gadoids in shallow inshore waters; what role does maerl play? ICES J Mar Sci 61: 422-429

Kendrick M, Huryn A, Bowden W, Deegan L and others (2018) Linking permafrost thaw to shifting biogeochemistry and food web resources in an arctic river. Glob Chang Biol 24: 5738-5750

Koivisto M and Westerbom M (2010) Habitat structure and complexity as determinants of biodiversity in blue mussel beds on sublittoral rocky shores. Mar Biol 157: 1463-1474

Konar B, Riosmena-Rodriguez R, Iken K (2006) Rhodolith bed: a newly discovered habitat in the North Pacific Ocean. Bot Mar 49: 355-35

Korczynski PC, Logan J, Faust JE (2002) Mapping monthly distribution of daily light integrals across the contiguous Unitded States. Horttechnology 12: 12-16

Krayeski-Self S, Schmidt WE, Phung D, Henry C and others (2017) Eukaryotic life inhabiots rhodolith-forming coralline algae (Hapaliadiales, Rhodophyta), remarkable marine benthic microhabitats. Sci Rep 7: 45850

Krom MD, Kress N, Brenner S, Gordon LI (1991) Phosphorus limitation of primary productivity in the eastern Mediterranean Sea. Limnol Oceanogr 36: 424-43

Lang A, Yang S, Kass E (2017) Sea ice thickness and recent Arctic warming. Geophys Res Lett 44: 409-418

Lapointe BE, Littler MM, Littler DS (1993) Modification of benthic community structure by natural eutrophication: the Belize barrier reef. Proc. 7th Int Coral Reef Symp 1: 323-334

Larned ST (1998) Nitrogen-versus phosphorus-limited growth and sources of nutrients for coral reef macroalgae. Mar Biol 132: 409-421

Lebrato M, Andersson AJ, Ries JB, Aronson AB and others (2016) Benthic marine calcifiers co-exist with $CaCO_3$-undersaturated seawater worldwide. Global Biogeochem Cycles 30: 1038-105

Levitus S, Antonov JI, Boyer TP, Baranova OK and others (2012) World ocean heat content and thermosteric sea level change (0–2000 m), 1955–2010. Geophys Res Lett 39: L10603

Lewis B and Diaz-Pulido G (2017) Suitability of three fluorochrome markers for obtaining *in situ* growth rates of coralline algae. J Exp Mar Biol Ecol 490: 64-73

Lischka S, Stange P, Riebesell U (2018) Response of pelagic calcifiers (Foraminifera, Thecosomata) to ocean acidification during oligotrophic and simulated up-welling conditions in the subtropical North Atlantic off Gran Canaria.

Littler MM, Littler DS, Blair SM, Norris JN (1985) Deepest known plant life discovered on an uncharted seamount. Science 227: 57-59

Littler MM, Littler DS, Brooks BL (2010) The effects of nitrogen and phosphorus enrichment on algal community development: Artificial mini-reefs on the Belize barrier reef sedimentary lagoon. Harmful Algae 9: 255-263

Long MH, Rheuban JE, Berg P, Zieman JC (2012) A comparison and correction of light intensity loggers to photosynthetically active radiation sensors. Limnol Oceanogr- Meth 10: 416-42

Lüning K (1984) Temperature tolerance and biogeography of seaweeds: the marine algal flora of Helgoland (North Sea) as an example. Helgoländer Meeresunters 38: 305-317

MacArthur R and Wilson EO (1967) The theory of island biogeography. Wilson EO (ed). Princeton University Press, Princeton, N.J.

Macaya EC, Riosmena-Rodríguez R, Melzer RR, Meyer R and others (2015) Rhodolith beds in the South-East Pacific. Mar Biodiv 45: 153-154

MacDiarmid A, Bowden D, Cummings V, Morrison M, and others (2013) Sensitive marine benthic habitats defined. Prepared for Ministry for the Environment. NIWA Client Report No: WLG2013-18

Maillet G, Bélanger D, Doyle G, Robar A and others (2019) Optical, chemical, and biological oceanographic conditions on the Newfoundland and Labrador Shelf during 2016-2017. DFO Can Sci Advis Sec Res Doc 2019/055. viii + 35 p.

Manly BFJ (1997) Randomization, bootstrap and Monte Carlo methods in biology. In: Manly BFJ (ed), 2nd ed. Chapman & Hall, Londo

Martin S, Cohu S, Vignot C, Zimmerman G and others (2013) One-year experiment on the physiological response of the Mediterranean crustose coralline alga, *Lithophyllum cabiochae*, to elevated p CO_2 and temperature. Ecol Evol 3: 676-693

Martin S and Gattuso JP (2009) Response of Mediterranean coralline algae to ocean acidification and elevated temperature. Glob Chang Biol 15: 2089-2100

Matsuda S, Iryu Y (2011) Rhodoliths from deep fore-reef to shelf areas around Okinawa-jima, Ryukyu Islands, Japan. Mar Geol 282: 215-230

Meadows PS, Meadows A, Murray JMH (2012) Biological modifiers of marine benthic seascapes: their role as ecosystem engineers. Geomorphology 157-158: 31-48

Mendoza ML and Cabioch J (1998) Étude comparée de la reproduction de *Phymatolithon calcareum* (Pallas) Adey & McKibbin et *Lithohtamnion corallioides* (P. & H. Crouan) (Corallinales, Rhodophyta), et reconsidérations sur la définition des genres. Can J Bot 76 : 1433-1445

McConnico L, Carmona G, Morales J, Rodríguez R (2017) Temporal variation in seaweed and invertebrate assemblages in shallow rhodolith beds of Baja California Sur, México. Aquat Bot 139: 37

McCoy ED and Bell SS (1991) Habitat structure: The evolution and diversification of a complex topic. Habitat structure. Springer, p. 3-27

McCoy SJ and Pfister CA (2014) Historical comparisons reveal altered competitive interactions in a guild of crustose coralline algae. Ecol Lett 17: 475-483

Merzouk A and Johnson LE (2011) Kelp distribution in the northwest Atlantic Ocean under a changing climate. J Exp Mar Biol Ecol 400: 90-98

Millar KR, Gagnon P (2018) Mechanisms of stability of rhodolith beds: sedimentological aspects. Mar Ecol Prog Ser 584: 65-83

Myhre L, Forsgren E, Amundsen T (2013) Effects of habitat complexity on mating behavior and mating success in a marine fish. Behav Ecol 24: 553-563

Nash MC, Diaz-Pulido G, Harvey AS, Adey W (2019) Coralline algal calcification: a morphological and process-based understanding. PLoS ONE 14: e0221396

Nelson WA (2009) Calcified macroalgae – critical to coastal ecosystems and vulnerable to change: a review. Mar Freshw Res 60: 787-801

Novaczek E, Howse V, Pretty C, Devillers R, Edinger E and other (2017) Limited contributions of small marine protected areas to regional biodiversity: the example of a small Canadian no-take MPA. Front Mar Sci 4: 174

Newfoundland Aquaculture Industry Association. https://naia.ca/index.php/aquaculture-nl/production-stats. Page visited on 29 April 2020

Officer CB, Smayda TJ, Mann R (1982) Benthic filter feeding: a natural eutrophication control. Mar Ecol Prog Ser 9: 203-21

Ogston AS and Field ME (2010) Predictions of turbidity due to enhanced sediment resuspension resulting from sea-level rise on a fringing coral reef: Evidence from Molokai, Hawaii. J Coast Res 26: 1027-1037

Ólafsson E (2017) Marine macrophytes as foundation species. CRC Press, Boca Raton, Fl, 277 p.

Olischläger M and Wiencke C (2013) Ocean acidification alleviates low-temperature effects on growth and photosynthesis of the red alga *Neosiphonia harveyi* (Rhodophyta). J Exp Bot 64: 5587-5597

Ossola A, Nash MA, Christie FJ, Hahs AK, Livesley SJ (2015) Urban habitat complexity affects species richness but not environmental filtering of morphologically-diverse ants. PeerJ 3: e1356-e1356

Pardo C, Guillemin ML, Peña V and others (2019) Local coastal configuration rather than latitudinal gradient shape clonal diversity and genetic structure of *Phymatolithon calcareum* maerl beds in North European Atlantic. Front Mar Sci 6: 149

Pascelli C, Riul P, Riosmena-Rodríguez R, Scherner F, Nunes M, Hall-Spencer J, Oliveira ECd, Horta P (2013) Seasonal and depth-driven changes in rhodolith bed structure and associated macroalgae off Arvoredo Island (southeastern Brazil). Aquat Bot 111: 62-65

Pearce CM, Scheibling RE (1990) Induction of metamorphosis of larvae of the green sea urchin, *Strongylocentrotus droebachiensis*, by coralline red algae. Biol Bull 179: 304-311

Peña V, Bárbara I (2004) Diferenciación morfológica y anatómica entre *Lithothamnion corallioides* y *Phymatolithon calcareum* (Corallinales, Rhodophyta) en dos bancos de maërl de la Ría de Arousa (N.O. Península Ibérica). Anales de Biología 26: 21-27

Peña V, Hernández-Kantún JJ, Grall J and others (2014a) Detection of gametophytes in the maerl-forming species maerl-forming species *Phymatolithon calcareum* (Meobesioideae, Corallinales) assessed by DNA barcoding. Cryptogam Algol 35: 15-25

Peña V, Rousseau F, de Reviers B, Le Gall L (2014b) First assessment of the diversity of coralline species forming mearl and rhodoliths in Guadeloupe, Caribbean using an integrative systematic approach. Phytotaxa 190: 190-215

Perry CT, Spencer T, Kench PS (2008 Carbonate budgets and reef production states: a geomorphic perspective on the ecological phase-shift concept. Coral Reefs 27: 853-866

Pettibone MH (1963) Marine polychaete worms of the New England region: 1. Families Aphroditidae through trochochaetidae. U.S. National Museum Bulletin 227. Smithsonian Institution, Washington. 356 p.

Pocklington P (1989) Polychaetes of eastern Canada: an illustrated key to polychaetes of eastern Canada including the eastern Arctic. Department of Fisheries and Oceans Canada, Mont-Joli 274 p.

Pollock LW (1998) A practical guides to the marine animals of the northeasterns North America. Rutgers University Press, New Brunswick MA, 367 p.

Preston FW (1960) Time and space and the variation of species. Ecology 41: 611-627

Quinn GP and Keough MJ (2002) Experimental design and data analysis for biologists. Cambridge University Press, Cambridge, UK; New Yor

R Core Team (2019) R: a language and environment for statistical computing. R foundation for statistical computing, Vienna

Radashevsky V and Pankova V (2013) Shell-boring versus tube-dwelling: Is the mode of life fixed or flexible? Two cases in spionid polychaetes (Annelida, Spionidae). Mar Biol 160: 1619-1624

Rasband WS, ImageJ, U. S. National Institutes of Health, Bethesda, Maryland, USA, https://imagej.nih.gov/ij/, 1997-2018.

Rasher D, Engel S, Bonito V, Fraser G, Montoya J, Hay M (2012) Effects of herbivory, nutrients, and reef protection on algal proliferation and coral growth on a tropical reef. Oecologia 169: 187-198

Ries JB, Cohen AL, McCorkle DC (2009) Marine calcifiers exhibit mixed responses to CO_2-induced ocean acidification. Geology 37: 1131-1134

Riosmena-Rodriguez R (2017) Rhodolith/maërl beds: A global perspective. Springer International Publishing, Cham, Cham

Riosmena-Rodríguez R (2017) Natural history of rhodolith/maërl beds: their role in near-shore biodiversity and management. In: Riosmena-Rodríguez R, Nelson W, Aguirre J (eds) Rhodolith/maërl beds: a global perspective. Springer International Publishing, Switzerland, p 105-138

Riul P (2008) Decrease in *Lithothamnion* sp. (rhodophyta) primary production due to the deposition of a thin sediment layer. J Mar Biol Assoc U K 88: 17-19

Ronowicz M, Kukliński P, Włodarska-Kowalczuk M (2018) Diversity of kelp holdfast-associated fauna in an arctic fjord - inconsistent responses to glacial mineral sedimentation across different taxa. Estuar Coast Shelf Sci 205: 100-109

Ryther JH and Dunstan WM (1971) Nitrogen, phosphorus, and eutrophication in the coastal marine environment. Science 171: 1008-1013

Saier B (2001) Direct and indirect effects of seastars *Asterias rubens* on mussel beds (*Mytilus edulis*) on Waden Sea. J Sea Res 46: 29-42

Santos IR, de Weys J, Tait DR, Eyre BD (2013) The contribution of groundwater discharge to nutrient exports from a coastal catchment: post-flood seepage increases estuarine N/P ratios. Estuaries Coast 36: 56-73

Scanlan CN, Foden J, Wells E, Best MA (2007) The monitoring of opportunistic macroalgal blooms for the water framework directive. Mar Pollut Bull 55: 162-171

Schoenrock KM, Bacquet M, Pearce D, Rea BR and others (2018) Influences of salinity on the physiology and distribution of the arctic coralline algae, *Lithothamnion glaciale* (Corallinales, Rhodophyta). J Phycol 54: 690

Schoenrock KM, Vad J, Muth A, Pearce DM and others (2018) Biodiversity of kelp forest and coralline algae habitats in southwestern Greenland. Diversity 10: 117

Schubert N, Salazar VW, Rich WA, Vivanco Bercovich M, Almeida Saá AC, Fadigas SD, Silva J, Horta PA (2019) Rhodolith primary and carbonate production in a changing ocean: The interplay of warming and nutrients. Sci Total Environ 676: 455-468

Sciberras M, Rizzo M, Mifsud JR, Camilleri K, Borg JB, Lafranco E, Schembri PJ (2009) Habitat structure and biological characteristics of a maerl bed off the northeastern coast of the Maltese Islands (central Mediterranean). Mar Biodiv 39: 251-26

Schwarz AM, Hawes I, Andrew N, Mercer S and others (2005) Primary production potential of non-geniculate coralline algae at Cape Evans, Ross Sea, Antarctica. Mar Ecol Prog Ser 294: 131-140

Selman M, Greenhalgh S, Diaz R, Sugg Z (2008) Eutrophication and hypoxia in coastal areas: A global assessment of the state of knowledge. Washington, DC: World Resources Institute

Simkiss K (1964) Phosphate as crystal poisons of calcification. Biol Rev 39: 487-505

Sletten HR, Andrus CFT, Guzmán HM, Halfar J (2017) Re-evaluation of using growth patterns for paleoenvironmental reconstruction: an example from the Gulf of Panama. Paleogeogr Paleoclimatol Paleoecol 465: 264-277

Smale DA, Wernberg T, Olivier ECJ, Thomsen M and others (2019) Marine heatwaves threaten global biodiversity and the provision of ecosystem services. Nat Clim Chang 9: 306-312

Small C and Nicholls RJ (2003) A global analysis of human settlement in coastal zones. J Coast Res 19: 584-599

Smith S (1984) Phosphorus versus nitrogen limitation in the marine environment. Limnol Oceanogr 29: 1149-1160

Snedecor GW and Cochran WG (1989) Statistical methods. 8th ed (DH Jones, Ed.). Iowa State University Press, Ames

Sneed ED and Folk RL (1958) Pebbles in the lower Colorado River, Texas a study in particle morphogenesis. J Geol 66: 114-150

Sokal RR and Rohlf FJ (2012) Biometry: The principles and practice of statistics in biological research. 4th ed. New York: W.H. Freema

Spilling K, Ylöstalo P, Simis S, Seppälä J (2015) Interaction effects of light, temperature and nutrient limitations (N, P and Si) on growth, stoichiometry and photosynthetic parameters of the cold-water diatom *Chaetoceros wighamii*. PLoS ONE 10: e0126308

Squires HJ (1990) Decapod Crustacea of the Atlantic coast of Canada. Department of Fisheries and Oceans, Ottawa, Canadian Bulletin of Fisheries and Aquatic Sciences; 221. 532 p.

Sordo L, Santos R, Barrote I, Silva J (2019) Temperature amplifies the effect of high CO_2 on the photosynthesis, respiration, and calcification of the coralline algae *Phymatolithon lusitanicum*. Ecol Evol 9: 11000-11009

Steller D, Cáceres-Martínez C (2009) Coralline algal rhodoliths enhance larval settlement and early growth of the Pacific calico scallop *Argopecten ventricosus*. Mar Ecol Progr Ser 396: 40-60

Steller DL and Foster MS (1995) Environmental factors influencing distribution and morphology of rhodoliths in Bahía Concepción, B.C.S., México. J Exp Mar Biol Ecol 194: 201-212

Steller DL, Hernádez-Ayón JM, Riosmena-Rodríguez R, Cabello-Pasini A (2007) Effect of temperature on photosynthesis, growth and calcification rates of the free-living coralline alga *Lithophyllum margaritae*. Cienc Mar 33: 441-456

Steller DL, Riosmena-Rodríguez R, Foster MS, Roberts CA (2003) Rhodolith bed diversity in the Gulf of California: the importance of rhodolith structure and consequences of disturbance. Aquatic Conserv Mar Freshw Ecosyst 13: S5-S2

Steneck RS (1986) The ecology of coralline algal crusts: convergent patterns and adaptative strategies. Ann Rev Ecol Syst 17: 273-303

Steneck RS, Graham MH, Bourque BJ, Corbett D and others (2002) Kelp forest ecosystems: Biodiversity, stability, resilience and future. Environ Conserv 29: 436-459

St-Pierre A and Gagnon P (2020) Kelp-bed dynamics across scales: Enhancing mapping capability with remote sensing and GIS. J Exp Mar Biol Ecol 522: 151246

Tanaka Y, Suzuki A, Sakai K (2017) Effects of elevated seawater temperature and phosphate enrichment on the crustose coralline alga *Porolithon onkodes* (Rhodophyta). Phycol Res 65: 51-57

Taylor R (1997) Seasonal variation in assemblages of mobile epifauna inhabiting three subtidal brown seaweeds in northeastern New Zealand. Hydrobiologia 361: 25-35

Teed L, Bélanger D, Gagnon P, Edinger E (2020) Calcium carbonate ($CaCO_3$) production of a subpolar rhodolith bed: effect of bioturbators, methods of estimation, and global comparisons. Estuar Coast Shelf Sci 242: 106822

Teichert S (2014) Hollow rhodoliths increase Svalbard's shelf biodiversity. Sci Rep 4:6972

Teichert S and Freiwald A (2014) Polar coralline algal CaCO3 production rates correspond to intensity and duration of the solar radiation. Biogeosciences 11: 833-842

Teichert S, Woelkerling W, Rüggeberg A, Wisshak M and others (2014) Arctic rhodolith beds and their environmental controls (Spitsbergen, Norway). Facies 60: 15-37

Teichert S, Woelkerling W, Rüggeberg A, Wisshak M and others (2012) Rhodolith beds (Corallinales, Rhodophyta) and their physical and biological environment at 80°31'N in Nordkappbukta (Nordaustlandet, Svalbard Archipelago, Norway). Phycologia 51: 371-390

Tendal OS (1992) The North Atlantic distribution of the octocoral *Paragorgia arborea* (L., 1758) (Cnidaria, Anthozoa). Sarsia 77: 213-217

Tomascik T, Sander F (1985) Effects of eutrophication on reef-building corals. Mar Biol 87: 143-155

Tsuji Y, Yamazaki M, Suzuki I, Shiraiwa Y (2015) Quantitative analysis of carbon flow into photosynthetic products functioning as carbon storage in the marine coccolithophore *Emiliania huxleyi*. Mar Biotechnol 17: 428-440

Valiela I, Mcclelland J, Hauxwell J, Behr PJ, Hersh D, Foreman K (1997) Macroalgal blooms in shallow estuaries: Controls and ecophysiological and ecosystem consequences. Limnol Oceanogr 42: 1105-1118

van der Heijden LH, Kamenos NA (2015) Reviews and syntheses: Calculating the glogal contribution of coralline algae to total carbon burial. Biogeosciences 12: 6429-6441

Villas-Boas AB, Riosmena-Rodríguez R, Figueiredo MAO (2014) Community structure of rhodolith-forming beds on the central Brazilian continental shelf. Helgol Mar Res 68: 27-35

Walvoord MA and Striegl RG (2007) Increased groundwater to stream discharge from permafrost thawing in the Yukon River basin: Potential impacts on lateral export of carbon and nitrogen. Geophys Res Lett 34: L12402

Wang X, Olsen LM, Reithan KI, Olsen Y (2012) Discharge of nutrient wastes from salmon farms: environmental effects, and potential for integrated multi-trophic aquaculture. Aquacult Environ Interact 2: 267-283

Watling L, Rowley S, Guinott J (2013) The World's largest known gorgonian. Zootaxa 3630: 198-199

Wentworth CK (1922) A scale of grade and class terms for clastic sediments. J Geol 30: 377-392

Węsławski JM, Kendall AK, Włodarska-Kowalczuk M, Iken K and others (2011) Climate change effects of Arctic fjord and coastal microbenthic diversity – observations and predictions. Mar Biodiv 41: 71-85

Whalan S, Webster NS, Negri AP (2012) Crustose coralline algae and a cnidarian neuropeptide trigger larval settlement in two coral reef sponges. PLoS ONE 7: e30386

White WB, Lean J, Cayan DR, Dettinger MD (1997) Response of global upper ocean temperature to changing solar irradiance. J Geophys Res 102: 3255-326

Wiencke C and Dieck IT (1990) Temperature requirements for growth and survival of macroalgae from Antarctica and southern Chile. Mar Ecol Prog Ser 59: 157-170

William S, Adey W, Halfar J, Kronz A and others (2018) Effects of light and temperature on Mg uptake, growth, and calcification in the proxy climate archive *Clathromorphum compactum*. Biogeosciences 15: 5745-5759

Williamson CJ, Najorka, J, Perkins R, Yallop ML and others (2014) Skeletal mineralogy of geniculate corallines: providing context for climate change and ocean acidification research. Mar Ecol Prog Ser 513: 71-84

Wilson S, Blake C, Berges JA, Maggs CA (2004) Environmental tolerances of free-living coralline algae (maerl): implications for European marine conservation. Biol Conserv 120: 279-289

Woelkerling WJ and Irvine LM (1986) The typification and status of *Phymatolithon* (Corallinaceae, Rhodophyta). Br Phycol J 21: 55-80

Woelkerling WMJ, Irvine LM, Harvey AS (1993) Growth-forms in non-geniculate coralline red algae (Corallinales, Rhodophyta). Aust Syst Bot 6: 277-293

Wolff C and Gerberding M (2015) "Crustacea": Comparative aspects of early development. Evolutionary Developmental Biology of Invertebrates 4. Springer, p. 39-61

Worm B, Reusch TBH, Lotze HK (2000) *In situ* nutrient enrichment: Methods for marine benthic ecology. Int Rev Hydrobiol 85: 359-37

Wong MC, Dowd M (2015) Patterns in taxonomic and functional diversity in macrobenthic invertebrates across seagrass habitats: a case study in Atlantic Canada. Estuar Coast 38: 2323-233

Wozniak B and Dera J (2007) Light absorption in sea water. In: Mysak LA, Hamilton K (eds) Springer-Verlag, New York

Zhang Q, Warwick RM, McNeil CL, Widdicombe CE, Sheehan A, Widdicombe S. (2015) An unusually large phytoplankton spring bloom drives rapid changes in benthic diversity and ecosystem function. Prog Oceanogr 137: 533-545

Zuur AF, Ieno EN, Walker NJ, Saveliev AA, Smith GM (2009) Mixed effects models and extensions in ecology with R. In: Ieno EN, Walker N, Saveliev AA, Smith GM and SpringerLink (Online service) (eds). New York, NY

APPENDICES

Appendix A

Nutrient release

We carried out pre-experimental trials to characterize patterns of nutrient release and underwater lifetime of the Osmocote® fertilizer prills used in the present study. Several quantities of Osmocote® were tested along with the custom-built nutrient dispensers (Figure A.1, Appendix A) to create a consistently repeatable pattern of nutrient release with detectable levels of nitrate, ammonia, and phosphorus. The present appendix reports on the methods and results for the pattern of release chosen to carry out the laboratory mesocosm and field experiments.

Trials were carried out in three, 180-L flow-through (1 L min^{-1}) glass mesocosms (those used in the laboratory experiment); one for each of the three targeted nutrient concentrations: ambient, intermediate, or high. All mesocosms replicated the same general conditions as in the laboratory experiment (see "Mesocosm enrichment experiment" for details on mesocosm setup), except they contained no rhodoliths. Trials lasted 31 d and began on 1 June, 2015, with the introduction of two, 25-cm-long nutrient dispensers to each mesocosm. Each dispenser in the ambient, intermediate, and high nutrient concentration mesocosms contained 0, 62.5, and 125 g of fertilizer, respectively, for a total of 0, 125, or 250 g of fertilizer in the mesocosms. Water samples were collected from each mesocosm every 24 h from days 1 to 5, every 48 h from days 6 to 25, and every 72 h from days 26 to 31, for a total of 17 samples per mesocosm, and analyzed with the same protocols as in the laboratory mesocosm experiment (see "Water sampling and nutrient analysis"). Water temperature was recorded every 5 min with one temperature logger (HOBO Pendant; Onset Computer Corporation) on the bottom of each mesocosm.

Patterns of nitrate (NO_3^-), ammonia (NH_3), and phosphate (PO_4^{3-}) release were similar for the intermediate and high nutrient concentration treatments, with a quick release to peak concentrations within the first 24 h, followed by a quasi exponential decline over the following 8 to10 d to relatively low and stable concentrations (Figure A.1, Appendix A). The diminishing phase was more abrupt for nitrate and ammonia, which both decreased by an order of magnitude, than for phosphate, which decreased by 75% and 85% in the intermediate and high enrichment treatments, respectively. As expected, concentrations of nitrate, ammonia, and phosphate in the ambient treatment were quite stable throughout the trials (Figure A.1, Appendix A). Nitrate and ammonia were continuously lower in the ambient than intermediate and high concentration treatments, whereas phosphate exhibited no clear differences among the three treatments beyond 10 d (Figure A.1, Appendix A). Daily mean water temperature during the pre-experimental trials generally increased from ~4°C on 1 Jun, 2015, to ~10°C on 1 July, 2015, averaging 7.8 ± 2.1 (SD) °C during this period. These results helped us anticipate nutrient depletion, while guiding the number and size of nutrient dispensers and frequency at which we changed them in the laboratory (see "Mesocosm enrichment experiment") and field (see "Field nutrient enrichment") experiments.

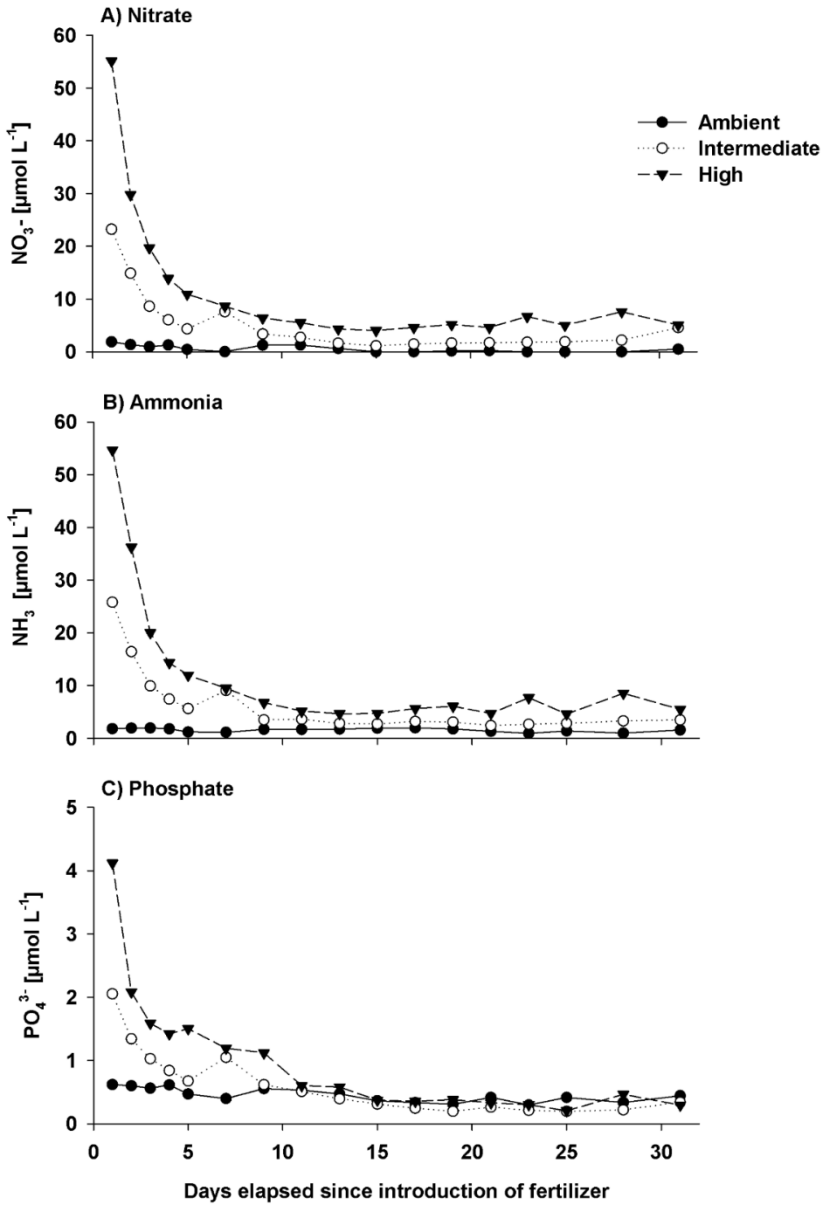

Figure A.1. Concentration of (A) nitrate [NO_3^-], (B) ammonia [NH_3], and (C) phosphate [PO_4^{3-}] for each nutrient concentration treatment (ambient [0 g of fertilizer], intermediate [125 g] and high [250 g]) for each of the 17 water collections during the 31-d pre-experiment trials. Concentration was measured every 24 h from days 1 to 5, every 48 h from days 6 to25, and every 72 h from days 25 to 31, from a single water sample per collection event (n = 17 for each concentration treatment).

Appendix B

Determination of lux to PAR conversion factors

The following procedures were applied to calculate numerical factors for conversion of illuminance values (in lx) of artificial actinic light and sunlight measured in the lab and field, to irradiance (PAR) values (in µmol photons m^{-2} s^{-1}).

B.1. Artificial actinic light

Illuminance and irradiance at the bottom of one mesocosm were recorded simultaneously for 15 min for each of two actinic fluorescent tubes at each of the three experimental irradiances (low, intermediate, and high). Tubes were chosen randomly from the pool of tubes used in the laboratory experiment. The two trials were performed in the dark to measure the sole contribution of each tube to light environment. Illuminance was recorded once every minute with the same model of temperature and light logger (HOBO Pendant; Onset Computer Corporation) used in the mesocsom experiment. Irradiance was recorded 240 times min^{-1} with a quantum sensor (LI-192; LI-COR). One conversion factor was calculated for each tube and irradiance treatment. This was done by averaging illuminance and irradiance data for each of the 15 min that each trial lasted, and then by dividing each mean illuminance by corresponding mean irradiance. Means of the resulting 15 conversion factors (one per minute for each combination of irradiance and tube) were similar for both tubes within a same irradiance treatment, and hence averaged, yielding one overall conversion factor per irradiance treatment (Table B.1).

Table B.1. Mean (± SD) illuminance to PAR conversion factors (in $\frac{\text{lx}}{\mu\text{mol photons m}^{-2}\text{s}^{-1}}$) for each of the two actinic fluorescent tubes chosen randomly among the five tubes used in the laboratory experiment, at each of the three experimental irradiances (n = 15 for each combination of tube and irradiance and 30 for each of the three overall factors pooled across tubes).

	Irradiance		
Actinic tube	Low	Intermediate	High
1	13.9 (0.9)	18.4 (0.9)	21.6 (0.7)
2	15.5 (0.9)	17.8 (0.5)	22.6 (0.6)
Tubes pooled	14.7 (1.2)[2]	18.1 (0.8)[2]	22.1 (0.8)[1, 2]

[1]Overall factors used to convert individual actinic illuminance values to PAR values in the laboratory mesocosm experiment of Chapter II

[2]Overall factors used to convert individual actinic illuminance values to PAR values in the low, intermediate, and high irradiance treatments of the laboratory mesocosm experiment of Chapter III.

B.2 Sunlight

Illuminance and irradiance above the rhodolith bed were recorded simultaneously for 15 min at each of the three experimental depths (8, 15, and 25 m), on a partly cloudy day with low winds in both April and August, when phytoplankton abundance was respectively high (during spring bloom) and low (after spring bloom) (Parrish et al. 2005). Illuminance was recorded once every second with the same model of temperature and light logger (HOBO Pendant; Onset Computer Corporation) used in the laboratory mesocosm experiment. Irradiance was recorded 240 times min^{-1} with a quantum sensor (LI-192; LI-COR). Both instruments were attached next to one another on a metal frame deposited on the surface of the rhodolith bed and pointed towards the sea surface. One conversion factor was calculated for each depth on each sampling day. This was done by averaging illuminance and irradiance data for each of the 15 min that each trial lasted, and then by dividing each mean illuminance by corresponding mean irradiance. Means of the resulting 15 conversion factors (one per minute for each combination of depth and day) were similar among the six combinations of depth and day, and hence averaged, yielding one overall conversion factor applicable to all depths (Table S1.2).

Table B.2. Mean (± SD) illuminance to PAR conversion factors (in $\frac{\text{lx}}{\mu\text{mol photons m}^{-2}\text{s}^{-1}}$) for each of the three depths of the field experiment, based on measurement of illuminance and irradiance above the rhodolith bed on a partly cloudy day with low winds in both April and August, when phytoplankton abundance was respectively high and low (n = 15 for each conversion factor per depth and day, 30 for each factor per depth pooled across days, 45 for each factor per day pooled across depths, and 90 for the overall factor pooled across depths and days).

	Depth (m)			
Sampling day	8	15	25	Depths pooled
1 (April)	21.3 (1.0)	25.0 (0.1)	25.9 (0.2)	24.1 (2.0)
2 (August)	24.0 (1.6)	21.9 (0.5)	22.1 (1.0)	22.7 (1.5)
Days pooled	22.7 (1.9)	23.5 (1.6)[1]	24.0 (2.1)	23.4 (1.9)[2]

[1] Overall factor used to convert sunlight illuminance values to PAR values in the field experiment of Chapter II.

[2] Overall factor used to convert sunlight illuminance values to PAR values in the field experiment of Chapter III.

Appendix C

Comparison of water temperatures between the first and second runs of the laboratory mesocosm experiment

Daily mean water temperature (DMWT) in the controlled temperature mesocoms (2, 4, 7, and 10°C) was generally similar between the first and second experimental runs (Figure C.1). The accidental reduction of seawater delivery to mesocosms at 2 and 4°C during the acclimation period of the second run increased temperature by ~4.5°C above that of the first experimental run over approximately three days. Such a small and short-lived difference was deemed inconsequential to rhodolith growth.

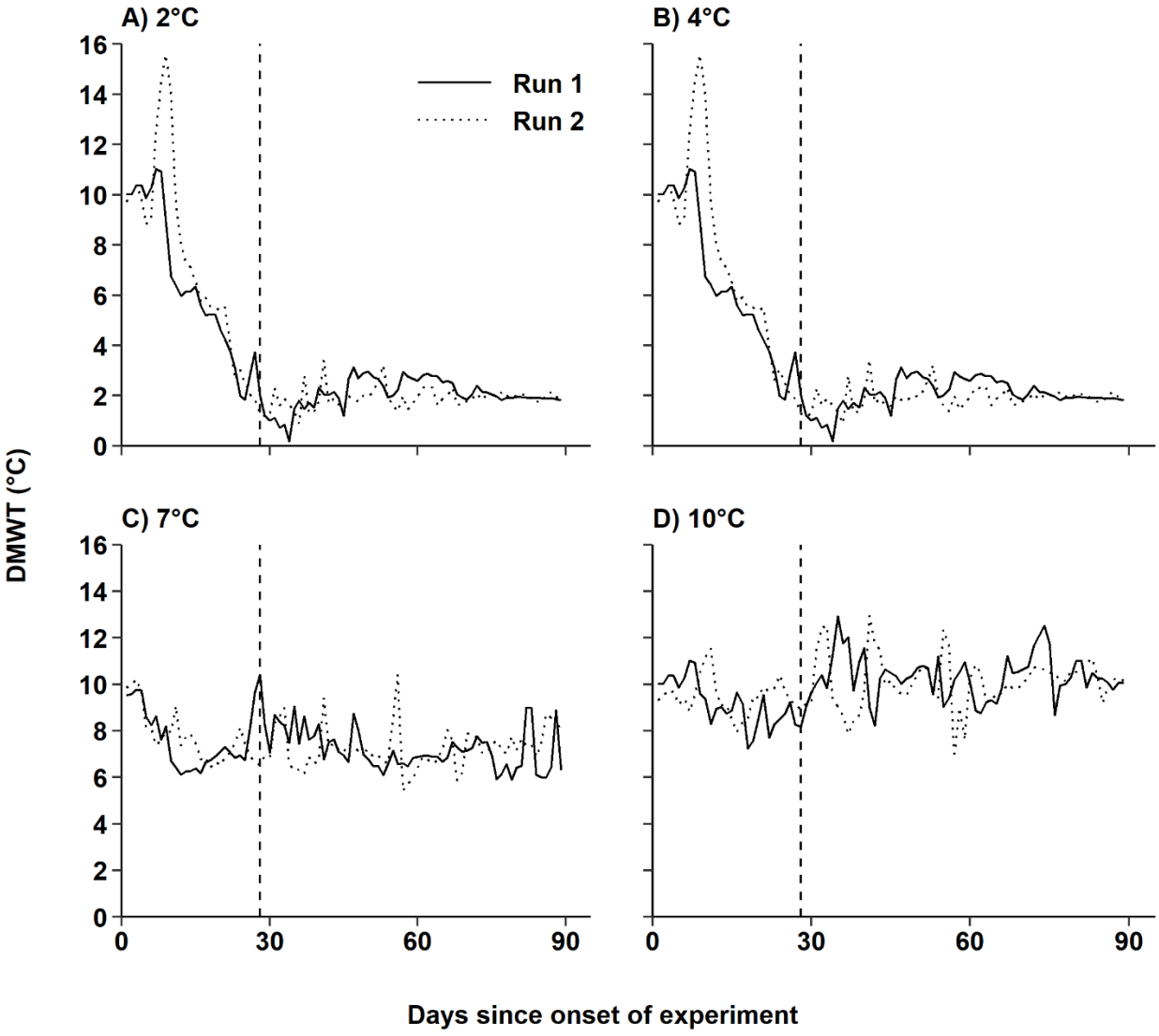

Figure C.1. Daily mean water temperature (DMWT) in each of the four mesocosms with controlled temperature [2, 4, 7, and 10°C] during the first 89 d of the first experimental run and 89 d that the second experimental run lasted. Vertical dashed lines mark the end of acclimation during which rhodoliths in mesocosms at 2, 4, and 7°C were exposed to decreasing temperatures from an initial temperature of 10°C.

Appendix D

Summary of similarity percentage (SIMPER) analyses

Table D.1. Summary of SIMPER analysis of seafloor composition between sampling sites (SP15 and SP18) and among seasons (spring, summer, fall, and winter). Second column indicates the average contribution of each seafloor type to the overall dissimilarity between contrasted sites or seasons. Third column indicates the cumulative dissimilarity. Fourth column indicates the probability of getting a larger or equal average contribution of each seafloor type to overall dissimilarity in random permutation of sampling sites or season (n = 9999 permutations). Asterisks indicate seafloor types significantly contributing to overall dissimilarity ($\alpha = 0.01$). Results are only presented for significant contrasts detected by pairwise comparison.

Seafloor type	Average dissimilarity (%)	Cumulative dissimilarity (%)	p	
SP15 vs SP18				
Dead shells	3.21	3.21	0.000	*
Sediment	2.07	5.28	0.418	
Pebbles	1.90	7.18	0.358	
Dead rhodoliths	1.24	8.43	0.118	
Live rhodoliths	1.20	9.63	0.234	
Cobbles	1.07	10.70	0.487	
Spring vs Winter				
Sediment	3.21	3.21	0.003	*
Pebbles	1.99	5.20	0.416	
Dead shells	1.97	7.17	0.829	
Live rhodoliths	1.92	9.09	0.001	*
Dead rhodoliths	1.21	10.30	0.453	
Cobbles	0.89	11.19	0.796	

Table D.2. Summary of similarity percentage (SIMPER) analysis of macrofaunal assemblages between sampling sites (SP15 and SP18) and among seasons (spring, summer, fall, and winter). Second column indicates the average contribution of each seafloor type to the overall dissimilarity between contrasted sites or seasons. Third column indicates the cumulative dissimilarity. Fourth column indicates the probability of getting a larger or equal average contribution of each taxa to overall dissimilarity in random permutation of sampling sites or season (n = 9999 permutations). Asterisks indicate taxa significantly contributing to overall dissimilarity ($\alpha = 0.01$). Results are only presented for significant contrasts detected by pairwise comparison.

Taxa	Average dissimilarity (%)	Cumulative dissimilarity (%)	p	
SP15 vs SP18				
Ophiopholis aculeata	1.65	1.65	0.504	
Ophiura robusta	1.54	3.29	0.999	
Tonicella marmorea	1.16	4.83	0.001	*
Sabellidae	1.07	6.00	0.694	
Hiatella arctica	1.04	7.07	0.003	*
Dexamine thea	0.98	8.10	0.000	*
Nematoda	0.96	9.08	0.010	*
Harpacticoida	0.89	10.04	0.033	
Puncturella noachina	0.83	10.94	0.223	
Phascolionidae	0.83	11.77	0.000	*
Stenosemus albus	0.78	12.60	0.001	*
Munna sp.	0.71	13.37	0.599	
Ostracoda	0.67	14.09	0.000	*
Boreocingula castanea	0.66	14.75	0.000	*
Cirratulidae	0.65	15.41	0.000	*
Orbiniidae	0.64	16.06	0.001	*
Crassicorophium bonellii	0.56	16.70	0.000	*
Moelleria costulata	0.53	17.26	0.579	
Phyllodocidae	0.53	17.79	0.000	*
Terebellidae	0.51	18.32	0.698	
Strongilocentrotus droebachiensis	0.48	18.83	0.981	
Asterias rubens	0.46	19.31	0.026	
Boltenia sp.	0.45	19.77	0.512	

Taxa	Average dissimilarity (%)	Cumulative dissimilarity (%)	p	
Syllidae	0.45	20.22	0.012	
Modiolus modiolus	0.44	20.67	0.027	
Heteranomia squamula	0.44	21.12	0.207	
Micrura sp.	0.44	21.56	0.994	
Hippolytidae	0.42	22.00	0.610	
Ecrobia truncata	0.42	22.41	0.509	
Margarites costalis	0.41	22.83	0.008	*
Nudibranchia	0.41	23.24	0.780	
Flabelligeridae	0.41	23.65	0.987	
Acari	0.41	24.05	0.978	
Dacrydium vitreum	0.40	24.46	0.336	
Capitellidae	0.40	24.86	0.535	
Testudinalia testudinalis	0.39	25.25	0.022	
Hardametopa carinata	0.38	25.65	0.000	*
Diaphana minuta	0.37	26.03	0.997	
Spionidae	0.35	26.39	0.401	
Maldanidae	0.34	26.74	0.966	
Nereididae	0.34	27.09	0.147	
Notoplana atomata	0.33	27.43	0.138	
Velutina velutina	0.33	27.76	0.245	
Crenella decussata	0.33	28.10	0.004	*
Lacuna vincta	0.29	28.42	0.746	
Deflexilodes tesselatus	0.28	28.72	0.888	
Turbonilla sp.	0.26	29.00	0.347	
Arenicolidae	0.25	29.26	1.000	
Sphaerodoridae	0.25	29.51	1.000	
Scalibregmidae	0.24	29.75	0.000	*
Pontogeneia inermis	0.22	29.99	0.665	
Pectinariidae	0.20	30.21	0.976	
Serpulidae	0.18	30.41	0.055	
Pleusymtes glaber	0.17	30.59	0.501	
Parvicardium pinnulatum	0.16	30.77	0.076	
Ampharetidae	0.16	30.93	0.378	
Cuccumaria frondosa	0.15	31.09	0.696	
Buccinum sp.	0.15	31.24	0.998	
Polynoidae	0.14	31.38	0.062	
Thyasira sp.	0.13	31.52	0.157	
Phoxocephalus holbolli	0.12	31.65	1.000	
Apherusa megalops	0.12	31.78	0.996	
Palio dubia	0.10	31.90	0.249	
Margarites helicinus	0.10	32.00	0.116	

Taxa	Average dissimilarity (%)	Cumulative dissimilarity (%)	p	
Hyas araneus	0.10	32.11	0.002	*
Isopoda	0.08	32.20	0.110	
Pholoidae	0.08	32.28	0.128	
Crossaster papposus	0.08	32.36	0.920	
Psolus sp.	0.08	32.43	0.993	
Onchidoris muricata	0.07	32.51	1.000	
Oenopota sp.	0.07	32.58	0.570	
Cyclocardia sp.	0.06	32.65	0.995	
Mytilus edulis	0.06	32.71	1.000	
Musculus discors	0.06	32.77	0.298	
Cancer irroratus	0.03	32.82	0.001	*
Littorina sp.	0.03	32.85	0.989	
Glyceridae	0.03	32.89	0.001	*
Lysianassidae	0.03	32.92	0.998	
Dotilla sp.	0.03	32.95	0.541	
Pagurus pubescens	0.03	32.98	0.997	
Pagurus sp.	0.02	33.00	0.999	
Metridium senile	0.02	33.03	0.001	*
Paraonidae	0.02	33.05	0.002	*
Orchomene sp.	0.01	33.07	0.999	
Solamen glandula	0.01	33.08	0.997	
Macoma calcarea	0.01	33.09	0.997	
Pagurus arcuatus	0.01	33.10	0.003	*
Ischyrocerus anguipes	0.01	33.11	0.003	*
Summer vs Fall				
Ophiura robusta	1.51	1.51	0.598	
Ophiopholis aculeata	1.35	3.02	0.985	
Sabellidae	1.23	4.37	0.050	
Nematoda	1.17	5.60	0.001	*
Tonicella marmorea	1.10	6.77	0.432	
Puncturella noachina	0.93	7.88	0.087	
Hiatella arctica	0.88	8.81	0.859	
Dexamine thea	0.85	9.68	0.255	
Harpacticoida	0.78	10.54	0.893	
Phascolionidae	0.75	11.31	0.306	
Stenosemus albus	0.70	12.06	0.636	
Boltenia sp.	0.62	12.76	0.000	*
Cirratulidae	0.61	13.38	0.416	
Phyllodocidae	0.59	13.99	0.009	*
Orbiniidae	0.58	14.57	0.691	

Taxa	Average dissimilarity (%)	Cumulative dissimilarity (%)	p	
Terebellidae	0.58	15.15	0.078	
Nudibranchia	0.57	15.73	0.000	*
Moelleria costulata	0.55	16.30	0.431	
Ostracoda	0.50	16.85	0.895	
Boreocingula castanea	0.49	17.34	0.933	
Syllidae	0.47	17.84	0.123	
Crassicorophium bonellii	0.44	18.31	0.903	
Heteranomia squamula	0.43	18.75	0.526	
Modiolus modiolus	0.43	19.19	0.476	
Acari	0.41	19.62	0.546	
Strongilocentrotus droebachiensis	0.41	20.03	0.932	
Munna sp.	0.40	20.43	1.000	
Hippolytidae	0.40	20.83	0.807	
Lacuna vincta	0.39	21.23	0.001	*
Testudinalia testudinalis	0.39	21.62	0.359	
Capitellidae	0.39	22.02	0.571	
Diaphana minuta	0.38	22.41	0.388	
Micrura sp.	0.38	22.79	0.901	
Arenicolidae	0.38	23.17	0.000	*
Notoplana atomata	0.36	23.54	0.053	
Spionidae	0.36	23.90	0.394	
Flabelligeridae	0.35	24.26	0.991	
Margarites costalis	0.35	24.61	0.861	
Dacrydium vitreum	0.35	24.96	0.908	
Hardametopa carinata	0.35	25.31	0.285	
Asterias rubens	0.35	25.66	0.974	
Ecrobia truncata	0.34	26.01	0.987	
Maldanidae	0.34	26.35	0.578	
Nereididae	0.33	26.69	0.702	
Velutina velutina	0.30	27.01	0.864	
Crenella decussata	0.29	27.32	0.624	
Deflexilodes tesselatus	0.27	27.61	0.681	
Pontogeneia inermis	0.27	27.88	0.067	
Sphaerodoridae	0.25	28.15	0.527	
Turbonilla sp.	0.25	28.40	0.705	
Ampharetidae	0.22	28.65	0.015	
Pectinariidae	0.18	28.87	0.798	
Serpulidae	0.17	29.05	0.570	
Polynoidae	0.16	29.22	0.173	
Apherusa megalops	0.16	29.39	0.155	
Scalibregmidae	0.15	29.55	0.939	

Taxa	Average dissimilarity (%)	Cumulative dissimilarity (%)	p	
Cuccumaria frondosa	0.15	29.70	0.529	
Buccinum sp.	0.14	29.85	0.654	
Isopoda	0.14	29.99	0.003	*
Mytilus edulis	0.12	30.13	0.004	*
Pholoidae	0.11	30.24	0.101	
Hyas araneus	0.10	30.35	0.283	
Psolus sp.	0.10	30.45	0.177	
Parvicardium pinnulatum	0.10	30.55	0.984	
Cyclocardia sp.	0.10	30.65	0.046	
Pleusymtes glaber	0.09	30.75	0.976	
Musculus discors	0.07	30.83	0.343	
Crossaster papposus	0.06	30.90	0.797	
Thyasira sp.	0.05	30.96	0.996	
Onchidoris muricata	0.05	31.01	0.885	
Phoxocephalus holbolli	0.05	31.06	0.984	
Margarites helicinus	0.04	31.10	0.977	
Glyceridae	0.04	31.15	0.177	
Oenopota sp.	0.04	31.19	0.882	
Paraonidae	0.04	31.22	0.153	
Orchomene sp.	0.03	31.26	0.048	
Littorina sp.	0.02	31.29	0.746	
Pagurus sp.	0.02	31.31	0.739	
Metridium senile	0.02	31.33	0.534	
Palio dubia	0.00	31.35	1.000	
Dotilla sp.	0.00	31.35	1.000	
Solamen glandula	0.00	31.35	1.000	
Macoma calcarea	0.00	31.35	1.000	
Cancer irroratus	0.00	31.35	1.000	
Pagurus arcuatus	0.00	31.35	1.000	
Pagurus pubescens	0.00	31.35	1.000	
Lysianassidae	0.00	31.35	1.000	
Ischyrocerus anguipes	0.00	31.35	1.000	
Summer vs Winter				
Ophiopholis aculeata	1.78	1.78	0.197	
Ophiura robusta	1.70	3.56	0.260	
Sabellidae	1.21	5.26	0.080	
Tonicella marmorea	1.15	6.46	0.279	
Munna sp.	1.12	7.61	0.000	*
Nematoda	1.10	8.74	0.019	
Hiatella arctica	1.02	9.83	0.364	

Taxa	Average dissimilarity (%)	Cumulative dissimilarity (%)	p	
Dexamine thea	0.98	10.85	0.005	*
Puncturella noachina	0.95	11.82	0.061	
Stenosemus albus	0.78	12.77	0.256	
Phascolionidae	0.77	13.55	0.192	
Harpacticoida	0.75	14.32	0.938	
Orbiniidae	0.66	15.08	0.184	
Nudibranchia	0.60	15.74	0.000	*
Phyllodocidae	0.58	16.34	0.012	
Cirratulidae	0.56	16.93	0.729	
Boreocingula castanea	0.56	17.48	0.666	
Terebellidae	0.53	18.04	0.412	
Ostracoda	0.51	18.57	0.847	
Moelleria costulata	0.49	19.08	0.784	
Strongilocentrotus droebachiensis	0.49	19.57	0.482	
Micrura sp.	0.47	20.06	0.324	
Dacrydium vitreum	0.45	20.53	0.078	
Asterias rubens	0.45	20.98	0.509	
Heteranomia squamula	0.44	21.42	0.460	
Testudinalia testudinalis	0.43	21.86	0.061	
Margarites costalis	0.42	22.30	0.215	
Crassicorophium bonellii	0.42	22.72	0.970	
Boltenia sp.	0.42	23.14	0.853	
Modiolus modiolus	0.42	23.56	0.617	
Ecrobia truncata	0.42	23.98	0.531	
Syllidae	0.41	24.39	0.695	
Flabelligeridae	0.41	24.80	0.549	
Acari	0.39	25.21	0.746	
Hippolytidae	0.38	25.60	0.930	
Capitellidae	0.35	25.98	0.857	
Hardametopa carinata	0.35	26.33	0.192	
Nereididae	0.35	26.69	0.265	
Velutina velutina	0.35	27.04	0.222	
Arenicolidae	0.33	27.39	0.002	*
Diaphana minuta	0.33	27.72	0.904	
Spionidae	0.33	28.04	0.745	
Notoplana atomata	0.32	28.37	0.682	
Deflexilodes tesselatus	0.31	28.69	0.187	
Maldanidae	0.31	29.00	0.859	
Pleusymtes glaber	0.26	29.31	0.011	*
Turbonilla sp.	0.25	29.57	0.726	
Crenella decussata	0.24	29.82	0.992	

Taxa	Average dissimilarity (%)	Cumulative dissimilarity (%)	p	
Lacuna vincta	0.23	30.06	0.982	
Serpulidae	0.22	30.29	0.131	
Pontogeneia inermis	0.22	30.50	0.516	
Sphaerodoridae	0.21	30.72	0.977	
Ampharetidae	0.21	30.93	0.036	
Pectinariidae	0.18	31.14	0.846	
Cuccumaria frondosa	0.16	31.32	0.330	
Buccinum sp.	0.15	31.48	0.438	
Scalibregmidae	0.15	31.63	0.948	
Palio dubia	0.15	31.79	0.024	
Isopoda	0.14	31.94	0.002	*
Parvicardium pinnulatum	0.14	32.08	0.804	
Polynoidae	0.14	32.21	0.536	
Margarites helicinus	0.10	32.35	0.537	
Onchidoris muricata	0.10	32.45	0.213	
Mytilus edulis	0.09	32.54	0.114	
Apherusa megalops	0.08	32.64	0.855	
Thyasira sp.	0.08	32.72	0.932	
Oenopota sp.	0.08	32.80	0.250	
Pholoidae	0.08	32.88	0.492	
Crossaster papposus	0.08	32.96	0.547	
Cyclocardia sp.	0.08	33.04	0.302	
Psolus sp.	0.07	33.11	0.640	
Pagurus pubescens	0.06	33.18	0.028	
Musculus discors	0.05	33.24	0.541	
Hyas araneus	0.04	33.29	0.964	
Cancer irroratus	0.04	33.33	0.318	
Glyceridae	0.04	33.37	0.291	
Orchomene sp.	0.03	33.41	0.312	
Pagurus sp.	0.02	33.44	0.470	
Paraonidae	0.02	33.46	0.407	
Lysianassidae	0.02	33.48	0.874	
Pagurus arcuatus	0.02	33.50	0.461	
Metridium senile	0.02	33.52	0.656	
Phoxocephalus holbolli	0.02	33.54	0.999	
Littorina sp.	0.00	33.55	1.000	
Dotilla sp.	0.00	33.55	1.000	
Solamen glandula	0.00	33.55	1.000	
Macoma calcarea	0.00	33.55	1.000	
Ischyrocerus anguipes	0.00	33.55	1.000	

Table D.3. Summary of similarity percentage (SIMPER) analysis of mollusc assemblages between sampling sites (SP15 and SP18) and among seasons (spring, summer, fall, and winter). Second column indicates the average contribution of each seafloor type to the overall dissimilarity between contrasted sites or seasons. Third column indicates the cumulative dissimilarity. Fourth column indicates the probability of getting a larger or equal average contribution of each taxa to overall dissimilarity in random permutation of sampling sites or season (n = 9999 permutations). Asterisks indicate taxa significantly contributing to overall dissimilarity ($\alpha = 0.01$). Results are only presented for significant contrasts detected by pairwise comparison.

Taxa	Average dissimilarity (%)	Cumulative dissimilarity (%)	p	
SP15 vs SP18				
Tonicella marmorea	3.29	3.29	0.001	*
Hiatella arctica	2.93	6.22	0.002	*
Puncturella noachina	2.36	8.59	0.226	
Stenosemus albus	2.22	10.81	0.001	*
Boreocingula castanea	1.85	12.65	0.000	*
Moelleria costulata	1.51	14.16	0.530	
Modiolus modiolus	1.25	15.41	0.026	
Heteranomia squamula	1.25	16.66	0.190	
Ecrobia truncata	1.17	17.84	0.508	
Nudibranchia	1.16	19.00	0.614	
Margarites costalis	1.16	20.16	0.007	*
Dacrydium vitreum	1.12	21.28	0.308	
Testudinalia testudinalis	1.12	22.40	0.023	
Diaphana minuta	1.04	23.44	0.992	
Velutina velutina	0.94	24.37	0.223	
Crenella decussata	0.92	25.30	0.003	*
Lacuna vincta	0.83	26.13	0.682	
Turbonilla sp.	0.73	26.85	0.353	
Parvicardium pinnulatum	0.46	27.31	0.088	
Buccinum sp.	0.41	27.72	0.994	
Thyasira sp.	0.36	28.08	0.160	
Palio dubia	0.30	28.38	0.264	

Taxa	Average dissimilarity (%)	Cumulative dissimilarity (%)	p	
Margarites helicinus	0.29	28.67	0.091	
Onchidoris muricata	0.22	28.89	0.998	
Oenopota sp.	0.18	29.07	0.627	
Cyclocardia sp.	0.17	29.24	0.980	
Mytilus edulis	0.16	29.41	0.995	
Musculus discors	0.16	29.56	0.192	
Littorina sp.	0.09	29.65	0.980	
Dotilla sp.	0.08	29.73	0.680	
Solamen glandula	0.03	29.77	0.985	
Summer vs Fall				
Tonicella marmorea	3.12	3.12	0.444	
Puncturella noachina	2.65	5.77	0.097	
Hiatella arctica	2.48	8.25	0.855	
Stenosemus albus	2.00	10.25	0.621	
Nudibranchia	1.61	11.87	0.000	*
Moelleria costulata	1.54	13.41	0.438	
Boreocingula castanea	1.39	14.80	0.933	
Heteranomia squamula	1.23	16.03	0.518	
Modiolus modiolus	1.22	17.25	0.451	
Testudinalia testudinalis	1.12	18.37	0.350	
Lacuna vincta	1.12	19.49	0.001	*
Diaphana minuta	1.08	20.56	0.375	
Margarites costalis	0.99	21.55	0.866	
Dacrydium vitreum	0.98	22.53	0.905	
Ecrobia truncata	0.97	23.50	0.987	
Velutina velutina	0.86	24.36	0.879	
Crenella decussata	0.83	25.19	0.623	
Turbonilla sp.	0.70	25.89	0.676	
Buccinum sp.	0.39	26.29	0.652	
Mytilus edulis	0.33	26.61	0.004	*
Cyclocardia sp.	0.28	26.89	0.043	
Parvicardium pinnulatum	0.28	27.17	0.983	
Musculus discors	0.19	27.36	0.326	
Onchidoris muricata	0.14	27.50	0.877	
Thyasira sp.	0.14	27.64	0.996	
Margarites helicinus	0.12	27.76	0.976	
Oenopota sp.	0.11	27.87	0.880	
Littorina sp.	0.06	27.93	0.724	

Taxa	Average dissimilarity (%)	Cumulative dissimilarity (%)	p
Palio dubia	0.00	27.93	1.000
Dotilla sp.	0.00	27.93	1.000
Solamen glandula	0.00	27.93	1.000

Table D.4. Summary of similarity percentage (SIMPER) analysis of polychaete assemblages between sampling sites (SP15 and SP18) and among seasons (spring, summer, fall, and winter). Second column indicates the average contribution of each seafloor type to the overall dissimilarity between contrasted sites or seasons. Third column indicates the cumulative dissimilarity. Fourth column indicates the probability of getting a larger or equal average contribution of each taxa to overall dissimilarity in random permutation of sampling sites or season (n = 9999 permutations). Asterisks indicate taxa significantly contributing to overall dissimilarity ($\alpha = 0.01$). Results are only presented for significant contrasts detected by pairwise comparison.

Taxa	Average dissimilarity (%)	Cumulative dissimilarity (%)	p	
SP15 vs SP18				
Sabellidae	5.99	5.99	0.981	
Cirratulidae	3.66	9.65	0.001	*
Orbiniidae	3.61	13.26	0.001	*
Phyllodocidae	2.86	16.12	0.000	*
Syllidae	2.52	18.64	0.017	
Flabelligeridae	2.32	20.95	0.988	
Capitellidae	2.23	23.19	0.775	
Spionidae	1.97	25.16	0.466	
Maldanidae	1.96	27.12	0.999	
Nereididae	1.92	29.04	0.255	
Sphaerodoridae	1.37	30.42	1.000	
Arenicolidae	1.35	31.77	1.000	
Scalibregmidae	1.32	33.08	0.000	*
Pectinariidae	1.09	34.17	0.982	
Serpulidae	0.99	35.16	0.073	
Ampharetidae	0.87	36.03	0.824	
Polynoidae	0.79	36.82	0.077	
Pholoidae	0.41	37.24	0.093	
Glyceridae	0.15	37.39	0.001	*
Paraonidae	0.10	37.49	0.002	*

Taxa	Average dissimilarity (%)	Cumulative dissimilarity (%)	p	
Summer vs Fall				
Sabellidae	6.66	6.66	0.131	
Cirratulidae	3.36	10.01	0.526	
Orbiniidae	3.16	13.17	0.789	
Phyllodocidae	3.14	16.30	0.019	
Syllidae	2.57	18.87	0.253	
Capitellidae	2.15	21.02	0.676	
Arenicolidae	2.00	23.02	0.000	*
Spionidae	1.96	24.98	0.538	
Flabelligeridae	1.91	26.89	0.997	
Maldanidae	1.89	28.78	0.692	
Nereididae	1.79	30.57	0.803	
Sphaerodoridae	1.35	31.92	0.709	
Ampharetidae	1.15	33.07	0.026	
Pectinariidae	0.95	34.02	0.877	
Polynoidae	0.90	34.92	0.221	
Serpulidae	0.89	35.81	0.671	
Scalibregmidae	0.81	36.62	0.956	
Pholoidae	0.56	37.19	0.144	
Glyceridae	0.20	37.38	0.190	
Paraonidae	0.18	37.57	0.172	

Table D.5. Summary of similarity percentage (SIMPER) analysis of crustacean assemblages between sampling sites (SP15 and SP18) and among seasons (spring, summer, fall, and winter). Second column indicates the average contribution of each seafloor type to the overall dissimilarity between contrasted sites or seasons. Third column indicates the cumulative dissimilarity. Fourth column indicates the probability of getting a larger or equal average contribution of each taxa to overall dissimilarity in random permutation of sampling sites or season (n = 9999 permutations). Asterisks indicate taxa significantly contributing to overall dissimilarity ($\alpha = 0.01$). Results are only presented for significant contrasts detected by pairwise comparison.

Taxa	Average dissimilarity (%)	Cumulative dissimilarity (%)	p	
SP15 vs SP18				
Dexamine thea	8.33	8.33	0.000	*
Harpacticoida	8.25	16.58	0.096	
Isopoda	5.96	22.54	1.000	
Ostracoda	5.89	28.43	0.000	*
Crassicorophium bonellii	4.97	33.40	0.000	*
Hippolytidae	3.69	37.09	1.000	
Hardametopa carinata	3.23	40.31	0.000	*
Deflexilodes tesselatus	2.34	42.65	1.000	
Pontogeneia inermis	1.75	44.40	1.000	
Pleusymtes glaber	1.36	45.76	1.000	
Phoxocephalus holbolli	1.09	46.85	1.000	
Apherusa megalops	0.90	47.75	1.000	
Hyas araneus	0.78	48.53	0.001	*
Pagurus spp.	0.45	48.98	1.000	
Lysianassidae	0.27	49.25	1.000	
Cancer irroratus	0.23	49.49	0.000	*
Orchomene sp.	0.12	49.61	1.000	
Ischyrocerus anguipes	0.08	49.69	0.000	*
Spring vs Summer				
Harpacticoida	15.56	15.56	0.000	*
Dexamine thea	8.43	23.99	0.004	*
Isopoda	7.16	31.14	0.012	

Taxa	Average dissimilarity (%)	Cumulative dissimilarity (%)	p	
Ostracoda	5.97	37.11	0.002	*
Crassicorophium bonellii	5.52	42.63	0.001	*
Hippolytidae	4.28	46.91	0.048	
Hardametopa carinata	2.41	49.32	0.992	
Phoxocephalus holbolli	2.15	51.47	0.000	*
Deflexilodes tesselatus	1.93	53.39	0.965	
Pontogeneia inermis	1.47	54.86	0.872	
Pleusymtes glaber	0.76	55.62	0.971	
Hyas araneus	0.65	56.27	0.579	
Lysianassidae	0.46	56.74	0.136	
Orchomene sp.	0.28	57.02	0.056	
Cancer irroratus	0.17	57.19	0.523	
Ischyrocerus anguipes	0.15	57.35	0.057	
Apherusa megalops	0.14	57.49	0.997	
Pagurus spp.	0.00	57.49	1.000	
Spring vs Fall				
Isopoda	10.47	10.47	0.009	*
Dexamine thea	7.20	17.67	0.674	
Crassicorophium bonellii	6.81	24.48	0.003	*
Ostracoda	5.43	29.91	0.138	
Hippolytidae	5.25	35.15	0.061	
Hardametopa carinata	4.24	39.39	0.072	
Deflexilodes tesselatus	3.19	42.58	0.492	
Phoxocephalus holbolli	2.45	45.03	0.000	*
Pontogeneia inermis	2.21	47.23	0.279	
Apherusa megalops	2.01	49.25	0.040	
Hyas araneus	1.42	50.66	0.023	
Pleusymtes glaber	1.06	51.72	0.965	
Lysianassidae	0.80	52.52	0.137	
Pagurus spp.	0.45	52.97	0.916	
Cancer irroratus	0.22	53.19	0.560	
Ischyrocerus anguipes	0.17	53.36	0.202	
Orchomene sp.	0.15	53.51	1.000	
Spring vs Winter				
Harpacticoida	8.11	8.11	0.506	
Dexamine thea	6.88	14.99	0.611	
Isopoda	4.96	19.95	0.992	
Ostracoda	4.83	24.78	0.535	

Taxa	Average dissimilarity (%)	Cumulative dissimilarity (%)	p	
Crassicorophium bonellii	4.72	29.49	0.182	
Hippolytidae	3.65	33.15	0.674	
Hardametopa carinata	3.01	36.16	0.261	
Deflexilodes tesselatus	2.67	38.83	0.186	
Pleusymtes glaber	2.09	40.91	0.011	
Phoxocephalus holbolli	1.82	42.73	0.026	
Pontogeneia inermis	1.36	44.09	0.934	
Pagurus spp.	0.84	44.93	0.016	
Apherusa megalops	0.75	45.68	0.769	
Hyas araneus	0.54	46.21	0.779	
Lysianassidae	0.51	46.72	0.122	
Cancer irroratus	0.40	47.12	0.105	
Ischyrocerus anguipes	0.13	47.25	0.492	
Orchomene sp.	0.00	47.25	1.000	
Summer vs Fall				
Dexamine thea	7.86	7.86	0.051	
Harpacticoida	7.83	15.69	0.639	
Ostracoda	4.83	20.52	0.523	
Crassicorophium bonellii	4.29	24.82	0.616	
Hippolytidae	3.91	28.72	0.333	
Isopoda	3.75	32.47	1.000	
Hardametopa carinata	3.10	35.57	0.141	
Pontogeneia inermis	2.44	38.00	0.012	
Deflexilodes tesselatus	2.43	40.44	0.508	
Apherusa megalops	1.35	41.78	0.067	
Hyas araneus	0.88	42.66	0.189	
Pleusymtes glaber	0.81	43.47	0.956	
Phoxocephalus holbolli	0.41	43.89	0.981	
Orchomene sp.	0.27	44.16	0.184	
Pagurus spp.	0.22	44.38	0.914	
Cancer irroratus	0.00	44.38	1.000	
Lysianassidae	0.00	44.38	1.000	
Ischyrocerus anguipes	0.00	44.38	1.000	
Summer vs Winter				
Isopoda	8.65	8.65	0.000	*
Dexamine thea	8.27	16.92	0.010	*
Harpacticoida	6.77	23.69	0.951	
Ostracoda	4.45	28.14	0.884	

Taxa	Average dissimilarity (%)	Cumulative dissimilarity (%)	p	
Crassicorophium bonellii	3.68	31.82	0.980	
Hippolytidae	3.29	35.11	0.962	
Hardametopa carinata	3.08	38.19	0.154	
Deflexilodes tesselatus	2.69	40.88	0.163	
Pleusymtes glaber	2.09	42.97	0.007	*
Pontogeneia inermis	1.79	44.76	0.548	
Pagurus spp.	0.84	45.60	0.015	
Apherusa megalops	0.66	46.26	0.843	
Hyas araneus	0.29	46.55	0.981	
Cancer irroratus	0.28	46.82	0.377	
Orchomene sp.	0.24	47.06	0.495	
Lysianassidae	0.16	47.22	0.770	
Phoxocephalus holbolli	0.14	47.36	0.998	
Ischyrocerus anguipes	0.00	47.36	1.000	
Fall vs Winter				
Isopoda	8.44	8.44	0.000	*
Dexamine thea	5.82	14.26	0.991	
Harpacticoida	5.09	19.36	1.000	
Ostracoda	4.05	23.41	0.992	
Hippolytidae	3.32	26.73	0.949	
Crassicorophium bonellii	2.99	29.72	1.000	
Hardametopa carinata	2.85	32.57	0.570	
Deflexilodes tesselatus	2.66	35.23	0.187	
Pleusymtes glaber	2.06	37.29	0.012	
Pontogeneia inermis	1.98	39.27	0.310	
Apherusa megalops	1.51	40.78	0.016	
Pagurus spp.	0.90	41.68	0.004	*
Hyas araneus	0.73	42.41	0.466	
Phoxocephalus holbolli	0.47	42.88	0.974	
Cancer irroratus	0.27	43.14	0.403	
Lysianassidae	0.16	43.30	0.793	
Orchomene sp.	0.00	43.30	1.000	
Ischyrocerus anguipes	0.00	43.30	1.000	

Appendix E

List and abundance of macrofaunal taxa

Table E.1. List of macrofaunal taxa identified in the St. Philip's bed. Numbers indicate mean density (± SE) per 30 x 30 cm quadrat (0.09 m^2) at the two sampling stations (data pooled across seasons), and each sampling seasons (data pooled across sites) (see Table 4.1 for collection dates). Dashes (---) indicate the absence of taxa for a given collection. Crosses (x) indicate taxa that were present but not tallied due to a high level of fragmentation. Blanks indicate species of polychaetes that were identified from subsamples but not tallied for quantitative analyses.

Taxa	SP15	SP18	Spring	Summer	Fall	Winter
Echinodermata						
Asteroidea						
Asterias rubens (Linnaeus, 1758)	17.4 (1.5)	12.8 (1.0)	14.9 (2.3)	14.9 (1.6)	14.9 (1.1)	15.7 (2.3)
Crossaster papposus (Linnaeus, 1767)	0.1 (0.1)	0.1 (0.1)	0.2 (0.1)	0.1 (0.1)	0.1 (0.1)	0.1 (0.1)
Echinoidea						
Strongylocentrotus droebachiensis (O.F. Müller, 1776)	26.3 (1.6)	24.4 (1.9)	23.7 (2.6)	26.7 (2.4)	26.1 (2.3)	24.9 (2.8)
Holothuroidea						
Cuccumaria frondosa (Gunnerus, 1767)	0.3 (0.1)	0.3 (0.1)	0.3 (0.2)	0.4 (0.2)	0.2 (0.1)	0.3 (0.2)
Psolus fabricii (Düben & Koren, 1846)	0.1 (0.0)	0.1 (0.1)	---	0.1 (0.1)	0.2 (0.1)	0.2 (0.1)

Taxa	SP15	SP18	Spring	Summer	Fall	Winter
Ophiuroidea						
Ophiura robusta (Ayres, 1852)	137 (12)	148 (15)	131 (18)	170 (19)	124 (16)	145 (21)
Ophiopholis aculeata (Linnaeus, 1767)	119 (19)	103 (14)	98 (16)	104 (14)	66 (11)	176 (38)
Mollusca						
Polyplacophora						
Tonicella marmorea (O. Fabricius, 1780)	117 (9)	77 (6)	94 (12)	128 (14)	85 (9)	84 (9)
Stenosemus albus (Linnaeus, 1767)	20.9 (2.2)	34.1 (2.7)	20.3 (2.7)	32.0 (4.7)	29.8 (3.3)	27.9 (3.9)
Gastropoda						
Boreocingula castanea (Møller, 1842)	9.9 (1.6)	2.7 (0.6)	6.7 (1.9)	5.6 (1.4)	4.4 (1.2)	8.4 (2.8)
Buccinum sp. (Linnaeus, 1758)	0.3 (0.1)	0.3 (0.1)	0.3 (0.1)	0.3 (0.1)	0.2 (0.1)	0.3 (0.2)
Diaphana minuta (T. Brown, 1827)	2.1 (0.4)	2.4 (0.4)	1.9 (0.5)	1.3 (0.2	3.6 (0.7)	2.2 (0.6)
Ecrobia truncata (Vanatta, 1924)	2.5 (0.6)	1.9 (0.5)	3.1 (0.9)	1.7 (0.3)	0.6 (0.2)	3.3 (1.1)
Lacuna vincta (Montagu, 1823)	1.1 (0.3)	0.8 (0.2)	0.5 (0.2)	0.3 (0.2)	2.1 (0.6)	0.8 (0.3)
Littorina sp. (Férussac, 1822)	< 0.1 (0.0)	0.1 (0.0)	0.1 (0.1)	---	0.1 (0.1)	---
Margarites costalis (Gould, 1841)	10.1 (1.0)	6.9 (0.8)	8.4 (0.9)	8.5 (1.1)	7.9 (1.2)	9.1 (1.8)
Margarites helicinus (Phipps, 1774)	0.2 (0.1)	0.1 (0.0)	0.2 (0.1)	0.1 (0.1)	0.1 (0.1)	0.3 (0.1)
Moelleria costulata (Möller, 1842)	12.1 (1.6)	9.0 (1.2)	16.5 (2.5)	11.9 (1.5)	5.4 (1,1)	8.3 (1.7
Oenopota sp. (Mörch, 1852)	0.1 (0.1)	0.1 (0.0)	0.1 (0.1)	---	0.1 (0.1)	0.2 (0.1)
Puncturella noachina (Linnaeus, 1771)	41.3 (3.9)	33.5 (3.6)	46.4 (5.7)	50.4 (5.3)	24.1 (2.9)	28.6 (4.6)
Testudinalia testudinalis (Müller, 1776)	2.1 (0.3)	3.7 (0.4)	3.3 (0.4)	3.5 (0.7)	3.3 (0.6)	1.3 (0.4)
Turbonilla sp. (Risso, 1826)	0.8 (0.2)	0.7 (0.1)	0.7 (0.2)	0.5 (0.2)	0.8 (0.2)	0.9 (0.3)
Velutina velutina (O.F. Müller, 1776)	1.9 (0.3)	1.4 (0.3)	1.8 (0.4)	1.8 (0.4)	0.9 (0.2)	2.1 (0.5)
Dotilla sp. (Stimpson, 1858)	0.1 (0.0)	< 0.1 (0.0)	0.2 (0.1)	---	---	---
Onchidoris muricata (O.F. Müller, 1776)	0.1 (0.1)	0.1 (0.1)	0.2 (0.1)	0.1 (0.1)	---	0.2 (0.1)
Palio dubia (M. Sars, 1829)	0.5 (0.1)	0.4 (0.1)	0.4 (0.2)	---	---	0.5 (0.2)
Nudibranchia indet. (Cuvier, 1817)	4.0 (0.5)	4.2 (0.6)	3.9 (0.5)	1.1 (0.4)	5.1 (0.7)	6.3 (1.0)
Bivalva						
Crenella decussata (Montagu, 1808)	1.6 (0.3)	0.5 (0.1)	1.7 (0.4)	0.7 (0.3)	1.2 (0.4)	0.8 (0.2)
Cyclocardia sp. (Conrad, 1867)	0.1 (0.1)	0.1 (0.1)	---	0.2 (0.1)	0.2 (0.1)	0.1 (0.1)

Taxa	SP15	SP18	Spring	Summer	Fall	Winter
Dacrydium vitreum (Møller, 1842)	2.4 (0.7)	1.3 (0.3)	0.7 (0.3)	0.7 (0.2)	2.2 (0.9)	3.9 (1.1)
Heteranomia squamula (Linnaeus, 1758)	2.8 (0.4)	2.4 (0.6)	1.6 (0.5)	3.1 (0.9)	1.9 (0.6)	3.9 (06)
Hiatella arctica (Linnaeus, 1767)	48.3 (4.9)	30.5 (3.9)	30.2 (5.0)	48.8 (6.6)	35.7 (5.4)	42.9 (8.4)
Macoma calcarea (Gmelin, 1791)	---	< 0.1 (0.0)	0.1 (0.1)	---	---	---
Modiolus modiolus (Linnaeus, 1758)	3.4 (0.6)	1.3 (0.2)	4.7 (1.0)	2.8 (0.6)	1.1 (0.3)	0.7 (0.2)
Musculus discors (Linnaeus, 1767)	---	0.2 (0.1)	0.1 (0.1)	0.1 (0.1)	0.1 (0.1)	0.1 (0.1)
Mytilus edulis (Linnaeus, 1758)	0.1 (0.0)	0.1 (0.1)	---	0.3 (0.1)	0.1 (0.1)	---
Parvicardium pinnulatum (Conrad, 1831)	0.4 (0.1)	0.2 (0.1)	0.4 (0.1)	0.1 (0.1)	0.3 (0.1)	0.5 (0.2)
Solamen glandula (Totten, 1834)	---	< 0.1 (0.0)	0.1 (0.1)	---	---	---
Thyasira sp. (Lamarck, 1818)	0.4 (0.1)	0.1 (0.1)	0.7 (0.3)	0.1 (0.1)	0.1 (0.1)	0.2 (0.1)
Annelida						
Polychaeta						
Ampharetidae (Malmgren, 1866)	0.4 (0.1)	0.3 (0.1)	0.4 (0.2)	0.7 (0.2)	0.1 (0.1)	0.2 (0.1)
Arenicolidae (Johnston, 1835)	0.3 (0.1	0.4 (0.1)	0.3 (0.1)	0.8 (0.2)	0.1 (0.1)	0.2 (0.1)
Capitellidae (Grube, 1862)	3.7 (0.6)	2.9 (0.5)	3.0 (0.7)	4.9 (1.1)	2.4 (0.5)	2.7 (0.6)
Cirratulidae (Ryckholt, 1851)	16.3 (1.6)	8.4 (1.1)	14.1 (2.6)	15.4 (2.3)	8.1 (1.3)	11.7 (1.8)
Cirratulus cirratus (O. F. Müller, 1776)						
Dodecaceria concharum (Örsted, 1843)						
Polydora sp. (Bosc, 1802)						
Tharyx sp. (Webster & Benedict, 1887)						
Flabelligeridae (de Saint-Joseph, 1894)	2.3 (0.4)	2.1 (0.4)	2.8 (0.6)	1.2 (0.3)	1.7 (0.5)	3.2 (0.6)
Flabelligera affinis (M. Sars, 1829)						
Glyceridae (Grube, 1850)	0.1 (0.0)	---	0.1 (0.1)	0.1 (0.1)	---	---
Glycera sp. (Lamarck, 1818)						
Maldanidae (Malmgren, 1867)	4.6 (0.4)	5.6 (0.7)	3.9 (0.6)	5.7 (0.8)	4.8 (0.9)	5.9 (0.9)
Clymenella zonalis (Verrill, 1874)						
Nicomache (Malmgren, 1865)						
Praxillella gracilis (M. Sars, 1861)						
Nereididae (Blainville, 1818)	1.7 (0.3)	1.3 (0.3)	1.2 (0.3)	1.7 (0.4)	1.4 (0.4)	1.7 (0.5)

Taxa	SP15	SP18	Spring	Summer	Fall	Winter
Nereis zonata (Malmgren, 1867)						
Orbiniidae (Hartman, 1942)	11.7 (1.8)	5.0 (0.8)	9.0 (2.3)	9.9 (2.0)	5.7 (1.4)	8.8 (2.6)
Naineris quadricuspida (Fabricius, 1780)						
Phylo ornatus (Verrill, 1873)						
Paraonidae (Cerruti, 1909)	0.1 (0.0)	---	---	0.1 (0.1)	0.1 (0.1)	---
Aricidea sp. (Webster, 1879)						
Pectinariidae (Quatrefages, 1866)	0.5 (0.1)	0.4 (0.1)	0.9 (0.2)	0.6 (0.2)	0.1 (0.1)	0.1 (0.1)
Cistenides granulata (Linnaeus, 1767)						
Pholoidae (Kinberg, 1858)	0.2 (0.1)	0.1 (0.1)	0.1 (0.1)	0.3 (0.2)	0.2 (0.1)	0.1 (0.1)
Pholoe minuta (Fabricius, 1780)						
Phyllodocidae (Örsted, 1843)	11.7 (1.5)	5.3 (0.7)	9.4 (1.8)	13.8 (2.3)	5.9 (1.3)	4.7 (0.7)
Eteone longa (Fabricius, 1780)						
Eteone sp. (Savigny, 1822)						
Eteone trilineata (Webster & Benedict, 1887)						
Eumida sp. (Malmgren, 1865)						
Eulalia viridis (Linnaeus, 1767)						
Phyllodoce (Lamarck, 1818)						
Polynoidae (Kinberg, 1856)	0.4 (0.1)	0.1 (0.1)	0.3 (0.2)	0.3 (0.1)	0.3 (0.2)	0.2 (0.1)
Harmothoe sp. (Kinberg, 1856)						
Sabellidae (Latreille, 1825)	34.3 (5.1)	29.5 (4.6)	24.9 (4.5)	50.0 (7.9)	17.8 (3.1)	34.9 (0.3)
Myxicola infundibulum (Montagu, 1808)						
Pseudopotamilla reniformis (Bruguière, 1789)						
Scalibregmatidae (Malmgren, 1867)	0.9 (0.2)	0.1 (0.0)	0.9 (0.3)	0.3 (0.1)	0.3 (0.1)	0.3 (0.1)
Serpulidae (Rafinesque, 1815)	0.7 (0.2)	0.2 (0.1)	0.4 (0.2)	0.7 (0.3)	0.1 (0.1)	0.6 (0.3)
Spirorbis (Spirorbis) spirorbis (Linnaeus, 1758)						
Sphaerodoridae (Malmgren, 1867)	0.7 (0.2)	0.7 (0.2)	0.9 (0.2)	0.6 (0.2)	0.8 (0.3)	0.6 (0.1)
Sphaerodorum gracilis (Rathke, 1843)						
Spionidae (Grube, 1850)	3.1 (0.5)	2.1 (0.3)	3.9 (0.6)	2.7 (0.6)	2.1 (0.6)	1.8 (0.5)
Polydora sp. (Bosc, 1802)						
Prionospio steenstrupi (Malmgren, 1867)						

Taxa	SP15	SP18	Spring	Summer	Fall	Winter
Scolelepis (Scolelepis) squamata (O.F. Muller, 1806)						
Spiophanes sp. (Grube, 1860)						
Syllidae (Grube, 1850)	3.5 (0.7)	1.3 (0.2)	2.9 (0.8)	3.6 (0.9)	2.1 (0.9)	1.2 (0.3)
Exogone sp. (Claparède 1868)						
Parapionosyllis longicirrata (Webster & Benedict, 1884)						
Parexogone hebes (Webster & Benedict, 1884)						
Terebellidae (Johnston, 1846)	14.9 (1.7)	13.4 (1.5)	14.9 (2.3)	18.8 (2.4)	9.2 (1.1)	13.7 (2.3)
Amphitrite cirrata Müller, 1776						
Eupolymnia sp. (Verrill, 1900)						
Nicolea venustula (Montagu, 1819)						
Polycirrus medusa (Grube, 1850)						
Arthropoda						
Amphipoda						
Apherusa megalops (Buchholz, 1874)	0.3 (0.2)	0.3 (0.1)	0.1 (0.1)	---	0.8 (0.4)	0.2 (0.1)
CrassiCrassicorophium bonelliii (H. Milne Edwards, 1830)	4.9 (0.9)	1.4 (0.4)	6.0 (1.6)	3.2 (0.7)	2.1 (0.6)	1.4 (0.4)
Dexamine thea (Boeck, 1861)	20.4 (2.7)	4.9 (0.9)	15.9 (3.6)	2.8 (1.1)	12.9 (2.5)	18.9 (4.2)
Hardametopa carinata (Hansen, 1887)	2.0 (0.3)	0.6 (0.1)	0.9 (0.3)	0.5 (0.1)	1.8 (0.5)	2.0 (0.4)
Ischyrocerus anguipes (Krøyer, 1838)	< 0.1 (0.0)	---	0.1 (0.1)	---	---	---
Lysianassidae (Dana, 1849)	< 0.1 (0.0)	0.1 (0.0)	0.1 (0.1)	-	---	0.1 (0.1)
Orchomene sp. (Boeck, 1871)	---	0.1 (0.1)	---	0.1 (0.1)	---	---
Phoxocephalus holbolli (Krøyer, 1842)	0.2 (0.1)	0.4 (0.2)	0.9 (0.5)		0.2 (0.1)	0.1 (0.1)
Pleusymtes glaber (Boeck, 1861)	0.7 (0.5)	0.3 (0.1)	0.1 (0.1)	0.1 (0.1)	0.2 (0.1)	1.6 (0.9)
Deflexilodes teselatus (Schneider, 1883)	0.7 (0.2)	1.0 (0.2)	0.5 (0.2)	0.4 (0.2)	1.0 (0.4)	1.4 (0.4)
Pontogeneia inermis (Krøyer, 1838)	0.3 (0.1)	0.7 (0.2)	0.1 (0.1)	0.6 (0.3)	0.9 (0.4)	0.4 (0.1)
Copepoda						
Harpacticoida indet. (Sars G.O., 1903)	22.8 (3.4)	12.9 (1.9)	3.8 (1.5)	30.4 (3.6)	20.4 (4.3)	16.8 (3.8)
Decapoda						
Cancer irroratus (Say, 1817)	0.1 (0.0)	---	0.1 (0.1)	---	---	0.1 (0.1)
Hyas araneus (Linnaeus, 1858)	0.3 (0.1)	< 0.1 (0.0)	0.2 (0.1)	0.1 (0.1)	0.3 (0.1)	0.1 (0.1)

Taxa	SP15	SP18	Spring	Summer	Fall	Winter
Hippolytidae (Spence Bate, 1888)	2.8 (0.5)	2.0 (0.4)	2.9 (0.7)	2.2 (0.5)	1.7 (0.4)	2.7 (0.8)
Pagurus arcuatus (Squires, 1864)	< 0.1 (0.0)	---	---	---	---	0.1 (0.1)
Pagurus pubescens (Krøyer, 1838)	< 0.1 (0.0)	0.1 (0.0)	---	---	---	0.2 (0.1)
Pagurus sp. (Fabricius, 1775)	---	0.1 (0.0)	---	---	0.1 (0.1)	0.1 (0.1)
Isopoda						
Munna sp. (Krøyer, 1839)	6.4 (1.3)	7.4 (1.6)	8.3 (1.4)	1.1 (0.4)	2.3 (0.7)	16.1 (2.6)
Idotea sp. (Fabricius, 1798)	---	< 0.1 (0.0)	---	0.1 (0.1)	---	---
Isopoda indet. (Latreille, 1817)	0.1 (0.1)	< 0.1 (0.0)	< 0.1 (0.0)	0.1 (0.1)	---	<0.1 (0.0)
Ostracoda						
Ostracoda indet. (Latreille, 1802)	6.2 (1.0)	1.2 (0.3)	3.4 (1.3)	3.8 (0.9)	3.5 (1.2)	3.9 (1.3)
Acari						
Acari indet. (Leach, 1817)	2.5 (0.5)	2.4 (0.5)	3.2 (0.8)	2.3 (0.8)	1.9 (0.6)	2.4 (0.4)
Cnidaria						
Metridium senile (Linnaeus, 1761)	0.1 (0.0)	---	0.1 (0.1)	0.1 (0.1)	---	---
Platyhelminthes						
Notoplana automata (Müller OF, 1776)	0.9 (0.2)	1.8 (0.3)	1.6 (0.3)	1.8 (0.5)	0.3 (0.1)	1.7 (0.3)
Nemertea						
Micrura sp. (Ehrenberg, 1828)	9.7 (1.0)	9.9 (0.9)	10.9 (1.5)	11.1 (1.2)	8.8 (1.2)	8.3 (1.4)
Tunicata						
Boltenia sp. (Savigny, 1816)	2.5 (0.6)	2.0 (0.5)	1.6 (0.6)	0.6 (0.3)	4.3 (3.8)	2.6 (0.8)
Nematoda						
Nematoda indet.	25.0 (3.8)	15.1 (2.1)	16.1 (3.6)	35.6 (5.6)	15.2 (3.4)	14.2 (3.0)

Taxa	SP15	SP18	Spring	Summer	Fall	Winter
Sipuncula						
Phascolion (Phascolion) strombus (Montagu, 1804)	15.3 (2.1)	4.1 (0.7)	7.8 (0.2)	16.3 (3.8)	6.4 (1.3)	8.2 (2.1)
Porifera						
Didemnum sp. (Savigny, 1816)	x	x	x	x	x	x
Sycon sp. (Risso, 1827)	x	x	x	x	x	x
Porifera indet. (Grant, 1836)	x	x	x	x	x	x